JULIANA ALVES DO VALE

PROSPECÇÃO DE COMPOSTOS DERIVADOS DO ÁCIDO CINÂMICO COM POTENCIAL ANTIMELANOMA

Tese apresentada à Universidade Federal de Viçosa, como parte das exigências do Programa de Pós-Graduação em Biologia Celular e Estrutural, para obtenção do título de *Doctor Scientiae*.

Orientadora: Mariana Machado Neves

Coorientadora: Graziela D. de Almeida Lima

VIÇOSA - MINAS GERAIS
2022

Ficha catalográfica elaborada pela Biblioteca Central da Universidade Federal de Viçosa - Campus Viçosa

T
V149p
2022

Vale, Juliana Alves do, 1992-
Prospecção de compostos derivados do ácido cinâmico com potencial antimelanoma / Juliana Alves do Vale. – Viçosa, MG, 2022.
1 tese eletrônica (199 f.): il. (algumas color.).

Texto em português e inglês.
Orientador: Mariana Machado Neves.
Tese (doutorado) - Universidade Federal de Viçosa, Departamento de Biologia Geral, 2022.
Inclui bibliografia.
DOI: https://doi.org/10.47328/ufvbbt.2022.275
Modo de acesso: World Wide Web.

1. Melanoma. 2. Ácido cinâmico. 3. Agentes antineoplásicos. I. Neves, Mariana Machado, 1977-.
II. Universidade Federal de Viçosa. Departamento de Biologia Geral. Programa de Pós-Graduação em Biologia Celular e Estrutural. III. Título.

CDD 22. ed. 616.99477

Bibliotecário(a) responsável: Alice Regina Pinto CRB6 2523

JULIANA ALVES DO VALE

PROSPECÇÃO DE COMPOSTOS DERIVADOS DO ÁCIDO CINÂMICO COM POTENCIAL ANTIMELANOMA

Tese apresentada à Universidade Federal de Viçosa, como parte das exigências do Programa de Pós-Graduação em Biologia Celular e Estrutural, para obtenção do título de *Doctor Scientiae*.

APROVADA: 07 de março de 2022.

Assentimento:

Juliana Alves do Vale
Juliana Alves do Vale
Autora

Mariana Machado Neves
Orientadora

Às flores do meu jardim, que perfumaram
e coloriram o fim dessa exímia trajetória:
Beatriz e Helena.

AGRADECIMENTOS

A Deus, sem o qual eu não sou nada;

À Nossa Senhora, amparo em todos os momentos;

Aos meus pais, fortaleza, apoio e proteção em toda caminhada e em toda a minha vida;

Ao meu esposo amado, por estar sempre comigo na alegria e na tristeza, nos fins de semana tranquilos e de estudo, nas noites serenas e mal dormidas. Obrigada, meu amor, por ser esse esposo tão parceiro, cuidadoso e apoiador. O amo!;

Às minhas filhas que, segundo o professor Róbson, são duas sínteses completas mais que perfeitas;

À minha rede de apoio na maternidade: meus pais, meus sogros e minha cunhada, sem os quais eu não teria conseguido finalizar essa tese em tempo hábil;

Aos meus avós já falecidos, em especial a querida vovó Geni (Nega), e a toda família que sonhou juntamente comigo;

À minha querida e tão amada orientadora Mariana Neves, que incontáveis vezes me segurou pelas mãos e me ensinou a ser pesquisadora e a escrever. Obrigada, Mari, pelos quase 11 anos de parceria, amizade e orientação;

Aos amigos de caminhada, do JSC, do ESC e da vida por serem amparo em todos os momentos;

Aos amigos do laboratório, especialmente às querydas, que foram mais que companhias acadêmicas, mas, inúmeras vezes, apoio emocional;

À Grazi e à Gabi, as quais foram cruciais para o meu aprendizado sobre o cultivo celular. Obrigada, meninas, por toda paciência e tempo gasto em me ensinar;

À Michelle, Fabíola e Deborah, orientadas do professor Róbson, que se tornaram amigas. Obrigada pela síntese dos compostos e pela parceria nos trabalhos, meninas!;

Ao professor Róbson, que é um grande exemplo de pessoa e professor a ser seguido;

Aos professores Leandro e Gustavo, pela parceria e valiosa contribuição nos trabalhos desenvolvidos;

À professora Juliana Fietto, pelos recursos disponibilizados para esta pesquisa e por abrir as portas do seu laboratório para mim;

Aos professores do laboratório de Biologia Estrutural, em especial ao professor Sérgio da Matta, pelas longas e profundas conversas e pelo imenso incentivo e confiança depositados a mim;

Aos professores da pós-graduação em Biologia Celular e Estrutural, que contribuíram enormemente para a minha formação profissional;

Aos servidores e técnicos do programa de pós-graduação, em especial à Beth, pelas partilhas trocadas e pelo apoio durante todo o percurso;

Ao Núcleo de Microscopia e Microanálise, pelos equipamentos fornecidos para as análises de apoptose e ciclo celular;

Aos membros efetivos da banca, Clóvis Andrade Neves, Gabriela Alves Moreira, Leandro Licursi e Róbson Teixeira, que aceitaram participar desta banca e fornecerem valiosas contribuições ao trabalho;

Aos suplentes, Alisson Almeida e Gustavo Bressan, pelo aceite e disponibilidade; À UFV, pela oportunidade ímpar de crescimento pessoal e profissional.

À Universidade Federal de Viçosa, pela oportunidade ímpar de crescimento pessoal e profissional;

À CAPES, FAPEMIG e CNPq pela concessão da bolsa de estudos e pelo suporte financeiro do projeto.

RESUMO

VALE, Juliana Alves do, D.Sc. Universidade Federal de Viçosa, março de 2022. **Prospecção de compostos derivados do ácido cinâmico com potencial antimelanoma**. Orientadora: Mariana Machado Neves. Coorientadora: Graziela Domingues de Almeida Lima.

Melanoma é um tipo de câncer altamente agressivo e letal. As altas taxas de mortalidade estão atreladas à sua capacidade de gerar metástases. Uma vez que os tratamentos atuais apresentam resultados insatisfatórios e o melanoma tem se mostrado resistente a muitos deles, faz-se necessária a prospecção de novos compostos com potencial antimelanoma. Nesse contexto, compostos sintéticos têm sido produzidos com o intuito de melhorar outros que servem como *scaffold* para a síntese de novas moléculas, como derivados do ácido cinâmico. O ácido cinâmico é um ácido graxo de ocorrência natural muito utilizado na criação de novos compostos. Derivados do ácido cinâmico já apresentaram diversas atividades biológicas, inclusive antitumoral. Desse modo, o objetivo geral desse estudo foi avaliar o potencial antimelanoma de derivados do ácido cinâmico em modelo experimental *in vitro* de melanoma murino B16-F10. No primeiro capítulo foi feita uma introdução geral do assunto, com uma justificativa do trabalho. No segundo capítulo foi realizada uma extensa revisão do uso de células de melanoma como modelo para o *screening* de drogas. Já os capítulos três e quatro são artigos de pesquisa com derivados do ácido cinâmico. Em ambos os artigos foram feitos a síntese dos compostos e ensaios biológicos de citotoxicidade, proliferação e metástase para avaliação da atividade antimelanoma dos compostos. No capítulo três o composto **6b** *((((oxybis(ethane-2,1-diyl))bis(oxy))bis(ethane-2,1-diyl))bis(1H-1,2,3-triazole-1,4-diyl))bis(methylene) (2E,2'E)-bis(3-phenylacrylate)* foi selecionado por apresentar melhor Índice de citotoxicidade (IC_{50}), sendo esse de 57.66 µM. Além disso, em concentrações abaixo do IC_{50}, o composto interferiu no ciclo celular e no comportamento metastático de células B16-F10, diminuindo migração, invasão celular e a formação de colônias. Já o capítulo quatro, o composto **3q** *(phenyl 2,3-dibromo-3-phenylpropanoate)* foi selecionado, apresentando IC_{50} de 60.28 µM. Esse composto não interferiu na viabilidade de células não-tumorais. Além disso, em concentração acima do IC_{50} provocou apoptose nas células de melanoma, enquanto em baixas concentrações impactou o ciclo celular e a proliferação, além de reduzir o comportamente metastático das células, como pode ser visto nos ensaios de migração, invasão, adesão, colonização celular e polimerização da actina. Enquanto o composto **3q** é um éster de ácido cinâmico, um cinamato com átomos de bromo em sua

composição, o composto **6b** é um bis cinamato contendo porções 1,2,3-triazólicas. Mesmo com características diferentes, os compostos apresentaram significativa atividade biológica em células de melanoma B16-F10. Portanto, os derivados do ácido cinâmico são compostos promissores para o tratamento do melanoma.

Palavras-chave: Ácido cinâmico. Atividade antitumoral. Melanoma.

ABSTRACT

VALE, Juliana Alves do, D.Sc., Universidade Federal de Viçosa, March, 2022. **Prospection of cinnamic acid derivatives compounds with antimelanoma potential**. Adviser: Mariana Machado Neves. Co-adviser: Graziela Domingues de Almeida Lima.

Melanoma is a highly aggressive and lethal type of cancer. The high mortality rates are linked to its ability to generate metastases. Since current treatments show unsatisfactory results and melanoma has been shown to be resistant to many of them, it is necessary to prospect new compounds with anti-melanoma potential. In this context, synthetic compounds have been produced to improve others that serve as scaffolds for the synthesis of new molecules, such as cinnamic acid derivatives. Cinnamic acid is a naturally occurring fatty acid widely used in the creation of new compounds. Derivatives of cinnamic acid have already shown several biological activities, including antitumor. Thus, the general objective of this study was to evaluate the antimelanoma potential of cinnamic acid derivatives in an *in vitro* experimental model of B16-F10 murine melanoma. In the first chapter, a general introduction of the subject was made, with a justification of the work. In the second chapter, an extensive review of the use of melanoma cells as a model for drug screening was carried out. Chapters three and four are research articles with cinnamic acid derivatives. In both articles, the synthesis of compounds and biological assays of cytotoxicity, proliferation and metastasis were performed to evaluate the antimelanoma activity of the compounds. In chapter three the compound **6b** *(((oxybis(ethane-2,1-diyl))bis(oxy))bis(ethane-2,1-diyl))bis(1H-1,2,3-triazole-1,4-diyl))bis(methylene) (2E,2'E)-bis(3-phenylacrylate)* was selected because it had the best cytotoxicity index (IC_{50}), which was 57.66 µM. Furthermore, at concentrations below the IC_{50}, the compound interfered with the cell cycle and metastatic behavior of B16-F10 cells, decreasing migration, cell invasion, and colony formation. Chapter four, the compound **3q** *(phenyl 2,3-dibromo-3-phenylpropanoate)* was selected, showing IC_{50} 60.28 µM. This compound did not interfere with the viability of non-tumor cells. Additionally, at concentrations above the IC_{50}, it triggered apoptosis in melanoma cells, while at low concentrations it impacted the cell cycle and proliferation, in addition to reducing the metastatic behavior of cells, as can be seen in cell migration, invasion, adhesion, colonization and actin polymerization assays. While compound **3q** is a cinnamic acid ester, a cinnamate with bromine atoms in its composition, compound **6b** is a bis cinnamate containing 1,2,3-triazole moieties. Even with different characteristics, the compounds showed significant

biological activity in B16-F10 melanoma cells. Therefore, cinnamic acid derivatives are promising compounds for the treatment of melanoma.

Keywords: Cinnamic acid. Antitumor activity. Melanoma.

SUMÁRIO

CAPÍTULO 1 – APRESENTAÇÃO GERAL

1. JUSTIFICATIVA

O câncer é a segunda maior causa de mortes e sua incidência global está aumentando rapidamente. Dentre os diversos tipos de cânceres, o câncer de pele é bastante comum no Brasil e no mundo. Enquanto o câncer de pele não-melanoma apresenta baixa letalidade, o melanoma é considerado de elevadíssimo impacto clínico devido ao mau prognóstico dos pacientes e ao risco metastático precoce. Desse modo, o melanoma é considerado uma doença de alta agressividade. Quando detectado em seu estágio inicial, o melanoma pode ser retirado por excisão cirúrgica. Entretanto, quando detectado em estágios avançados, radioterapia, quimioterapia e/ou imunoterapia são os tratamentos indicados. Contudo, o melanoma é resistente a muitos desses tratamentos e os medicamos disponíveis no mercado para o melanoma metastático demonstraram e numerosos efeitos colaterais, contribuindo para maior recidiva da doença. Portanto, são imprescindíveis novos estudos de prospecção de compostos com potencial antimelanoma.

Nesse contexto, nosso grupo de pesquisa trabalha com a prospecção de compostos com potencial contra o melanoma *in vitro* e *in vivo* (Vale et al., 2022; Santos et al., 2021; Almeida et al., 2021; Vale et al., 2020; Lima et al., 2018; Moreira et al., 2018), com o intuito de encontrar possíveis candidatos para o tratamento desse câncer. Diante disso, o ácido cinâmico tem se mostrado uma importante substância de partida, uma vez que modificações em sua estrutura permitem a descoberta de compostos com atividade biológica e eficácia aprimorada. Derivados do ácido cinâmico já apresentaram efeito antimicrobiano, antifúngico, anti-inflamatório, antioxidante, leishmanicida e antitumoral, inclusive contra o melanoma. Portanto, com base no presente exposto, esse trabalho teve como objetivo geral avaliar o potencial antimelanoma de derivados do ácido cinâmico em modelo experimental *in vitro* de melanoma murino B16-F10.

A presente tese foi dividida em quatro capítulos. O primeiro capítulo é uma introdução geral sobre o melanoma, bem como sobre o ácido cinâmico e seus derivados, características e aplicações, com o intuito de complementar nosso estudo sobre esse tipo de câncer e sobre o principal composto que originou os compostos utilizados nos artigos científicos. Já o segundo deles é um capítulo de livro, no qual são abordadas as diferentes possibilidades de uso das células do melanoma para o *screening* de drogas. O terceiro e o quarto capítulos são artigos de

pesquisa em que são avaliados derivados do ácido cinâmico em melanoma murino B16-F10. Além disso, duas patentes derivadas dos artigos de pesquisa foram escritas e submetidas.

2. INTRODUÇÃO GERAL

2.1 Melanoma e metástase

O melanoma é um tipo de câncer de pele extremamente agressivo e letal. A exposição crônica à radiação ultravioleta e a predisposição genética são fatores de risco determinantes para o seu desenvolvimento [1], uma vez que tais fatores induzem danos no DNA de melanócitos, mutações genéticas e aumentam a resposta inflamatória, contribuindo para o surgimento e progressão do melanoma [2]. O melanoma surge da transformação maligna de melanócitos, células especializadas encontradas, por exemplo, na pele e nos olhos, e são responsáveis pela produção, maturação e secreção de melanina, compostos poliméricos responsáveis pela pigmentação da pele [3]. A melanina exerce função protetora, ao absorver parte da radiação ultravioleta proveniente do sol e/ou neutralizar radicais livres que surgem devido ao dano no DNA dos melanócitos [4]. Esse pigmento pode ser produzido de forma constitutiva, que é o nível de pigmento basal da pele, ou adaptativa, quando induzido pela radiação ultravioleta. A radiação solar induz a síntese de melanina pela via do fator de transcrição MITF (*Microphthalmia-associated transcription fator*), o qual pode ativar oncogenes e genes relacionados à proliferação do melanócito, como CDK2 [5], e, portanto, induzir a progressão tumoral.

A transformação maligna dos melanócitos inicia-se pela mutação inicial de um único melanócito que, ao ter seu DNA mutado em genes importantes para a proliferação e sobrevivência celular, como BRAF e NRAS, induz a inativação de genes supressores tumorais e à ativação de genes responsáveis pela proliferação celular [6,7]. O melanócito transformado prolifera e gera um nevo benigno, tumores geralmente benignos não invasivos. O nevo benigno pode evoluir para nevo displásico, com presença de melanócitos atípicos, e entrar em uma fase de crescimento radial do melanoma, ou seja, o primeiro estágio maligno da doença. Melanoma em estágio de crescimento radial pode evoluir para uma fase de crescimento vertical, fase em que o melanoma é potencialmente metastático (Figura 1).

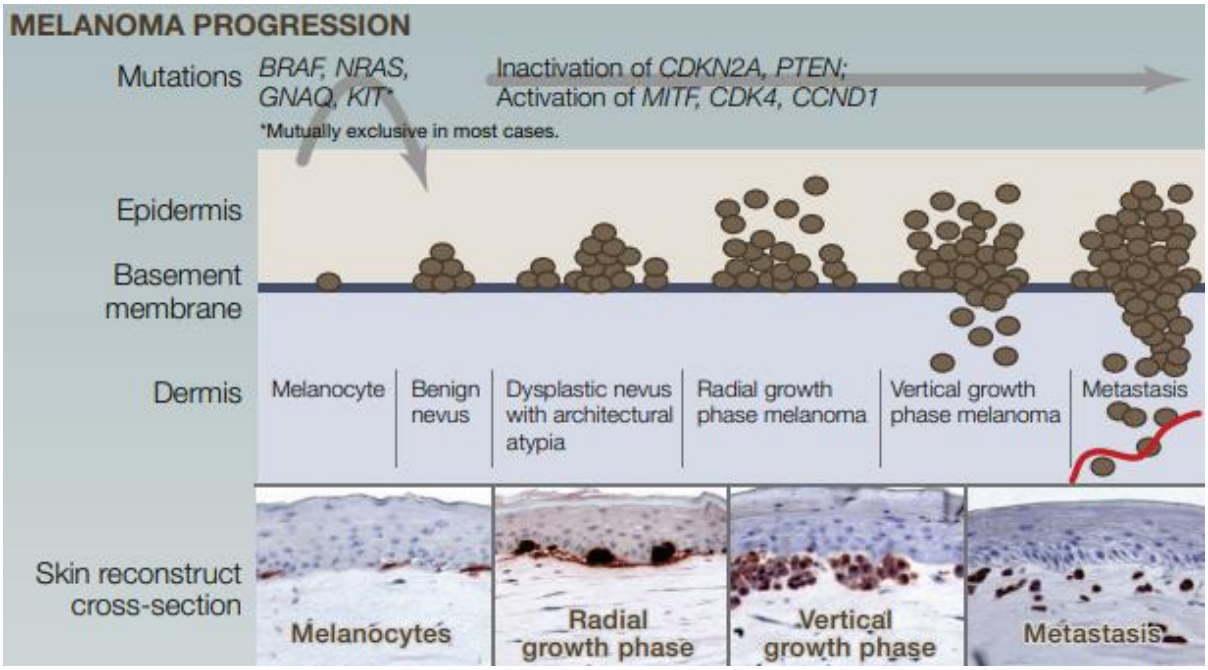

Figura 1 - Progressão do melanoma.
Fonte: Vultur and Herlyn (2013) [6].

A metástase é um processo que ocorre por meio de uma série de etapas progressivas (Figura 2). A partir de mutações em um único melanócito, ocorre a proliferação celular descontrolada, dando origem ao tumor primário. Os melanócitos transformados proliferam-se e passam pela transformação epitélio-mesenquimal, onde as células mudam a sua morfologia e seu padrão de expressão gênica. Nessa transformação, apresentam um fenótipo mesenquimal, perdendo a polaridade característica das células epiteliais, expressando N-caderina e vimentina e apresentam habilidade para migrar e invadir. Além disso, secretam proteinases, como as metaloproteinases de matriz, responsáveis pela degradação de componentes na matriz extracelular e favorecendo a invasão das células tumorais. Uma vez que se desprenderam do tumor primário, as células tumorais migram e invadem o estroma, rico em vasculatura, o que facilita o intravasamento das células na corrente sanguínea e na circulação linfática. Na corrente sanguínea, as células cancerosas podem se prender em leitos capilares estreitos, expressando receptores que se ligam a sítios de apoio à metástases, ou se ligando à plaquetas, as quais as protegem do sistema imune. A circulação das células cancerosas ocorre por meio do fluxo sanguíneo e por interações entre elas e órgãos secundários que irão colonizar [8]. As células cancerosas colonizam órgãos específicos devido à existência de nichos pré-metastáticos, ou seja, sítios de colonização “preferíveis”, tais como linfonodos, pulmão, fígado, osso e cérebro. Esses nichos pré-metastáticos são

formados antes da chegada das células tumorais e induzem um microambiente favorável à sobrevivência das células, com vasos sanguíneos, fatores de crescimento e citocinas, as quais contribuem para atrair as células tumorais para esse novo local. Caso sobrevivam aos processos de morte celular e não entrem em dormência, quando alcançam o sítio secundário extravasam da corrente sanguínea, aderem e colonizam o novo local [9]. Para proliferar no sítio secundário, as células cancerosas aliciam o ambiente local por liberarem substâncias pró-inflamatórias e proteinases que induzem as células vizinhas a liberarem fatores de crescimento [10].

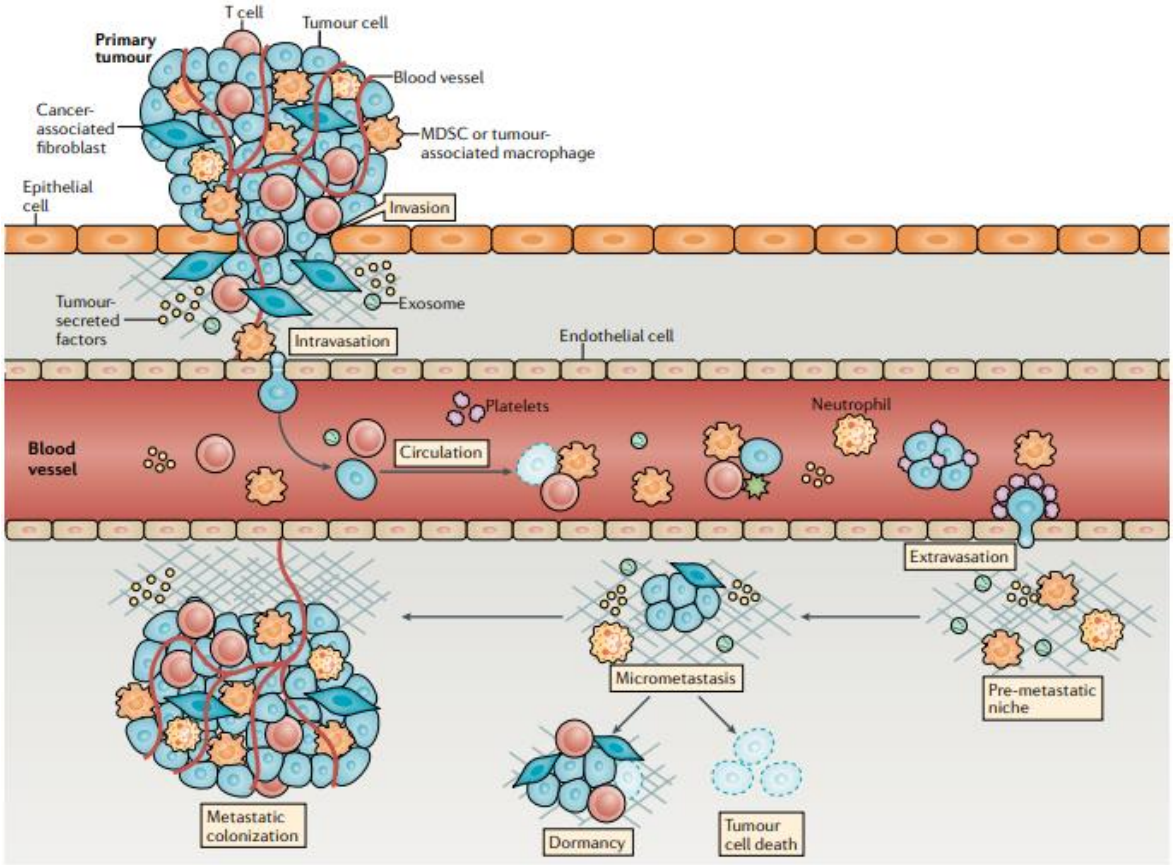

Figura 2 - Etapas do processo metastático de tumores sólidos.
Fonte: Anderson et al. (2019) [9].

As etapas do processo metastático são controladas por complexas vias de sinalização celular e são potenciais meios para a determinação de estratégias terapêuticas [11, 12]. As vias de sinalização mais envolvidas na progressão do melanoma são a MAPK e a PI3K-AKT (Figura 3). Tais vias estão relacionadas à progressão do ciclo celular, sobrevivência e angiogênese. Mutações em BRAF e NRAS levam à ativação contínua da via MAPK,

enquanto a deleção de PTEN inativa o controle da via PI3K/AKT. Já mutações em CDKN2A inativam as proteínas supressoras tumorais p16 e p14. Portanto, alterações em qualquer componente dessas vias podem alterar os fenótipos de proliferação, migração e sobrevivência celular [13, 14]. Além disso, a super ativação das vias MAPK e PI3K-AKT pode modificar a expressão de enzimas que degradam componentes da matriz extracelular, como as metaloproteinases. Com isso, pode favorecer a invasão e a propagação do melanoma, uma vez que uma etapa crucial para o desenvolvimento do melanoma metastático é a invasão de vasos sanguíneos e linfáticos, para a posterior colonização de outros órgãos [15]. Diversos compostos já apresentaram ação nas diferentes etapas metastáticas do melanoma, como compostos derivados do ácido cinâmico e inibidores de proteínas quinases SRPKs [11, 12, 16, 17].

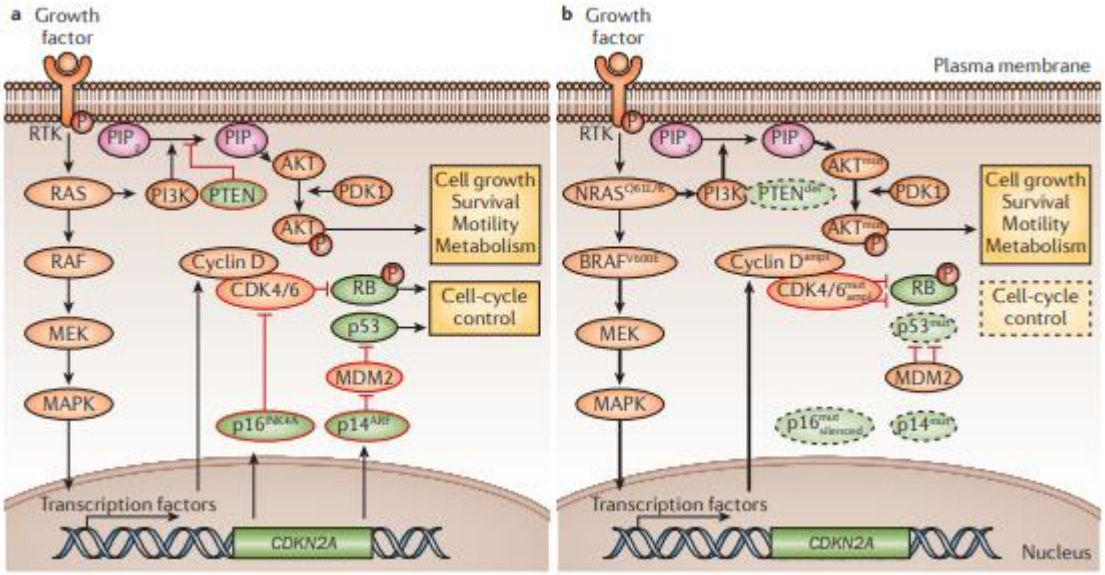

Figura 3 - Vias de sinalização no melanoma. Em (a) as vias de sinalização estão sob condições normais, e em (b) estão super ativadas no melanoma.
Fonte: Schadendorf et al. (2015) [7].

Quando detectado precocemente, o prognóstico dos pacientes com melanoma pode ser considerado bom. Porém, se diagnosticado tardiamente, o melanoma encontra-se em estágio de crescimento avançado, podendo acometer outros órgãos. Os estágios de crescimento do melanoma são descritos segundo o sistema da *American Joint Commission on Cancer Tumor–Node–Metastasis* (Figura 4). O estágio zero indica que a doença está confinada a epiderme, sendo chamada de melanoma *in situ*; o estágio um representa melanoma cutâneo localizado,

com menos de 1 mm de espessura e pode ou não ter ulceração. O estágio dois compreende lesões maiores, entre 1 e 4 mm de espessura com ulceração ou maior que 4 mm de profundidade, sem ulceração; o estágio três engloba o comprometimento de nódulos linfáticos, ou seja, o câncer se difunde para um ou mais linfonodos; e, por fim, o estágio quatro consiste na propagação metastática para outras partes do corpo [18]. Nos estágios zero e um, o melanoma pode ser tratado por excisão cirúrgica, enquanto que no estágio dois o melanoma é tratado por meio de excisão cirúrgica e com adjuvantes, como o interferon. Já no estágio três, é feita excisão cirúrgica com ampla margem de ressecção, além da terapia com adjuvantes. Caso o paciente não responda, inicia-se o tratamento com o creme imiquimod, radioterapia e quimioterapia. Já no estágio quatro, quando as células cancerosas invadem o sistema linfático e vascular e aderem ao novo sítio, o que torna o melanoma agressivo e potencialmente letal [3], o tratamento pode ser feito, por exemplo, com dacarbazine e temozolomide, individualmente ou em combinação com interleucina-2 e/ou interferon [19].

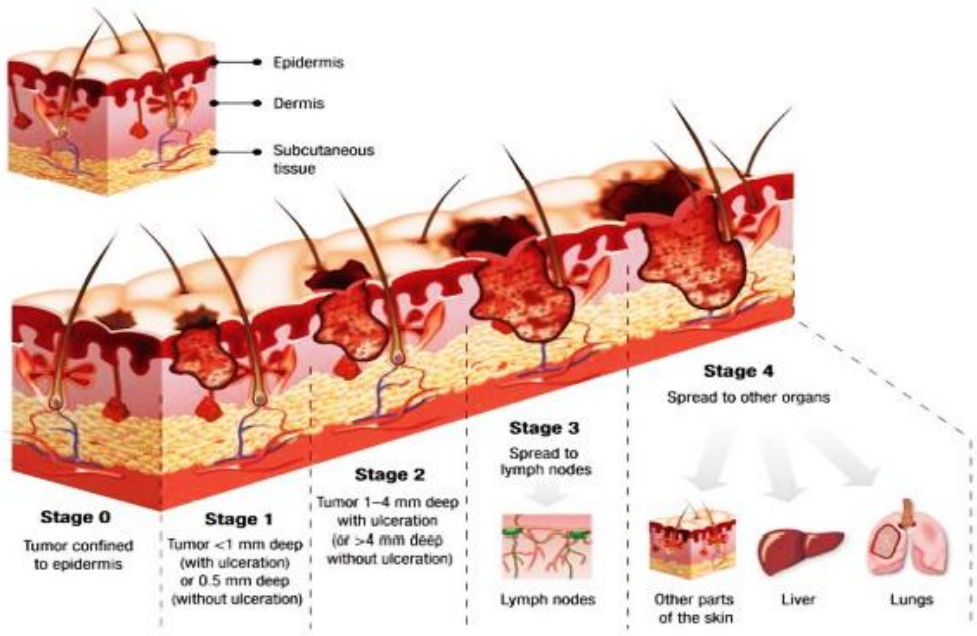

Figura 4 - Estágios do desenvolvimento do melanoma.
Fonte: Moqadam et al. (2018) [20].

As drogas antitumorais podem ser multifuncionais, por possuírem ação antimetastática e, ao mesmo tempo, antiproliferativa, por exemplo [21-25]. Outras drogas podem agir por meio de indução das células à apoptose ou por interromperem o ciclo celular de células tumorais [26-28]. A principal forma de quimioterapia para o melanoma inclui fármacos antineoplásicos, como a cisplatina e o 5-fluorouracil [29]. Contudo, o melanoma é

frequentemente refratário aos medicamentos anticâncer existentes e isso se deve à habilidade das células cancerosas de escaparem dos processos apoptóticos, ao acúmulo de mutações no decorrer do desenvolvimento do melanoma, à sua instabilidade genômica, além da ausência de mecanismos de manutenção/reparo do DNA nestas células [3, 30, 31]. A resistência do melanoma aos tratamentos é um processo multifatorial e é relacionado não apenas ao subtipo da neoplasia, ao genótipo do tumor e heterogeneidade, mas também às características de cada paciente [32].

Devido à resistência encontrada no melanoma para os tratamentos convencionais, aos vários efeitos colaterais relatados pelos pacientes, aos altos custos inerentes aos longos períodos de tratamento e à necessidade de drogas com melhor eficácia terapêutica, o desenvolvimento de novos fármacos é de suma importância [3, 29, 33-35]. Nesse contexto, produtos naturais e sintéticos destacam-se como fontes de diferentes compostos com potencial atividade antitumoral. Dentre esses compostos, o ácido cinâmico e seus derivados apresentam ação antitumoral e antimetastática promissora contra o câncer [11, 36-38].

2.2 Ácido cinâmico

Quimicamente denominado de ácido 3-fenil-2-propenoico, o ácido cinâmico consiste em um ácido aromático de ocorrência natural, sintetizado por organismos vivos a partir da fenilalanina e resultante do metabolismo secundário das plantas. Pertence ao grupo das auxinas, hormônios vegetais responsáveis por regular o crescimento e a diferenciação celular em plantas [36]. Sua principal fonte é a casca de canela (*Cinnamomum sp*), mas também pode ser encontrado em exsudatos de plantas como bálsamo [39, 40]. No entanto, a concentração do composto encontrada na natureza ainda é baixa, enquanto a quantidade do mesmo produzida por meio da síntese orgânica, pela desaminação da fenilalanina, é satisfatória para seu uso em escala [40].

O ácido cinâmico tem uma natureza cristalina, possui baixa solubidade em água e é solúvel em quase todos os solventes orgânicos [41]. A molécula do ácido cinâmico pode ser encontrada na natureza nas formas *cis* e *trans* (Figura 5), sendo normalmente encontrada na forma *trans* [36, 42]. Além disso, o ácido cinâmico pode ser encontrado tanto em sua forma livre, quanto na forma de ésteres e é considerado um composto de baixa toxicidade [40, 43].

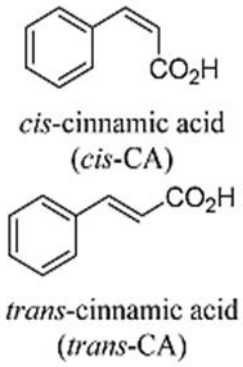

Figura 5 - Estrutura química do ácido cinâmico.
Fonte: Okuda et al. (2014) [42].

O ácido cinâmico já era utilizado desde os primórdios da civilização. Seu uso era atrelado a múltiplas ações terapêuticas, como antisséptica, inseticida e estimulante [40, 44]. Atualmente, sabe-se que o ácido cinâmico também pode exercer outras atividades biológicas, como antimicrobiana, antifúngica e antitumoral, até mesmo contra o melanoma [27, 36, 45-47]. No câncer seu mecanismo de ação é diverso, uma vez que pode interferir no ciclo celular [48], gerar danos irreversíveis ao DNA, induzindo morte celular por apoptose [27], pode agir no citoesqueleto, promovendo sua desorganização [27], e sobre a capacidade invasiva das células cancerosas, reduzindo-a [36]. Entretanto, apesar de induzir morte celular por apoptose, o efeito citotóxico do ácido cinâmico ainda é baixo [27].

Por meio de modificações em sua estrutura química é possível sintetizar novos compostos derivados do ácido cinâmico, os quais podem vir a ter maior eficácia antitumoral e antimetastática do que o mesmo. É possível realizar modificações estruturais em três locais reativos da estrutura do ácido cinâmico (Figura 6): no anel aromático, na cadeia lateral alifática e/ou no grupo carboxila, a fim de produzir diversas substâncias bioativas, com múltiplas ações mecanicistas e biológicas [40, 44].

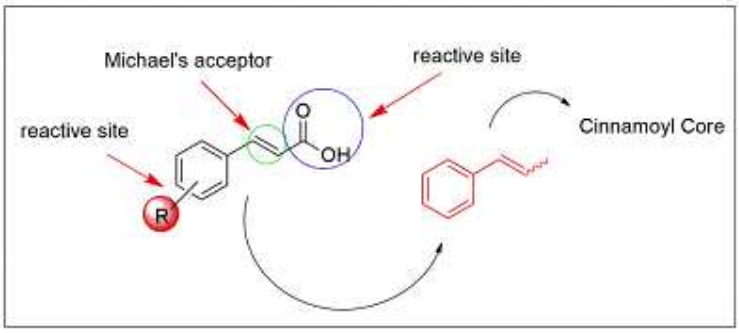

Figura 6 - Locais reativos na molécula do ácido cinâmico.
Fonte: França et al. (2021) [40], De et al. (2011) [44].

Portanto, o ácido cinâmico é considerado uma estrutura versátil e que pode ser utilizada como *scaffold* para o desenvolvimento de novos fármacos contra o câncer [43]. Desse modo, muitos compostos derivados do ácido cinâmico têm sido sintetizados com o núcleo cinamoil preservado [49].

2.3 Derivados do ácido cinâmico

Derivados do ácido cinâmico já foram relatados com diversas atividades biológicas, como antimicrobiana [50], antiparasítica [51], neurológica [52], antidiabética [53], antioxidante [54], anti-inflamatória [55] e antitumoral sobre diversos tipos de cânceres [49, 56, 57], até mesmo o melanoma [11, 58]. Nestes últimos trabalhos, os derivados do ácido cinâmico apresentaram atividade antiproliferativa e antimetastática contra o melanoma, ao reduzir a proliferação, migração, invasão, adesão e colonização celular.

Os efeitos biológicos dos derivados do ácido cinâmico são relacionados aos locais reativos na estrutura do ácido cinâmico, como a adição de grupos conjugados ao anel cinamoil, os quais contribuem gradativamente para a atividade inibitória de células neoplásicas, bem como a presença de grupos hidroxilas e halogênios, os quais possibilitam a interação dos compostos com proteínas relacionadas à progressão da metástase [56, 59]. Além disso, estudos mostraram que as moléculas mais promissoras que apresentam o núcleo cinamoil são aquelas que possuem funções éster e amida [40].

Ácidos cinâmicos podem ser utilizados como precursores para a síntese de importantes ésteres derivados do ácido cinâmico, também chamados de cinamatos. Tais ésteres podem ser encontrados em várias plantas e seu uso está correlacionado à indústria farmacêutica [43]. Por meio da reação de esterificação Steglich [60] entre o ácido *trans*-cinâmico e compostos hidroxilados é possível formar cinamatos que podem vir a ter atividade biológica superior ao ácido cinâmico [58, 61]. Além disso, cinamatos contendo porções 1,2,3-triazólicas também são interessantes compostos com significativa atividade biológica, até mesmo contra o câncer [11, 62]. Da mesma forma, existem amidas derivadas do ácido cinâmico, também chamadas de cinamidas, que possuem diferentes propriedades farmacológicas, como antidiabética, antiviral e anticâncer [41].

3. HIPÓTESE E OBJETIVOS

Baseado no presente exposto e na hipótese de que derivados do ácido cinâmico possuem atividade contra o melanoma, os objetivos desse estudo foram:

Objetivo Geral:

Avaliar o potencial antimelanoma de derivados do ácido cinâmico em modelo experimental *in vitro* de melanoma murino B16-F10.

Objetivos Específicos:

→ Capítulo 1

- Discorrer sobre a biologia do melanoma e as características e aplicações do ácido cinâmico, bem como de seus derivados.

→ Capítulo 2

- Discutir as estratégias desenvolvidas para teste e seleção de fármacos em linhagens celulares de melanoma por métodos *in silico*, *in vitro* e *in vivo*.

→ Capítulo 3

- Descrever a síntese de uma série de novas cinamidas e um bis cinamato contendo fragmento 1,2,3-triazólico;
- Avaliar a atividade antimelanoma dos compostos em células de melanoma murino B16-F10.

→ Capítulo 4

- Descrever a síntese de 17 ésteres de cinamato derivados do ácido cinâmico;
- Avaliar a atividade biológica dos compostos em células de melanoma murinho B16-F10.

4. REFERÊNCIAS

[1] Champine, M.; Kohlmann, W.; Leachman, S. A. Genetic Counseling and Testing for Hereditary Melanoma: An Updated Guide for Dermatologists. Hereditary Genetics. 2013; S2: 004.

[2] Lo, J. A. and Fisher, D. E. The melanoma revolution: from UV carcinogenesis to a new era in therapeutics. Science. 2014; 346(6212): 945–949.

[3] Gray-Schopfer, V.; Wellbrock, C.; Marais, R. Melanoma biology and new targeted therapy. Nature, 2007; 445.

[4] Sullivan, R. J., Fisher, D. E. Understanding the biology of melanoma and therapeutic implications. Hematol Oncol Clin North Am. 2014; 28(3): 437–453.

[5] Kawakami, A.; Fisher, D. E. The master role of microphthalmia-associated transcription factor in melanocyte and melanoma biology. Lab. Investig. 2017; 97: 649–656.

[6] Vultur, A.; Herlyn, M. SnapShot: Melanoma. Cancer Cell. 2013; 23: 706-706.e1.

[7] Schadendorf, D.; Fisher, D. E.; Garbe, C.; Gershenwald, J. E.; Grob, J.; Halpern, A.; Herlyn, M.; Marchetti, M. A.; McArthur, G.; Ribas, A.; Roesch, A.; Hauschild, A. Melanoma. Nat. Rev. Dis. Primers. 2015; 1: 1-20.

[8] Schroeder, A.; Heller, D. A.; Winslow, M. M.; Dahlman, J. E.; Pratt, G. W.; Langer, R.; Jacks, T.; Anderson, D. G. Treating metastatic cancer with nanotechnology. Nat. Rev. Cancer. 2012; 12: 39-50.

[9] Anderson, R. L.; Balasas, T.; Callaghan, J.; Coombes, R. C.; Evans, J.; Hall, J. A.; Kinrade, S.; Jones, D.; Jones, P. S.; Jones, R.; Marshall, J. F.; Panico, M. B.; Shaw, J. A.; Steeg, P. S.; Sullivan, M.; Tong, W.; Westwell, A. D.; Ritchie, J. W. A. A framework for the development of effective anti- metastatic agents. Nat. Rev. 2019; 16: 185-204.

[10] Joyce, J. A. and Pollard, J. W. Microenvironmental regulation of metastasis. Nat. Rev. Cancer. 2009; 9(4): 239–252.

[11] Lima, G. D. A.; Rodrigues, M. P.; Mendes, T. A. O.; Moreira, G. A.; Siqueira, R. P.; da Silva, A. M.; Vaz, B. G.; Fietto, J. L. R.; Bressan, G. C.; Machado-Neves, M.; Teixeira, R. R. Synthesis and antimetastatic activity evaluation of cinnamic acid derivatives containing 1,2,3-triazolic portions.Toxicol. *In Vitro*. 2018; 53: 1-9.

[12] Moreira, G. A.; Lima, G. D. A.; Siqueira, R. P.; Barros, M. V. A.; Adjanohoun, A. L. M.; Santos, V. C.; Barbosa, E. A. A.; Loterio, R. K.; Paiva, J. C.; Gonçalves, V. H. S.; Viol, L. C. S.; Marques-da-Silva, E. A.; Júnior, A. S.; Almeida, M. R.; Fietto, J. L. R.; Machado-Neves, M.; Ferreira, R. S.; Teixeira, R. R.; Bressa, G. C. Antimetastatic effect of the pharmacological inhibition of serine/arginine-rich protein kinases (SRPK) in murine melanoma. Toxicol. Appl. Pharmacol. 2018; 356: 214-223.

[13] Nikiforov, Y. E.; Nikiforova, M. N. Molecular genetics and diagnosis of thyroid cancer. Nat. Rev. Endocrinol. 2011; 7: 569–580.

[14] Yajima, I.; Kumasaka, M. Y.; Thang, N. D.; Goto, Y.; Takeda, K.; Yamanoshita, O.; Iida, M.; Ohgami, N.; Tamura, H.; Kawamoto, Y.; Kato, M. RAS/RAF/MEK/ERK and PI3K/PTEN/AKT Signaling in Malignant Melanoma Progression and Therapy. Dermatol. Res. Pract. 2012; 1-5.

[15] Guan, X. Cancer metastases: challenges and opportunities. Acta Pharmaceutica Sinica B. 2015; 5(5): 402–418.

[16] Wang, Z.; Wang, D.; Liu, L.; Guo, D.; Yuc, B.; Zhang, B.; Hanc, B.; Sun, X.; Zhenga, Q. Alteronol inhibits the invasion and metastasis of B16F10 and B16F1 melanoma cells *in vitro* and *in vivo*. Life Sci. 2014; 98: 31-38.

[17] Li, C.; Wang, Q.; Shen, S.; Wei, X.; Li, G. Oridonin inhibits migration, invasion, adhesion and TGF-β1-induced epithelial-mesenchymal transition of melanoma cells by inhibiting the activity of PI3K/Akt/GSK-3β signaling pathway. Oncol. Lett. 2018; 15: 1362-1372.

[18] Balch, C. M.; Gershenwald, J. E.; Soong, S.; Thompson, J. F.; Atkins, M. B.; Byrd, D. R.; Buzaid, A. C.; Cochran, A. J.; Coit, D. G.; Ding, S.; Eggermont, A. M.; Flaherty, K. T.; Gimotty, P. A.; Kirkwood, J. M.; McMasters, K. M.; Mihm Jr, M. C.; Morton, D. L.; Ross, M. I.; Sober, A. J.; Sondak, V. K. Final Version of 2009 AJCC Melanoma Staging and Classification. J. Clin. Oncol. 2009; 27(36): 6199-6206.

[19] Couto, G. K.; Segatto, N. V.; Oliveira, T. L.; Seixas, F. K.; Schachtschneider, K. M.; Collares, T. The Melding of Drug Screening Platforms for Melanoma. Front. Oncol. 2019; 9: 512.

[20] Moqadam, S. M.; Grewal, P. K.; Haeri, Z.; Ingledew, P. A.; Kohli, K.; Golnaraghi, F. Cancer detection based on electrical impedance spectroscopy: A clinical study. J. Electr. Bioimp. 2018; 9: 17-23.

[21] Reddy, N. D.; Shoja, M. H.; Biswas, S.; Nayak, P. G.; Kumar, N.; Rao, C. M. An appraisal of cinnamyl sulfonamide hydroxamate derivatives (HDAC inhibitors) for anti-cancer, anti-angiogenic and anti-metastatic activities in human cancer cells. Chemo-Bio Interact. 2016.

[22] Qi, G.; Chen, J.; Shi, C.; Wang, Y.; Mi, S.; Shao, W.; Yu, X.; Ma, Y.; Ling, J.; Huang, J. Cinnamic Acid (CINN) Induces Apoptosis and Proliferation in Human Nasopharyngeal Carcinoma Cells. Cell. Physiol. Biochem. 2016; 40: 589-596.

[23] Ling, Y.; Guo, J.; Yang, Q.; Zhu, P.; Miao, J.; Gao, W.; Peng, Y.; Yang, J.; Xu, K.; Xiong, B.; Liu, G.; Tao, J.; Luo, L.; Zhu, Q.; Zhang, Y. Development of novel β-carboline-based hydroxamate derivatives as HDAC inhibitors with antiproliferative and antimetastatic activities in human cancer cells. Eur. J. Med. Chem. 2018.

[24] Peng, X.; Wang, Z.; Liu, Y.; Peng, X.; Liu, Y.; Zhu, S.; Zhang, Z.; Qiu, Y.; Jin, M.; Wang, R.; Zhang, Q.; Kong, D. Oxyfadichalcone C inhibits melanoma A375 cell proliferation and metastasis via suppressing PI3K/Akt and MAPK/ERK pathways.Life Sci. 2017.

[25] Sinka, I.; Kiss, A.; Mernyák, E.; Wölfling, J.; Schneider, G.; Ocsovszki, I.; Kuo, C.Y.; Wang, H.; Zupkó, I. Antiproliferative and antimetastatic properties of 3-benzyloxy-16-hydroxymethylene-estradiol analogs against breast cancer cell lines. Eur. J. Pharm. Sci. 2018; 123: 362–370.

[26] Faião-Flores, F.; Coelho, P. R.; Arruda-Neto J. D. T.; Maria-Engler, S. S.; Tiago, M.; Capelozzi, V. L.; Giorgi, R. R.; Maria, D. A. Apoptosis through Bcl-2/Bax and cleaved caspase up-regulation in melanoma treated by boron neutron capture therapy. PLoS One. 2013; 8(3): e59639.

[27] Niero, E. L.; Machado-Santelli, G. M. Cinnamic acid induces apoptotic cell death and cytoskeleton disruption in human melanoma cells. J. Exp. Clin. Cancer Res. 2013; 32:31

[28] Baharara, J.; Amini, E.; Nikdel, N.; Salek-Abdollahi, F. The cytotoxicity of Dacarbazine potentiated by Sea Cucumber Saponin in resistant B16F10 melanoma cells through apoptosis induction. Avicenna J. Med. Biotechnol. 2016; 8(3):112-119.

[29] Mattia, G.; Puglisi, R.; Ascione, B.; Malorni, W.; Carè, A.; Matarrese, P. Cell death-based treatments of melanoma: conventional treatments and new therapeutic strategies. Cell Death Dis 2018; 9(2): 112.

[30] Shaffer, S. M.; Dunagin, M. C.; Torborg, S. R.; Torre, E. A.; Emert, B.; Krepler, C.; Beqiri, M.; Sproesser, K.; Brafford, P. A.; Xiao, M.; Eggan, E.; Anastopoulos, I. N.; Vargas-Garcia, C. A.; Singh, A.; Nathanson, K. L.; Herlyn, M.; Raj, A. Rare cell variability and drug-induced reprogramming as a mode of cancer drug resistance. Nature. 2017; 546(7658): 431–435.

[31] Hanahan, D.; Weinberg, R. A. Hallmarks of Cancer: The Next Generation. Cell. 2011; 144: 646-674.

[32] Dean, M.; Fojo, T.; Bates, S. Tumour stem cells and drug resistance. Nat. Rev. Cancer. 2005; 5(4):275-284.

[33] Vale, J.A., Lima, G.D.A., Almeida, A.A., Teixeira, R.R., Neves, M.M., 2020. Melanoma cell lines as a model for high-throughput drug screening, in: Watanabe, H.S. (Ed.), Horizons in cancer research. Nova Science Publishers, Nova York, pp. 85-145.

[34] American Cancer Society Treatments and side effects. Disponível em < https://www.cancer.org/treatment/treatments-and-side-effects.html>. Acesso em: 24 de jan. 2022.

[35] Garbe, C.; Terheyden, P.; Keilholz, U.; Kölbl, O.; Hauschild, A. Treatment of Melanoma. Dtsch Arztebl Int. 2008; 105(49): 845–51.

[36] Liu, L.; Hudgins, W. R.; Shack, S.; Yin, M. Q.; Samid, D. Cinnamic Acid: a natural product with potential use in cancer intervention. Int. J. Cancer. 1995; 62: 345-350.

[37] Yang, G.; Jiang, J.; Lu, W. Ferulic Acid exerts anti-angiogenic and anti-tumor activity by targeting fibroblast growth factor Receptor 1-Mediated angiogenesis. Int. J. Mol. Sci. 2015; 16:24011-24031.

[38] Park, H.; Cho, J.; Hong, S.; Kim, D.; Jung, H.; Kang, I.; Cho, Y. Whitening and anti-wrinkle activities of ferulic acid isolated from Tetragonia tetragonioides in B16F10 melanoma and CCD986sk fibroblast cells. J. Nat. Med. 2017.

[39] Hoskins, J. A. The Occurrence, Metabolism and Toxicity of Cinnamic Acid and Related Compounds. J. Appl. Toxicol. 1984; 4: 283-292.

[40] França, S. B.; Correia, P. R. S.; Castro, I. B. D.; Júnior, E. F. S.; Barros, M. E. S. B.; Lima, D. J. P. Synthesis, applications and Structure-Activity Relationship (SAR) of cinnamic acid derivatives: a review. Res. Soc. Dev. 2021; 10 (1): e28010111691.

[41] Gaikwad, N.; Nanduri, S.; Madhavi, Y. V. Cinnamamide: An insight into the pharmacological advances and structureeactivity relationships. Eur. J. Med. Chem. 2019; 181, 111561.

[42] Okuda, K.; Nishikawa, K.; Fukuda, H.; Fujii, Y.; Shindo, M. cis-Cinnamic Acid Selective Suppressors Distinct from Auxin Inhibitors. Chem. Pharm. Bull. 2014; 62(6): 600–607.

[43] Sharma, P. Cinnamic acid derivatives: A new chapter of various pharmacological activities. J. Chem. Pharm. Res. 2011; 3(2): 403-423.

[44] De, P.; Baltas, M.; Bedos-Belval, F. Cinnamic acid derivatives as anticancer agents - A review. Curr. Med. Chem. 2011; 18: 1672-1703.

[45] Laverty, G.; McCloskey, A. P.; Gorman, S. P.; Gilmore, B. F. Anti-biofilm activity of ultrashort cinnamic acid peptide derivatives against medical device-related pathogens. J. Pept. Sci. 2015; 21: 770-778.

[46] Tawata, S.; Taira, S.; Kobamoto, N.; Zhu, J.; Ishihara, M.; Toyama, S. Synthesis and Antifungal Activity of Cinnamic Acid Esters. Biosci. Biotech. Biochem. 1996; 60(5): 909-910.

[47] Ekmekcioglu, C.; Feyertag, J.; Marktl, W. Cinnamic acid inhibits proliferation and modulates brush border membrane enzyme activities in Caco-2 cells. Cancer Lett. 1998; 128(2): 137-144.

[48] Sova, M.; Zizac, Z.; Stankovic, J. A. A.; Prijatelj, M.; Turk, S.; Jurani, Z. D.; Mlinari -Rascan, I.; Gobec, S. Cinnamic Acid derivatives induce cell cycle arrest in carcinoma cell lines. J. Med. Chem. 2013; 9: 633-641.

[49] Pontiki, E.; Hadjipavlou-Litina, D.; Litinas, K.; Geromichalos, G. Novel Cinnamic Acid derivatives as antioxidant and anticancer agents: design, synthesis and modeling studies. Molecules. 2014; 19: 9655-9674.

[50] Malheiro, J. F.; Maillard, J.-Y.; Borges, F.; Simões, M. Evaluation of cinnamaldehyde and cinnamic acid derivatives in microbial growth control. Int. Biodeterior. Biodegrad. 2018; 141: 71–78.

[51] Chen et al., 2018 Chen, D-D.; Zhang, B-Y.; Liu, X-X.; Li, X-Q; Yang, X-J.; Zhou, L. Bioactivity and structure–activity relationship of cinnamic acid derivatives and its heteroaromatic ring analogues as potential high-efficient acaricides against Psoroptes cuniculi. Bioorganic Med. Chem. Lett. 2018; 28: 1149–1153.

[52] Lan, J-S.; Hou, J-W.; Liu, Y.; Ding, Y.; Zhang, Y.; Li, L.; Zhang, T. Design, synthesis and evaluation of novel cinnamic acid derivatives bearing N-benzyl pyridinium moiety as multifunctional cholinesterase inhibitors for Alzheimer's disease. J. Enzyme Inhib. Med. Chem. 2017; 32 (1): 776–788.

[53] Xu, X-T.; Deng, X-Y.; Chen, J.; Liang, Q-M.; Zhang, K.; Li, D-L.; Wu, P-P.; Zheng, X.; Zhou, R-P.; Jiang, Z-Y.; Ma, A-J.; Chen, W-H.; Wang, S-H. Synthesis and biological

evaluation of coumarin derivatives as aglucosidase inhibitors. Eur. J. Med. Chem. 2020; 189: 112013.

[54] Mazzone, G.; Russo, N.; Toscano, M. Antioxidant properties comparative study of natural hydroxycinnamic acids and structurally modified derivatives: Computational insights. Computat. Theor. Chem. 2016; 1077: 39-47.

[55] Taofiq et al., 2019 Taofiq, O.; Heleno, S. A.; Calhelha, R. C.; Fernandes, I. P.; Alves, M. J.; Barros, L.; González-Paramás, A. M.; Ferreira, I. C. F. R.; Barreiro, M. F. Phenolic acids, cinnamic acid, and ergosterol as cosmeceutical ingredients: Stabilization by microencapsulation to ensure sustained bioactivity. Microchem. J. 2019; 147: 469–477.

[56] Tsai, C. M.; Yen, G. C.; Sun, F. M.; Yang, S. F.; Weng, C. J. Assessment of the anti-invasion potential and mechanism of select cinnamic acid derivatives on human lung adenocarcinoma cells. Mol. Pharm. 2013; 10(5):1890-900.

[57] Rathee, D.; Lather, V.; Grewal, A. S.; Dureja, H. Targeting matrix metalloproteinases with novel diazepine substituted cinnamic acid derivatives: design, synthesis, *in vitro* and *in silico* studies. Chem. Cent. J. 2018; 12: 41.

[58] Santos, F. S.; Vale, J. A.; Santos, L. S.; Gontijo, T. B.; Lima, G. D. A.; Oliveira, L. L.; Machado-Neves, M.; Teixeira, R. R.; Freitas, R. P. Synthesis of Novel Cinnamides and a Bis Cinnamate Bearing 1,2,3-Triazole Functionalities with Antiproliferative and Antimetastatic Activities on Melanoma Cells. J. Braz. Chem. Soc. 2021; 32(12): 2174-2185.

[59] Melo, E. B. A QSAR Study of Matrix Metalloproteinases Type 2 (MMP-2) Inhibitors with Cinnamoyl Pyrrolidine Derivatives. Sci Pharm. 2012; 80: 265–281.

[60] Sova, M.; Perdih, A.; Kotnik, M.; Kristan, K.; Rižner, T. L.; Solmajer, T.; Gobec, S. Flavonoids and cinnamic acid esters as inhibitors of fungal 17β-hydroxysteroid dehydrogenase: A synthesis QSAR and modelling study. Bioorganic Med. Chem. 2006; 14: 7404–7418.

[61] Vale, J. A.; Rodrigues, M. P.; Lima, A. M. A.; Santiago, S. S.; Lima, G. D. A.; Almeida, A. A.; Oliveira, L. L.; Bressan, G. C.; Teixeira, R. R.; Machado-Neves, M. Synthesis of cinnamic acid ester derivatives with antiproliferative and antimetastatic activities on murine melanoma cells. Biomed. Pharmacother. 2022; 148: 112689.

[62] Dheer, D.; Singh, V.; Shankar, R. Medicinal attributes of 1,2,3-triazoles: Current developments. Bioorg. Chem. 2017; 71: 30–54.

CAPÍTULO 2 – CAPÍTULO DE LIVRO

Melanoma Cell Lines as a Model for High-throughput Drug Screening

Juliana Alves do Vale[1],
Graziela Domingues de Almeida Lima[1], Alisson Andrade Almeida[2],
Róbson Ricardo Teixeira[3] and Mariana Machado Neves[1]

[1]General Biology Department, Federal University of Viçosa, Viçosa,
Minas Gerais State, Brazil
[2]Biochemistry and Molecular Biology Department, Federal University of Viçosa, Viçosa,
Minas Gerais State, Brazil
[3]Chemistry Department, Federal University of Viçosa, Viçosa,
Minas Gerais State, Brazil

Publicado: Horizons in Cancer Research. 1ed.New York: Nova Science Publishers, 2020, v. 77, p. 85-145

ABSTRACT

Malignant melanoma is the most aggressive form of skin cancer. The high incidence and mortality rates of this disease are related to its strong ability to metastasize. Several treatments exist for patients with metastatic melanoma; however, the disease is refractory to most systemic therapies, which negatively impacts the prognosis of patients. Therefore, there is a need to search for new drugs with antimelanoma activity. In this context, melanoma cell lines are an important model for high-throughput drug screening. This approach permits a wide range of tests using molecules with potential activity against melanoma. After the selection of promising drugs by *in vitro* assays, *in vivo* studies can be performed to verify their efficacy and safety. Alternatively, *in silico* tests may contribute to the selection of the most promising compounds during drug discovery, as well as for the optimization of existing molecules. This chapter aims to review the strategies used to screen potential antimelanoma drugs, especially those involved in evaluating drugs in cancer cell lines, *in vitro* and *in vivo*, as well as *in silico* tests used for drug selection.

Keywords: cancer, computational methods, drug leads, antimelanoma

1. INTRODUCTION

Melanoma is a malignancy that originates from the growth out of control of melanocytes in clear skin without precursor lesions [1-3]. Melanocytes are neural crest-derived cells responsible for producing melanin [4]. They are located in several parts of the body, mainly in the bottom layer of the epidermis, in the middle layer of the eye, and in mucosal (e.g., vagina, rectum, and conjunctiva), subungual, and acral sites [5, 6]. Melanomas can occur on the body at different locations via several etiologies [6-8]. Cutaneous melanoma is the most common melanoma and the most aggressive type of skin cancer. This is due to the metastatic phenotype of the melanocytes constituting the tumor, which promotes rapid and aggressive metastases, and resistance to current therapeutic strategies [9, 10].

Several risk factors are associated with susceptibility to cutaneous melanoma, inclusing genetic mutations, excessive exposure to ultraviolet radiation, severe sunburn, outdoor training, advanced age, and sex [8]. Epidemiological studies have shown that the incidence of melanoma is increasing worldwide, mainly in men aged > 65 years [11-13]. There have been an estimated 100,350 new cases of melanoma to the year of 2020 in the United States, with 6,850 deaths, and an estimated 8,450 new cases in Brazil [13, 14]. Despite the lower incidence of melanoma globally than that of other cutaneous malignancies, it accounts for the highest number of deaths due to skin cancer. For example, the prognosis of patients 5 years after tumor detection and with treatment is poor. Taken together, these observations highlight the severity of this disease [15-18]. Thus, the diagnosis and treatment of patients with cutaneous melanoma in the early stages are crucial for achieving optimal outcomes.

The management and treatment of patients with melanoma remain challenging. The standard treatment for patients with cutaneous melanoma is surgical excision, which remains the best therapeutic option [17, 19]. Chemotherapy has subsequently become the mainstay of treatment for patients with advanced-stage melanoma. However, neither treatment has been shown to significantly increase the overall survival rate. This is because the rate of cutaneous melanoma recurrence is high, due to its strong metastatic ability and resistance to available drugs. The latter is related to complex cell signaling pathways (e.g., RAS-RAF-MEK-ERK pathway) that modulate the proliferation of tumor cells and their ability to escape from apoptotic processes [20-24].

Targeted molecular therapy and immunotherapy are promising candidates with potential to overcome the challenges associated with standard melanoma treatments [10, 19,

25]. Significant efforts have been made to identify and develop new drugs to improve therapeutic strategies and prognosis for patients with this cancer [20, 24, 26, 27]. Within this framework, melanoma cell lines are an interesting model for use in drug screening. The ability of these cell lines to mimic the tumor microenvironment underlies their clinical relevance, providing a rich source of biological material for experimental purposes [28]. Moreover, under adequate conditions, melanoma cell lines preserve many features of the original tissue, which makes the results of studies more reliable [29]. In this chapter, the strategies developed for drug testing and selection on melanoma cell lines by *in silico* methods, and *in vitro* and *in vivo* studies, have been discussed.

2. MELANOMA TREATMENT AND THE MAIN TARGETS OF SIGNALING PATHWAY

Several small-molecule drugs currently used for the treatment of melanoma are listed by the National Cancer Institute (NCI) (Table 1) [30]. Other small-molecule drug alternatives have been reported for the treatment of melanoma [31-33]. Importantly, these new drugs have passed through required preclinical and clinical trials before being critically reviewed by regulatory agencies such as the Food and Drug Administration (FDA, United States). Drugs can only be commercialized after all these steps [34].

Most of the approved drugs used for the treatment of melanoma are BRAF [35] or MEK1 and MEK2 [36] kinase inhibitors (Table 1). These kinases are an integral components of the RAS-RAF-MEK-ERK (mitogen-activated protein kinase) signal transduction pathway, which regulates cellular growth, proliferation, differentiation, and survival in response to extracellular signals, including growth factors, cytokines, and hormones. Approximately 50% of patients with metastatic melanoma have mutations in BRAF, one of three RAF family members, and over 95% of these mutations are in BRAF exon 15 at V600. This mutation results in a valine to glutamic acid substitution at codon 600. The most common V600 mutations are V600E and V600K, accounting for 66–91% and 7–30% of all BRAF V600 mutations, respectively [53-57]. These mutations stimulate cells to grow and proliferate quickly. Since these mutations are harbored by many patients with melanoma, they have been explored for the development of targeted compounds capable of slowing or stopping cancer cell growth. These compounds include dabrafenib, vemurafenib, encorafenib, and cobimetinib, which are usually used for the treatment of melanoma in combinations [58]. MEK1 and MEK2 are closely related, dual-specificity tyrosine/threonine protein kinases. The

combination of a BRAF- and a MEK inhibitor can lead to enhanced efficacy and reduced toxicity.

Overall, the compounds shown in Table 1 are aromatic. Additionally, amide (-NHCO-) and sulfonamide (-SO_2NH-) groups are predominant in their structures. Another important structural feature in most of these compounds is the presence of halogen atoms. Still, the majority of those compounds exerts their therapeutic effect by acting on specific molecules, and is thus considered to be targeted therapies. Typically, these molecular targets include proteins, the expression or overexpression of which plays a role in the development of several cancers, including melanoma.

During the past few decades, several potential therapeutic targets in melanoma have been discovered [58] and explored for the development of new chemotherapeutic agents. For example, imatinib and dasatinib act on one of these targets, the c-KIT protein (Table 2) [59]. c-KIT is a growth factor receptor in epidermal melanocytes and plays an essential role in the differentiation and migration of melanocytic cells during embryonic development. Moreover, the compounds shown in Table 2 have already been used for the treatment of other cancers and have demonstrated beneficial results in melanoma [59].

Immunotherapies have been used besides to small drugs-molecules (Table 3). In terms of the development of alternative treatments for melanoma, one important point deserves mention. Nature is a formidable reservoir of compounds that can be explored for the development of new therapeutic agents against cancer [70, 71]. Newman and Cragg (2016) reported that among all anticancer drugs approved from 1981 to 2014, 83% were natural products *per se*, were based on natural products, or mimicked natural products [72]. In this context, a review by Chinembiri and collaborators (2014) described natural products with antimelanoma activity [73]. Their structures are presented in Figure 1, and specific details concerning the antimelanoma effects of these compounds can be found in reference [73].

Although useful, conventional treatments are associated with numerous side effects and are unsatisfactory, as they do not result in the total eradication of the tumor [10]; therefore, there is an urgent need to screen new drugs with therapeutic potential that are also safe.

Table 1 - Compounds used in the chemotherapy of melanoma

Chemical Structure	Name	Brand Names	Synonims/Code Names	Comments	References
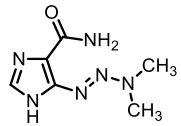	Dacarbazine	Asercit Dacatic Deticene Detimedac Fauldetic	Biocarbazine Dacarbazina Dacarbazina Almirall Dacarbazine - DTIC Dakarbazin Dimethyl (triazeno) imidazolecarboxamide Dimethyl Triazeno Imidazol Carboxamide Dimethyl Triazeno Imidazole Carboxamide Imidazole Carboxamide Imidazole Carboxamide Dimethyltriazeno	Dacarbazine is an imidazole derivative possessing a carboxamide and a triezenyl groups. It is a compound used for the treatment of metastatic melanoma and Hodgkin´s lymphoma (Hodgkin´s diseases). It has been used for more than 30 years as a standard drug for the chemotherapy treatment of metastic melanoma. However, the patient response for the administration of dacarbazine alone is low. For this reason, this drug is used in combination with other cancer drugs. Dacarbazine is an alkylating agent. After activation in the liver, it methylates nucleic acids, producing DNA damage leading to growth arrest and cell death. Dacarbazine is administered by the intravenous route.	[30], [37], [38], [39]
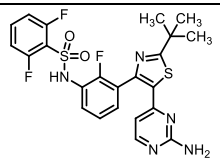	Dabrafenib	Tafinlar	GSK-2118436	This benzosulphonamide, which also presents in its structure a thiazole and an amynopiridine rings, is a potent, selective, and efficacious inhibitor of B-RAF V600E. In 2013, the Food and Drug Administration (FDA) approved dabrafenib mesylate to be used alone or in combination with trametinib for the treatment of melanoma cancer in: i) patients who have had surgery to remove cancer that has spread to the lymph nodes; ii) patients whose cancer cannot be removed by surgery or has metastasized.	[30], [40], [41], [42], [43]
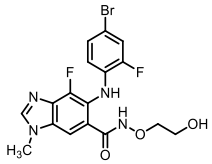	Binimetinib	Mektovi	ARRY-162 ARRY-438162 MEK162	Binimetinib is a benzimidazol derivative approved by FDA in 2018. It is a reversible inhibitor of the kinase activity of mitogen-activated extracellular signal-regulated kinase MEK1 and MEK2. It is an orally administered drug used in combination with encorafenib for the treatment of adult patients with with unresectable or metastatic melanoma with a BRAF V600 mutation.	[30], [44], [45]

Table 1 - (Continued)

Chemical Structure	Name	Brand Names	Synonims/Code Names	Comments	References
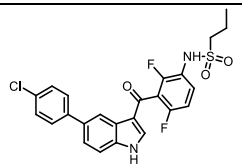	Vemurafenib	Zelboraf	BRAF(V600E) kinase inhibitor RO5185426, PLX4032, RG7204, RO5185426	This oral drug is another inhibitor of BRAF kinase and it was approved by FDA in 2011. It was the first small-drug molecule approved as serine/threonine kinase BRAF inhibitor. It is approved for the treatment of patients with unresectable or metastatic melanoma with BRAF V600E mutation.	[30], [46], [47]
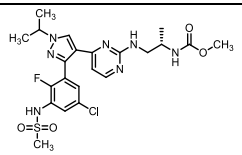	Encorafenib	Braftovi	LGX818	Alike other BRAF kinase inhibitors, encorafenib is a chiral benzenosufonamide. On June 27, 2018, the Food and Drug Administration approved encorafenib and binimetinib in combination for patients with unresectable or metastatic melanoma with a BRAF V600E or V600K mutation.	[30], [48], [49], [50], [51]
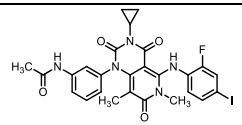	Trametinib	Mekinist	GSK1120212 JTP-74057 TMT212	This polifunctionalized acetamide was approved to be used in combination with drabrafenib for the treatment of melanomas. It inhibits MEK1 and MEK2.	[30], [49], [52]
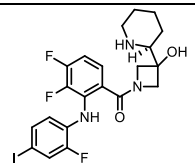	Cobimetinib	Cotellic	GDC-0973, XL-518	Cobimetinib, an amide bearing a chiral center, is approved to be used along with vemurafenib for the treatment of melanoma.	[30], [49]

Table 2 - Compounds that target c-Kit protein

Chemical Structure	Name	Comments
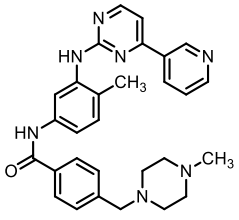	Imatinib	This amide was tested in phase II trials in patients with melanoma: First trial – it had the participation of patients with metastatic melanomas that expressed at least one protein tyrosine kinase [c-KIT, platelet-derived growth factor receptors (PDGFRs), c-abl, or abl-related gene]. It was observed response in only 1 patient, who had the highest level of c-KIT expression. It should be mentioned that c-KIT mutations were not required prior to entry in this trial. Second trial – It had the participation of 28 patients with c-KIT mutations and amplifications with advanced unresectable melanoma arising from acral, mucosal, and chronic sun-induced skin damage were orally administered 400 mg imatinib mesylate twice daily in 6-week cycles until disease progression or unacceptable toxicity.
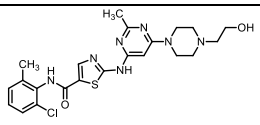	Dasatinib	During the 45th ASCO meeting in 2009, the phase II trial results were presented, showing that daily treatment with dasatinib has modest activity in patients with melanoma. Accrual is almost complete. Toxicity is frequent; therefore, alternate schedules to allow breaks in dosing might be better and should be evaluated.

3. DRUG SCREENING

Different approaches may be used for the discovery and development of new drugs for melanoma. Among them, drug screening is a relevant tool for the discovery of substances with potential biological activities. Previously, screening has been conducted using classical strategies based on the forward pharmacology approach. While animals were tested prior to *in vitro* experiments, *in vitro* assays were commonly used for mechanistic studies. Although this approach was effective at that time, it was challenging and time-consuming [74-76]. In addition, resistance to antimelanoma therapies made this approach unsuitable [15, 26].

Over the past decades, the advent of modern molecular biology has qualified reverse pharmacology as a new strategy for drug screening. This begins with the *in silico* or *in vitro* screening of compound libraries against predetermined protein targets followed by validation using *in vivo* models [76-80]. Strategies for identifying potential new therapeutic targets may follow two approaches. The first involves the use of high-throughput screening based on proteomics, metabolomics, and transcriptomics methods [81-85]. The second involves the identification of new molecules with biological activity on protein targets from well-known signaling pathways, such as BRAF inhibitors in melanoma [79, 86-89]. *In silico* or *in vitro*

high-throughput screening of compound libraries may be validated by *in vivo* models [76-80, 88, 90].

Table 3 - FDA approved immunotherapies

Agent	Names	Comments	References
Ipilimumab	Yervoy (brand name), MDX-010	It is a monoclonal antibody that acts by binding to the protein CTLA-4 protein which, in turn, is found in T cells. Ipilimumab may block CTLA-4 and help the immune system destroy cancer cells. It is used: • as adjuvant therapy in patients with melanoma in the skin and lymph nodes who have already had surgery; • in adults and children 12 years and older whose disease cannot be removed by surgery or has metastasized (spread to other parts of the body). Sometimes, ipilimumab is used in combination with nivolumab	[30], [60], [61], [62]
Nivolumab	Opdivo or Opdivo Injection (brand names)	This monoclonal antibody binds to a protein name PD-1 which is also found in T cells. The binding of nivolumab to PD-1 may block the action of this protein and help immunosystem to kill cancer cells.	[30], [61], [63]
Pembrolizumab	Keytruda (brand name)	It is another type of monoclonal antibody that binds do PD-1 protein.	[30], [64]
Talimogene Laherparepvec	IMLYGIC or T-Vec (brand names)	Talimogene laherparepvec is made with a form of the herpesvirus that has been changed in the laboratory to infect and break down cancer cells without harming normal cells. It may also help the immune system kill cancer cells. Talimogene laherparepvec is injected directly into tumors in the skin and lymph nodes.	[30], [65]
INα2b	Intron A (brand name)	Interferon alfa-2b is a non-glycosilated recombinant form of the protein interferon alfa-2. Interferon alfa-2b presents antiviral and antineoplastic activities	[30], [66]
Pegylated INα2b	Peginterferon Alfa-2b, Sylatron (brand name), Peg-Intron (brand name)	Pegylated INα2b corresponds to the conjugated interferon alfa-2b with monomethoxy polyethylene glycol (PEG). Peginterferon alfa-2b was approved in March 2011 for adjuvant treatment in node-positive melanoma following definitive surgical resection.	[30], [67]
Aldesleukin (interleukin-2; IL-2)	Proleukin (brand name)	Aldesleukin (interleukin-2 [IL-2]) is a recombinant product produced by a genetically engineered *E. coli* strain that has been used for the treatment of melanoma that has metastasized.	[30], [68], [69]

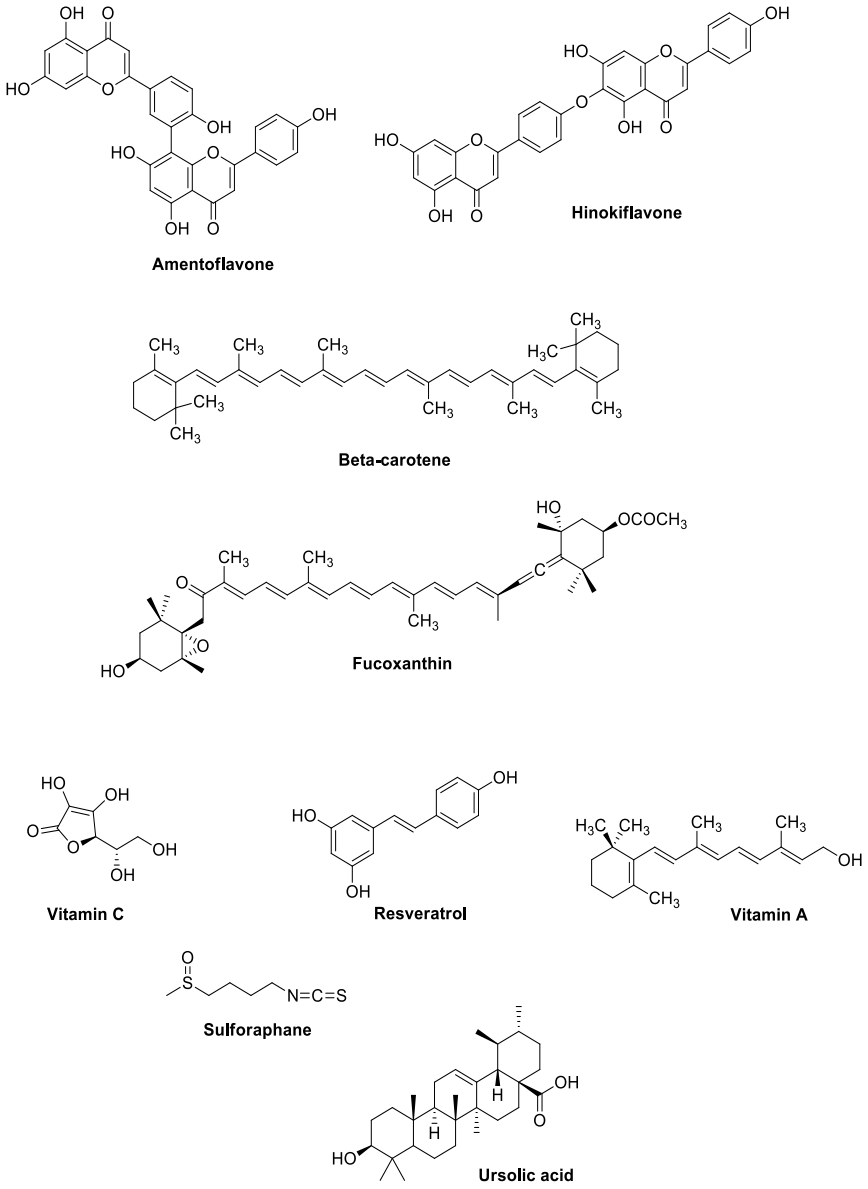

Figure 1 - Selected chemical structures of natural products, described in the review of Chinembiri and co-authors, presenting antimelanoma effects.

3.1 Virtual High-Throughput Screening

Virtual screening is an *in silico* technique that is complementary to the high-throughput screening used in large-scale drug discovery. This approach is based on the search of virtual libraries or databases of small molecules (Table 4) to identify structures most likely to bind a target of interest [91-93]. Virtual screening methods can be divided into two approaches: the first uses structure-based virtual screening (SBVS), while the second uses ligand-based virtual screening (LBVS). SBVS uses computational programs to dock ligands into the target protein active site. Binding affinities of the ligands to the target protein are then

estimated [24, 94, 95]. The LBVS, in turn, is based on a similarity and substructure search, quantitative structure-activity relationships, and mainly pharmacophore mapping (i.e., the region of the molecule that binds to its receptor) [94, 96, 97].

However, the main goal of virtual high-throughput screening (VHTS) is to identify an adequate number of substances for use as starting scaffolds for the development of new drugs, rather than identifying all possible compounds in databases. The main limiting factors of this approach are the occurrence of false positives and the requirement for infrastructure to mitigate this problem. Nonetheless, it is still considered the method of choice by pharmaceutical companies [91]. Compounds identified using starting scaffolds for the development of new antimelanoma drugs are listed in Table 5. Several *in silico* tools have been used to investigate different targets in melanoma, such as BRAF and TRAF6 inhibitors, and proteins involved in metalloproteinases dynamics [88, 90, 97].

3.2 Cell-Based High-Throughput Screening

Melanoma targets can also be assessed by cell-based high-throughput screening, which combines both VHTS and cell-based assays (Table 6). Cell-based screening assays are of interest, particularly for the identification of new antimelanoma drugs, because they can identify targets in a cell signaling pathway of interest within the physiological environment of a tumor cell, with interaction networks (e.g., cell-to-cell communication and cell-to-matrix interaction). Thus, this approach has been considered a more physiological alternative to assays involving isolated biochemical reactions or computational simulations [100, 101]. Moreover, the use of cell-based assays in combination with other methods, such as robotic platforms, high-performance equipment, and 384-, 1536-, and 3456-well plate formats, permits the large-scale screening of antimelanoma substances from compound libraries [34, 79, 80, 86, 98]. Researchers have evaluated many compounds *in vitro* following their identification from databases of substances for high-throughput screening (Table 6). In addition, all studies used melanoma cell lines, and in some cases, *in vivo* approaches were used. Another promising strategy is the integration of different approaches: for example, a workflow that integrates the compound library synthesized by the researchers, cell-based screening, and computational tools for molecules validation (Table 7).

Thus, associating *in silico* studies with cell-based assays is important to accelerate the selection of promising compounds. This association substantially improves the knowledge of these compounds and their potential effects under physiological conditions. In this regard,

integrative approaches based on *in vitro* and *in vivo* assays are essential to investigative identified drugs with potential antimelanoma activity. In the next section, we will review methods that use melanoma cell lines to evaluate potential drug candidates for antimelanoma treatment.

Table 4 - List of databases of molecules and compounds for high-throughput screening

Library	**Website**	**Compound number**
ZINC	http://zinc.docking.org/	More than 230 million
PubChem	https://pubchem.ncbi.nlm.nih.gov/	102,703,829
ChemSpider	http://www.chemspider.com/	More than 82 million
Enamine	http://www.enamine.net/	2,701,170
ChEMBL	https://www.ebi.ac.uk/chembl/	1,961,462
ChemDiv	http://www.chemdiv.com/products/screening-libraries/	More than 1,5 million
ChemBridge	https://www.chembridge.com/screening_libraries/	1.3 million
Life Chemicals	http://www.lifechemicals.com/	1 million
BindingDB	https://www.bindingdb.org/bind/index.jsp	815,305
Specs	http://www.specs.net/	500,000
SelleckChem	https://www.selleckchem.com/screening/express-pick-library-premium-version.html	99,040
Maybridge	http://www.maybridge.com	53,000
DrugBank	http://www.drugbank.ca/	13,574
NPACT	https://ncats.nih.gov/preclinical/core/compound/npact	11,000
GRAC	http://www.guidetopharmacology.org/about.jsp	10,053
MedChemExpress	https://www.medchemexpress.com/screening-libraries.html	10,000
Spectrum Collection	http://www.msdiscovery.com/spectrum.html	2,560
Prestwick	http://www.prestwickchemical.com/libraries-screening-lib-pcl.html	1,520
LOPAC	https://www.sigmaaldrich.com/life-science/cell-biology/bioactive-small-molecules.html	1,280
Tocris	https://www.tocris.com/product-type/tocriscreen-compound-libraries-and-toolboxes	1,280

Table 5- Studies that used an approach of molecule library-based screening using *In Silico* tools

Melanoma target studied	**Virtual Screening-based screening**	***In silico* tool**	**Other assays/techniques performed**	**References**
Metalloproteinase inducer (Fyn/CD147)	Molecule database (PubChem and ZINC databases).	• Virtual screening • Pharmacophores analysis • Molecular docking • Molecular modeling • Analysis performed using Schrodinger system.	• Cell proliferation (Human: SK-Mel-5, SK-Mel-28) • Immunoblotting • Kinase assay • Antimetastatic assays (wound healing; invasion) • *In vivo*/ xenografts tumor	[97]
BRAF(V600E)	Molecule database (TCM Database @Taiwan databatse).	• Virtual screening • Homology modeling • Quantitative structure-activity relationship (QSAR) • Molecular dynamics (GROningen MAchine)	Not applicable	[88]
TRAF6 inhibitors	Molecule database (ZINC database).	• Virtual screening (GOLD 5.2 package) • ADME (admetSAR) • Molecular docking (PatchDock) • Molecular dynamics (Discovery Studio 2.5 software package; GROMACS; CHARMm force-field; LINCS algorithms)	Not applicable	[90]
Antiproliferative activity	Molecule database (University of Cincinnati Drug Discovery Center Compound Library)	• Connectivity-based search (citegic Pipeline Pilot from Accelerys) • Pharmacophores analysis (Schrodinger system)	• Cell viability (Human: A375; mouse: B16-F1)	[94]

Table 6 - Studies that used an approach of molecule library-based screening and tested using cell-based high-throughput screening

Melanoma target studied	Library	Number of compounds	Basic infrastructure to cell-based screening	Melanoma cell line	Other biologic assays performed	Reference
BRAF(V600E) and BCL2 family	SelleckChem Bioactive Compound Library	2,123 molecules	• Microplate reader; 384-well	Human: A-375, WM88, WM3311 and WM3743	• Cell viability • Flow cytometry • Viral vector tools • Immunoblotting • Immunofluorescence • *In vivo xenografts tumor*	[80]
Enzyme thymine DNA glycosylase	LOPAC^{1280} library from Sigma Aldrich	1,280 molecules	• Robotic platforms • Microplate reader; 1536-well • Multidrop combi dispenser	Human: SK28, 888-Mel, Mel501 and MNT-1	• Immunoblotting • Viral vector tools • Cell viability • Cell proliferation • Flow cytometry • Clonogenic • Immunofluorescence • *In vivo xenografts tumor*	[98]
NF-kB and Bromodomain	Tocris chemical library	1,280 molecules	• Microplate reader; 96-well • Multidrop combi dispenser	Human: Omm1.3, Omm1, 92.1, UM004 and Mewo	• Cell viability • RNA-seq • Viral vector tools • Immunoblotting • Real-Time PCR • *In vivo experiment tumor*	[99]
Synergism between drugs	Prestwick chemical library	1,280 molecules	• Microplate reader; 384-well	Mouse: B16-F10	• Cell viability • Flow cytometry • Immunofluorescence • Real-Time PCR • *In vivo experiment tumor*	[78]

Table 6 - (Continued)

Melanoma target studied	Library	Number of compounds	Basic infrastructure to cell-based screening	Melanoma cell line	Other biologic assays performed	Reference
BRAF inhibitors	Walter and Eliza Hall Institute	10,560 molecules	• Microplate reader	Human: MM200 and Mel-JD	• Viral vector tools • Cell viability • Clonogenic • Immunoblotting • Immunohistochemistry • *In vivo xenografts tumor*	[86]
BRAF(V600E) and IFNγ	NPACT Chemical Library	466 molecules	• Microplate reader; 1536-well • Multidrop combi dispenser • Kalypsys pintool	Human: SK-Mel 28 Mouse: SB3123p	• Immunohistochemistry • Immunoblotting • ELISA • Real-Time PCR	[89]
BRAF(V600E) and Mitochondrial Complex I	MicroSource Spectrum Collection and OTRADI Siga Collection	2,000 and 6,720 molecules	• Microplate reader; 384-well • Multidrop combi dispenser • Digital dispenser	Human: A2058	• Cell viability • Live-Cell metabolic • Immunoblotting • Immunohistochemistry	[79]

Table 7 - Studies that performed an approach cell-based screening and used i*n silico* tools and *in vitro* assays to validate their molecules

Melanoma target studied	**Compound library**	**Melanoma cell line**	***In silico* tool**	**Other biologic assays performed**	**Reference**
Serine/arginine-rich protein kinases inhibitor	4 compounds synthesized by the researchers.	Mouse: B16-F10	• Comparative modeling • Molecular docking (Glide SP, Fit • Docking, Schrodinger system)	• Cell viability • Antimetastatic assays (wound healing; colony formation; invasion; migration) • Immunofluorescence • *In vivo experiment tumor*	[102]
BRAF(V600E)	15 compounds synthesized by the researchers.	Human melanoma cell lime: A375; WM266-4; WM1361	• Molecular docking (Accelrys Discovery Studio version 3.5; CDOCKER) • Molecular dynamics (GROMACS)	• Kinase inhibition • Cell proliferation • Cell apoptosis • Caspase 3 • Cell cycle • Immunoblotting • - *In vivo/xenografts tumor*	[103]
Apoptosis inhibitors and Bcl-2 family	22 compounds synthesized by the researchers.	Human melanoma cell lime: A375	• Molecular docking (Schrodinger system) • Pharmacophores analysis (Schrodinger system) • ADME (QikProp)	• Cytotoxicity • Antioxidant activity • Apoptotic assays (acridine orange/ethidium bromide; TUNEL; FITC-Annexin V) • Antimetastatic assays (wound healing; colony formation; invasion; migration) • Cell cycle • Cyt c and mitochondrial membrane potential • DNA fragmentation • Caspases (8; 9; 2) • GSH estimation	[104]

Table 7 - (Continued)

Melanoma target studied	**Compound library**	**Melanoma cell line**	***In silico* tool**	**Other biologic assays performed**	**Reference**
BRAF inhibitors	15 compounds synthesized by the researchers.	Human melanoma cell line: Lu1205	• Molecular docking (AutoDock4 program) • Molecular dynamics (Amber software package; Particle Mesh Ewald method; SHAKE algorithm; PTRAJ.)	• Cytotoxicity	[87]
Metalloproteinases 9 and 2	26 compounds synthesized by the researchers.	Mouse: B16-F10	• Molecular docking • ADME (pkCSM)	• Cell viability • Cell proliferation • Antimetastatic assays (wound healing; colony formation; invasion; migration) • Gelatin zymography	[24]

4. BIOLOGICAL APPROACHES TO DRUG SCREENING

Biological approaches, including *in vitro* and *in vivo* methodologies, are used widely for cancer research and drug development. HeLa cells, derived from a cervical cancer, were the first human cancer cell line to be established *in vitro* [105]. That study highlights research on cancer cells, allowing drug screening and molecular cancer biology studies to be performed. In the past decade, studies have resulted in the large-scale genetic and pharmacological characterization of human cancer cell lines [106, 107]. Human cell lines that capture the genomic diversity of their respective cancers can be used in *in vitro* and *in vivo* studies, allowing reliable results to be obtained that reflect the disease from which they are derived. In addition, cell lines can provide an unlimited supply of biological material for use in multiple assays, making studies more feasible and promising for drug discovery [29, 108, 109].

Regarding melanoma, different cell lines are required to cover the genetic variety of tumors [10]. Therefore, metastatic melanoma cell lines vary according to the level of genetic complexity. This must be considered for biological studies that require such complexity to analyze tumor heterogeneity [34]. It is important that selected cell lines are capable of sustaining their original features.

4.1 Melanoma Cell Lines

Most melanoma cells used for *in vitro* and *in vivo* studies are derived from human tumors [80, 86, 97, 99, 110-112]. They can be divided into melanotic (pigmented) and amelanotic (non-pigmented) cell lines. Overall, both types of cell lines can be used for drug screening assays, and melanin is a target molecule since it acts as a chelating agent in chemoresistance assays [113]. Although existing cell lines are diverse, only a few melanogenic cell lines retain their *in vivo* characteristics. For example, SK-MEL-1, RPMI-7951, UACC-62, MALME-3M, and UACC-257 are melanotic cell lines, while SK-MEL-2, SK-MEL-5, SK-MEL-28, LOX IMVI, M14, M19-MEL, and A375 are amelanotic [34].

Additionally, the use of murine melanoma cell lines is important for cancer research [24, 78, 89, 94, 102]. The cell lines K1735, Cloudman S91-M3, and B16-F10 are most commonly used in models of murine melanoma [114]. B16 sublines that are more invasive than B16-F10 exist, including B16-BL6 and Mmb16 cells [34, 115]. To date, the most widely used cell line is B16-F10. The B16 murine melanoma cell line was first identified in 1954, when a tumor spontaneously arose in a C57BL/6J mouse [116]. This is the most widely used

animal model for the screening of potential melanoma drugs, owing to its well-estabilished genetic and histological characteristics [34]. In 1973, it was published the process that gave rise to the B16 (F1, F10) sublines with different metastatic potentials [117]. The B16-F10 cell line maintains wild-type copies of BRAF, TP3, and NRAS, therefore being very similar to human melanoma. Moreover, this cell line presents alterations in the p16INK4A/p19Arf, p53, and RAS-MAPK pathways, which favor the development of murine melanoma [34, 118].

The use of melanoma cell lines has driven our understanding of molecular cancer biology and led to numerous landmark discoveries, including the prevalence of BRAF V600E mutations in melanomas [119]. The identification of molecular biomarkers can help to predict cancer progression and therapeutic efficacy. Diverse biomarkers associated with melanoma metastasis have been investigated for their prognostic value and application for the treatment of patients [120]. The genomic, epigenomic, and metabolomic characterization of cell lines allows investigators to identify and evaluate oncogenic molecular mechanisms in depth [121]. Thus, an understanding of melanoma cell biology has been instrumental in the development of more effective treatments for the disease.

The progression of melanoma is commonly associated with mutations in the BRAF/NRAS/KIT, INK4A/CDK4, and ARF/TP53 genes, resulting in altered regulation of the RAS-RAF-MEK-ERK, p16INK4A-CDK4-RB, and ARF-p53 pathways, respectively. Subsequently, activation of the MAPK/ERK, PI3K/AKT, and Wnt signaling pathways have been identified in melanoma tumorigenesis [20, 122]. Changes in any component of these pathways can alter the cell proliferation, migration and survival phenotypes, favoring melanoma progression [123, 124]. Therefore, components of these signaling pathways in melanomas are important molecular targets for potential antitumor molecules. Therefore, studying melanoma cells enhances our knowledge of these potential targets [79, 80, 88, 90]. For example, combination treatment targeting the MAPK and PI3K signaling pathways with the PI3K inhibitor buparlisib and the MEK1/2 inhibitor, trametinib is a promising strategy for patients with melanoma [125]. Thus, several opportunities exist for the appropriate use of melanoma cell line panels for preclinical evaluation of cancer drugs [86, 98, 109].

4.2 2D and 3D Cell Culture

In the laboratory, cell-based experiments have been indispensable for the study of biochemical interactions and cell-to-cell communication. Cultures of two-dimensional (2D) and three-dimensional (3D) cells are the main cell-based systems used to investigate the

genetics and biology of different types of cancer [126]. Two-dimensional cell monolayers consist of a static dish culture system with mainly adherent cells, except for blood cells (e.g., leukemia cells). This cell culture matrix is still widely used in research aiming to identify novel anticancer agents. The advantages of 2D cell culture include high reproducibility, the ability for long-term culture, facile cell observation, environmental control, and inexpensive biological tests and media [127]. Based on these characteristics, 2D cell culture is used widely in cell-based high-throughput screening [24, 78, 80, 86, 98]. However, 2D-cultured cancer cells cannot precisely simulate tumor characteristics *in vivo*, since essential cellular functions that are present in tissues are lacking [128]. For that reason, following the identification of new molecules, the use of *in vitro* assays with 3D cultures is a viable approach, as this model can simulate physiological conditions that more closely mimic those of the living organism [128].

Three-dimensional cancer cell models mimic the *in vivo* physiology of organs and their external environment, reducing the gap between cell culture and live tissue [129]. This method provides a better representation of important tumor features, such as hypoxia, dormancy, anti-apoptotic potential, and drug resistance, making the collected data more predictable than those obtained from 2D models [128]. Different types of 3D culture technologies exist, including multicellular spheroids, organoids, scaffolds, hydrogels, organs-on-chips, and 3D bioprinting. For more details of the key features of these technologies, see Fang and Eglen (2017) [130].

The benefits of 3D culture involve proper cell-cell and cell-extracellular environment interactions, the preservation of morphology, interactions between different cell types, and the replacement of animals, which is attractive for both ethical and economic reasons. However, 3D-cultured cells have some limitations due to their structural complexity. They demand more advanced laboratory technologies in terms of sample handling and microscopy, which makes this process expensive and time-consuming [126, 129]. Other limitations of 3D cell cultures include their worse reproducibility than 2D models, sensitivity to the culturing method used, and the presence of undesirable elements, such as growth factors and viruses [127, 131]. Notably, 3D culture platforms have been developed using B16-F10 cells to mimic the complex network of cell interactions present in melanomas [132, 133]. This demonstrates that melanoma cell lines are valuable tools for studying malignant cells and tumor formation [122].

4.3 Preclinical Assays

4.3.1 *In vitro* Melanoma Cell Experiments

Malignant cells present important hallmarks, such as sustained proliferation, resistance to cell death, replicative immortality, angiogenesis, metastasis, and reprograming of signaling pathways [134]. Different *in vitro* assays can be used to detect these cellular hallmarks. The selection of an appropriate validation method to evaluate these multi-step events is challenging, because it depends on factors such as the cell model system, cost of reagents, and instrumentation availability. The first methods developed to detect proliferative events used different dyes, and are based on the principle that viable cells exclude certain dyes. In contrast, these dyes can pass through damage membranes, thereby labeling non-viable cells [104, 135].

The most common cell proliferation assays include 3-(4,5-dimethyl-2-thiazolyl)-2,5-diphenyl-2H-tetrazolium bromide (MTT) and sulforhodamine B (SRB) assays. These are often used to evaluate the cytotoxicity of compounds during the drug discovery process via cell viability. The colorimetric MTT assay results in the enzymatic reduction of tetrazolium salt (yellow substrate) to the lipophilic formazan (dark blue product), which is then quantified by absorbance [136, 137]. The SRB assay, in turn, uses a protein-bound dye to measure the total protein content that is directly proportional to cell proliferation [138]. However, these assays have some disadvantages, such as low absorption by cells arranged in clusters and the high cytotoxicity of some reagents. Besides that, the physiology of metastatic melanoma cells shows important metabolic changes, such as the change from mitochondrial oxidative phosphorylation to cytoplasmic aerobic glycolysis, which contributes to reducing the efficiency of these tests [34, 139]. Conversely, they are low-cost tests that require only simple manipulation and provide reliable preliminary results [135].

Another marker of cell proliferation is telomerase activity. Telomerases elongate telomeric DNA and compensate for its shortening during replication, which is essential for the long-term viability of cells [140]. Normal cells pass through a limited number of cell cycles; however, cancer cells have high telomerase activity, resulting in replicative immortality. Therefore, the use of telomerase inhibitors may be helpful in the search for anticancer drugs [141].

Moreover, other methods, such as membrane alterations, DNA fragmentation, and mitochondrial damage, have been established to detect the type of cell death based on apoptotic markers [104, 142]. Apoptosis is a natural phenomenon of programed cell death,

which leads to morphological and biochemical alterations, genome fragmentation, and mitochondrial dysfunction. During apoptosis, chromatin is fragmented by endonucleases, reducing the amount of DNA staining by propidium iodide. Pro-apoptotic pathways include an extrinsic pathway mediated by cell surface death receptors (Fas or TNF-R), and an intrinsic pathway activated by the release of mitochondrial cytochrome c [104, 143].

Angiogenesis assays have also contributed to the evaluation of drugs with potential antimelanoma activity. Angiogenesis is the process through which new blood vessels are formed in normal tissues. In tumors, neoplastic cells induce vessel formation to increase the source of nutrients and oxygen [144]. Vascular endothelial growth factor (VEGF) induces angiogenesis and promotes vessel growth in several tissues, such as human umbilical vein endothelial cells (HUVEC). The latter is an example of a cell line that can be used to evaluate the activity of inhibitory agents, such as antimelanoma drugs, on the proliferation, differentiation, and migration of cells involved in the formation of capillary-like structures [145].

Metastasis includes multiple complex steps, such as the loss of cell adherence proteins, alterations in cell morphology, increased motility, and expression of the enzymes responsible to the extracelullar matrix (EM) dynamics: the matrix metalloproteinases (MMPs) [9]. MMPs are involved in degradation of EM components, such as collagen, elastin, laminin, and fibronectin. This changes the microenvironment of EM and modulates the activity of biologically active molecules, as growth factors, in addition to act on the activity of proteases. Thus, MMPs are essential for the progression of metastasis, once they promote the necessary conditions for metastatic cells to invade the basement membrane of blood and lymph vessels and colonize other tissues and organs [146-150]. Therefore, in view of the foregoing, MMPs represent promising therapeutic targets in the development of new drugs with antimetastatic activity [148, 151, 152].

Cancer cells have differentiated energy physiology; they have high rates of glucose uptake and lactate secretion, even in the presence of oxygen, which normally favors aerobic glycolysis (i.e., Warburg effect). Rapid glucose uptake allows tumor cells to contribute to macromolecular synthesis, such as that of ribose for nucleotides, more quickly and efficiently [153, 154]. Due to this differential energetic dynamics, quantification of glucose consumption can identify altered cancer cells metabolism and be used to analyze the mode of action of anticancer drugs.

Exposure to oxidative stress has been implicated in cancer development. For instance, glutathione (GSH) is a natural antioxidant that prevents cell damage in tissue due to attack by

oxyradicals. High levels of GSH have been reported in various types of tumors and are associated with drug resistance [155]. Moreover, GSH levels are associated with the proliferation and metastasis of melanoma cells [156]. This highlights the importance of antioxidant activity assays for evaluating potential antimelanoma drugs.

In the Table 8, we present a summary of some *in vitro* assays employed in combination by our group to assess the potential efficacy of novel compounds from natural products and organic synthesis targeting in each hallmark of melanoma cancer cells [157-159]. We emphasize those with low cost and feasibility in most research laboratories.

4.3.2 *In vivo* Melanoma Models

In vitro assays provide useful preliminary information on the cytotoxicity of screened compounds and important insights into mechanistic actions in cell models. However, during the rational process of development and the approval of new melanoma drugs, *in vivo* experiments are mandatory. The use of animal models is necessary to evaluate the efficacy and safety of potential drugs. Therefore, *in vivo* studies are a crucial stage for the screening of drugs with antimelanoma potential, respecting the 3R principles: reduction, replacement, and refinement of animal use [80, 99, 102, 103].

Various animal models are used to study radio- and chemotherapy, each with different applications. Nevertheless, malignant melanoma only develops spontaneously in a few models: Sinclair miniature swine, Munich miniature swine troll, and Melanoma-bearing Libechov minipigs (MeLiM) [182, 183]. Thus, since the rise of spontaneous melanoma is extremely rare in animal models, the induction of tumor formation is necessary to create biological models of melanoma [117].

Over the years, several animal models have emerged, including non-mammalian models, such as *Drosophila melanogaster* and zebrafish (*Danio rerio*) [184, 185]. Zebrafish xenografts have been used as a fast and sensitive *in vivo* vertebrate model for testing novel compounds against melanoma [186]. Among the animal models used in melanoma research, zebrafish are less expensive and have been considered a substitute for murine animal models. Interestingly, fish have a low occurrence of natural cancer formation. However, elevated levels of tumorigenesis have been observed in animals following exposure to cytotoxic compounds [127]. Different aspects of cancer can be investigated by using zebrafish, including apoptosis, tubulin binding, angiogenesis, microangiography, transgenesis, and toxicity.

Regarding preclinical models, mice are the most commonly used, followed by other mammals, such as dogs, horses and pigs [183]. This is because different genetic alterations identified in human melanoma have been recapitulated in mice [187]. In addition, murine models of melanoma present important characteristics that make them a great choice for drug screening: small size, established genetics, easy handling, and low cost [34, 80, 99, 103]. However, it is important to emphasize that the use of animals in experiments should be performed consciously, rationally using the appropriate number of animals.

Table 8 - *In vitro* assays that could be applied to detect disturbance on the main hallmarks of melanoma cancer cells

Hallmark	Assays	Principle	Equipment required	References
Sustaining proliferation	Colony formation	Based on the ability of a single cell replicate and form colony, consisted at least 50 cells. Colonies are stained with crystal violet.	Any specialized equipment	[160]
	Trypan blue exclusion	Live cells possess intact membranes that exclude trypan blue. As a result, the cytoplasm of dead cells is positively stained.	Hemocytometer	[161]
	Lactate dehydrogenase (LDH)	Dead cells leak LDH into the culture medium, where NADH is generate. NADH reduce resazurin into the fluorogenic resorufin.	Spectrophotometer	[162]
	BrdU (bromodeoxyuridine)	BrdU incorporates into DNA of dividing cells and will be passed down to daughter cells following division. Be detected by antibodies.	Fow cytometry or immunohistochemistry	[163]
Resisting cell death	Acridine orange (AO) and ethidium bromide (EB)	AO permeates all cells. EB dominates over AO and is take by cells with damage membrane. As a result, lives, apoptotic and necrotic cells have green, orange and red nucleus, respectively.	Fluorescent microscopy	[164]
	Hoechst 33342	Hoechst binds to adenine-thymine-rich regions of DNA, which can be used to observe nuclear condensation distinguishing apoptotic from healthy or necrotic cells.	Fluorescent microscopy	[165]
	DAPI (4′,6-diamidino-2-phenylindole)	DAPI associates with the minor groove of double-stranded DNA preferably for the adenine-thymine clusters.	Fluorescent microscopy	[166]
	Propidium iodide (PI) exclusion	It is based on the principle that apoptotic cells present DNA fragments, reducing PI staining.	Flow cytometry or fluorescent microscopy	[167]
	TUNEL (terminal deoxynucleotidyl transferase (TdT)-mediated dUTP Nick End Labeling)	Rely on the use of exogenous terminal deoxynucleotidyl transferase which either directly attaches the fluorochrome conjugated triphosphodeoxynucleotides to 3′OH DNA termini generates by endonucleases. This method detects early apoptosis.	Flow cytometry	[168]
	Annexin V-FITC	Apoptotic cells show phosphatidyl-serine on the outer surface, which can be detected using Annexin V-FITC staining. Using AnnexinV-FITC in combination with PI permits quantification of viable (double negative), early apoptotic (Annexin V-FITC positive/PI negative) and late apoptotic cells (double positive).	Flow cytometry	[169]
	JC-1	JC-1 is a carbocyanine with positive charge, which can be used to exploit live mitochondria. The potential of matrix (negative inside) promoted a directional uptake of JC-1, that alter color reversibly from green to red with increasing membrane potentials.	Fluorescent microscopy	[170]

Table 8 - (Continued)

Hallmark	Assays	Principle	Equipment required	References
Resisting cell death	Cytochrome c	In apoptotic cells cytochrome c are released from the mitochondrial intermembrane space to the cytoplasm. Techniques to assay cytochrome c release rely on cellular fractionation followed by western blotting, immunocytochemistry or GFP-tagged cytochrome c.	Fluorescent microscopy	[171]
	Bcl-2, Bax, Fas, p53, and CDK	Expression of apoptosis-regulating proteins. Pro-apoptotic (p53, p21, bax, bak, fas) and anti-apoptotic (bcl-2, bcl-x).	Fluorescent microscopy	[172], [173]
	Caspases	Caspase is a cysteine protease activated during apoptosis. The aggregation of caspases into dimers or macromolecules, result in controlled demolition of cellular components. Detection can be performed with specific antibodies by immunoprecipitation or immunoblot, or with fluorescent probes.	Fluorescent microscopy and flow cytometer	[174]
Replicative immortality	TRAP (telomerase repeat amplification)	Measure the telomerase activity. Telomerase adds telomeric repeats to the telomere-imitating oligonucleotide, after which synthesized DNA is amplified by using specific primers.	RT-PCR	[141]
	Cell cycle blockage	Based on the analysis of cellular DNA distribution between cycle phases by PI staining	Flow cytometry	[175]
Angiogenesis	Chemoinvasion	HUVEC (human umbilical vein endothelial cells) cells can be used to access migration ability when exposed to VEGF (chemotaxis).	Boyden-chamber assay	[145]
	Capillary-like structures forming	HUVEC cells form capillary-like structures when plated on top of a basement membrane of fibrin, collagen or Matrigel.	Microscopy	[176]
	Angiogenesis activators	Detection of known factors effecting angiogenesis (VEGF, FGF, EGF family) by antibodies.	Immunoblot or ELISA	[177]
Metastasis	Scratch (*wound healing*)	The confluent cellular monolayer is wounded by scraping. At regular time intervals, images are captured to track the migration of cells until wound close.	Microscopy	[178]
	Adhesion	The cells were seed into a microplate well coated with matrigel. Nonattached cells were removed by washing. Attached cells are fixed and stained with glutaraldehyde and crystal violet, respectively.	Spectrophotometer	[179]
	Migration and invasion	Cells are seeded in the upper side, and migrate through a porous membrane to the lower side by chemotaxis. Coating the porous with matrigel or collagen, the device is suitable for invasion measurement. Migrated and invaded cells can be visualized by cytological dyes such as toluidine blue.	Transwell chamber and microscopy	[145]
Reprogramming signaling pathways	Glutathione (GSH)	Based on the reduction of small molecule CBT-Cys(SEt) by GSH, that condenses and consequent self-assembles into nanostructures.	Spectrophotometer	[180]
	Glucose uptake	Radioactive hexoses FDG (fluoro-deoxyglucose), 2DG (2-deoxy-D-glucose) and 3MG (3-O-methylglucose) are quantified from cell lysates to study glucose uptake efficiency. Fluorescent glucose analogs can be measured as well.	Liquid scintillation counter and fluorescence microscopy	[181]

4.3.2.1 Syngeneic Models

Overall, tumor induction is required in murine models, because mice do not develop melanoma spontaneously; this can be performed by inoculating mice with human or murine melanoma cells. Thus, syngeneic models involve the inoculation of mouse melanoma cells into inbred animals of the same genetic background [183]. This model has the advantage of preserving the immune system of the animal and is often used to evaluate immunotherapies and the relationship between the immune system and the tumor. A syngeneic model is also used to evaluate the formation of metastases and the behavior of melanomas [102, 183, 188]. However, the use of murine cells instead of human cells is a limitation of the B16 syngeneic model, due to differences in the expression of adhesion proteins, the production of growth factors, and anti-apoptotic mechanisms [189].

Models of syngeneic transplantation include K1735 melanoma in C3H mice, Harding-Passey melanoma in BALB/c•DBA/2F1 mice, Cloudman S91 melanoma in DBA/2 mice, and B16 melanoma in C57BL/6 mice [114, 188]. While the first animal model remains poorly characterized and is rarely used for drug screening, C57BL/6 mice are used widely for melanoma drug screening and 70% of studies reported up to 2018 utilized mice bearing B16 grafts for *in vivo* evaluation [34, 78, 102, 190]. Sublines of B16 melanoma, such as B16-F0, B16-BL6, and Mmb16 lines, exist [191]; however, the two most well-established and widely used sublines, B16-F1 and B16-F10, were obtained from *in vivo* passaging [117]. The first is characterized by its low potential for lung colonization, and is therefore useful for studying primary tumor growth. In contrast, B16-F10 cell lines display a high metastatic potential, most notably in the lungs, and are therefore ideal for use in metastatic investigations *in vivo* [78, 102, 189].

B16 melanoma cells can be inoculated into C57BL/6 mice via subcutaneous, intraperitoneal, or intravenous routes [102, 159]. The cell number and the experiment time vary depending on the study. For example, mice are commonly inoculated subcutaneously on the back or flank with 1 or 2 x 10^5 cells and maintained for 2 weeks; longer durations impair animal health and welfare. A recent study used this animal model to evaluate a compound that showed antitumor potential *in vitro*. C57BL/6 mice were inoculated with 2 x 10^5 cells on their backs; treatments began as soon as the tumors became visible. The compound used recruited the immune system and did not demonstrated signs of toxicity for the animal [159].

Intravenous injection of B16-F10 has also been used to investigate the action of new compounds on metastases [102]. Since metastatic melanoma is considered an intractable

cancer [18], this model allows the evaluation of new substances with antimetastatic potential. The injection of cells into the animal tail vein generates organ metastases, mainly in the lungs. One study revealed that treatment of animals with SRPIN340 derivatives for 3 weeks after inoculation of 2 x 10^5 cells reduced the number of lung tumor nodules compared with a vehicle-control [102], demonstrating the antimetastatic potential of this compound.

These models are useful for the preclinical evaluation of new compounds. However, they are limited by the use of murine cells instead of human cells. To overcome this, other animal models are available that use human melanoma cell lines, such as xenograft models [80, 97, 98].

4.3.2.2 Xenograft Models

Melanoma cells can be used in serial xenotransplantation animal assays in non-adherent (spheroid) or adherent cultures. Melanoma culture expansion as spheroids (melanospheres), which were originally established as an *in vitro* culture system for cancer stem cells, present high tumorigenic potential in immunodeficient mice compared with that of melanoma cells expanded as adherent cultures [192].

Xenograft models allow the transplantation of human melanoma cells into immunodeficient mice. In recent years, human tumor xenograft models have been widely used to evaluate metastases and for drug screening [190]. As tumor cells are obtained from humans, the mouse immune system used in this model is suppressed in order to avoid graft rejection. Unlike the syngeneic model, in the xenograft model, the mice lack a functional immune system, which hampers the study of immunotherapies [183]. In addition, some human cell lines are not tumorigenic in mice, limiting the utility of this model to study the effects of chemotherapeutic agents *in vivo*. In addition, the xenograft model allows human melanoma cells to interact with the bloodstream and lymphatic vessels, beyond the murine stroma, allowing interactions between tumor cells and host animals to be studied. This provides a valuable method of investigating the behavior and response of human melanoma cells to drugs *in vivo* [193].

Mice used in xenograft models include severe compromised immunodeficient (SCID; T-cell and B-cell deficient) and athymic nude mice (T-cell deficient). Similar to the syngeneic models, approximately 2 x 10^5 melanoma cells are inoculated subcutaneously in immunodeficient mice to generate xenograft models of human melanoma [34]. Gammons and collaborators (2014) evaluated the pharmacological inhibition of serine/arginine-rich protein

kinases, protein kinases involved in alternative splicing, and observed a decrease in the growth of subcutaneous melanoma after treatment with SRPIN340 [6]. In that study, an A375 human melanoma cell line, one of the most commonly used human cell lines, was used in a nude mouse model.

Some researchers have performed assays using the hollow fiber model, before initiating tests on xenograft models. The hollow fiber consists of semipermeable hollow fibers filled with tumor cells that are implanted into animals. This assay is similar to the xenograft test since the cells are disseminated and treated directly in a mouse with all of the associated pharmacokinetic, pharmacodynamic, and toxicologic dimensions of an *in vivo* assay. The hollow fiber assay is commonly used as an early *in vivo* model for anticancer drug screening, prior to assessment in more complex tumor models. It acts as a filter to enable researchers to select the most suitable steps for further analysis in a xenograft assay in a time- and cost-effective manner [194, 195].

Although xenograft models are excellent tools for studying human melanoma, they require the use of immunodeficient mice, which does not permit the analysis of immunotherapies, and results in a less realistic tumor microenvironment. In addition, this model is often poorly predictive of clinical outcomes, and drugs that demonstrate efficacy in this model often fail in clinical trials [196]. To overcome this, other animal models can be used to evaluate novel anticancer therapies, such as patient-derived xenografts (PDXs), humanized PDX mouse models, and genetically engineered mice.

4.3.2.3 Patient-Derived Xenograft Models

PDX models, unlike xenograpft models, are generated by the implantation of fresh human tumors into immunodeficient mice [197]. A critical limitation is the requirement for immunosuppressed mice, making tests of immunotherapies unfeasible. Conversely, this model preserves tumor heterogeneity and key characteristics of the patient's tumor and, therefore, is renowned to be superior for drug screening [198]. Thus, PDX models represent valuable predictive platforms for therapeutic outcomes [199].

PDX models enable the provision of a personalized medicine approach, because the animal model is developed using tumor cells originating from a patient. This allows researchers to evaluate drug efficacy and therapies using a patient's own cells [34]. One study used melanomas from 25 patients and showed reproducible differences in the rate of spontaneous metastasis after transplantation into mice, which were correlated with clinical

outcomes in the patients [200]. Therefore, this model allows the study of personalized treatment approaches for each patient.

To overcome the deficiency of the immune system in immunodeficient mice, humanized PDX mouse models have been developed. In these models, the human immune system is introduced into mice previously subjected to gamma irradiation-induced myeloablation by grafting purified human $CD34^+$ hematopoietic stem cells [196]. Using humanized PDX mouse models, it is possible to test immunotherapeutic strategies, allowing different classes of antitumor drugs to be tested.

While this approach is relatively new, expensive, and technically complicated, classic genetically defined predisposed mouse models provide useful information, which complements that obtained from *in vitro* and xenograft studies [193].

4.3.2.4 Genetically Engineered Models

Genetically engineered models (GEMs) are used to eluidate gene function and identify possible targets for melanoma treatment [187]. In these models, the tumor exists in the presence of a competent immune system, which makes the microenvironment more realistic. As previously stated, the development of melanomas is rare in mice. Thus, they can be generated using GEMs by activating oncogenes relevant to human melanoma, such as mutant BRAF or mutant NRAS, or through inactivation of key tumor suppressors, including CDKN2A and PTEN [196]. This enables treatment with drugs that have specific targets, such as genes carrying mutations.

A disadvantage of GEMs is that they target a limited number of genes that usually do not reflect the complex heterogeneity of human tumor cells. Furthermore, tumor development in animals is slow and variable. Finally, development is generally costly and time-consuming, and often requires years of work before validation [201].

Recently, a novel immunogenic mouse model of melanoma was developed for the preclinical assessment of combined targeted and immune-based therapy [202]. In this model, the authors rationally designed combinations of target therapy and immunotherapy to overcome the poor response rates of the individual therapies. The development and characterization of a new immunogenic variant of the BrafV600ECdkn2a−/−Pten−/−YUMM1.1 tumor model was described, which expresses the immunogen ovalbumin (YOVAL1.1). This new model is transplantable, immunogenic, and

sensitive to clinical therapies, making it suitable for the development of new combined therapies for melanoma.

4.3.2.5 Chemically Induced Models

Models using melanoma cell lines have been described. In addition, chemically induced models have been utilized, in which melanoma cells are not used. However, drugs can be tested using this animal model, considering the differences in the physiology of human and rodent skin [203].

In chemically induced models, melanoma is chemically induced by carcinogens, such as 7,12-dimethylbenz(a)anthracene (DMBA), an immune-suppressing polycyclic aromatic hydrocarbon, and 12-O-tetradecanoyl-phorbol-13-acetate (TPA), a phorbol ester. Both compounds can be applied topically to induce skin irritation and to generate black lesions, which develop into melanoma [190]. One advantage of this model is that the immune system is functional; therefore, the mice can be used to test immunotherapies. Meanwhile, the main disadvantage is the lack of clinical relevance to human disease, due to chemical induction [187].

5. CONCLUSION

This chapter provides an overview of strategies used to demonstrate the utility of melanoma cell lines for drug screening. Novel models have been created to optimize and validate the employed techniques, such as 3D culture models, xenograft models and *in silico* studies. Furthermore, a great deal of progress has been made in understanding the biology of cancer, enabling the development of tumor- and patient-specific therapies. However, there remains no effective treatment that is of low cost and without side effects for patients with metastatic melanoma. Therefore, in future, new drugs are needed, or the use of available drugs should be improved, for patients with melanoma. Notably, the role of melanoma cell lines in this process remains incomplete. The advent of -omics technologies and the generation of a comprehensive public database that describes the molecular and cellular alterations of each cell line have renewed their importance as indispensable tools for cancer research and drug discovery. *In vitro* studies are essential tools for testing potential therapies, but do not recapitulate the complexity of the whole organism and the microenvironment in which tumors develop. Thus, *in vivo* models in conjunction with *in silico* studies are relevant to increase and improve our understanding of melanoma biology. Taken together, this

combined knowledge brings us closer to developing more effective treatments for patients with metastatic melanoma.

6. REFERENCES

[1] Uong, A. & Zon, L. I. (2010). Melanocytes in development and cancer. Journal of Cellular Physiology, 222(1), 38–41. doi:10.1002/jcp.21935.

[2] Moon, H., Donahue, L. R., Choi, E., Scumpia, P. O., Lowry, W. E., Grenier, J. K., Zhu, J. & White, A. C. (2017). Melanocyte stem cell activation and translocation initiate cutaneous melanoma in response to UV exposure. Cell Stem Cell, 21, 665–678. doi:10.1016/j.stem.2017.09.001.

[3] Yang, K., Oak, A. S., W., Slominski, R. M., Brożyna, A. A. & Slominski, A. T. (2020). Current molecular markers of melanoma and treatment targets. International Journal of Molecular Sciences, 21, 3535. doi:10.3390/ijms21103535.

[4] Kinsler, V. A. & Larue, L. (2018). The patterns of birthmarks suggest a novel population of melanocyte precursors arising around the time of gastrulation. Pigment Cell & Melanoma Research, 31, 95–109. doi:10.1111/pcmr.12645.

[5] Kierszenbaum, Abraham L. & Tres, Laura L. (2007). Histology and cell biology: an introduction to pathology. Philadelphia: Elsevier.

[6] Gammons, M. V., Lucas, R., Dean, R., Coupland, S. E., Oltean, S. & Bates, D. O. (2014). Targeting SRPK1 to control VEGF-mediated tumour angiogenesis in metastatic melanoma. British. Journal of Cancer, 111, 477–485. doi:10.1038/bjc.2014.342.

[7] Glatz-Krieger, K., Pache, M., Tapia, C., Fuchs, A., Savic, S., Glatz, D., Mihatsch, M. & Meyer, P. (2006). Anatomic site-specific patterns of gene copy number gains in skin, mucosal, and uveal melanomas detected by fluorescence in situ hybridization. Virchows Archiv, 449, 328–333. doi:10.1007/s00428-006-0167-8.

[8] Landi, M. T., Bishop, D. T., MacGregor, S., Machiela, M. J., Stratigos, A. J., Ghiorzo, P., Brossard, M., Calista, D., Choi, J., Fargnoli, M. C., Zhang, T., Rodolfo, M., Trower, A. J., Menin, C., Martinez, J., Hadjisavvas, A., Song, L., Stefanaki, I., Scolyer, R., Yang, R., Goldstein, A. M., Potrony, M., Kypreou, K. P., Pastorino, L., Queirolo, P., Pellegrini, C., Cattaneo, L., Zawistowski, M., Gimenez-Xavier, P., Rodriguez, A., Elefanti, L., Manoukian, S., Rivoltini, L., Smith, B. H., Loizidou, M. A., Regno, L. D., Massi, D., Mandala, M., Khosrotehrani, K., Akslen, L. A., Amos, C. I., Andresen, P. A., Avril, M., Azizi, E., Soyer, H. P., Bataille, V., Dalmasso, B., Bowdler, L. M., Burdon, K. P., Chen, W. V., Codd, V., Craig, J. E., Dębniak, T., Falchi, M., Fang, S., Friedman, E., Simi, S., Galan, P., Garcia-Casado, Z., Gillanders, E. M., Gordon, S., Green, A., Gruis, N. A., Hansson, J., Harland, M., Harris, J., Helsing, P., Henders, A., Hočevar, M., Höiom, V., Hunter, D., Ingvar, C., Kumar, R., Lang, J., Lathrop, G. M., Lee, J. E., Li, X., Lubiński, J., Mackie, R. M., Malt, M., Malvehy, J., McAloney, K., Mohamdi, H., Molven, A., Moses, E. K., Neale, R. E., Novaković, S., Nyholt, D. R., Olsson, H., Orr, N., Fritsche, L. G., Puig-Butille, J. A., Qureshi8, A. A., Radford-Smith, G. L., Randerson-Moor, J., Requena, C., Rowe, C., Samani, N. J., Sanna, M., Schadendorf, D., Schulze, H., Simms, L. A., Smithers, M., Song, F., Swerdlow, A. J., van der

Stoep, N., Kukutsch, N. A., Visconti, A., Wallace, L., Ward, S. V., Wheeler, L., Sturm, R. A., Hutchinson, A., Jones, K., Malasky, M., Vogt, A., Zhou, W., Pooley, K. A., Elder, D. E., Han, J., Hicks, B., Hayward, N. K., Kanetsky, P. A., Brummett, C., Montgomery, G. W., Olsen, C. M., Hayward, C., Dunning, A. M., Martin, N. G., Evangelou, E., Mann, G. J., Long, G., Pharoah, P. D. P., Easton, D. F., Barrett, J. H., Cust, A. E., Abecasis, G., Duffy, D. L., Whiteman, D. C., Gogas, H., Nicolo, A. D., Tucker, M. A., Newton-Bishop, J. A., GenoMEL Consortium, Q-MEGA and QTWIN Investigators, ATHENS Melanoma Study Group, 23andMe, The SDH Study Group, IBD Investigators, Essen-Heidelberg Investigators, AMFS Investigators, MelaNostrum Consortium, Peris, K., Chanock, S. J., Demenais, F., Brown, K. M., Puig, S., Nagore, E., Shi, J., Iles, M. M. & Law, M. H. (2020). Genome-wide association meta-analyses combining multiple risk phenotypes provide insights into the genetic architecture of cutaneous melanoma susceptibility. Nature Genetics, 52, 494–504. doi:10.1038/s41588-020-0611-8.

[9] Kumar, S. & Weaver, V. M. (2009). Mechanics, malignancy and metastasis: the force journey of a tumor cell. Cancer and Metastasis Reviews, 28, 113–127. doi:10.1007/s10555-008-9173-4.

[10] Mattia, G., Puglisi, R., Ascione, B., Malorni, W., Carè, A. & Matarrese, P. (2018). Cell death-based treatments of melanoma: conventional treatments and new therapeutic strategies. Cell Death and Disease, 9(2), 112. doi:10.1038/s41419-017-0059-7.

[11] Apalla, Z., Lallas, A., Sotiriou, E., Lazaridou, E. & Ioannides, D. (2017). Epidemiological trends in skin cancer. Dermatology Practical and Conceptual, 7(2), 1–6. doi:10.5826/dpc.0702a01.

[12] Siegel, R. L., Miller, K. D. & Jemal, A. (2020). Cancer statistics, 2020. CA: A Cancer Journal for Clinicians, 70(1), 7-30. doi:10.3322/caac.21590.

[13] American Cancer Society. (2020). Cancer Facts & Figures 2020. Atlanta: American Cancer Society, 76 pages.

[14] Instituto Nacional do Câncer. (2019). Estimates 2020: Incidence of cancer in Brazil. Rio de Janeiro: José Alencar Gomes da Silva National Cancer Institute, 122 pages.

[15] Bhatia, S., Tykodi, S. S. & Thompson, J. A. (2009). Treatment of metastatic melanoma: an overview. Oncology, 23(6), 488–496. PMID: 19544689.

[16] Maio, M., Grob, J., Aamdal, S., Bondaremnko, I., Robert, C., Thomas, L., Garbe, C., Chiarion-Silene, V., Testori, A., Chen, T. T., Tschaika, M. & Wolchik, J. D. (2015). Five-years survival rates for treatment-naive patients with advanced melanoma who received ipilimumab plus dacarbazine in a phase III trial. Journal of Clinical Oncology, 33 (10), 1191–1196. doi:10.1200/JCO.2014.56.6018.

[17] Matthews, N. H., Li, W., Qureshi, A. A., Weinstock, M. A. & Cho, E. (2017). Epidemiology of melanoma. In Cutaneous Melanoma: Etiology and Therapy, edited by Ward, W. H. and Farma, J. M., 3-22. Brisbane: Codon Publications. doi:10.15586/ codon.cutaneousmelanoma.2017.

[18] Qin, B. D., Jiao, X. D., Liu, K., Wu, Y., He, X., Liu, J., Qin, W. X., Wang, J. & Zang, Y. S. (2019). Basket trials for intractable cancer. Frontiers in Oncology, 229 (9), 1-11. doi:10.3389/fonc.2019.00229.

[19] Pavri, S. N., Clune, J., Ariyan, S. & Narayan, D. (2016). Malignant melanoma: beyond the basics. Plastic and Reconstructive Surgery, 138(2), 330e-340e. doi:10.1097/PRS.0000000000002367.

[20] Gray-Schopfer, V., Wellbrock, C. & Marais, R. (2007). Melanoma biology and new targeted therapy. Nature, 445, 851-87. doi:10.1038/ nature05661.

[21] Elias, E. G., Hasskamp, J. H. & Sharma, B. K. (2010). Biology of human cutaneous melanoma. Cancers, 2, 165–189. doi:10.3390/cancers2010165.

[22] Siegel, R. L., Miller, K. D. & Jemal, A. (2015). Cancer statistics, 2015. CA: A Cancer Journal for Clinicians, 65, 5–29. doi:10.3322/caac.21254.

[23] Agaësse, G., Barbollat-Boutrand, L., El Kharbili, M., Berthier-Vergnes, O. & Masse, I. (2017). p53 targets TSPAN8 to prevent invasion in melanoma cells. Oncogene, 6, e309. doi:10.1038/ oncsis.2017.11.

[24] Lima, G. D. A., Rodrigues, M. P., Mendes, T. A. O., Moreira, G. A., Siqueira, R. P., da Silva, A. M., Vaz, B. G., Fietto, J. L. R., Bressan, G. C., Machado-Neves, M. & Teixeira, R. R. (2018). Synthesis and antimetastatic activity evaluation of cinnamic acid derivatives containing 1,2,3-triazolic portions. Toxicology *In Vitro*, 53, 1-9. doi:10.1016/j.tiv.2018.07.015.

[25] Rozeman, E. A., Dekker, T. J. A., Haanen, J. B. A. G. & Blank, C. U. (2017). Advanced melanoma: current treatment options, biomarkers, and future perspectives. American Journal of Clinical Dermatology. doi:10.1007/s40257-017-0325-6.

[26] Shaffer, S. M., Dunagin, M. C., Torborg, S. R., Torre, E. A., Emert, B., Krepler, C., Beqiri, M., Sproesser, K., Brafford, P. A., Xiao, M., Eggan, E., Anastopoulos, I. N., Vargas-Garcia, C. A., Singh, A., Nathanson, K. L., Herlyn, M. & Raj, A. (2017). Rare cell variability and drug-induced reprogramming as a mode of cancer drug resistance. Nature, 546(7658), 431–435. doi:10.1038/nature22794.

[27] Cristiani, C. M., Garofalo, C., Passacatini, L. C. & Carbone, E. (2019). New avenues for melanoma immunotherapy: Natural Killer cells? NK cells and solid tumors immune therapy. Scandinavian Journal of Immunology, 91, e12861. doi:10.1111/SJI.12861.

[28] Gillet, J. P., Varma, S. & Gottesman, M. M. (2013). The clinical relevance of cancer cell lines. Journal of National Cancer Institute, 105, 452–458. doi:10.1093/jnci/djt007.

[29] Mirabelli, P., Coppola, L. & Salvatore, M. (2019). Cancer cell lines are useful model systems for medical research. Cancers, 11 (1098), 1-18. doi:10.3390/cancers11081098.

[30] National Cancer Institute (NCI). 2020. “Dictionary of cancer terms.” Accessed May 2020. https://www.cancer.gov/ publications/ dictionaries/cancer-terms.

[31] Wróbel, S., Przybylo, M. & Stepień, E. (2019). The clinical trial landscape for melanoma therapies. Journal of Clinical Medicine, 8, 368. doi:10.3390/jcm8030368.
[32] Daponte, A., Ascierto, P. A., Gravina, A., Melucci, M., Scala, S., Ottaiano, A., Simeone, E., Palmieri, G. & Comella, G. (2005). Temozolomide and cisplatin in advanced malignant melanoma. Anticancer Research, 25, 14441-1448. PMID: 15865103.

[33] Gupta, A., Gomes, F. & Lorigan, P. (2017). The role for chemotherapy in the modern management of melanoma. Melanoma Management, 4(2), 125-136. doi:10.2217/mmt-2017-0003.

[34] Couto, G. K., Segatto, N. V., Oliveira, T. L., Seixas, F. K., Schachtschneider, K. M. & Collares, T. (2019). The melding of drug screening platforms for melanoma. Frontiers in Oncology, 9, 512. doi:10.3389/fonc.2019.00512.

[35] Leich, D. L., Balan, V., Kaplun, A., Singh-Gupta, V., Kaplum, L., Dobson, M. & Tzivion, G. (2007). Raf kinases: Function, regulation and role in human cancer. Biochimica et Biophysical Acta, 1773(8), 1196-1212. doi:10.1016/j.bbamcr.2007.05.001.

[36] Caunt, C. J., Sale, M. J., Smith, P. D. & Cook, S. J. (2015). MEK1 and MEK2 inhibitors and cancer therapy: the long and winding road. Nature Reviews Cancer, 15(10), 577-592. doi:10.1038/nrc4000.

[37] Al-Badr, A. A. & Alodhaib, M. M. (2016). Dacarbazine. In: Profiles of Drug Substances, Excipients and Related Methodology, Vol. 41, Burlington: Academic Press, pp. 323-377. ISBN: 978-0-12-804784-2.

[38] Eggermont, A. M. M. & Kirkwood, J. M. (2004). Re-evaluating the role of dacarbazine in metastaic melanoma: what have we learned in 30 years? European Journal of Cancer, 40(12), 1825-1836. doi:10.1016/j.ejca.2004.04.030.

[39] Jiang, G., Li, R. H., Sun, C., Liu, Y. Q. & Zheng, J. N. (2014). Dacarbazine combined targeted therapy versus dacarbazine alone in patients with malignant melanoma: A meta-analysis. Plos One, 9(12), e111920. doi:10.1371/journal.pone.0111920.

[40] Rheault, T. R., Stellwagen, J. C., Adjabeng, G. M., Homberger, K. R., Petrov, K. G., Waterson, A. G., Dickerson, S. H., Mook, Jr., R. A., Laquerre, S. G., King, A. J., Rossanese, O. W., Arnone, M. R., Smitheman, K. N., Kane-Carson, L. S., Han, C., Moorthy, G. S., Moss, K. G. & Uehling, D. E. (2013). Discovery of dabrafenib: A selective inhibitor of raf kinases with antitumor activity against B-Raf-driven tumors. ACS Medicinal Chemistry Letters, 4(3), 358-362. doi:10.1021/ml4000063.

[41] Arkenau, H. T., Saggese, M. & Lemech, C. (2012). Drabrafenib. Serine/threonine-protein kinase B-raf inhibitor, Oncolitic. Drugs of the Future, 37(7), 469. doi:10.1358/dof.2012.037.07.1820872.

[42] Medina, T., Amaria, M. N. & Jimeno, A. (2013). Drabrafenib in the treatment of advanced melanoma. Drugs Today, 49(6), 377. doi:10.1358/dot.2013.49.6.1968669.

[43] Rai, S. K., Gunnam, A., Mannava, M. K. C. & Nangia, A. K. (2020). Improving the dissolution rate of the anticancer drug drabrafenib. Crystal Growth and Design, 20(2), 1035-1046. doi:10.1021/acs.cgd.9b01365.

[44] Koelblinger, P., Dornbiere, J. & Dummer, R. (2017). A review of binimetinib for the treatment of mutant cutaneous melanoma. Future Oncology, 13(20), 1755-1766. doi:10.2217/fon-2017-0170.

[45] Specenie, P. (2020). An overview of binimetinib for the treatment of melanoma. Expert Opinion on Pharmacoterapy, 26, 1-8. doi:10.1080/14656566.2020.1729122.

[46] Flaherty, K. T., Yasothan, U. & Kirkpatrick, P. (2011). Vemurafenib. Nature Review Drug Discovery, 10(11), 811-812. doi:10.1038/nrd3579.

[47] Fisher, R. & Larkin, J. (2012). Vemurafenib: a new treatment for BRAF-V600 mutated advanced melanoma. Cancer Management and Research, 4, 243-252. doi:10.2147/CMAR.S25284.

[48] Koelblinger, P., Thuerigen, O. & Dummer, R. (2018). Development of encorafenib for BRAF-mutated advanced melanoma. Current Opinion in Oncology, 30(2), 125-133. doi:10.1097/ CCO.0000000000000426.

[49] Hamid, O., Cowey, C. L., Offner, M., Faries, M. & Carvajal, R. D. (2019). Efficacy, safety, and tolerability of approved combination BRAF and MEK inhibitor regimens for BRAF-mutant melanoma. Cancers, 11(11), pii E1642. doi:10.3390/cancers11111642.

[50] Shirley, M. (2018). Encorafenib and binimetinib: First global approvals. Drugs, 78(12), 1277-1284. doi:10.1007/s40265-018-0963-x.

[51] Trojaniello, C., Festino, L., Vanella, V. & Ascierto, P. A. (2019). Encorafenib in combination with binimetinib for unresectable or metastic melanoma with BRAF mutations. Expert Review of Clinical Pharmacology, 12(3), 259-266. doi:10.1080/ 17512433.2019.1570847.

[52] Long, G. V., Hauschild, A., SAntinami, M., Atkinson, V., mandala, M., Chiarion-Sileni, V., Larkin, J., Nyakas, M., Dutriaux, C., Haydon, A., Robert, C., Mortier, L., Schachter, J., Schadendorf, D., Lesimple, T., Plummer, R., Ji, R., Zhang, P., Mookerjee, B., Legos, J., Kefford, R., Dummer, R. & Kirkwood, J. M. (2017). Adjuvante dabrafenib plus trametinib in stage III BRAF-mutated melanoma. The New England Journal of Medicine, 377(19), 1813-1823. doi:10.1056/NEJMoa1708539.

[53] Greaves, W. O., Verma, S., Patel, K. P., Davies, M. A., Barkoh, B. A., Galbincea, J. M., Yao, H., Lazar, A. J., Aldape, K. D., Medeiros, L. J. & Luthra, R. (2013). Frequency and spectrum of BRAF mutations in a restropective, single-institution study of 1112 cases of melanoma. Journal of Molecular Diagnosis, 15(2), 220-226. doi:10.1016/j.jmoldx.2012.10.002.

[54] Colombino, M., Capone, M., Lissia, A., Cossu, A., Rubino, C., De Giorgi, V., Massi, D., Fonsatti, E., Staibano, S., Nappi, O., Pagani, E., Casula, M., Manca, A., Sini, M. C., Franco, R., Botti, G., Caracò, C., Mozillo, N., Ascierto, P. A. & Palmieri, G. (2012).

BRAF/NRAS mutation frequencies among primary tumors and metástases in patients with melanoma. Journal of Clinical Oncology, 30(20), 2522-2529. doi:10.1200/JCO.2011.41.2452.

[55] Davie, H., Bignelli, G. R., Cox, G., Stephens, P., Edkins, S., Clegg, S., Teague, J., Woffendin, H., Garnett, M. J., Bottomley, W., Davis, N., Dicks, E., Ewing, R., Floyd, Y., Gray, K., Hall, S., Hawes, R., Hughes, J., Kosmidou, V., Menzies, A., Mould, C., Parker, A., Stevens, C., Watt, S., Hooper, S., Wilson, R., Jayatilake, H., Gusterson, B. A., Cooper, C., Shipley, J., Hargrave, D., Pritchard-Jones, K., Maitland, N., Chenevix-Trench, G., Riggins, G. J., Bigner, D. D., Palmieri, G., Cossu, A., Flanagan, A., Nicholson, A., Ho, J. W. C., Leung, S. Y., Yuen, S. T., Weber, B. L., Seigler, H. F., Darrow, T. L., Peterson, H., Marais, R., Marshall, C. J., Wooster, R., Stratton, M. R. & Futreal, P. A. (2002). Mutations of the BRAF gene in human cancer. Nature, 417(6892), 949-954. doi:10.1038/nature00766.

[56] Jakob, J. A., Bassett Jr, R. L., Ng, C. S., Curry, J. L., Joseph, R. W., Alvarado, G. C., Rohlfs, M. L., Richard, J., Gershenwald, J. E., Hwu, P., Kim, K. B., Lazar, A. J. & Davies, M. A. (2012). NRAS mutation status is and independent prognostic factor in metastaic melanoma. Cancer, 118(16), 4014-4023. doi:10.1002/cncr.26724.

[57] Flaherty, K. T., Hodi, F. S. & Fisher, D. E. (2012). From genes to drugs: targeted strategis for melanoma. Nature Review Cancer, 12(5), 349-361. doi:10.1038/nrc3218.

[58] Griffin, M., Scotto, D., Josephs, D. H., Mele, S., Crescioli, S., Bax, H. J., Pellizzari, G., Wynne, M. D., Nakamura, M., Hoffmann, R. M., Ilieva, K. M., Cheung, A., Spicer, J. F., Papa, S., Lacy, K. E. & Karagiannis, S. N. (2017). BRAF inhibitors: resistance and the promise of combination treatments for melanoma. Oncotarget, 8(44), 78174-78192. doi:10.18632/oncotarget.

[59] Tseng, H. W., Li, T. & Hsieh, J. S. (2013). Targeted agents for the treatment of melanoma: an overview. In Recent advances in the biology, therapy, and management of melanoma, edited by Davids, L., 231-251. London: In Tech. doi:10.5772/54938.

[60] Chambers, C. A., Kuhns, M. S., Egen, J. G. & Alisson, J. P. (2001). CLTA-4-mediated inhibition in regulation of T cell respondes: mechanism and manipulation in tumor immunotherapy. Annual Review of Immunology, 19, 565-594. doi:10.1146/ annurev.immunol.19.1.565.

[61] Acharya, U. H. & Jeter, J. M. (2013). Use of ipilimumab in the treatment of melanoma. Clinical Pharmacology: Advances and Applications, 5, (Suppl 1), 21–27. doi:10.2147/CPAA.S45884.

[62] Somasundaram, R. & Herlyn, M. (2015). Nivolumab in combination with ipilimumab for the treatment of melanoma. Expert Reviews in Anticancer Therapy, 15(10), 1135-1141. doi:10.1586/ 14737140.2015.1093418.

[63] Czarnecka, A. & Rutkowski, P. (2020). An update on the safety of nivolumab for the treatment of advanced melanoma. Expert Opinion on Drug Safety, 409-421. doi:10.1080/14740338.2020.1757068.

[64] Poole, R. M. (2014). Pembrolizumab: first global approval. Drugs, 74, 1973-1981. doi:10.1007/s40265-014-0314-5.

[65] Raman, S. S., Hecht, J. R. & Chan, E. (2019). Talimogene laherparepvec: review of its mechanism of action and clinical efficacy and safety. Immunotherapy, 11(8), 705-723. doi:10.2217/imt-2019-0033.

[66] Tarhini, A. A., Gogas, H. & Kirkwood, J. (2012). INF-α in treatment of melanoma. Journal of Immunology, 189(8), 3789-3793. doi:10.4049/jimmunol.1290060.

[67] Patel, J. N. & Walko, C. M. (2012). Sylatron: a pegylated interferon for use in melanoma. Annals of Pharmacotherapy, 46(6), 830-838. doi:10.1345/aph.1Q791.

[68] Amaria, R. N., Reuben, A., Cooper, Z. A. & Wargo, J. A. (2015). Update on use of aldesleukin for treatment of high-risk metastatic melanoma. Immuno Targets and Therapy, 4, 79-89. doi:10.2147/ITT.S61590.

[69] Mizui, M. (2019). Natural and modified IL-2 for the treatment of cancer and autoimune diseases. Clinical Immunology, 206, 63-70. doi:10.1016/j.clim.2018.11.002.

[70] Kim, J. & Park, E. J. (2002). Cytotoxic anticancer candidates from natural resoures. Current Medicinal Chemistry – Anticancer Agents, 2(4), 485-537. doi:10.2174/1568011023353949.

[71] Bhanot, A., Sharma, R. & Noolvi, M. N. (2011). Natural sources as potential anti-cancer agents: a review. International Journal of Phytomedicine, 3, 09-26.

[72] Newman, D. J. & Cragg, G. M. (2016). Natural products as sources of new drugs from 1981 to 2014. Journal of Natural Products, 79(3), 629-661. doi:10.1021/acs.jnatprod.

[73] Chinembiri, T. N., du Plessis, L. H., Gerber, M., Hamman, J. H. & du Plessis, J. (2014). Review of natural compounds for potential skin cancer treatment. Molecules, 19(8), 11679-11721. doi:10.3390/molecules190811679.

[74] Durkin, W. J., Ghanta, V. K., Balch, C. M., Davis, D. W. & Hiramoto, R. N. (1979). A methodological approach to the prediction of anticancer drug effect in humans. Cancer Research, 39(2 Pt 1), 402-407.

[75] Dobrynin, Y. V. & Vyshinskaya, G. V. (1980). *In vitro* anticancer drug sensitivity testing. Antibiotics and Chemotherapy, 28, 13-14. doi:10.1159/000386053.

[76] Atanasov, A. G., Waltenberger, B., Pferschy-Wenzig, E. V, Linderd, T., Wawroscha, C., Uhrine, P., Temmlf, V., Wanga, L., Schwaigerb, S., Heissa, E. H., Rollingera, J. M., Schusterf, D., Breusse, J. M., Bochkovg, V., Mihovilovicd, M. D., Koppa, B., Bauerc, R., Dirscha, V. & Stuppner, H. (2015). Discovery and resupply of pharmacologically active plant-derived natural products: a review. Biotechnology Advances, 33, 1582–1614. doi:10.1016/j.biotechadv.2015.08.001.

[77] Takenaka, T. (2001). Classical vs reverse pharmacology in drug discovery. BJU International, 88(Suppl 2), 7-10. doi:10.1111/j.1464-410x.2001.00112.x.

[78] Riedel, T., Demaria, O., Zava, O., Joncic, A., Gilliet, M. & Dyson, P. J. (2017). Drug repurposing approach identifies a synergistic drug combination of an antifungal agent and an

experimental organometallic drug for melanoma treatment. Molecular Pharmaceutics, 15(1), 116-126 doi:10.1021/ acs.molpharmaceut.7b00764.

[79] Carpenter, E. L., Chagani, S., Nelson, D., Cassidy, P. B., Laws, M., Ganguli-Indra, G. & Indra, A. K. (2019). Mitochondrial complex I inhibitor deguelin induces metabolic reprogramming and sensitizes vemurafenib-resistant BRAFV600E mutation bearing metastatic melanoma cells. Molecular Carcinogenesis, 1-11. doi:10.1002/mc.23068.

[80] Kim, Y., Tsang, T., Anderson, G. R., Posimo, J. M. & Brady, D. C. (2020). Inhibition of BCL2 family members increases the efficacy of copper chelation in BRAFV600E - driven melanoma. Cancer Research, 80, 1387–1400. doi:10.1158/0008-5472.CAN-19-1784.

[81] Zampieri, M., Sekar, K., Zamboni, N. & Sauer, U. (2017). Frontiers of high-throughput metabolomics. Current Opinion in Chemical Biology, 36, 15-23. doi:10.1016/j.cbpa.2016.12.006.

[82] Huang, M., Qi, T. F., Li, L., Zhang, G. & Wang, Y. (2018). A targeted quantitative proteomic approach assesses the reprogramming of small GTPases during melanoma metastasis. Cancer Research, 78(18), 5431-5445. doi:10.1158/0008-5472.CAN-17-3811.

[83] Miao, W., Li, L. & Wang, Y. (2018). A targeted proteomic approach for heat shock proteins reveals DNAJB4 as a suppressor for melanoma metastasis. Analytical Chemistry, 90(11), 6835–6842. doi:10.1021/acs.analchem.8b00986.

[84] Joshi, P., Seki, T., Kitamura, S., Bergano, A., Lee, B. & Perera, R. J. (2019). Transcriptome stability profiling using 5'- bromouridine IP chase (BRIC-seq) identifies novel and functional microRNA targets in human melanoma cells. RNA Biology, 16(10), 1355-1363. doi:10.1080/15476286.2019.1629769.

[85] Paulitschke, V., Eichhoff, O., Gerner, C., Paulitschke, P., Bileck, A., Mohr, T., Cheng, P. F., Leitner, A., Guenova, E., Saulite, I., Freiberger, S. N., Irmisch, A., Knapp, B., Zila, N., Chatziisaak, T., Stephan, J., Mangana, J., Kunstfeld, R., Pehamberger, H., Aebersold, R., Dummer, R. & Levesque, M. P. (2019). Proteomic identification of a marker signature for MAPKi resistance in melanoma. The EMBO Journal, 38, e95874. doi:10.15252/embj.201695874.

[86] Sutton, S. K., Carter, D. R., Kim, P., Tan, O., Arndt, G. M., Zhang, X. D., Baell, J., Noll, B. D., Wang, S., Kumar, N., McArthur, G. A., Cheung, B. B. & Marshall, G. M. (2016). A novel compound which sensitizes BRAF wild-type melanoma cells to vemurafenib in a TRIM16-dependent manner. Oncotarget, 7(32), 52166-52178. doi:10.18632/oncotarget.10700.

[87] Campos, L. E., Garibotto, F. M., Angelina, E., Kos, J., Tomašič, T., Zidar, N., Kikelj, D., Gonec, T., Marvanova, P., Mokry, P., Jampilek, J., Alvarez, S. E. & Enriz, R. D. (2019). Searching new structural scaffolds for BRAF inhibitors. An integrative study using theoretical and experimental techniques. Bioorganic Chemistry, 91, 103125. doi:10.1016/j.bioorg.2019.103125.

[88] Tang, H. & Chen, Y. (2015). Insight into molecular dynamics simulation of BRAF(V600E) and potent novel inhibitors for malignant melanoma. International Journal of Nanomedicine, 10, 3131–3146. doi:10.2147/IJN.S80150.

[89] Dextras, C., Dashnyam, M., Griner, L. A. M., Sundaresan, J., Chim, B., Yu, Z., Vodnala, S., Lee, C. R., Hu, X., Southall, N., Marugan, J. J., Jadhav, A., Restifo, N. P., Acquavella, N., Ferrer, M. & Singh, A. (2020). Identifcation of small molecule enhancers of immunotherapy for melanoma. Scientific Reports, 10, 5688. doi:10.1038/s41598-020-62369-1.

[90] Biswas, R., Chowdhury, N., Mukherjee, R. & Bagchi, A. (2018). Identification and analyses of natural compounds as potential inhibitors of TRAF6-Basigin interactions in melanoma using structure-based virtual screening and molecular dynamics simulations. Journal of Molecular Graphics and Modelling, 85, 281-293. doi:10.1016/j.jmgm.2018.09.008.

[91] Kontoyianni, M. (2017). Docking and virtual screening in drug discovery. In Proteomics for Drug Discovery: Methods and Protocols, Methods in Molecular Biology, edited by Lazar, I. M. et al., 1647, 255-266. Springer Science+Business Media LLC. doi:10.1007/978-1-4939-7201-2_18.

[92] Forli, S. (2015). Charting a path to success in virtual screening. Molecules, 20, 18732-18758. doi:10.3390/molecules201018732.

[93] Lin, X., Li, X. & Lin, X. (2020). A review on applications of computational methods in drug screening and design. Molecules, 25, 1375. doi:10.3390/molecules25061375.

[94] Wang, Z., Lu, Y., Seibel, W., Miller, D. D. & Li, W. (2009). Identifying novel molecular structures for advanced melanoma by ligand-based virtual screening. Journal of Chemical Information and Modeling, 49, 1420–1427. doi:10.1021/ci800445a.

[95] Lionta, E., Spyrou, G., Vassilatis, D. K. & Cournia, Z. (2014). Structure-based virtual screening for drug discovery: principles, applications and recent advances. Current Topics in Medicinal Chemistry, 14, 1923-1938. doi:10.2174/ 1568026614666140929124445.

[96] Banegas-Luna, A., Cerón-Carrasco, J. P. & Perez-Sánchez, H. (2018). A review of ligand-based virtual screening web tools and screening algorithms in large molecular databases in the age of big data. Future Medicinal Chemistry, 10(22), 2641–2658. doi:10.4155/fmc-2018-0076.

[97] Zhang, X., Huang, Z., Guo, Y., Xiao, T., Tang, L., Zhao, S., Wu, L., Su1, J., Zeng, W., Huang, H., Li, Z., Tao, J., Zhou, J., Chen, X. & Peng, C. (2020). The phosphorylation of CD147 by Fyn plays a critical role for melanoma cells growth and metastasis. Oncogene, 39, 4183–4197. doi:10.1038/s41388-020-1287-3.

[98] Mancuso, P., Tricarico, R., Bhattacharjee, V., Cosentino, L., Kadariya, Y., Jelinek, J., Nicolas, E., Einarson, M., Beeharry, N., Devarajan, K., Katz, R. A., Dorjsuren, D. G., Sun, H., Simeonov, A., Giordano, A., Testa, J. R., Davidson, G., Davidson, I., Larue, L., Sobol, R. W., Yen, T. J. & Bellacosa, A. (2019). Thymine DNA glycosylase as a novel target for melanoma. Oncogene, 38, 3710–3728. doi:10.1038/s41388-018-0640-2.

[99] Ambrosini, G., Do, C., Tycko, B., Realubit, R. B., Karan, C., Musi, E., Carvajal, R. D., Chua, V., Aplin, A. E. & Schwartz, G. K. (2019). Inhibition of NF-κB-dependent

signaling enhances sensitivity and overcomes resistance to BET inhibition in uveal melanoma. Cancer Research, 79(9), 2415-2425. doi:10.1158/0008-5472.CAN-18-3177.

[100] An, W. F. & Tolliday, N. (2010). Cell-based assays for high-throughput screening. Molecular Biotechnology, 45, 180–186. doi:10.1007/s12033-010-9251-z.

[101] Brogi, S. (2019). Computational Approaches for Drug Discovery. Molecules, 24, 3061. doi:10.3390/molecules24173061.

[102] Moreira, G. A., Lima, G. D. A., Siqueira, R. P., Barros, M. V. A., Adjanohoun, A. L. M., Santos, V. C., Barbosa, E. A. A., Loterio, R. K., Paiva, J. C., Gonçalves, V. H. S., Viol, L. C. S., Marques-da-Silva, E. A., Júnior, A. S., Almeida, M. R., Fietto, J. L. R., Machado-Neves, M., Ferreira, R. S., Teixeira, R. R. & Bressan, G. C. (2018). Antimetastatic effect of the pharmacological inhibition of serine/arginine-rich protein kinases (SRPK) in murine melanoma. Toxicology and Applied Pharmacology, 356, 214–223. doi:10.1016/j.taap.2018.08.012.

[103] Wang, J., Fang, P., Chase, P., Tshori, S., Razin, E., Spicer, T. P., Scampavia, L., Hodder, P. & Guo, M. (2017). Development of an HTS-compatible assay for discovery of melanoma-related microphthalmia transcription factor disruptors using alphascreen technology. SLAS Discovery, 22(1), 58–66. doi:10.1177/1087057116675274.

[104] Arya, J. S., Joseph, M. M., Sherin, D. R., Nair, J. B., Manojkumar, T. K. & Maiti, K. K. (2019). Exploring mitochondria-mediated intrinsic apoptosis by new phytochemical entities: an explicit observation of cytochrome c dynamics on lung and melanoma cancer cells. Journal of Medicinal Chemistry, 62, 8311−8329. doi:10.1021/acs.jmedchem.9b01098.

[105] Scherer, W. F., Syverton, J. T. & Gey, G. O. (1953). Studies on the propagation *in vitro* of Poliomyelitis viruses. The Journal of Experimental Medicine, 97, 695-710. doi:10.1084/jem.97.5.695.

[106] Barretina, J., Caponigro, G., Stransky, N., Venkatesan, K., Margolin, A. A., Kim, S., Wilson, C. J., Lehár, J., Kryukov, G. V., Sonkin, D., Reddy, A., Liu, M., Murray, L., Berger, M. F., Monahan, J. E., Morais, P., Meltzer, J., Korejwa, A., Jané-Valbuena, J., Mapa, F. A., Thibault, J., Bric-Furlong, E., Raman, P., Shipway, A., Engels, I. H., Cheng, J., Yu, G. K., Yu, J., Aspesi, P., de Silva, M., Jagtap, K., Jones, M. D., Wang, L., Hatton, C., Palescandolo, E., Gupta, S., Mahan, S., Sougnez, C., Onofrio, R. C., Liefeld, T., MacConaill, L., Winckler, W., Reich, M., Li, N., Mesirov, J. P., Gabriel, S. B., Getz, G., Ardlie, K., Chan, V., Myer, V. E., Weber, B. L., Porter, J., Warmuth, M., Finan, P., Harris, J. L., Meyerson, M., Golub, T. R., Morrissey, M. P., Sellers, W. R., Schlegel, R. & Garraway, L. A. (2012). The cancer cell line encyclopedia enables predictive modeling of anticancer drug sensitivity. Nature, 483(7391), 603–607. doi:10.1038/nature11003.

[107] Garnett, M. J., Edelman, E. E., Heidorn, S. J., Greenman, C. D., Dastur, A., Lau, K. W., Greninger, P., Thompson, I. R., Luo, X., Soares, J., Liu, Q., Iorio, F., Surdez, D., Chen, L., Milano, R. J., Bignell, G. R., Tam, A. T., Davies, H., Stevenson, J. A., Barthorpe, S., Lutz, S. R., Kogera, F., Lawrence, K., McLaren-Douglas, A., Mitropoulos, X., Mironenko, R., Thi, H., Richardson, L., Zhou, W., Jewitt1, F., Zhang, T., O'Brien, P., Boisvert, J. L., Price, S., Hur, W., Yang, W., Deng, X., Butler, A., Choi, H. G., Chang, J. W., Baselga, J., Stamenkovic, I., Engelman, J. A., Sharma, S. W., Delattre, O., Saez-Rodriguez, J., Gray, N.

S., Settleman, J., Futreal, P. A., Haber, D. A., Stratton, M. R., Ramaswamy, S., McDermott, U. & Benes, C. H. (2012). Systematic identification of genomic markers of drug sensitivity in cancer cells. Nature, 483(7391), 570–575. doi:10.1038/nature11005.

[108] Gonzalez-Nicolini, V. & Fusseneggera, M. (2005). *In vitro* assays for anticancer drug discovery—a novel approach based on engineered mammalian cell lines. Anti-Cancer Drugs, 16(3), 223–228. doi:10.1097/00001813-200503000-00001.

[109] Wilding, J. L. & Bodmer, W. F. (2014). Cancer cell lines for drug discovery and development. Cancer Research, 74(9), 2377-2384. doi:10.1158/0008-5472.CAN-13-2971.

[110] Keijzer, W., Mulder, M. P., Langeveld, J. C. M., Smit, E. M. E., Bos, J. L., Bootsma, D. & Hoeijmakers, J. H. J. (1989). Establishment and characterization of a melanoma cell line from a xeroderma pigmentosum patient: activation of N-ras at a potential pyrimidine dimer site. Cancer Research, 49, 1229-1235. PMID: 2645048.

[111] Zaffaroni, N., Villa, R., Silvestro, L., Sanfilippo, O. & Silvestrini, R. (1990). Cytotoxic activity of azelaic acid against human melanoma primary cultures and established cell lines. Anticancer Research, 10(6), 1599-602. PMID: 2285231.

[112] Van Muijen, G. N. P., Jansen, K. F. J., Cornelissen, I. M. H. A., Smeets, D. F. C. M., Beck, J. L. M. & Ruiter, D. J. (1991). Establishment and characterization of a human melanoma cell line (MV3) which is highly metastatic in nude mice. International Journal of Cancer, 48, 85-91. doi:10.1002/ijc.2910480116.

[113] Chen, K. G., Leapman, R. D., Zhang, G., Lai, B., Valencia, J. C., Cardarelli, C. O., Vieira, W. D., Hearing, V. J. & Gottesman, M. M. (2009). Influence of melanosome dynamics on melanoma drug sensitivity. Journal of the National Cancer Institute, 101, 1256–1271. doi:10.1093/jnci/djp259.

[114] Peter, I., Mezzacasa, A., LeDonne, P., Dummer, R. & Hemmi, S. (2001). Comparative analysis of immunocritical melanoma markers in the mouse melanoma cell lines B16, K1735 and S91-M3. Melanoma Research, 11, 21-30. doi:10.1097/00008390-200102000-00003.

[115] Giavazzi, R. & Decio, A. (2014). Syngeneic murine metastasis models: B16 melanoma. Methods in Molecular Biology, 1070, 131–140. doi:10.1007/978-1-4614-8244-4_10.

[116] Alvarez, E. (2010). B16 Murine Melanoma: Historical Perspective on the Development of a Solid Tumor Model. In Tumor Models in Cancer Research, Cancer Drug Discovery and Development, edited by Teicher, B. A., 79-95. Watertown: Springer Link. doi:10.1007/ 978-1-60761-968-0_4.

[117] Fidler, I. J. (1973). Selection of sucessive tumour lines for metastasis. Nature: New Biology, 242, 148-149. doi:10.1038/newbio242148a0.

[118] Melnikova, V. O., Bolshakov, S. V., Walker, C. & Ananthaswamy, H. M. (2004). Genomic alterations in spontaneous and carcinogen-induced murine melanoma cell lines. Oncogene, 23, 2347–2356. doi:10.1038/sj.onc.1207405.

[119] Vincent, K. M. & Postovit, L. M. (2017). Investigating the utility of human melanoma cell lines as tumour models. Oncotarget, 8(6), 10498-10509. doi:10.18632/oncotarget.14443.

[120] Kim, H. Y., Lee, H., Kim, S. H., Jin, H., Bae, J. & Choi, H. K. (2017). Discovery of potential biomarkers in human melanoma cells with different metastatic potential by metabolic and lipidomic profiling. Scientific Reports, 7, 8864. doi:10.1038/s41598-017-08433-9.

[121] Huang, Y. & Vakoc, C. R. (2016). A biomarker harvest from one thousand cancer cell lines. Cell, 166, 536-537. doi:10.1016/j.cell.2016.07.010.

[122] Dahl, C. & Guldberg, P. (2007). The genome and epigenome of malignant melanoma. Acta Pathologica, Microbiologica, et Immunologica Scandinavica, 115, 1161–76. doi:10.1111/j.1600-0463.2007.apm_855.xml.x.

[123] Nikiforov, Y. E. & Nikiforova, M. N. (2011). Molecular genetics and diagnosis of thyroid cancer. Nature Reviews Endocrinology, 7, 569–580. doi:10.1038/nrendo.2011.142.

[124] Yajima, I., Kumasaka, M. Y., Thang, N. D., Goto, Y., Takeda, K., Yamanoshita, O., Iida, M., Ohgami, N., Tamura, H., Kawamoto, Y. & Kato, M. (2012). RAS/RAF/MEK/ERK and PI3K/PTEN/AKT signaling in malignant melanoma progression and therapy. Dermatology Research and Practice, 354191. doi:10.1155/2012/354191.

[125] Aasen, S. N., Parajuli, H., Hoang, T., Feng, Z., Stokke, K., Wang, J., Roy, K., Bjerkvig, R., Knappskog, S. & Thorsen, S. (2019). Effective treatment of metastatic melanoma by combining MAPK and PI3K signaling pathway inhibitors. International Journal of Molecular Sciences, 20, 4235. doi:10.3390/ijms20174235.

[126] Kapałczyńska, M., Kolenda, T. T., Przybyła, W., Zajączkowska, M., Teresiak, A., Filas, V., Ibbs, M., Bliźniak, R., Łuczewski, Ł. & Lamperska, K. (2018). 2D and 3D cell cultures – a comparison of different types of cancer cull cultures. Archives of Medical Science, 14(4), 910–919. doi:10.5114/aoms.2016.63743.

[127] Agarwal, G., Carcache, P. J. B., Addo, E. M. & Kinghorn, A. D. (2020). Current status and contemporary approaches to the discovery of antitumor agents from higher plants. Biotechnology Advances, 38, 1–27. doi:10.1016/j.biotechadv.2019.01.004.

[128] Imamura, Y., Mukohara, T., Shimono, Y., Funakoshi, Y., Chayahara, N., Toyoda, M., Kiyota, N., Takao, S., Kono, S., Nakatsura, T. & Minami, H. (2015). Comparasion of 2D- and 3D-culture models as drug-testing platforms in breast cancer. Oncology Reports, 33, 1837–1843. doi:10.3892/or.2015.3767.

[129] Pampaloni, F., Reynaud, E. G. & Stelzer, E. H. K. (2007). The third dimension bridges the gap between cell culture and live tissue. Nature Reviews: Molecular Cell Biology, 8, 839–845. doi:10.1038/nrm2236.

[130] Fang, Y. & Eglen, R. M. (2017). Three-dimensional cell cultures in drug discovery and development. SLAS Discovery, 22(5), 456–472. doi:10.1177/1087057117696795.

[131] Jensen, J. B. & Parmar, M. (2006). Strengths and limitations of the neurosphere culture system. Molecular Neurobiology, 34, 153–61. doi:10.1385/MN:34:3:153.

[132] Pandya, H. J., Dhingra, K., Prabhakar, D., Chandrasekar, V., Natarajan, S. K., Vasan, A. S., Kulkarni, A. & Shafiee, H. (2017). A microfluidic platform for drug screening in a 3D cancer microenvironment. Biosensors and Bioelectronics, 94, 632–642. doi:10.1016/j.bios.2017.03.054.

[133] Fontoura, J. C., Viezzer, C., Dos Santos, F. G., Ligabue, R. A., Weinlich, R., Puga, R. D., Antonow, D., Severino, P. & Bonorino, C. (2020). Comparison of 2D and 3D cell culture models for cell growth, gene expression and drug resistance. Materials Science and Engineering: C, 107, 110264. doi:10.1016/j.msec.2019.110264.

[134] Menyhárt, O., Harami-Papp, H., Sukumar, S., Shäfer, R., Magnani, L., Barrios, O. & Győrffy, B. (2016). Guidelines for the selection of functional assays to evaluate the hallmarks of cancer. Biochimica et Biophysica Acta, 1866, 300–319. doi:10.1016/j.bbcan.2016.10.002.

[135] Riss, T., Niles, A., Moravec, R., Karassina, N. & Vidugiriene, J. (2019). Cytotoxicity Assays: *In Vitro* Methods to Measure Dead Cells. In Assay Guidance Manual, edited by Sittampalam, G. S., Grossman, A., Brimacombe, K., et al. Bethesda (MD): Eli Lilly & Company and the National Center for Advancing Translational Sciences.

[136] Mosmann, T. (1983). Rapid colorimetric assay for cellular growth and survival: application to proliferation and cytotoxicity assays. Journal of Immunological Methods, 16, 693–697. doi:10.1016/0022-1759(83)90303-4.

[137] Stockert, J. C., Horobin, R. W., Colombo, L. L. & Blázquez-Castro, A. (2018). Tetrazolium salts and formazan products in Cell Biology: Viability assessment, fluorescence imaging, and labeling perspectives. Acta Histochemica, 120, 159–167. doi:10.1016/j.acthis.2018.02.005.

[138] Orellana, E. A. & Kasinski, A. L. (2016). Sulforhodamine B (SRB) assay in cell culture to investigate cell proliferation. Bio-Protocol, 6(21), e1984. doi:10.21769/BioProtoc.1984.

[139] Abildgaard, C. & Guldberg, P. (2015). Molecular drivers of cellular metabolic reprogramming in melanoma. Trends in Molecular Medicine, 21, 164–71. doi:10.1016/j.molmed.2014.12.007.

[140] Blackburn, E. H. (1991). Structure and function of telomeres. Nature, 350(6319), 569-573. doi:10.1038/350569a0.

[141] Skvortsov, D. A., Zvereva, M. E., Shpanchenko, O. V. & Dontsova, O. A. (2011). Assays for detection of telomerase activity. Acta Naturae, 3(1), 48–68. PMID: 22649673.

[142] Banfalvi, G. (2017). Methods to detect apoptotic cell death. Apoptosis, 22, 306–323. doi:10.1007/s10495-016-1333-3.

[143] Elmore, S. (2007). Apoptosis: a review of programmed cell death. Toxicologic Pathology, 35(4), 495–516. doi:10.1080/ 01926230701320337.

[144] Auerbach, R., Lewis, R., Shinners, B., Kubai, L. & Akhtar, N. (2003). Angiogenesis assays: a critical overview. Clinical Chemistry, 49(1), 32–40. doi:10.1373/49.1.32.

[145] Albini, A. & Benelli, R. (2007). The chemoinvasion assay: a method to assess tumor and endothelial cell invasion and its modulation. Nature Protocols, 2, 504–511. doi:10.1038/nprot.2006.466.

[146] Lambert, E., Dassé, E., Haye, B. & Petitfrère, E. (2004). TIMPs as multifacial proteins. Critical Reviews in Oncology/Hematology, 49, 187–198. doi:10.1016/j.critrevonc.2003.09.008.

[147] Lu, Z., Lu, N., Li, C., Li, F., Zhao, K., Lin, B. & Guo, Q. (2012). Oroxylin A inhibits matrix metalloproteinase-2/9 expression and activation by up-regulating tissue inhibitor of metalloproteinase-2 and suppressing the ERK1/2 signaling pathway. Toxicology Letters, 209, 211–220. doi:10.1016/j.toxlet.2011.12.022.

[148] Ansari, M. A., Shaikh, S., Muteeb, G., Rizvi, S. M. D., Shakil, S., Alam, A., Tripathi, R., Ghazal, F., Rehman, A., Ali, S. Z., Pandey, A. K. & Ashraf, G. M. (2013). Role of matrix metalloproteinases in cancer. In Advances in Protein Chemistry, edited by Ashraf, G. M. and Sheikh, I. A. Foster City: OMICS Group eBooks. doi:10.4172/978-1-63278-016-4-017.

[149] Guan, X. (2015). Cancer metastases: challenges and opportunities. Acta Pharmaceutica Sinica B, 5(5), 402–418. doi:10.1016/j.apsb.2015.07.005.

[150] Cui, N., Hu, M. & Khalil, R. A. (2017). Biochemical and Biological Attributes of Matrix Metalloproteinases. In Progress in Molecular Biology and Translational Science, edited by Tplow, D. Philadelphia: Elsevier. doi:10.1016/bs.pmbts.2017.02.005.

[151] Lin, H., Chen, J., Chou, D. & Wang, C. (2010). Protocatechuic acid inhibits cancer cell metastasis involving the down-regulation of Ras/Akt/NF-kB pathway and MMP-2 production by targeting RhoB activation. British Journal of Pharmacology, 162, 237–254. doi:10.1111/j.1476-5381.2010.01022.x.

[152] Ross, S. H., Spanjaard, E., Post, A., Vliem, M. J., Kristyanto, H., Bos, J. L. & Rooij, J. (2012). Rap1 can bypass the FAK-Src-Paxillin cascade to induce cell spreading and focal adhesion formation. PLoS ONE, 7(11), e50072. doi:10.1371/journal.pone.0050072.

[153] Liberti, M. V. & Locasale, J. W. (2016). The warburg effect: how does it benefit cancer cells? Trends in Biochemical Sciences, 41(3), 211-218. doi:10.1016/j.tibs.2015.12.001.

[154] DeBerardinis, R. J. & Chandel, N. S. (2020). We need to talk about the Warburg effect. Nature Metabolism, 2, 127–129. doi:10.1038/s42255-020-0172-2.

[155] Traverso, N., Ricciarelli, R., Nitti, M., Marengo, B., Furfaro, A. L., Pronzato, M. A., Marinari, U. M. & Domenicotti, C. (2013). Role of glutathione in cancer progression and chemoresistance. Oxidative Medicine and Cellular Longevity, 972913. doi:10.1155/2013/972913.

[156] Carretero, J., Obrador, E., Anasagasti, M. J., Martin, J. J., Vidal-Vanaclocha, F. & Estrela, J. M. (1999). Growth-associated changes in glutathione content correlate with liver

metastatic activity of B16 melanoma cells. Clinical and Experimental Metastasis, 17(7), 567–574. doi:10.1023/a:1006725226078.

[157] Almeida, A. A., Lima, G. D. A., Simão, M. V. R. C., Moreira, G. A., Siqueira, R. P., Zanatta, A. C., Vilegas, W., Machado-Neves, M., Bressan, G. C. & Leite, J. P. V. (2020). Screening of plants from the Brazilian Atlantic Forest let to identification of Athenaea velutina (Solanacea) as a novel source of antimetastatic agents. International Journal of Experimental Pathology, 54, 1-9. doi:10.1111/iep.12351.

[158] Siqueira, R. P., Caetano, M. M. M., De Souza, L. Â., Dos Passos, P. M. S., Simaroli, N. B., Barros, M. V. A., De SOUZA, A. P. M., De Oliveira, L. L., Júnior, A. S., Fietto, J. L. R., Teixeira, R. R., Teixeira, F. R. & Bressan, G. C. (2020). Combined SRPK and AKT pharmacological inhibition is synergistic in T-cell acute lymphoblastic leukemia cells. Toxicology *In Vitro*, 65, 104777. doi:10.1016/j.tiv.2020.104777.

[159] Vale. J. A. Souza, A. P. M., Lima, G. D. A., Gonçalves, V. H. S, Moreira, G. A., Barros, M. V. A., Pereira, W. L., Lazaroni e Merchid, N. C., Fietto, J. L. R., Bressan, G. C., Teixeira, R. R. & Neves, M. M. (2020). Effect of the topical administration of N-(2-(4-bromophenylamino)-5-(trifluoromethyl)phenyl)nicotinamide compound in a murine subcutaneous melanoma model. Anti-Cancer Drugs, 31(7): 718-727.

[160] Franken, N. A. P., Rodermond, H. M., Stap, J., Haveman, J. & van Bree, C. (2006). Clonogenic assay of cells *in vitro*. Nature Protocols, 1(5), 2325–2319. doi:10.1038/nprot.2006.339.

[161] Strober, W. (2001). Trypan blue exclusion test of cell viability. Current Protocols of Immunology, 21(1). doi:10.1002/ 0471142735.ima03bs21.

[162] Korzeniewski, C. & Callewaert, D. M. (1983). An enzyme-release assay for natural cytotoxicity. Journal of Immunological Methods, 64(3), 313–20. doi:10.1016/0022-1759(83)90438-6.

[163] Wojtowicz, J. & Kee, N. (2006). BrdU assay for neurogenesis in rodents. Nature Protocols, 1, 1399–1405. doi:10.1038/ nprot.2006.224.

[164] Ribble, D., Goldstein, N. B., Norris, D. A. & Shellman, Y. G. (2005). A simple technique for quantifying apoptosis in 96-well plates. BMC Biotechnology, 5(12), 1–7. doi:10.1186/1472-6750-5-12.

[165] Chazotte, B. (2011). Labeling Nuclear DNA with Hoechst 33342. Cold Spring Harbor Protocols. doi:10.1101/pdb.prot5557.

[166] Chazotte, B. (2011). Labeling Nuclear DNA Using DAPI. Cold Spring Harbor Protocols, (1). doi:10.1101/pdb.prot5556.

[167] Riccardi, C. & Nicoletti, I. (2006). Analysis of apoptosis by propidium iodide staining and flow cytometry. Nature Protocols, 1(3), 1458–1461. doi:10.1038/nprot.2006.238.

[168] Li, X. & Darzynkiewicz, Z. (1995). Labelling DNA strand breaks with BrdUTP. Detection of apoptosis and cell proliferation. Cell Proliferation, 28(1), 571–579. doi:10.1111/j.1365-2184.1995.tb00045.x.

[169] Koopman, G., Reutelingsperger, C. P., Kuijten, G. A., Keehnen, R. M., Pals, S. T. & van Oers, M. H. (1994). Annexin V for flow cytometric detection of phosphatidylserine expression on B cells undergoing apoptosis. Blood, 84 (5), 1415–1420. PMID: 8068938.

[170] Reers, M., Smith, T. W. & Chen, L. B. (1991). J-aggregate formation of a carbocyanine as a quantitative fluorescent indicator of membrane potential. Biochemistry, 30(18), 4480–4486. doi:10.1021/ bi00232a015.

[171] Waterhouse, N. & Trapani, J. (2003). A new quantitative assay for cytochrome c release in apoptotic cells. Cell Death & Differentiation, 10, 853–855. doi:10.1038/sj.cdd.4401263.

[172] Golsteyn, R. M. (2005). Cdk1 and Cdk2 complexes (cyclin dependent kinases) in apoptosis: a role beyond the cell cycle. Cancer Letters, 217(2), 129–138. doi:10.1016/j.canlet.2004.08.005.

[173] Porebska, I., Wyrodek, E., Kosacka, M., Adamiak, J., Jankowska, R. & Harłozińska-Szmyrka, A. (2006). Apoptotic markers p53, Bcl-2 and Bax in primary lung cancer. *In Vivo*, 20(5), 599–604. PMID: 17091766.

[174] Mizukami, S., Kikuchi, K., Higuchi, T., Urano, Y., Mashima, T., Tsuruo, T. & Nagano, T. (1999). Imaging of caspase-3 activation in HeLa cells stimulated with etoposide using a novel fluorescent probe. FEBS Letters, 453(3), 356–360. doi:10.1016/s0014-5793(99)00755-3.

[175] Pozarowski, P. & Darzynkiewicz, Z. (2004). Analysis of cell cycle by flow cytometry. Methods in Molecular Biology, 281, 301-11. doi:10.1385/1-59259-811-0:301.

[176] Arnaoutova, I., George, J., Kleinman, H. K. & Benton, G. (2009). The endothelial cell tube formation assay on basement membrane turns 20: state of the science and the art. Angiogenesis, 12(3), 267–274. doi:10.1007/s10456-009-9146-4.

[177] Inoue, T., Kibata, K., Suzuki, M., Nakamura, S., Motoda, R. & Orita, K. (2000). Identification of a vascular endothelial growth factor (VEGF) antagonist, sFlt-1, from a human hematopoietic cell line NALM-16. FEBS Letters, 469(1), 14–18. doi:10.1016/s0014-5793(00)01246-1.

[178] Liang, C. C., Park, A. Y. & Guan, J. L. (2007). *In vitro* scratch assay: a convenient and inexpensive method for analysis of cell migration *in vitro*. Nature Protocols, 2(2), 329–333. doi:10.1038/nprot.2007.30.

[179] Humphries, M. J. (1998). Cell-substrate adhesion assays. Current Protocols in Cell Biology, 9.1.1-9.1.11. doi:10.1002/ 0471143030.cb0901s00.

[180] Yuan, Y., Zhang, J., Wang, M., Mei, B., Guan, Y. & Liang, G. (2013). Detection of glutathione *in vitro* and in cells by the controlled self-assembly of nanorings. Analytical Chemistry, 85(3), 1280-1284. doi:10.1021/ac303183v.

[181] TeSlaa, T. & Teitell, M. A. (2014). Techniques to monitor glycolysis. Methods in Enzymology, 542, 91–114. doi:10.1016/B978-0-12-416618-9.00005-4.

[182] Misfeldt, M. L. & Grimm, D. R. (1994). Sinclair miniature swine: an animal model of human melanoma. Veterinary Immunology and Immunopathology, 43, 167-175. doi:10.1016/0165-2427(94)90133-3.

[183] Horak, V., Palanova, A., Cizkova, J., Miltrova, V., Vodicka, P. & Kupcova, H. (2019). Skalnikova Melanoma-Bearing Libechov Minipig (MeLiM): the unique swine model of hereditary. Metastatic Melanoma Genes, 10, 915. doi:10.3390/genes10110915.

[184] Cagan, R. L., Zon, L. I. & White, R. M. (2019). Modeling cancer with flies and fish. Developmental Cell, 49, 317–324. doi:10.1016/j.devcel.2019.04.013.

[185] Bootorabi, F., Manouchehri, H., Changizi, R., Barker, H., Palazzo, E., Saltari, A., Parikka, M., Pincelli, C. & Aspatwar, A. (2017). Zebrafish as a model organism for the development of drugs for skin cancer. International Journal of Molecular Sciences, 18, 1550. doi:10.3390/ijms18071550.

[186] Van der Ent, W., Burrello, C., Lange, M. J., van der Velden, P. A., Jochemsen, A. G., Jager, M. J. & Snaar-Jagalska, B. E. (2015). Embryonic zebrafish: different phenotypes after injection of human uveal melanoma cells. Ocular Oncology and Pathology, 1, 170–181. doi:10.1159/000370159.

[187] McKinney, A. J. & Holmen, S. L. (2011). Animal Models of Melanoma: A Somatic Cell Gene Delivery Mouse Model Allows Rapid Evaluation of Genes Implicated in Human Melanoma. Chinese Journal of Cancer, 30, 153–162. doi:10.5732/cjc.011.10007.

[188] Bobek, V., Kolostova, K., Pinterova, D., Kacprzak, G., Adamiak, J., Kolodziej, J., Boubelik, M., Kubecova, M. & Hoffman, R. M. (2010). A clinically relevant, syngeneic model of spontaneous, highly metastatic B16 mouse melanoma. Anticancer Research, 5, 4799–4803. PMID: 21187455.

[189] Herlyn, M. & Fukunaga-Kalabis, M. (2010). What is a good model for melanoma? Journal of Investigative Dermatology, 130, 911–912. doi:10.1038/jid.2009.441.

[190] Kuzu, O. F., Nguyen, F. D., Noory, M. A. & Sharma, A. (2015). Current state of animal (mouse) modeling in melanoma research. Cancer Growth and Metastasis, 8, 81–94. doi:10.4137/ CGM.S21214.

[191] Nakamura, K., Yoshikawa, N., Yamaguchi, Y., Kagoto, S., Shimozuka, K. & Kunitomo, M. (2002). Characterization of mouse melanoma cell lines by their mortal malignancy using an experimental metastatic model. Life Science, 70(7), 791–798. doi:10.1016/s0024-3205(01)01454-0.

[192] Perego, M., Tortoreto, M., Tragni, G., Mariani, L., Deho, P., Carbone, A., Santinami, A., Patuzzo, R., Mina, P. D., Villa, A., Pratesi, G., Cossa, G., Perego, P., Daidone, M. G. & Alison, M. R. (2010). Heterogeneous phenotype of human melanoma cells with *in vitro* and *in vivo* features of tumorinitiating cells. Journal of Investigative Dermatology, 130, 1877–1886. doi:10.1038/jid.2010.69.

[193] Beaumont, K. A., Mohana-Kumaran, N. & Haass, N. K. (2013). Modeling melanoma *in vitro* and *in vivo*. Healthcare, 2, 27–46. doi:10.3390/healthcare2010027.

[194] Zhang, G. J., Chen, T. B., Bednar, B., Connolly, B. M., Hargreaves, R., Sur, C. & Williams, Jr. D. L. (2007). Optical imaging of tumor cells in hollow fibers: evaluation of the antitumor activities of anticancer drugs and target validation. Neoplasia, 9(8), 652 – 661. doi:10.1593/neo.07421.

[195] Mi, Q., Pezzuto, J. M., Farnsworth, N. R., Wani, M. C., Kinghorn, A. D. & Swanson, S. M. (2009). Use of the *in vivo* hollow fiber assay in natural products anticancer drug discovery. Journal of Natural Products, 72(3), 573–580. doi:10.1021/np800767a.

[196] Merlino, G., Flaherty, K., Pesantes, N. A., Aplin, A., Holmen, S., Dyke, T. V. & Herlyn, M. (2013). The future of preclinical mouse models in melanoma treatment is now. Pigment Cell & Melanoma Research, 26, E8–14. doi:10.1111/pcmr.12099.

[197] Choi, Y., Lee, S., Kim, K., Kim, S. H., Chung, Y. J. & Lee, C. (2018). Studying cancer immunotherapy using patient-derived xenografts (PDXs) in humanized mice. Experimental & Molecular Medicine, 50, 1–9. doi:10.1038/s12276-018-0115-0.

[198] Harris, A. L., Joseph, R. W. & Copland, J. A. (2016). Patient-derived tumor xenograft models for melanoma drug discovery. Expert Opinion on Drug Discovery, 11, 895–906. doi:10.1080/17460441.2016.1216968.

[199] Kopetz, S., Lemos, R. & Powis, G. (2012). The promise of patient-derived xenografts: the best laid plans of mice and men. Clinical Cancer Research, 18(19), 5160–5162. doi:10.1158/1078-0432.CCR-12-2408.

[200] Quintana, E., Piskounova, E., Shackleton, M., Weinberg, D., Eskiocak, U., Fullen, D. R., Johnson, T. M. & Morrison, S. J. (2012). Human melanoma metastasis in NSG mice correlates with clinical outcome in patients. Science Translational Medicine, 4(159), 159ra149–159ra149. doi:10.1126/scitranslmed.3004599.

[201] Butterworth, K. T. (2019). Evolution of the supermodel: progress in modelling radiotherapy response in mice. Clinical Oncology, 31, 272e282. doi:10.1016/j.clon.2019.02.008.

[202] Lelliott, E. J., Cullinane, C., Martin, C. A., Walker, R., Ramsbottom, K. M., Souza-Fonseca-Guimaraes, F., Abuhammad, S., Michie, J., Kirby, L., Young, R. J., Slater, A., Lau, P., Meeth, K., Oliaro, J., Haynes, N., McArthur, G. A. & Sheppard, K. E. (2019). A novel immunogenic mouse model of melanoma for the preclinical assessment of combination targeted and immune-based therapy. Scientific Reports, 9, 1225. doi:10.1038/s41598-018-37883-y.

[203] Neagu, M., Caruntu, C., Constantin, C., Boda, D., Zurac, S., Spandidos, D. A. & Tsatsakis, A. M. (2016). Chemically induced skin carcinogenesis: Updates in experimental models (Review). Oncology Reports, 35, 2516-2528. doi:10.3892/or.2016.4683.

CAPÍTULO 3 – ARTIGO DE PESQUISA 1

Synthesis of Novel Cinnamides and a Bis Cinnamate Bearing 1,2,3-Triazole Functionalities with Antiproliferative and Antimetastatic Activities on Melanoma Cells

Fabíola S. Santos[1]§, Juliana A. do Vale[2]§,
Lucas da S. Santos[1], Talita B. Gontijo[1], Graziela D. A. Lima[2], Leandro L. de Oliveira[2],
Mariana Machado-Neves[2], Róbson R. Teixeira[3], Rossimiriam P. de Freitas[1]

[1]Department of Chemistry, Universidade Federal de Minas Gerais,
Belo Horizonte, Minas Gerais State, Brazil
[2]Department of General Biology, Universidade Federal de Viçosa,
Viçosa, Minas Gerais State, Brazil
[3]Department of Chemistry, Universidade Federal de Viçosa,
Viçosa, Minas Gerais State, Brazil

§These authors contributed equally to this work

Publicado: Journal of the Brazilian Chemical Society, Vol. 32, No. 12, 2174-2185, 2021

ABSTRACT

The present investigation describes the synthesis of novel cinnamides and a bis cinnamate bearing 1,2,3-triazole functionalities and investigation of their antiproliferative and antimetastatic effects on melanoma cells. The necessity for the development of new chemotherapeutic agents for melanoma treatment motivated this work. Sixteen derivatives were obtained with yields ranging from 23-81% and fully characterized by spectroscopic (^{1}H and ^{13}C nuclear magnetic resonance, infrared) and spectrometric high resolution mass spectrometry (HRMS) techniques. The derivatives were *in vitro* evaluated against B16-F10 murine melanoma cell line. The most effective compound (a bis cinnamate) (**6b**) reduced the melanoma cell viability, generated cell cycle arrest, and influenced the metastatic behavior of melanoma cells by decreasing migration, invasion, and colony formation. Based on these findings, it is believed that compound **6b** may represent an interesting scaffold to be explored toward the development of new antimelanoma agents.

Keywords: cinnamides, cinnamates, cinnamic acid, 1,2,3-triazoles, B16-F10 cell line

1. INTRODUCTION

Melanoma is the most serious type of skin cancer [1,2]. It is originated from uncontrolled growth of melanocytes that are dendritic-like cells responsible for skin pigmentation [3,4]. Melanoma accounts for the highest number of skin cancer deaths worldwide, and its incidence rate is increasing over the last years [5-7]. In 2020, new melanoma cases in the United states were estimated to be about 100,350 with 6,850 deaths, whereas in Brazil approximately 8,450 new cases were projected [5,8].

Genetic mutations, excessive ultraviolet radiation exposure, severe sunburn, outdoor training, advanced age, and gender are relevant factors related to melanoma susceptibility [2,9]. Additionally, melanoma has a high tendency to spread to other parts of the body. This metastatic behavior increases the challenge to treat this disease. Altogether, these facts evidence the melanoma severity [10-13].

Surgical resection is the main option available for patients with early stage of melanoma. Once present the metastatic form, systemic treatment is the mainstay of therapy, which includes radiotherapy, cytotoxic chemotherapy, immunotherapy, and targeted therapies [5,12]. Particularly, the chemotherapy has been using several compounds over the years, such as dacarbazine, dabrafenibe, binimetinib, vemurafenib, encorafenib, trametinib, and cobimetinib [12, 14-18]. However, these drugs still exhibit important side effects and low efficacy when used individually [19]. These facts justify the need for the development of new chemotherapeutic agents to be used in the treatment of metastatic melanoma.

In the search for new antimelanoma agents, natural products have been an extraordinary source of compounds with great chemical variability and biological activities [20-23], including antimelanoma [24, 25]. Newman and Cragg (2016) reported that 83% of anticancer drugs approved between 1981 and 2014 were either natural products *per se* or were based thereon [26]. For instance, Paclitaxel is an antimelanoma drug from natural sources derived from the bark of the Pacific yew tree (*Taxus brevifolia*) [12].

Cinnamic acid and its derivatives are natural plant-derived compounds that present antitumor and other biological activities. They have been used as templates for designing and arriving at newly compounds with antitumor activities [27, 28]. Our research group reported the preparation of a series of twenty-six cinnamic acid derivatives resulting from the connection of cinnamic acid with 1,2,3-triazole functionalities [28]. In the latter, B16-F10 cell line was used in *in vitro* assays to evaluate the antimelanoma activity of these compounds. The most potent cinnamate 3-(1-benzyl-1H-1,2,3-triazol-4-yl)propyl showed significant

antiproliferative and antimetastatic activities against B16-F10 cells by interacting with matrix metalloproteinase 9 (MMP-9) and MMP-2, which are directly involved in melanoma progression [28]. Indeed, compounds bearing the 1,2,3-triazole ring present a variety of therapeutic effects including antitumor activity [29, 30]. Due to this fact, this fragment is relevant to medicinal chemistry [29] and used as pharmacophore [31]. Likewise, cinnamides are cinnamic acid derivatives found in nature [32-34]. Also known as cinnamamides and cinnamic acid amides, they present a broad range of pharmacological activities, which include antitubercular, anti-trypanosomal activity, anti-diabetic, anti-microbial, antiviral, anti-inflammatory, anti-malarial, nervous disorders, and antitumor [35].

In our ongoing efforts to find useful compounds for the treatment of melanoma [28, 36, 37], and considering antitumor activity linked to cinnamides, cinnamates, and compounds displaying the 1,2,3-triazole functionality, it is herein described the synthesis and antimelanoma evaluation of a series novel cinnamides and a bis cinnamate bearing 1,2,3-triazole fragment(s).

2. EXPERIMENTAL

2.1 Synthesis

2.1.1 Generalities

The solvents were purchased from Vetec (Rio de Janeiro, Brazil), Sigma-Aldrich (St. Louis, MO, US), and Synth (Diadema, São Paulo, Brazil) and were distilled before use. Distilled water was used in the experiments. The reagents were procured from Vetec, Sigma-Aldrich, Synth and Oakwood Chemical (Estill, South Carolina, US) and used without further purification. The progress of the reactions was monitored by thin layer chromatography (TLC). For the purification of the reaction products, it was employed silica gel column chromatography (SiliCycle 0.035–0.070 mm, pore diameter 6 nm). The NMR spectra were recorded on Bruker (Billerica, Massachusetts, US) AVANCE DPX 200 MHz, AVANCE-III Onebay and Nanobay 400MHz and AVANCE-NEO 600 MHz instruments, using $CDCl_3$, CD_3OD, or DMSO-d_6 as deuterated solvents. The ^1H NMR data are presented as follows: chemical shift (δ) in ppm, multiplicity, number of hydrogens, J values in Hertz (Hz). Multiplicities are indicated by the following abbreviations: s (singlet), brs (broad singlet), d (doublet), dd (double of doublets), t (triplet), m (multiplet), q (quartet). For fluorine-containing derivatives, the multiplicity of some carbon signals are described along with J

values in Hertz. IR spectra were obtained using Varian 660-IR (Palo Alto, California, US) equipped with GladiATR scanning from 4000 to 500 cm^{-1}. Melting points were determined using a MQAPF-302 melting point apparatus (Microquímica, Santa Catarina, Brazil) and are uncorrected. High resolution mass spectra (HRMS) were obtained by electron spray ionization-mass spectrometry (ESI-MS) technique on a Q-Exactive (Thermo Scientific, Waltham, Massachusetts, United States of America) mass spectrometer and Solarix (Bruker Daltonics, Bremen, Germany) mass spectrometer. Details concerning the preparation of the intermediate compounds can be found in the supplementary material.

*2.1.2 Synthesis of compounds 3a-3m exemplified by the synthesis of N-((1-benzyl-1H-1,2,3-triazol-4-yl)methyl)cinnamamide (**3a**)*

To a 10.0 mL round-bottom flask, it was added azide (0.133 g, 1.00 mmol), water (2.00 mL), dichloromethane (2.00 mL), sodium ascorbate (39.6 mg, 0.200 mmol), *N*-(prop-2-yn-1-yl)cinnamamide (**1**) (0.185 g, 1.00 mmol) and $CuSO_4 \cdot 5H_2O$ (0.100 g, 0.400 mmol). The reaction mixture was vigorously stirred at room temperature for 30 min. Subsequently, water (10.0 mL) was added and the resulting aqueous phase was extracted with dichloromethane (3 x 20.0 mL). The organic extracts were combined, and the resulting organic phase was dried over anhydrous Na_2SO_4, filtered, and concentrated under reduced pressure. The compound **5a** was purified from the residue by silica gel column chromatography eluted with hexane/ethyl acetate/methanol (5:3:1 v/v). The described procedure gave compound **5a** with 58% yield (0.185 g, 0.580 mmol). White solid, m.p. 165.8-166.9 ºC, IR (ATR) ν_{max}/cm^{-1} 3229, 1614, 1565, 989, 729. ^{1}H NMR (400 MHz, DMSO-d_6) δ 4.41 (d, 2H, *J* 3.6 Hz), 5.55 (s, 2H), 6.63 (d, 1H, J_{trans} 16.0 Hz), 7.30-7.54 (m, 11Hz), 8.00 (s, 1H), 8.57 (brs, 1H). ^{13}C (100 MHz, DMSO-d_6) δ 35.0, 53.4, 122.6, 123.7, 128.2, 128.7, 128.8, 129.4, 129.6, 130.2, 135.5, 136.8, 139.7, 145.7, 165.5. HRMS (ESI^+) calcd. for $[C_{19}H_{19}N_4O]^+$ $[M+H]^+$: 319.1558, found: 319.1555.

Compounds **3b-3n** were prepared from the corresponding alkyne **2** and azides as described for compound **5a**. All the compounds were fully characterized by IR and NMR (^{1}H and ^{13}C) as well as high resolution mass spectrometry. Structures of the compounds are supported by the following data.

*2.1.3 N-((1-(4-(trifluoromethoxy)benzyl)-1H-1,2,3-triazol-4-yl)methyl)cinnamamide **(3b)***

White solid, obtained in 53% yield, m.p. 194.0-194.8 ºC, IR (ATR) ν_{max}/cm^{-1} 3247, 1649, 1598, 1538, 995. ^{1}H NMR (400 MHz, DMSO-d_6) δ 4.37 (d, 2H, *J* 5.6 Hz), 5.54 (s, 2H); 5.66 (s, 2H); 6.58 (d, 1H, J_{trans} 15.6 Hz); 7.25-7.7.39 (m, 8H); 7.45 (d, 2H, *J* 8.0 Hz); 7.99 (s, 1H); 8.53 (t, 1H, *J* 5.6 Hz). ^{13}C NMR (100 MHz, DMSO-d_6) δ 35.0, 52.5, 122.0, 122.5, 123.8, 128.2, 129.6, 130.2, 130.7, 135.5, 136.2, 139.7, 145.8, 148.7, 165.6. The signal for the carbon of the CF_3 group was note observed. However, the remaining spectroscopic and spectrometric data confirmed the structure of the compound. HRMS (ESI^+) calcd. for $[C_{20}H_{17}F_3N_4O_2Na]^+$ $[M+Na]^+$: 425.1201, found: 425.1196.

*2.1.4 N-((1-(4-methoxybenzyl)-1H-1,2,3-triazol-4-yl)methyl)cinnamamide (**3c**)*

White solid, obtained in 41% yield, m.p. 162.5-163.2 ºC, IR (ATR) ν_{max}/cm^{-1} 3235, 1649, 1609, 992. ^{1}H NMR (400 MHz, DMSO-d_6) δ 3.65 (s, 3H), 4.35 (d, 2H, *J* 5.6 Hz), 5.40 (s, 2H), 6.58 (d, 1H, J_{trans} 16 Hz), 6.84 (d, 2H, *J* 8.4 Hz), 7.22 (d, 2H, *J* 8.4 Hz), 7.28-7.34 (m, 3H), 7.38 (d, 1H, J_{trans} 16 Hz), 7.47 (d, 2H, *J* 7.6 Hz), 7.89 (s, 1H), 8.52 (t, 1H, *J* 5.6 Hz). ^{13}C NMR (100 MHz, DMSO-d_6) δ 35.0, 53.0, 55.8, 114.8, 122.5, 123.4, 128.2, 128.7, 129.6, 130.2, 130.4, 135.5, 139.7, 145.6, 159.8, 165.6. HRMS (ESI^+) calcd. for $[C_{20}H_{21}N_4O_2]^+$ $[M+H]^+$: 349.1664, found: 349.1658.

*2.1.5 N-((1-(4-iodobenzyl)-1H-1,2,3-triazol-4-yl)methyl)cinnamamide (**3d**)*

White solid, obtained in 69% yield, m.p. 208.2-209.6 ºC, IR (ATR) ν_{max}/cm^{-1} 3257, 1650, 1606, 999, 750. ^{1}H NMR (400 MHz, DMSO-d_6) δ 4.33 (d, 2H, *J* 5.6 Hz), 5.43 (s, 2H), 6.55 (d, 1H, J_{trans} 16 Hz), 7.02 (d, 2H, *J* 8.0 Hz), 7.24-7.32 (m, 3H), 7.35 (d, 1H, J_{trans} 16 Hz), 7.44 (d, 2H, *J* 6.8 Hz), 7.63 (d, 2H, *J* 8.0 Hz), 7.91 (s, 1H), 8.50 (t, 1H, *J* 5.6 Hz). ^{13}C NMR (100 MHz, DMSO-d_6) δ 35.0, 52.9, 95.0, 122.5, 123.8, 128.2, 129.6, 130.2, 131.0, 135.5, 136.5, 138.2, 139.8, 145.7, 165.6. HRMS (ESI^+) calcd. for $[C_{19}H_{18}IN_4O]^+$ $[M+H]^+$: 445.05254, found: 445.05201.

*2.1.6 N-((1-(4-fluorobenzyl)-1H-1,2,3-triazol-4-yl)methyl)cinnamamide (**3e**)*

White solid, obtained in 78% yield, m.p. 163.8-164.5ºC, IR (ATR) ν_{max}/cm^{-1} 3232, 1644, 1597, 1508, 992. ^{1}H NMR (600 MHz, DMSO-d_6) δ 4.44 (d, 2H, J 6.0 Hz), 5.57 (s, 2H), 6.66 (d, 2H, J_{trans} 15.6 Hz), 7.20 (t, 2H, J 8.7 Hz), 7.35-7.42 (m, 5H), 7.46 (d, 1H, J_{trans} 15.6 Hz), 7.55 (d, 2H, J 7.2 Hz), 8.03 (s, 1H), 8.60 (t, 1H, J 6.0 Hz). ^{13}C NMR (150 MHz, DMSO-d_6) δ 34.8, 52.4, 116.0 (d, J_{C-F} 21. Hz), 122.3, 123.4, 128.0, 129.4, 130.0, 130.8 (d, J_{C-F} 8.4 Hz), 132.8 (d, J_{C-F} 3.3 Hz), 135.3, 139.5, 145.5, 162.4 (d, J_{C-F} 243 Hz), 165.3. HRMS (ESI$^+$) calcd. for $[C_{19}H_{18}FN_4O]^+$ $[M+H]^+$: 337.14646, found: 337.14593.

*2.1.7 N-((1-(4-nitrobenzyl)-1H-1,2,3-triazol-4-yl)methyl)cinnamamide (**3f**)*

Yellow solid, obtained in 66% yield, m.p. 184.4-186.1 ºC, IR (ATR) ν_{max}/cm^{-1} 3353, 1649, 1610, 1518, 976, 723. ^{1}H NMR (400 MHz, DMSO-d_6) δ 4.45 (d, 2H, J 5.6 Hz), 5.77 (s, 2H), 6.66 (d, 1H, J_{trans} 16 Hz), 7.35-7.44 (m, 3H), 7.46 (d, 1H, J_{trans} 16 Hz), 7.53-7.56 (m, 4H), 8.11 (s, 1H), 8.24 (d, 2H, J 8.8 Hz), 8.63 (t, 1H, J 5.6 Hz). ^{13}C NMR (100 MHz, DMSO-d_6) δ 34.8, 52.3, 122.4, 124.0, 124.4, 128.0, 129.4, 129.6, 130.0, 135.3, 139.5, 144.0, 145.7, 147.7, 165. 6. HRMS (ESI$^+$) calcd. for $[C_{19}H_{18}N_5O_3]^+$ $[M+H]^+$: 364.14096, found: 364.14046.

*2.1.8 N-((1-(4-chlorobenzyl)-1H-1,2,3-triazol-4-yl)methyl)cinnamamide (**3g**)*

White solid, obtained in 72% yield, m.p. 185.6-186.8 ºC, IR(ATR) ν_{max}/cm^{-1} 3260, 1659, 1618, 972, 781. ^{1}H NMR (400 MHz, DMSO-d_6) δ 4.44 (d, 2H, J 5.5 Hz), 5.58 (s, 2H), 6.66 (d, 1H, J_{trans} 16 Hz), 7.34-7.46 (m, 8H), 7.56 (d, 2H, J 7.6 Hz), 8.04 (s, 1H), 8.60 (t, 1H, J 5.5 Hz). ^{13}C NMR (100 MHz, DMSO-d_6) δ 34.8, 52.3, 122.4, 123.9, 124.4, 128.0, 129.4, 129.6, 129,7, 135.3, 139.5, 144.0, 145.7, 147.7, 165.4. HRMS (ESI$^+$) calcd. for $[C_{19}H_{18}ClN_4O]^+$ $[M+H]^+$: 353.11691, found: 353.11642.

*2.1.9 N-((1-(4-bromobenzyl)-1H-1,2,3-triazol-4-yl)methyl)cinnamamide (**3h**)*

White solid, obtained in 81% yield, m.p. 196.4-197.5 ºC, IR (ATR) ν_{max}/cm^{-1} 3253, 1657, 1614, 1566, 971, 752. ^{1}H NMR (400 MHz, DMSO-d_6) δ 4.44 (d, 2H, J 5.6 Hz), 5.57 (s, 2H), 6.66 (d, 1H, J_{trans} 16,0 Hz), 7.29 (d, 2H, J 8.4 Hz), 7.37-7.44 (m, 3H), 7.46 (d, 1H, J_{trans} 16 Hz), 7.54-7.59 (m, 4H), 8.04 (s, 1H), 8.60 (t, 1H, J 5.6 Hz). ^{13}C NMR (100 MHz, DMSO-d_6) δ 34.8, 52.5, 121.9, 122.4, 123.6, 128.0, 129.4, 130.0, 130.7, 132.1, 135.3, 136.0, 139.5,

145.5, 165.3. HRMS (ESI$^+$) calcd. for $[C_{19}H_{17}BrN_4ONa]^+$ $[M+Na]^+$: 419.04834, found: 419.04788.

*2.1.10 N-((1-(4-methylbenzyl)-1H-1,2,3-triazol-4-yl)methyl)cinnamamide (**3i**)*

White solid, obtained in 78% yield, m.p. 182.8-183.8 ºC, IR (ATR) ν_{max}/cm^{-1} 3268, 1652, 1609, 1539, 988, 757. ^{1}H NMR (400 MHz, DMSO-d_6) δ 2.28 (s, 3H), 4.43 (d, 2H, J 5.6 Hz), 5.51 (s, 2H), 6.66 (d, 1H, J_{trans} 16 Hz), 7,17 (d, 2H, J 8 Hz), 7,23 (d, 2H, J 8 Hz), 7.16-7.24 (m, 4H), 7.36-7.41 (m, 3H), 7.46 (d, 1H, J_{trans} 16 Hz), 7.55 (d, 2H, J 6.4 Hz), 7.94 (s, 1H), 8.58 (t, 1H, J 5.6 Hz).^{13}C NMR (150 MHz, DMSO-d_6) δ 20.7, 34.4, 52.6, 121.9, 122.9, 127.6, 128.1, 129.0, 129.3, 129.5, 133.1, 134.9, 137.5, 139.1, 145.0, 164.9. HRMS (ESI$^+$) calcd. for $[C_{20}H_{21}N_4O]^+$ $[M+H]^+$: 333.17154, found: 333.17104.

*2.1.11 N-((1-(4-(trifluoromethyl)benzyl)-1H-1,2,3-triazol-4-yl)methyl)cinnamamide (**3j**)*

White solid, obtained in 71% yield, m.p. 214.1-215.3 ºC, IR(ATR) ν_{max}/cm^{-1} 3253, 1649, 1602, 1112. ^{1}H NMR (400 MHz, DMSO-d_6) δ 4.45 (d, 2H, J 5.4 Hz), 5.71 (s, 2H), 6.67 (d, 1H, J_{trans} 16 Hz), 7.35-7.43 (m, 3H), 7.47 (d, 1H, J_{trans} 16 Hz), 7.51-7.56 (m, 4H), 7.75 (d, 2H, J 8.4 Hz), 8.10 (s, 1H), 8.62 (t, 1H, J 5.4 Hz). ^{13}C NMR (100 MHz, DMSO-d_6) δ 34.8, 52.5; 122.4, 123.8, 126.1 (q, J 3.7 Hz), 128.0, 129.2, 129.4, 129.9, 135.3, 139.5, 141.2, 145.6, 165.4. HRMS (ESI$^+$) calcd. for $[C_{20}H_{18}F_3N_4O]^+$ $[M+H]^+$: 387.14327, found: 387.14283.

*2.1.12 N-((1-(4-isopropylbenzyl)-1H-1,2,3-triazol-4-yl)methyl)cinnamamide (**3k**)*

White solid, obtained in 72% yield, m.p. 199.1-200.5 ºC, IR (ATR) ν_{max}/cm^{-1} 3279, 1653, 1610, 992. ^{1}H NMR (400 MHz, DMSO-d_6) δ 1.17 (d, 6H, J 6.9 Hz), 2.86 (septet, 1H, J 6.9 Hz), 4.42 (d, 2H, J 5.3 Hz), 5.52 (s, 2H), 6.65 (d, 1H, J_{trans} 16 Hz), 7.22-7.28 (m, 4H), 7.35-7.43 (m, 3H), 7.45 (d, 1H, J_{trans} 16 Hz), 7.55 (d, 2H, J 7.3 Hz), 8.01 (s, 1H), 8.59 (t, 1H, J 5.3 Hz). ^{13}C NMR (100 MHz, DMSO-d_6) δ 24.2, 33.6, 34.8, 53.0, 122.4, 123.4, 127.1, 128.0, 128.6, 129.4, 130.0, 134.0, 135.3, 139.5, 145.4, 148.9, 165.3. HRMS (ESI$^+$) calcd. for $[C_{22}H_{25}N_4O]^+$ $[M+H]^+$: 361.20284, found: 361.20230.

*2.1.13 N-((1-(3,4-difluorobenzyl)-1H-1,2,3-triazol-4-yl)methyl)cinnamamide (**3l**)*

White solid, obtained in 77% yield, m.p. 149.3-150.8 ºC, IR (ATR) ν_{max}/cm^{-1} 3241, 1518. ^{1}H NMR (400 MHz, DMSO-d_6) δ 4.43 (d, 2H, *J* 5.5 Hz), 5.57 (s, 2H), 6.65 (d, 1H, J_{trans} 16 Hz), 7.20 (s, 1H), 7.35-7.47 (m, 6H), 7.55 (d, 2H, *J* 6.9 Hz), 8.06 (s, 1H), 8.59 (t, 1H, *J* 5.5 Hz). ^{13}C NMR (100 MHz, DMSO-d_6) δ 34.3, 51.5, 117.3 (d, *J* 17.4 Hz), 117.8 (d, *J* 17.4 Hz), 121.8, 123.0, 125.1-125.2 (m), 127.4, 128.9, 129.4, 133.6-133.7 (m), 134.7, 139.0, 145.0, 147.9-148.0 (m), 150.3-150.5 (m), 164.8. HRMS (ESI$^+$) calcd. for $[C_{19}H_{17}F_2N_4O]^+$ $[M+H]^+$: 355.13704, found: 355.13663.

*2.1.14 N-((1-(7-hydroxy-2-oxo-2H-chromen-3-yl)-1H-1,2,3-triazol-4-yl)methyl)cinnamamide (**3m**)*

White solid, obtained in 30% yield, m.p. 224.4-224.9 ºC, IR (ATR) ν_{max}/cm^{-1} 3250, 3065, 1728, 1600. ^{1}H NMR (400 MHz, DMSO-d_6) δ 4.54 (d, 2H, *J* 5.2 Hz), 6.69 (d, 1H, J_{trans} 15.6 Hz), 6.85-6.92 (s, 2H, m), 7.36-7.44 (m, 3H), 7.49 (d, 1H, J_{trans} 15.6 Hz), 7.56 (d, 2H, *J* 6.9 Hz), 7.75 (d, 1H, *J* 8.5 Hz), 8.44 (s, 1H), 8.58 (s, 1H), 8.73 (t, 1H, *J* 5.2 Hz). ^{13}C NMR (100 MHz, DMSO-d_6) δ 34.7, 102.6, 110.8, 114.8, 119.8, 122.3, 124.3, 128.0, 129.4, 130.0, 131.4, 135.3, 136.6, 139.6, 145.5, 155.1, 156.8, 163.0, 165.5. HRMS (ESI$^+$) calcd. for $[C_{19}H_{16}F_2N_4ONa]^+$ $[M+Na]^+$: 411.10693, found: 411.10663.

*2.1.15 N-((1-(7-(diethylamino)-2-oxo-2H-chromen-3-yl)-1H-1,2,3-triazol-4-yl)methyl)cinnamamide (**3n**)*

Yellow solid, obtained in 63% yield, m.p. 206.5-207.4 ºC, IR (ATR) ν_{max}/cm^{-1} 3332, 1731, 1613, 968. ^{1}H NMR (400 MHz, DMSO-d_6) δ 1.13-1.47 (m, 6H), 3.46-3.51 (m, 4H), 4.53 (s, 2H), 6.66-6.71 (m, 2H), 6.82 (d, 1H, *J* 9.6 Hz), 7.40-7.42 (m, 3H), 7.48 (d, 1H, J_{trans} 16 Hz), 7.56-7.64 (m, 3H), 8.40 (s, 1H), 8.45 (s, 1H), 8.71 (s, 1H).^{13}C NMR (100 MHz, DMSO-d_6) δ 12.5, 34.4, 44.4, 96.6, 106.7, 110.2, 116.5, 122.0, 123.9, 127.7, 129.1, 129.7, 130.7, 135.0, 136.7, 139.3, 145.0, 151.6, 155.8, 156.9, 165.1. HRMS (ESI$^+$) calcd. for $[C_{25}H_{26}N_5O_3]^+$ $[M+H]^+$: 444.20356, found: 444.20352.

*2.1.16 Synthesis of (2E,2'E)-N,N'-(((((oxybis(ethane-2,1-diyl))bis(oxy))bis(ethane-2,1-diyl))bis(1H-1,2,3-triazole-1,4-diyl))bis(methylene))bis(3-phenylacrylamide) (**6a**)*

This compound was prepared via the reaction between azide **4** and compound **2**, using the same methodology described for compound **3a**, however, 2.00 mmol of compound **2** was used for 1.00 mmol of azide **4**. A white solid was obtained in 34% yield, m.p. 152.4-153.5 ºC, IR (ATR) ν_{max}/cm^{-1} 3266, 1667, 1629, 971. ^{1}H NMR (400 MHz, CD_3OD) δ 3.48-3.53 (m, 8H), 3.82 (t, 4H, *J* 5.2 Hz), 4.52 (t, 4H, *J* 5.2 Hz), 4.55 (s, 4H), 6.62 (d, 2H, J_{trans} 16 Hz), 7.35-7.39 (m, 6H), 7.52-7.58 (m, 6H), 7.92 (s, 2H). ^{13}C NMR (100 MHz, CD_3OD) δ 35.8, 51.4, 70.3, 71.5, 121.6, 125.1, 128.9, 130.0, 130.9, 136.2, 142.2, 146.0, 168.4. HRMS (ESI^+) calcd. for $[C_{32}H_{38}N_8O_5Na]^+$ $[M+Na]^+$: 637.28629, found: 637.28741.

*2.1.17 ((((oxybis(ethane-2,1-diyl))bis(oxy))bis(ethane-2,1-diyl))bis(1H-1,2,3-triazole-1,4-diyl))bis(methylene) (2E,2'E)-bis(3-phenylacrylate) (**6b**)*

This compound was obtained in 23% as colorless oil from the reaction of azide **4** and ester **5**, using the same methodology described for compound **6a**, IR (ATR) ν_{max}/cm^{-1}:3136, 1713, 1636, 1160. ^{1}H NMR (400 MHz, $CDCl_3$) δ 3.53-3.60 (m, 8H), 3.86 (t, 4H, *J* 5.1 Hz), 4.54 (t, 4H, *J* 5.1 Hz), 5.36 (s, 4H), 6.43 (d, 2H, J_{trans} 16.0 Hz), 7.36-7.39 (m, 6H), 7.48-7.51 (m, 4H), 7.70 (d, 2H, J_{trans} 16 Hz), 7.85 (s, 2H). ^{13}C NMR (100 MHz, $CDCl_3$) δ 50.4, 57.5, 69.3, 70.46, 70.54, 117.5, 125.11, 128.1, 128.9, 130.5, 134.2, 142.6, 145.6, 166.7. HRMS (ESI^+) calcd. for $[C_{32}H_{37}N_6O_7]^+$ $[M+H]^+$: 617.27237, found: 617.27271.

2.2 Cell culture

Murine melanoma cells (B16-F10) were kindly provided by Dr. Mirian T. Paes Lopes (Department of Pharmacology, Universidade Federal de Minas Gerais, Belo Horizonte, Minas Gerais, Brazil). African green monkey kidney cell line (Vero) was kindly provided by Dr. Juliana Lopes Rangel Fietto (Department of Biochemistry and Molecular Biology, Universidade Federal de Viçosa, Viçosa, Minas Gerais, Brazil). The cells were grown in RPMI-1640 medium (Sigma Aldrich) supplemented with 10% (v/v) of fetal bovine serum (FBS) (LGC Biotecnologia, Cotia, Brazil), 100 g/mL streptomycin, and 100 units/mL penicillin at pH 7.2 and 37 °C under 5% CO_2 atmosphere.

2.3 Cell viability assay and cytotoxicity

B16-F10 cells were plated in 96-well at a concentration of 1.0 x 10^4 cells/well in a 96-well flat bottom microplate. The cells grew for 24 h and were treated with the concentration of 100 μM of each synthesized compound derived from cinnamic acid **3a**-**3n**, **6a** and **6b**. DMSO (0.4% v/v) and RPMI-1640 were used as control. After 48 h of treatment, the cell viability was determined by MTT (3-(4,5 dimethylthiazol-2-yl)-2,5 diphenyltetrazolium bromide) (Sigma Aldrich) metabolization. The MTT solution was added to each well (final concentration 5 mg/mL) and the plate was incubated for 3 h. Finally, 100 μL of DMSO was added to each well and the absorbance was measured in a plate reader (Sinergy HT, Biotek) at 540 nm. Results were normalized considering the cultures treated with 0.4% DMSO (control). The half-maximal inhibitory concentration (IC_{50}) of the most active compounds was also analyzed using the MTT method, after treating the B16-F10 cells with increasing doses (0–200.0 μM) of these compounds. The IC_{50} was calculated as previously reported [61].

2.4 Cell viability on non-tumor cell line

Vero cells, a non-tumor cell line, were plated at a concentration of 8.0 x 10^4 cells/well in a 96-well flat bottom microplate. The cells grew for 24 h and were treated with the concentration of 100.0 μM of the five best compounds selected after the cell viability test in B16-F10. DMSO (0.4% v/v) and RPMI-1640 were used as control. After 48 h of treatment, the cell viability was determined by MTT (3-(4,5 dimethylthiazol-2-yl)-2,5 diphenyltetrazolium bromide) (Sigma) metabolization. The MTT solution was added to each well (final concentration 5 mg/mL) and the plate was incubated for 3 h. Finally, 100 μL of DMSO was added to each well and the absorbance was measured in a plate reader (Sinergy HT, Biotek, Winooski, Vermont, USA) at 540 nm. Results were normalized considering the cultures treated with DMSO 0.4% v/v (control).

2.5 Cell cycle assay

B16-F10 cells were seeded on a 6-well plate at a density of 2.5 x 10^5 cells/well and treated with compound **6b** at the concentrations of 12.5, 25.0, and 50.0 μM for 48 h. DMSO (0.4%v/v) was used as vehicle control. Then the cells were fixed in 70% ethanol, washed in PBS, and incubated for 60 min in PBS containing propidium iodide (50 μg/mL, Sigma) and

RNase A (0.2 mg/mL, Invitrogen). The samples were analyzed by flow cytometry (FACS Verse, BD Bioscience, Franklanes, New Jersey, USA).

2.6 Cell migration assay

The wound-healing assay was conducted to evaluate the ability of the compound **6b** to inhibit cell migration. B16-F10 cells were seeded onto 24-well plate at a concentration of 1.0 x 10^5 cells/well and allowed to reach full confluence after incubation overnight at 37 °C under 5% CO_2 atmosphere. Monolayers were then wounded using a sterile 200 μL pipette tip. Cells were washed twice with phosphate-buffered saline (PBS) to remove detached cells and then treated with the compounds at the concentrations of 12.5, 25.0 and 50.0 μM. The DMSO vehicle treatment (0.4% v/v) was used as control. Photos of the wound were taken using an inverted microscope (Life Technologies, Carlsbad, California, USA). Wound closure rates were then calculated quantitatively as the difference between wound width at 0 and 24 h. Results were expressed as a percentage of cell migration.

2.7 Cell invasion assay

The matrigel matrix (BD Biosciences) was diluted with serum-free RPMI-1640 culture medium at 1:12 ratio. Subsequently, the upper chamber of the transwell (8.0 μm polycarbonate membrane, Corning) was coated with 35 μL diluted Matrigel matrix and incubated at 37 °C, for 2 h, for full condensation. Then, the B16-F10 cells were re-suspended with serum-free RPMI-1640, treated with **6b** at 12.5, 25.0, and 50.0 μM for 60 min, and inoculated into the upper chamber Matrigel-precoated (5.0 x 10^4 cells, 100 μL/well). The DMSO-vehicle treatment (0.4% v/v) was used as control. The well was filled with 650 μL of culture medium containing 10% v/v FBS as a chemoattractant. After 24 h, the chambers were fixed in methanol for 30 min, washed and stained with toluidine blue (1% v/v, Sigma Aldrich) for 15 min. Images from 10 fields were chosen at random/group, captured using an inverted microscope (Leica Microsystems, Wetzlar, Germany) and the cells were counted using the Image J software. The results were expressed as a percentage of cell invasion.

2.8 Cell colony assay

B16-F10 cells were seeded in 6-well plates in triplicate at the density of 1.0 x 10^3 cells/well. After 24 h, the cells were treated with the compound **6b** at 12.5, 25.0, and 50.0 μM

for 24 h. The complete medium was exchanged for complete medium with 2% FBS, and the cells were cultured for 7 d. The colonies formed were then fixed and stained with toluidine blue solution (1% v/v, Sigma Aldrich) and methanol (20% v/v). Colonies were counted by using ImageJ software and the results were expressed as a percentage of the untreated control cultures.

2.9 Statistical analysis

All numeric data were obtained from three independent experiments, each experiment with triplicate, and are shown as mean ± standard error of the mean (S.E.M.). The analyses were performed using Microsoft Excel (Microsoft Office Software System) and GraphPad Prism (GraphPad Software Inc.). The statistical analyses were carried out by one-way ANOVA followed by Dunn's or Dunnett's tests. *$p < 0.05$, **$p < 0.01$, ***$p < 0.001$ and ****$p < 0001$ were considered significant.

3. RESULTS AND DISCUSSION

3.1 Synthesis

The steps involved in the synthesis of cinnamides **3a-3n** are outlined in Scheme 1.

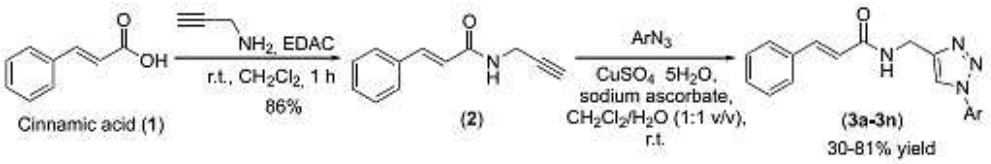

Compounds	Ar	Compounds	Ar
3a	benzyl	**3h**	4-bromobenzyl
3b	4-trifluoromethoxybenzyl	**3i**	4-methylbenzyl
3c	4-methoxybenzyl	**3j**	4-trifluoromethylbenzyl
3d	4-iodobenzyl	**3k**	4-isopropylbenzyl
3e	4-fluorobenzyl	**3l**	3,4-difluorobenzyl
3f	4-nitrobenzyl	**3m**	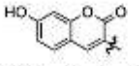
3g	4-chlorobenzyl	**3n**	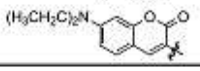

Scheme 1 – Synthesis of cinnamides **3a**-**3n**.

The amide **2** was prepared via the reaction of cinnamic acid (**1**) and propargyl amine [38]. The reaction was carried out in the presence of EDAC, which promoted coupling of the acid and the amine in good yield (86%). Then, the CuAAC reactions [39-42] between **2** and several aromatic azides afforded the cinnamides **3a-3n** with yields ranging from 30-81%.

The synthesis of cinnamides **3a-3n** required the preparation of twelve benzyl azides and two 3-azidocoumarins. The benzyl azides were prepared via conversion of benzyl alcohols to the corresponding ester sulphonates, followed by the treatment of these esters with sodium azide, as previously reported [43]. The 3-azidocoumarins, in turn, were obtained from the substituted salicylaldehyde and N-acetylglycine or ethyl nitroacetate through routes involving two and three steps, according to methodology previously described [44].

One aspect deserves comment at this point. In our previous work, we synthesized a series of cinnamates bearing 1,2,3-triazole functionalities [28]. Indeed, these cinnamates presented different degrees of efficiency against the melanoma B16-F10 cell line. Their efficiency depended on the benzyl groups present in the triazole functionality of the cinnamates. These benzyl groups, in turn, came from the benzyl azides. Herein, benzyl azides were also used in the preparation of cinnamides in order to make possible a comparison between the antimelanoma activity of cinnamates previously published by us [28] and the cinnamides herein investigated.

The structures of the new cinnamides **3a-3n** were confirmed based on IR, NMR, and HRMS analyses. The IR spectrum showed bands for the N-H stretching within the 3230-3279 cm^{-1} range. Also, carbonyl stretching vibrations for the amide groups were noticed within the interval 1615-1670 cm^{-1}. In the 1H-NMR, the coupling constants for the hydrogens of aliphatic double bonds were approximately equal to 16 Hz, which confirms the *trans* stereochemistry of these bonds. The singlet typically observed around 8 ppm confirmed the presence of the 1,2,3-triazole functionality in the structures of the cinnamides. The presence of the amide group was also confirmed by 13C NMR; the signals for the carbonyl groups of this functionality were noticed within the 164.8-168.4 ppm range. The molecular formulas of the cinnamides were confirmed via HRMS analyses.

Our research group has demonstrated important cytotoxic effects for symmetrical 1,4-disubstituted bis-1,2,3-triazoles [45]. Based on that, we decided to prepare the bis cinnamides **6a** and cinnamate **6b** as shown in Scheme 2. The synthesis of bis azide **4** has been previously reported [45].

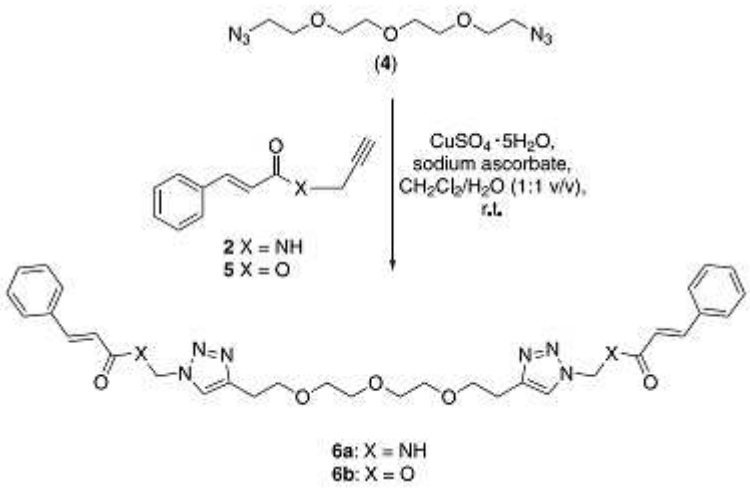

Scheme 2 – Preparation of compounds **6a** and **6b**.

The compound **6b** was prepared to compare the biological response of the bis ester cinnamate in relation to bis cinnamide **6a** (Scheme 2). The ester **5** was prepared via condensation of cinammic acid (**1**) and propargyl alcohol promoted by EDAC as previously published by us [28].

The spectroscopic data that confirmed the structures of cinnamic acid derivatives **3a**-**3n**, **6a** and **6b** are available in the supplementary material.

3.2 Effect of compounds 3a-3n, 6a and 6b on the viability and cytotoxicity of B16-F10 cells

In the current study, compounds **3c**, **3e**, **3f**, **3j**, and **6b** reduced significantly the viability of metastatic B16-F10 cells at 100 μM (Figure 1). Therefore, these five compounds were evaluated for the half-maximal inhibitory concentration (IC_{50}). While compound **3c** presents an electron-donating group (-OCH3) at the *para* position of the benzyl group, the compounds **3e** (-F), **3f** (-NO2), and **3j** (-CF3) have electron withdrawing ones. Besides, compound **6b** is a bis 1,2,3-triazole, a class of compounds endowed with antitumor activity [45]. The similar 1,2,3-triazolic cinnamate with a p-methoxy benzyl group, at the 100.0 μM, was inactive against B16-F10 cell line [28], the cinnamide **3c** could reduce cell viability in approximately 40%. On the contrary, the 1,2,3-triazolic cinnamates possessing the *p*-fluoro benzyl, *p*-nitro benzyl, and *p*-trifluoromethyl benzyl groups were equipotent to the cinnamides **3e**, **3f**, and **3j** counterparts.

Although metastatic B16-F10 is known to be very resistant to antitumor agents [46], the compounds **3j** and **6b** displayed superior cytotoxic activity (IC_{50} values of 153.4 and 57.7

μM, respectively) than cinnamic acid (> 200.0 μM, data not shown). In constrast, the cinnamides **3c**, **3e**, and **3f** showed IC_{50} value greater than 200.0 μM. The cytotoxic effects presented by compounds **3j** and **6b** corroborate with previous studies, in which cinnamic acid derivatives also have presented relevant cytotoxic effects on the metastatic melanoma cell line [28,47]. In this last, cytotoxic effects of representative cinnamic acid esters and amides were seen in different types of cancer *in vitro*, including melanoma. Besides that, the compounds tested showed selectivity of these cytotoxic effects on the malignant cell lines versus the peripheral blood mononuclear cells [47].

3.3 Effect of the compounds 3c, 3e, 3f, 3j, and 6b on non-tumoral cell viability

The cytotoxicity of compounds in non-tumoral cells was also evaluated by means of Vero fibroblast-like kidney cells treated with the compounds **3c**, **3e**, **3f**, **3j**, and **6b**. Vero cells showed sensitivity for the compounds **3e**, **3f**, and **6b** at 100.0 μM, being **3e** the most cytotoxic (Figure 2).

This assay is relevant to compare the effect of compounds on non-tumoral cells, once that novel cancer chemotherapy relies on the selection of malignant-cell specific drugs and non-toxic to normal cells [48]. Meantime, cytotoxic chemotherapy can kill more cancer cells than normal tissue, as seen in cytotoxic drugs used to treat cancer [49]. It was the case of the results observed for the compound **6b**, which presented certain cytotoxicity in non-tumor cells, but it was the most effective in B16-F10 tumor cells. Taking the findings together, we selected the derivative **6b** for the subsequent assays due to its activity against the melanoma cell line B16-F10 (lowest IC_{50}).

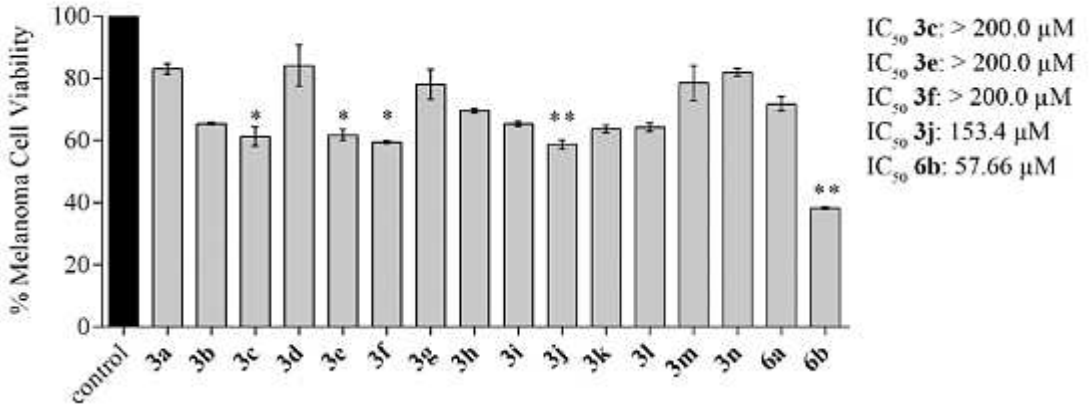

Figure 1 - Effect of compounds **3a**-**3n**, **6a** and **6b** on cell viability of melanoma cells. B16-F10 metastatic melanoma was treated with 100.0 μM of each compound for 48 h. Each bar shows the mean of percentage of survival of melanoma cells determined by MTT assay. The compounds that showed statistical difference in relation to the control were selected for IC_{50} evaluation. Data expressed as the mean ± S.E.M. *p < 0.05 and **p < 0.01 *versus* control (DMSO 0.4% v/v) by One-way ANOVA and Dunn's post-hoc test.

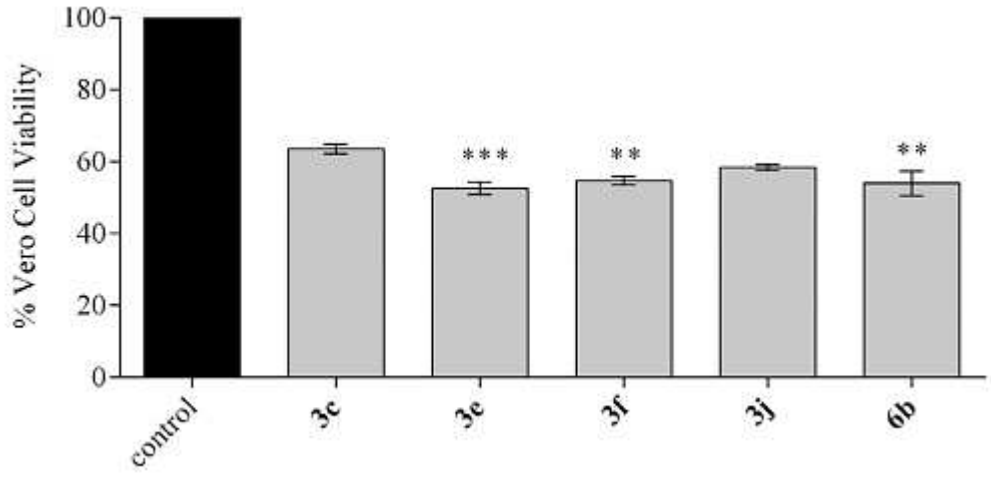

Figure 2 **-** Effect of compounds **3c**, **3e**, **3f**, **3j** and **6b** on cell viability of non-tumor cell line. Vero fibroblast-like kidney cells were treated with 100.0 μM of each compound derived from cinnamic acid for 48 h. Each bar shows the mean of percentage of survival of Vero cells determined by MTT assay. Data expressed as the mean ± S.E.M. **p < 0.01 and ***p < 0.001 *versus* control (DMSO 0.4% v/v) by One-way ANOVA and Dunn's post-hoc test.

3.4 Effect of compound 6b on the proliferation of melanoma cells

Cell proliferation was analyzed using the cell cycle assay. The compound **6b** induced a shift in the DNA content of B16-F10 cells after 48 h incubation (Figure 3). Specifically, the

percentage of cells in the G0/G1 phase was 75.40%, 78.10%, and 57.90% after incubation with **6b** compound at 12.5 μM ($p < 0.05$), 25.0 μM ($p < 0.05$), and 50.0 μM in contrast to the 45.43% of DMSO control cells. Further, the percentage of cells in the S phase corresponded to 45.9% in the DMSO control, and 21.7% ($p < 0.0001$), 14.3% ($p < 0.0001$), and 31.9% ($p < 0.01$) at 12.5 μM, 25.0 μM, and 50.0 μM. For the G2/M phase, the percentages were 8.70% (DMSO control), 2.86% (at 12.5 μM; $p < 0.0001$), 7.64% (at 25.0 μM), and 10.31% (at 50.0 μM; $p < 0.01$).

Thus, these data expressed a B16-F10 cells accumulation in the G0/G1 phase and fewer cells in the S-phase (phase of duplication of genetic material), resulting in growth inhibition/cell cycle arrest. Drugs that affect the tumor cell cycle are promising, as they negatively influence the proliferation of cancer cells [50]. In the case of cinnamic acid derivatives, previous studies have reported their capacity to induce cell cycle arrest in cancer cells [47, 51]. Therefore, our data corroborate the studies with cinnamic acid derivatives, since the compounds inhibited cell proliferation by disruption of cell cycle.

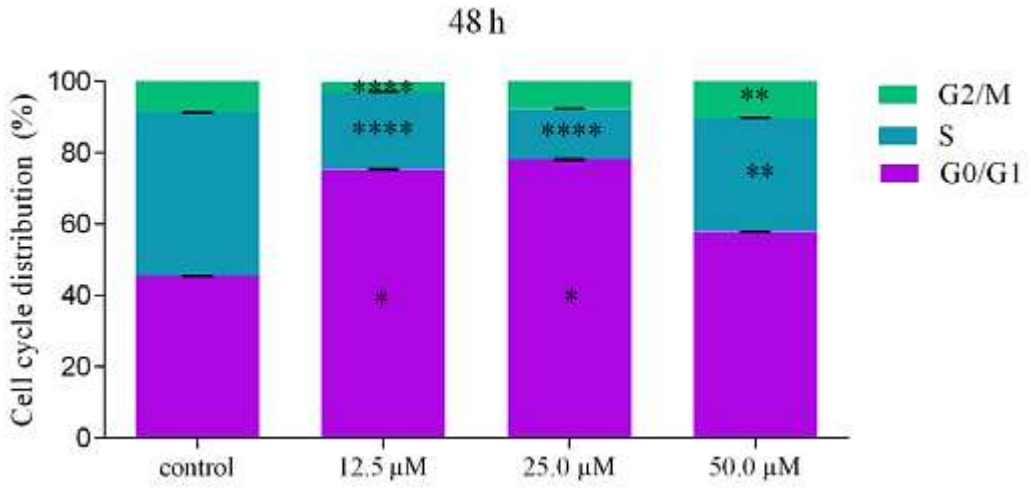

Figure 3 - Effect of compound **6b** on melanoma cell cycle. B16-F10 cells were treated with 12.5, 25.0, and 50.0 μM of compound **6b**. Cells treated with DMSO 0.4% v/v were used as control. Cell cycle was evaluated using propidium iodide, followed by cytometry analysis after 48 h of incubation. Data expressed as the mean ± S.E.M. *$p < 0.05$, **$p < 0.01$ and ****$p < 0.0001$ *versus* control (DMSO 0.4% v/v) by One-way ANOVA and Dunnett's post-hoc test.

3.5 Effect of compound 6b on the metastatic behavior of melanoma cells

Metastasis involves a series of progressive stages which include cell migration, invasion of blood and lymph vessels, cell colonization, and the ability of these cells to survive

in other organs [52, 53]. In order to analyze the cell migration, we evaluated the cell migration capacity through the wound healing assay using concentrations of 12.5, 25.0 and 50.0 μM of the compound **6b** for 24 h, all concentrations below the IC_{50} value. The compound **6b** significantly reduced in approximately 42% the cell migration at the concentration of 50.0 μM, in relation to the DMSO control (Figure 4).

Cinnamic acid and its derivatives normally interfere with cell dynamics, decreasing cell migration. Niero and Machado-Santelli (2013) observed that the treatment with cinnamic acid on melanoma cells caused cytoskeleton disruption [54]. Any change in the cell cytoskeleton interferes with cell locomotion, since these filaments are crucial for cell movement. Therefore, our data confirm the hypothesis that cinnamic acid derivatives interfere with cell migration.

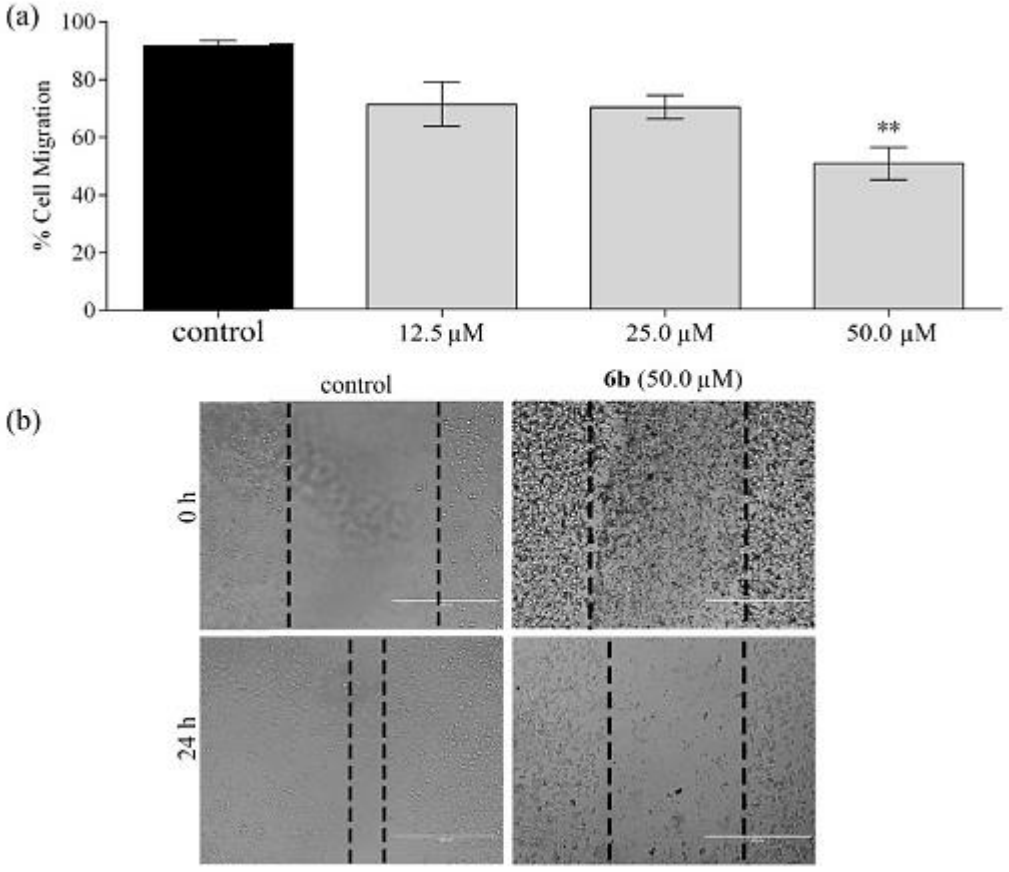

Figure 4 - Effect of compound **6b** on migration of B16-F10 melanoma cells *in vitro*. (A) B16-F10 metastatic melanoma was wounded with a pipette tip and then treated with 12.5, 25.0 and 50.0 μM of **6b** compound for 24 h. (B) Photos of the wound were taken at 0 and 24 h after treatment with 50.0 μM of the compound under 100x magnitude microscope. Data expressed as the mean ± S.E.M. **p < 0.01 versus control (0.04% DMSO) by One-way ANOVA and Dunnett's post-hoc test.

Once that **6b** interfered with cell migration and cell invasion is a key step of metastasis, invasion assay was performed. B16-F10 cells were treated with 12.5, 25.0 and 50.0 μM of the compound **6b**. Cell invasion decreased after 24 h of treatment with compound **6b** at 12.5 (35.9%), 25.0 (44.3%), and 50.0 (58.7%) μM compared to vehicle-treated cells (DMSO 0.4% v/v) (Figure 5).

Compounds with properties to reduce cellular invasion of cancer cells are interesting [55]. The ability of these synthetic cinnamic acid derivatives to inhibit the invasive capacity of melanoma cells *in vitro*, shows once again that cinnamic acid and its derivatives have anti-invasive properties against cancer cells, an effect also observed against colon carcinoma cells, human lung, adenocarcinoma, and even against melanoma cells [28, 56, 57]. This anti-invasion action of **6b** compound may be related to the activity of metalloproteinases (MMPs), since previous studies have shown that cinnamic acid derivatives are potent inhibitors of MMPs [28, 56, 57].

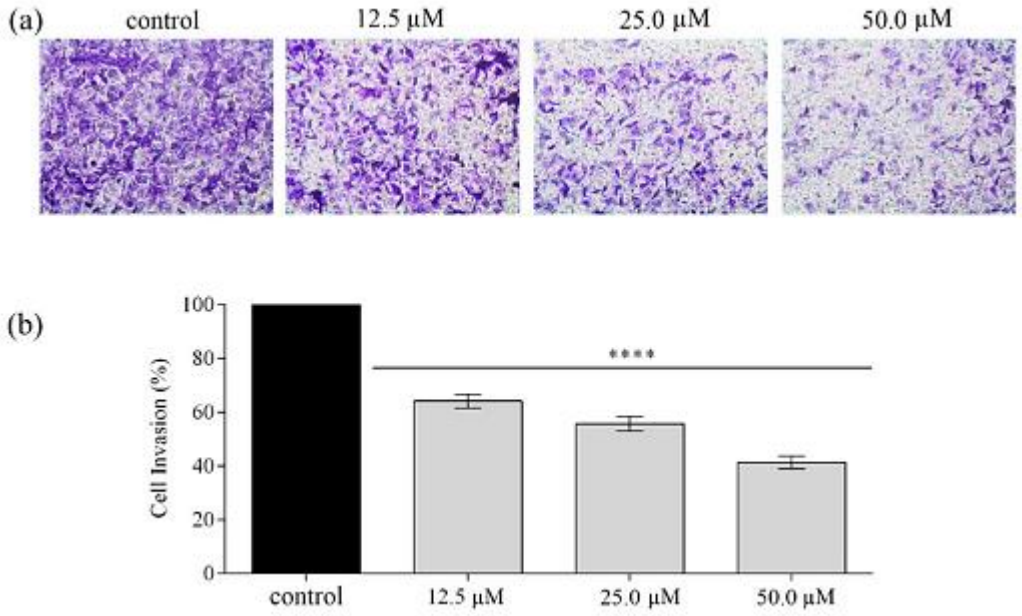

Figure 5 - Effect of compound **6b** on invasion of B16-F10 melanoma cells *in vitro*. (A) Photomicrography represents the cells invasion through matrigel-coated transwell. (B) The bar graph represents the percentage of invasive cell that was treated with 12.5, 25.0, and 50.0 μM of compound **6b** for 60 min. Data expressed as the mean ± S.E.M. ****$p < 0.0001$ *versus* control (DMSO 0.4% v/v) by One-way ANOVA and Dunnett's post-hoc test.

Finally, the colony formation was also assessed to evaluate the long-term effects of the compound **6b**. This compound significantly reduced colony formation, with a reduction in the

number of colonies at the concentrations of 12.5 (26.5%), 25.0 (41.6%) and 50.0 μM (53.3%) when compared to vehicle-treated cells (Figure 6). This important result is probably due to a set of factors, such as the negative action of compound **6b** on cell proliferation and its impact on cell mobility and invasion, as seen in previous *in vitro* assays [58].

Taken together, all the *in vitro* experiments performed suggested that the cinnamic acid derivative would render antiproliferative and antimetastatic effect in melanoma cells.

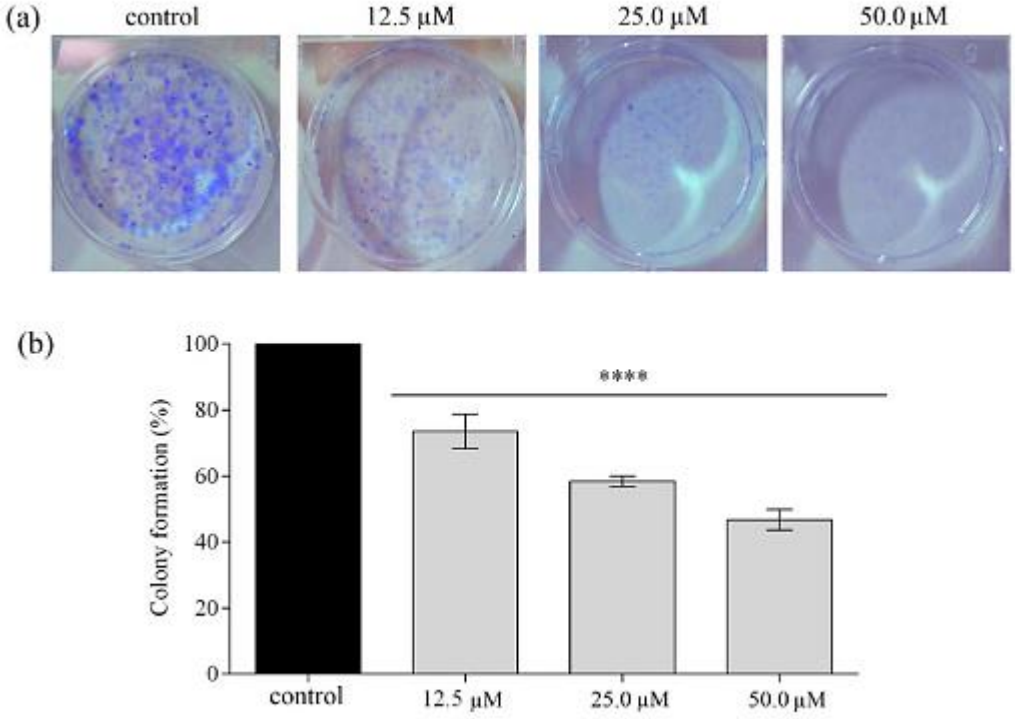

Figure 6 - Effect of compound **6b** on colony formation of B16-F10 melanoma cells *in vitro*. (A) Photomicrography showing the formation of B16-F10 colonies after treatment with 12.5, 25.0 and 50.0 μM of the compound **6b**. (B) The bar graph represents the percentage of colony formation after 7 days. Data expressed as mean ± S.E.M. ****$p < 0.0001$ *versus* control (DMSO 0.4% v/v) by One-way ANOVA and Dunnett's post-hoc test.

4. CONCLUSION

In summary, a series of novel triazole cinnamides and a hitherto unknown bis-triazole ester cinnamate were prepared and had their antiproliferative and antimetastastic activities evaluate *in vitro* on B16-F10 murine cell line. It was demonstrated that the derivative **6b**, the most effective compound, reduced the melanoma cell viability, generated cell cycle arrest and influenced the metastatic behavior of melanoma cells, by decreasing migration, invasion, and colony formation. Taken together, these results clearly showed the cytotoxic, antiproliferative

and antimetastatic potential of compound **6b** against melanoma cells and highlight the cinnamic acid derivative as possible therapeutic target for the treatment of metastatic cancers.

Supplementary Information

Supplementary data are available free of charge at http://jbcs.sbq.org.br as PDF file.

Acknowledgment

We are grateful to FAPEMIG, CNPq, and CAPES for financial support.

5. REFERENCES

[1]. Bishop, J. A. N.; Jewell, R.; In *Principles and Practice of Medical Genetics*, 6th ed.; Rimoin D., Pyeritz R., Korf B., eds; Academic Press: Cambridge, UK, 2013.

[2]. D´Orazio, J. A.; Jarrett, S.; Marsch, A.; Lagrew, J.; Clear, L.; In *Melanoma – Epidemiology, Genetics and Risk Factors;* Davids, L., ed.; IntechOpen: London, UK, 2013.

[3]. Bandarchi, B.; Ma, L.; Navab R.; Seth, A.; Rasty, G.; From melanocyte to metastatic malignant melanoma. *Dermatol. Res. Pract.* **2010**, *2010,* 1.

[4]. Cichorek, M.; Wachulska, M.; Stasiewicz, A.; Tyminska, A.; *Adv. Dermatol. Allergol*. **2013**, *30*, 30.

[5]. *Cancer Facts & Figures 2020.* Available at https://www.cancer.org/research/cancer-facts-statistics/all-cancer-facts-figures/cancer-facts-figures-2020.html, accessed in June 2021.

[6]. Apalla, Z.; Lallas, A.; Sotiriou, E.; Lazaridou, E.; Ioannides, D.; *Dermatol. Pract. Concept*. 2017, *7*, 1.

[7]. Siegel, R. L.; Miller, K. D.; Jemal, A.; *CA Cancer J.* Clin. **2020**, *70*, 7.

[8]. De Oliveira Santos, M.; *Rev. Bras. Cancerol*. **2020**, *66*, 1.

[9]. Landi, M. T.; Bishop, D. T.; MacGregor, S.; Machiela, M. J.; Stratigos, A. J.; Ghiorzo, P.; Brossard, M.; Calista, D.; Choi, J.; Fargnoli, M. C.; Zhang, T.; Rodolfo, M.; Trower, A. J.; Menin, C.; Martinez, J.; Hadjisavvas, A.; Song, L.; Stefanaki, I.; Scolyer, R.; Yang, R.; Goldstein, A. M.; Potrony, M.; Kypreou, K. P.; Pastorino, L.; Queirolo, P.; Pellegrini, C.; Cattaneo, L.; Zawistowski, M.; Gimenez-Xavier, P.; Rodriguez, A.; Elefanti, L.; Manoukian, S.; Rivoltini, L.; Smith, B. H.; Loizidou, M. A.; Regno, L. D.; Massi, D.; Mandala, M.; Khosrotehrani, K.; Akslen, L. A.; Amos, L. A.; Andresen, P. A.; Avril, M.-F.; Azizi, M.-F.; Soyer, H. P.; Bataille, V.; Dalmasso, B.; Bowdler, L. M.; Burdon, K. P.; Chen, W. V.; Codd, V.; Craig, J. E.; Dębniak, T.; Falchi, M.; Fang, S.; Friedman, E.; Simi, S.; Galan, P.; Garcia-Casado, Z.; Gillanders, E. M.; Gordon, S.; Green, A.; Gruis, N. A.; Hansson, J.; Harland, M.; Harris, J.; Helsing, P.; Henders, A.; Marko Hočevar, V.; Höiom, D.; Hunter, C.; Ingvar, R.; Kumar, J.; Lang, Lathrop, G. M.; Lee, J. E.; Li, X.; Lubiński, J.; Mackie, R. M.; Malt, M.; Malvehy, J.; McAloney, H.; Mohamdi,

K.; Molven, A.; Moses, E. K.; Neale, R. E.; Novaković, S.; Nyholt, D. R.; Olsson, H.; Orr, N.; Fritsche, L. G.; Puig-Butille, J. A.; Qureshi, A. A.; Radford-Smith, G. L.; Randerson-Moor, J.; Requena, C.; Rowe, C.; Samani, N. J.; Sanna, M.; Schadendorf, D.; Schulze, H.-J.; Simms, L. A.; Smithers, M.; Song, F.; Swerdlow, A. J.; van der Stoep, N.; Kukutsch, N. A.; Visconti, A.; Wallace, L.; Ward, S. V.; Wheeler, L.; Sturm, R. A.; Hutchinson, A.; Jones, K.; Malasky, M.; Vogt, A.; Zhou, W.; Pooley, K. A.; Elder, D. E.; Han, J.; Hicks, B.; Hayward, N. K.; Kanetsky, P. A.; Brummett, C.; Montgomery, G. W.; Olsen, C. M.; Hayward, C.; Dunning, A. M.; Martin, N. G.; Evangelou, E.; Mann, G. J.; Long, G.; Pharoah, P. D. P.; Easton, D. F.; Barrett, J. H.; Cust, A. E.; Abecasis, G.; Duffy, D. L.; Whiteman, D. C.; Gogas, H.; De Nicolo, A.; Tucker, M. A.; Newton-Bishop, M. A.; *Nat. Genet.* **2020**, *52*, 494.

[10]. Maio, M. M.; Grob, J.-J.; Aamdal, S.; Bondarenko, I.; Robert, C.; Thomas, L.; Garbe, C. V. C.-S.; Testori, A.; Chen, T.-T.; Tschaika, M.; Walchok, J. D; *J. Clin. Onc*. **2015**, *33*, 1191.

[11]. Mattia, G.; Puglisi, R.; Ascione, B.; Malorni, W.; Carè, A.; Matarrese, P.; *Cell Death Dis*. **2018**, *25*, 112.

[12]. Bhatia, S.; Tykodi, S. S.; Thompson, J. A.; *Oncology*. **2009**, *23*, 488.

[13]. Balch, C. M.; Buzaid, A. C.; Soong, S.-J.; Atkins, M. B.; Cascinelli, N.; Coit, D. G.; Fleming, I. D.; Gershenwald, J. E.; Houghton Jr, A.; Kirkwood, J. M.; McMasters, K. M.; Mihm, M. F.; Morton, D. L.; Reintgen, D. S.; Ross, M. I.; Sober, A.; Thompson, J. A.; Thompson, J. F.; *J. Clin. Onc*. **2009**, *19*, 3635.

[14]. Atallah, E.; Flaherty, L.; *Curr. Treat. Options Oncol*. **2005**, *6*, 185.

[15]. Domingues, B.; Lopes, J. M.; Soares, P.; Pópulo, H.; *ImmunoTargets Ther.* **2018**, *7*, 35.

[16]. Wróbel, S.; Przybylo, M.; Stepień, E.; *J. Clin. Med*. **2019**, *8*, 368.

[17]. *National Cancer Institute. Drugs Approved for Melanoma.* Available at https://www.cancer.gov/about-cancer/treatment/drugs/melanoma, accessed in June 2020.

[18]. do Vale, J. A.; Lima, G. D. A.; Almeida, A. A.; Teixeira, R. R.; Neves, M. M.; In *Horizons in Cancer Research,* vol 77.; Watanabe, H. S., ed.; Nova Science Publishers: Nova York, USA, 2020.

[19]. Gupta, A.; Gomes, F.; Lorigan, P.; *Melanoma Manag.* **2017**, *4*, 125.

[20]. Harvey, A. L.; *Drug Discov. Today*. **2008**, *13*, 894.

[21]. Harvey, A. L.; Edrada-Ebel, R.; Quinn, R. J.; *Nat. Rev. Drug Discov*. **2015**, *14*, 111.

[22]. Thomford, N. E.; Senthebane, D. A.; Rowe, A.; Munro, D.; Seele, P.; Dzobo, A. M. K.; *Int. J. Mol. Sci.* **2018**, *19*, 1578.

[23]. Koparde, A. A.; Doijad, R. C.; Magdum, C. S.; In *Natural Products in Drug Discovery,* Intechopen: London, UK, 2019.

[24]. Chinembiri, T. N.; du Plessis, L. H.; Gerber, M.; Hamman, J. H.; du Plessis, J.; *Molecules*, **2014**, *19*, 11679.

[25]. Alqathama, A.; Prieto, J. M.; *Nat. Prod. Rep.* **2015**, *32*, 1170.

[26]. Newman, D. J.; Cragg, G. M.; *J. Nat. Prod*. **2016**, *79*, 629.

[27]. De P., Baltas, M.; Bedos-Belval, F.; *Curr. Med. Chem*. **2011**, *18*, 1672.

[28]. Lima, G. D. A.; Rodrigues, M. P.; Mendes, T. A. O.; Moreira, G. A.; Siqueira, R. P.; da Silva, A. M.; Vaz, B. G.; Fietto, J. L. R.; Bressan, G. C.; Neves, M. M.; Teixeira, R. R.; *Toxic. In Vitro*. **2018**, *53*, 1.

[29]. Dheer, D.; Singhi, V.; Shankar, R.; *Bioorg. Chem.* **2017**, *71*, 30.

[30]. Agalave, S. G.; Maujan, S. R.; Pore, V. S.; *Chem. Asian J.* **2011**, *6*, 2696.

[31]. Xu, Z.; Zhao, S.-J.; Liu, Y.; *Eur. J. Med. Chem.* **2019**, *183*, 111700.

[32]. Liu, X.; Luo, J.; Kong, L.; *Nat. Prod. Commun*. **2011**, *6*, 851.

[33]. de Araújo-Vilges, K. M.; de Oliveira, S. V.; Couto, S. C. P.; Fokoue, H. H.; Romero, G. A. S.; Kato, M. J.; Romeiro, L. A. S.; Leite, J. R. A.; Kuckelhaus, S. A. S.; *Pharm. Biol*. **2017**, *55*, 1601.

[34]. Phuwaspraisiran, P.; Puksasook, T.; Jong-Aramruang, J.; Kokpol, U.; *Bioorg. Med. Chem. Lett.* **2008**, *18*, 4956.

[35]. Gaikwad, N.; Nanduri, S.; Madhavi, Y. V.; *Eur. J. Med. Chem*. **2019**, *181*, 111561.

[36]. Moreira, G. A.; Lima, G. D. A.; Siqueira, R. P.; Barros, M. V. A.; Adjanohoun, A. L. M.; Santos, V. C.; Barbosa, E. A. A.; Loterio, R. K.; de Paiva, J. C.; Gonçalves, V. H. S.; Viol, L. C. S.; Marques, E. S. A.; Júnior, A. S.; Almeida, M. R.; Fietto, J. L. R.; Neves, M. M.; Ferreira, R. S.; Teixeira, R. R.; Bressan, G. C.; *Toxicol. Appl. Pharm*. **2018**, *356*, 214.

[37]. do Vale, J. A.; de Souza, A. P. M.; Lima, G. D .A.; Gonçalves, V. H. S.; Moreira, G. A.; Barros, M. V. A.; Pereira, W. L.; Lazaroni e Merchid, N. C.; Fietto, J. L. R.; Bressan, G. C.; Teixeira, R. R.; Neves, M. M.; *Anticancer Drugs*. **2020**, *31*, 718.

[38]. Neises, B.; Steglich, W.; *Angew. Chem. Int. Ed.* **1978**, *17*, 522.

[39]. Kolb, H. C.; Finn, M. G.; Sharpless, K. B.; *Angew. Chem. Int. Ed*. **2001**, *40*, 2004.

[40]. Rostovtsev, V. V.; Green, L. G.; Fokin, V. V.; Sharpless, K. B.; *Angew. Chem. Int. Ed.* **2002**, *41*, 2596.

[41]. Tornϕe, C. W.; Christensen, C.; Meldal, M.; *J. Org. Chem*. **2002**, *67*, 3057.

[42]. Singh, M. S.; Chowdhury, S.; Koley, S.; *Tetrahedron*. **2016**, *72*, 5257.

[43]. Borgati, T. F.; Alves, R. B.; Teixeira, R. R.; de Freitas, R. P.; Perdigão, T. G.; da Silva, S. F.; dos Santos, A. A.; Bastidas, A. J. O.; *J. Braz. Chem. Soc.* **2013**, *24*, 953.

[44]. Sivakumar, K.; Xie, F.; Cash, M.; Long, S.; Barnhill, H. N.; Wang, Q.; *Org. Lett*. **2004**, *24*, 4603.

[45]. Reis, W. J.; Moreira, P. O. L.; Alves, R. B.; Oliveira, H. H. M.; Silva, L. M.; Varotti, F. P.; Freitas, R. P.; *Curr. Top. Med. Chem*. **2018**, *18*, 1475.

[46]. Dunagin, M. C.; Torborg, S. R.; Torre, E. A.; Emert, B.; Krepler, C.; Beqiri, M.; Sproesser, K.; Brafford, P. A.; Xiao, M.; Eggan, E.; Anastropoulos, J. N.; Vargas-Garcia, C. A.; Singh, A.; Nathanson, K. L.; Herlyn, M.; Raj, A.; *Nature*. **2017**, *546*, 431.

[47]. Sova, M.; Zizac, Z.; Stankovic, J. A. A.; Prijatelj, M.; Turk, S.; Jurani, Z. D.; Mlinari - Rascan, I.; Gobec, S.; *J. Med. Chem*. **2013**, *9*, 633.

[48]. Yang, Y.; Zhang, Y.; Li, N.; *J. Ethnopharmacol*. **2019**, *236*, 129.

[49]. Romaguera, J. E.; *Oncologic Imaging: A Multidisciplinary Approach*. Rohren, E.M., Erasmus, J.J., Szklaruk, J., Vining, D., Sandler, C.M., Kaur, H., Hagemeister, F.B., Madewell, J.E., Raval, B., Gladish, G., eds.; Elsevier Saunders: Philadelphia, USA, 2012.

[50]. Li, Y.; Zhang, G.; *Cancer Biol. Med.* **2017**, *14*, 348.

[51]. Hunke, M.; Martinez, W.; Kashyap, A.; Bokoskie, T.; Pattabiraman, M.; Chandra, S.; *Anticancer Res*. **2018**, *8*, 4469.

[52]. Gray-Schopfer, V.; Wellbrock, C.; Marais, R.; *Nature* **2007**, *445*, 851.

[53]. Balasas, T.; Callaghan, J.; Coombes, R. C.; Evans, J.; Hall, J. A.; Kinrade, S.; Jones, D.; Jones, P. S.; Jones, R.; Marshall, J. F.; Panico, M. B.; Shaw, J. A.; Steeg, P. S.; Sullivan, M.; Tong, W.; Westwell, A. D.; Ritchie, J. W. A.; *Nat. Rev*. **2019**, *16*,185.

[54]. Niero, E. L.; Machado-Santelli, G. M.; *J. Exp. Clin. Cancer Res*. **2013**, *32*, 1.

[55]. Rosel, D.; Fernandes, M.; Veselý, P.; Heneberg, P.; Cermák, V.; Petruželka, L.; Kumar, S.; Sanz-Moreno, V.; Brábek, J.; *Trends Cancer,* **2017**, *3*, 391.

[56]. Yen, G-C.; Chen, Y-L.; Sun, F-M.; Chiang, Y-L.; Lu, S-H.; Weng, C-J.; *Eur. J. Pharm. Sci.* **2011**, *44*, 281.

[57]. Tsai, C-M.; Yen, G. C.; Sun, F. M.; Yang, S. F.; Weng, C. J.; *Mol. Pharm*. **2013**, *10*, 1890.

[58]. Almeida, A. A.; Lima, G. D. A.; Simão, M. V. R. C.; Moreira, G. A.; Siqueira, R. P.; Zanatta, A. C.; Vilegas, W.; Machado-Neves, M.; Bressan, G. C.; Leite, J. P. V.; *Int. J. Exp. Path.* **2020**, *00*, 1.

[59]. Siqueira, R. P.; Barbosa, E. A. A.; Polêto, M. D.; Righetto, G. L.; Seraphim, T. V.; Salgado R. L.; Ferreira, J. G.; Barros, M. V. A.; de Oliveira, L. L.; Laranjeira, A. B. A.;

Almeida, M. R.; Júnior, A. S.; Fietto, J. L. R.; Kobarg, J.; de Oliveira, E. B.; Teixeira, R.R.; Borges, J. C.; Yunes, J. A.; Bressan, G.C.; *PLoS ONE*. **2015**, *10*, 1.

[60]. Rasband, W.S., *ImageJ*, version 1.49; U. S. National Institutes of Health,version, Bethesda, Maryland, USA, 2015.

[61]. Microsoft Corporation, *Microsoft Excel*, version 16.0; Microsoft Company, Redmond, WA, USA, 2016.

[62]. GraphPad Software, Inc., *GraphPad Prism*, version 6.01; Software Mackiey, San Diego, California, USA, 2012.

SUPPLEMENTARY INFORMATION

Synthesis of Novel Cinnamides and a Bis Cinnamate bearing 1,2,3-Triazole Functionalities with Antiproliferative and Antimetastatic Activities on Melanoma Cells

Fabíola S. Santos[a§], Juliana A. do Vale[b§], Lucas da S. Santos[a], Talita B. Gontijo[a], Graziela D. A. Lima[b], Leandro L. de Oliveira[b], Mariana Machado-Neves[b], Róbson R. Teixeira[c], Rossimiriam P. de Freitas[a*]

[§]These authors contributed equally to this work

[a]*Laboratório de Síntese Orgânica (LABSINTO), Departamento de Química, Universidade Federal de Minas Gerais(UFMG), CEP 31270-901 Belo Horizonte-MG, Brazil*

[b] *Departamento de Biologia Geral, Universidade Federal de Viçosa (UFV), CEP 36590-000 Viçosa-MG, Brazil*

[c]*Departamento de Química, Universidade Federal de Viçosa (UFV), CEP36590-000 Viçosa-MG, Brazil*

*rossimiriam@ufmg.br

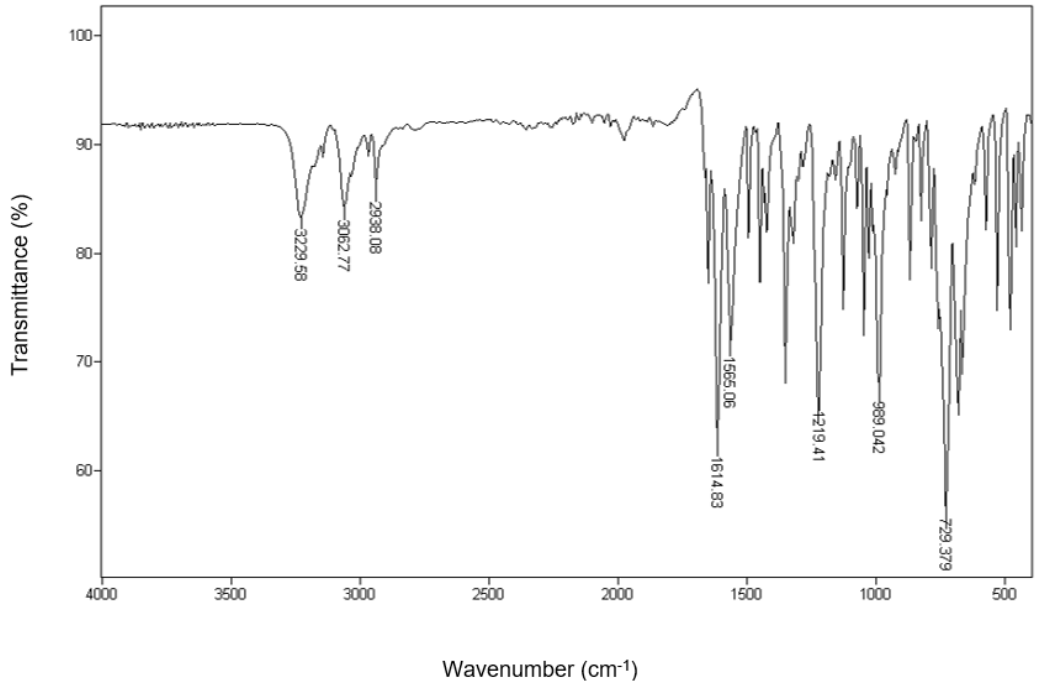

Figure S1 - IR spectrum (ATR) of **3a**.

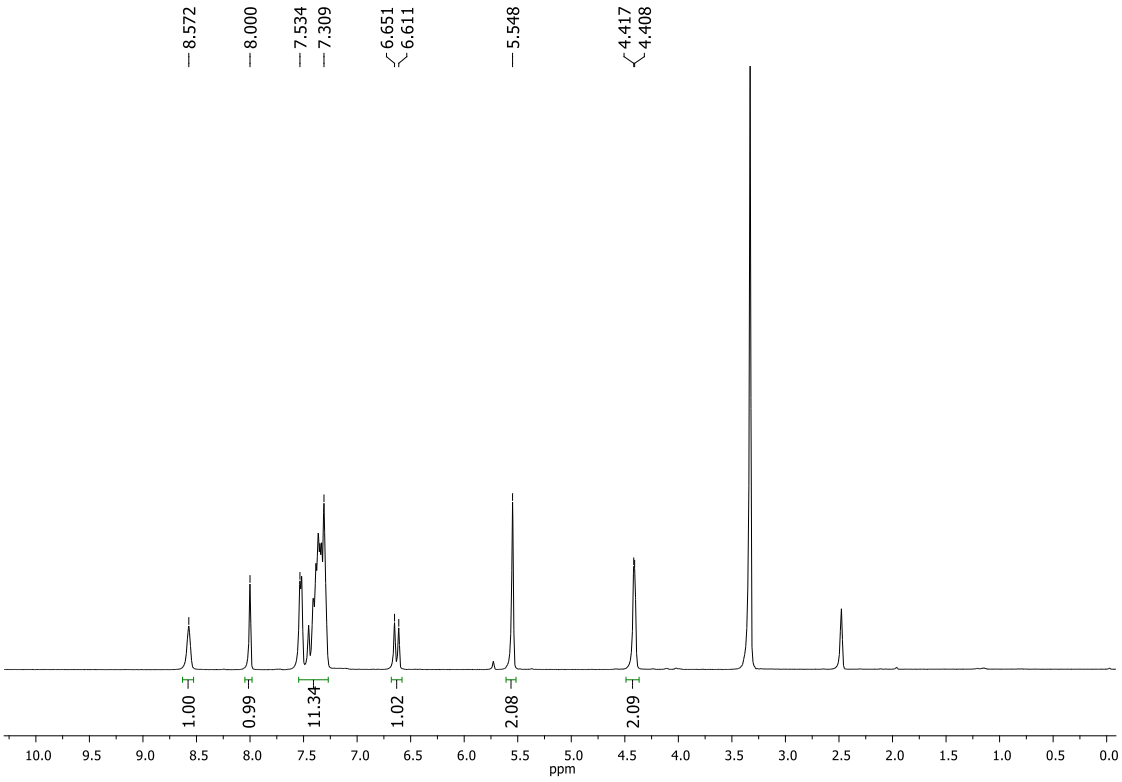

Figure S2 - ^{1}H NMR spectrum (400 MHz, DMSO-d_6) of **3a**.

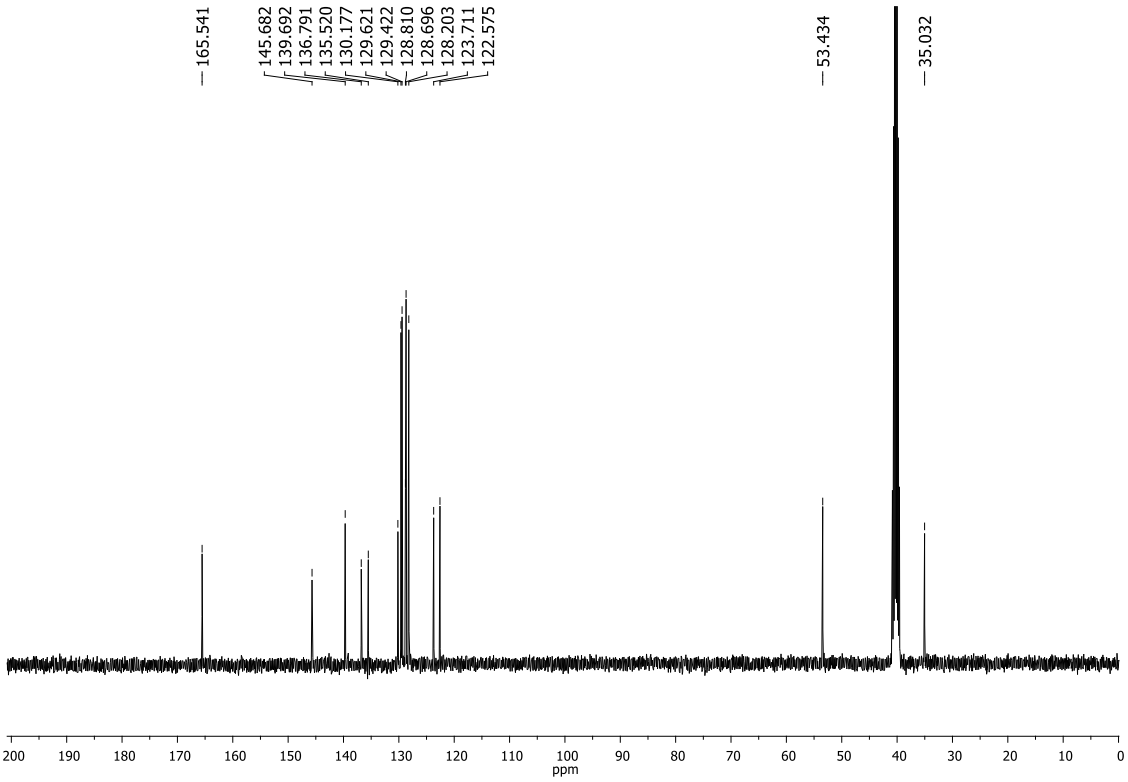

Figure S3 - ^{13}C NMR spectrum (100 MHz, DMSO-d_6) of **3a**.

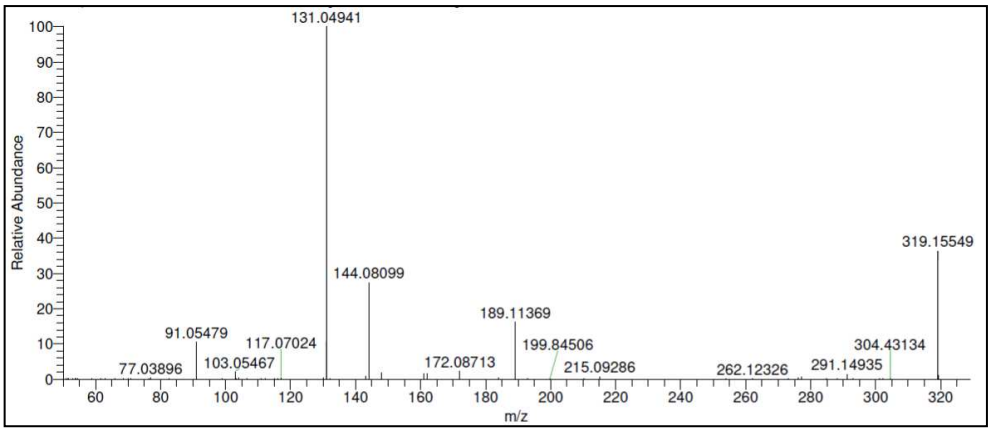

Figure S4 - HRMS spectrum of **3a**.

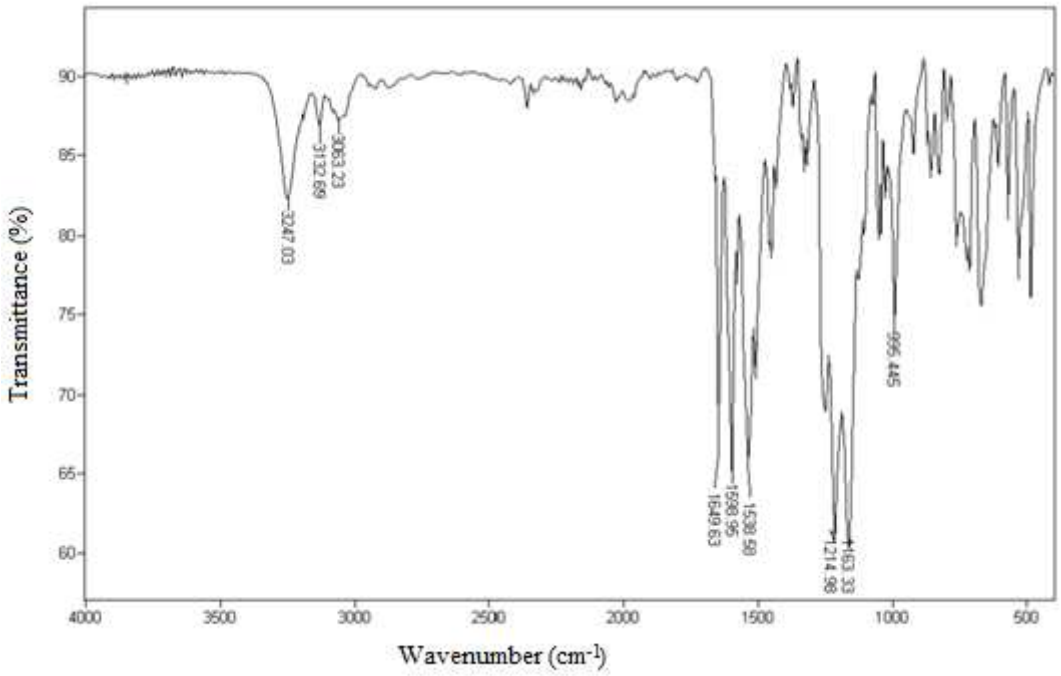

Figure S5 - IR spectrum (ATR) of **3b**.

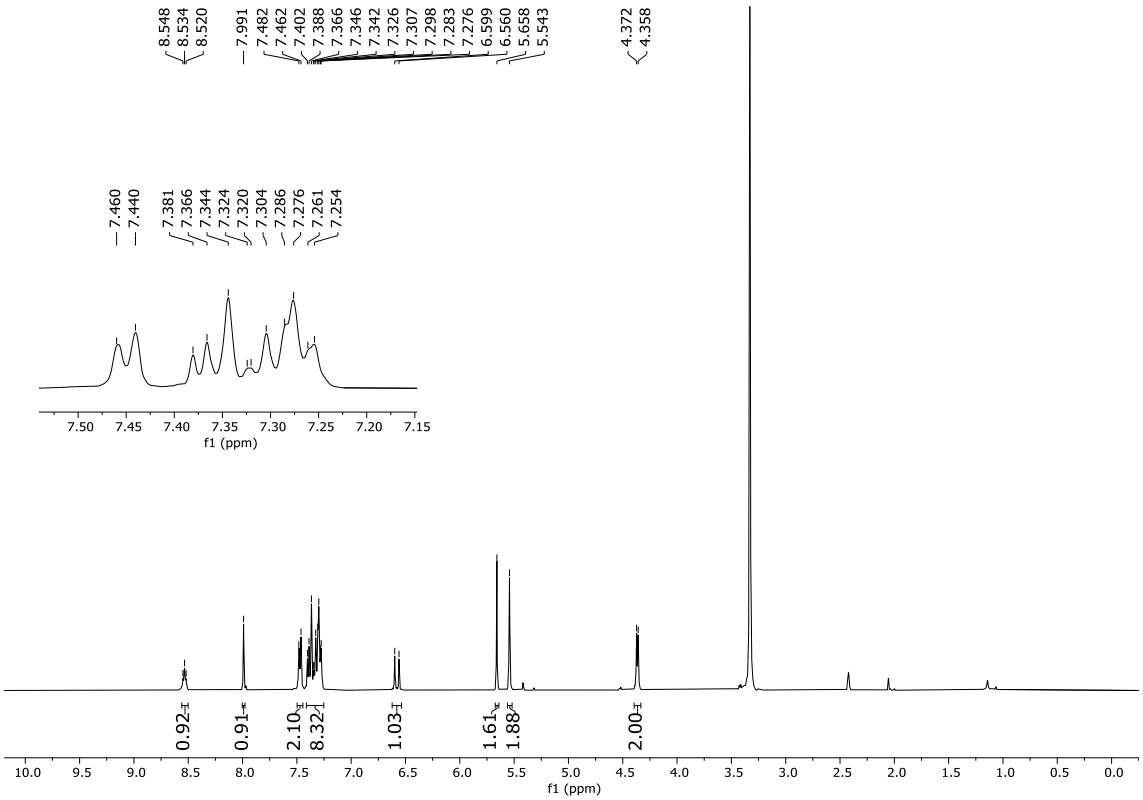

Figure S6 - ^{1}H NMR spectrum (400 MHz, DMSO-d_6) of **3b**.

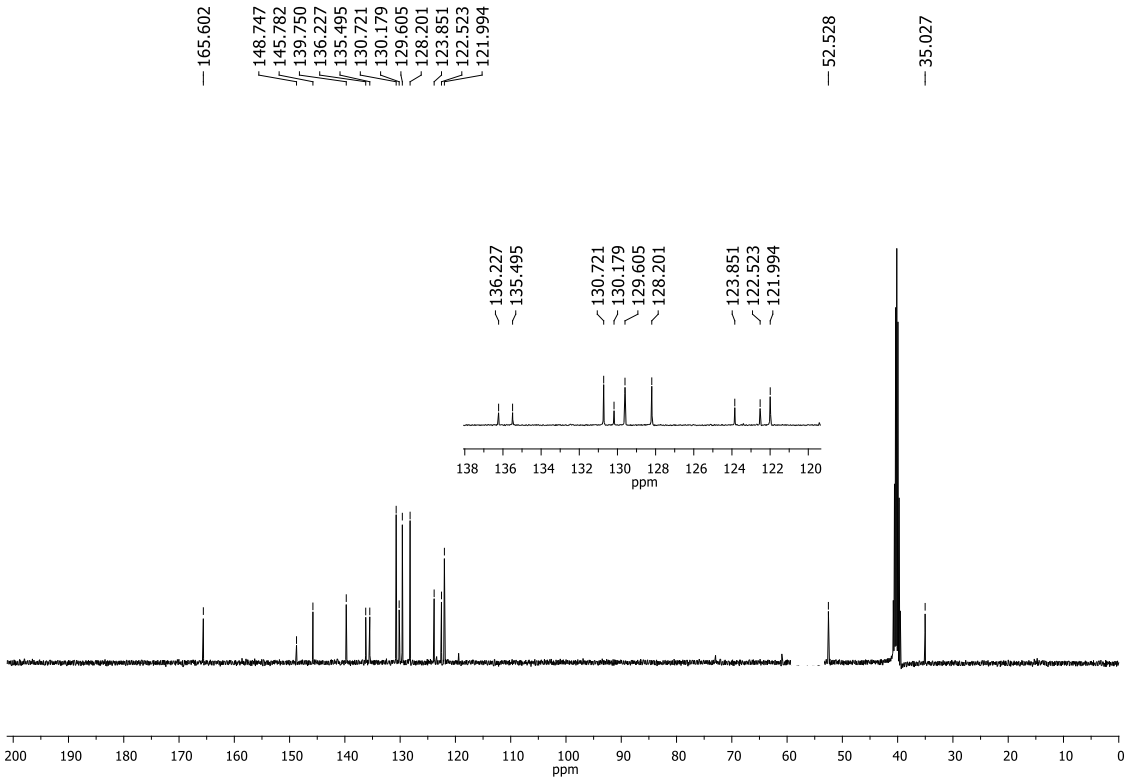

Figure S7 - ^{13}C NMR spectrum (100 MHz, DMSO-d_6) of **3b**.

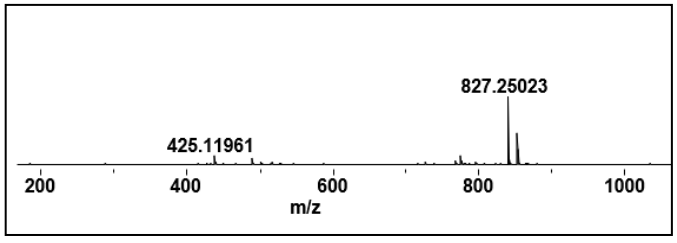

Figure S8 - HRMS spectrum of **3b**.

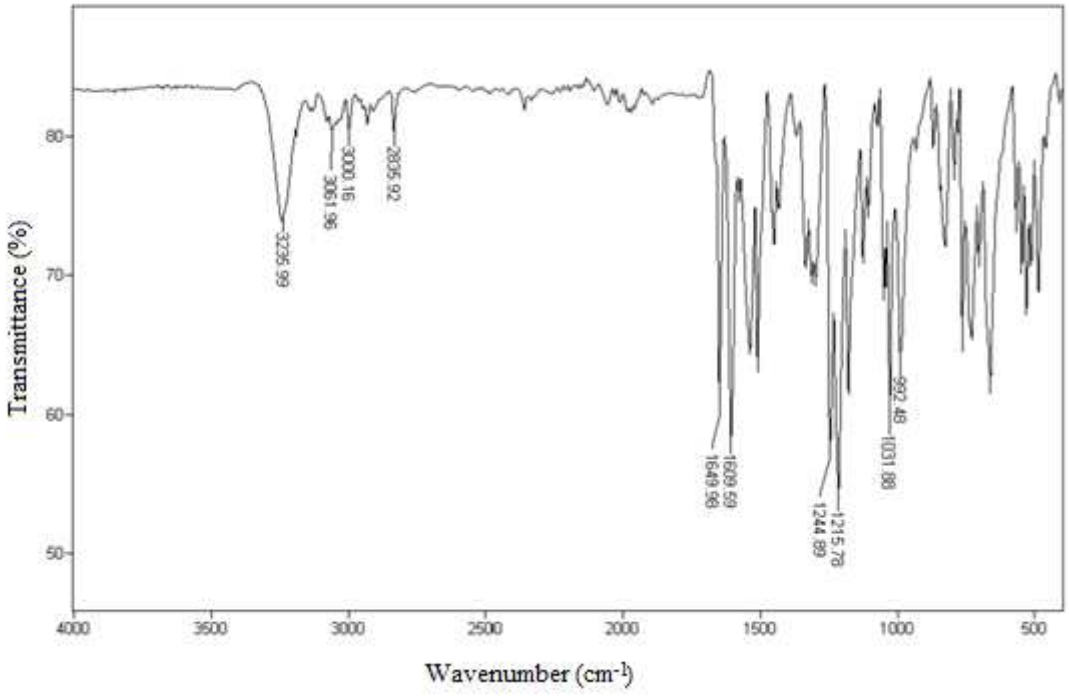

Figure S9 - IR spectrum (ATR) of **3c**.

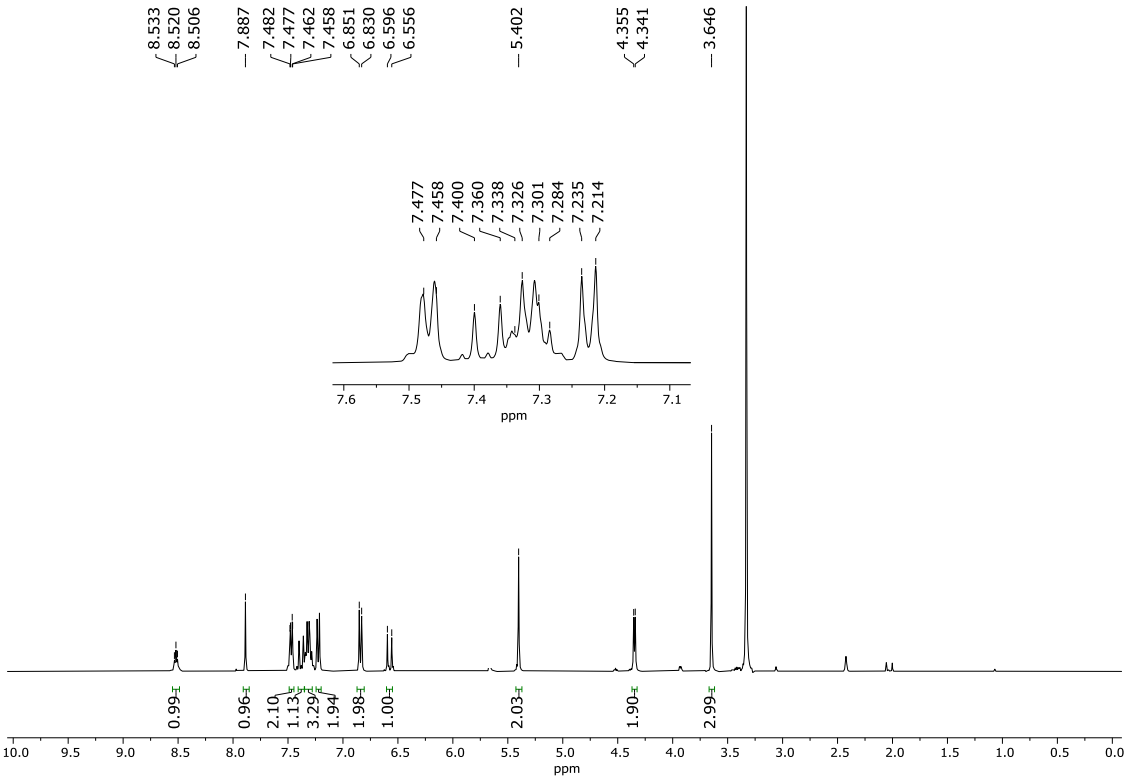

Figure S10 - ^{1}H NMR spectrum (400 MHz, DMSO-d_6) of **3c**.

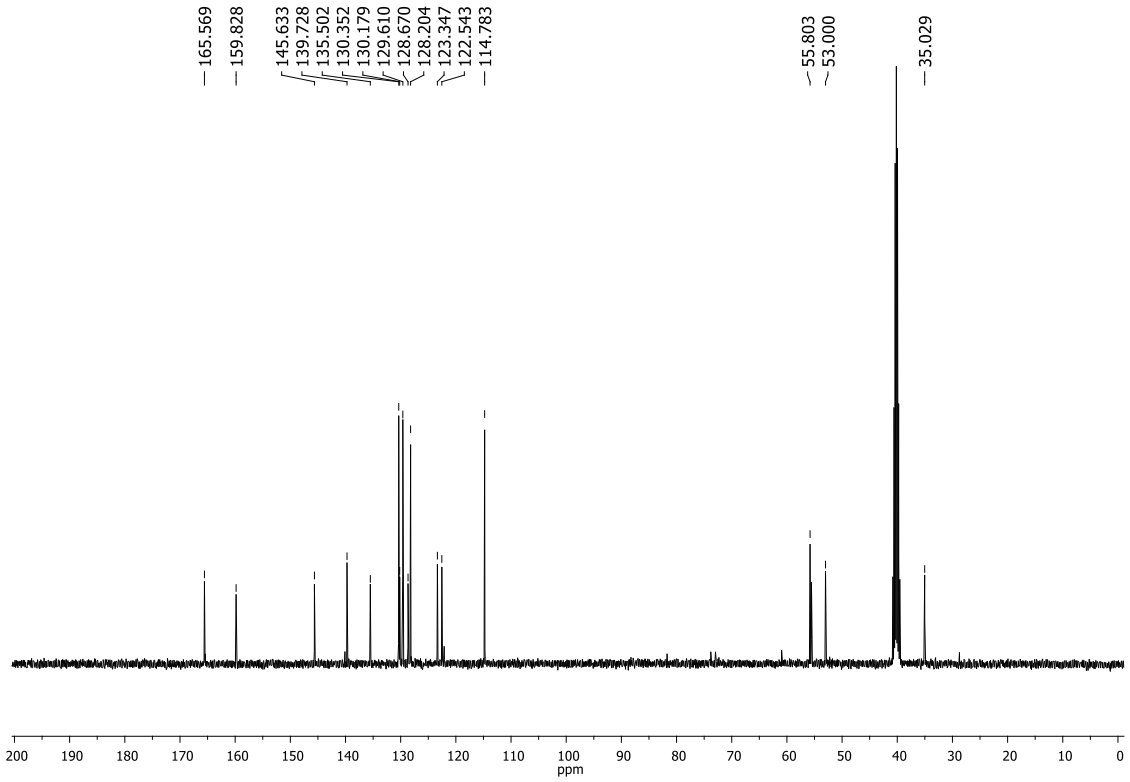

Figure S11 - ^{13}C NMR spectrum (100 MHz, DMSO-d_6) of **3c**.

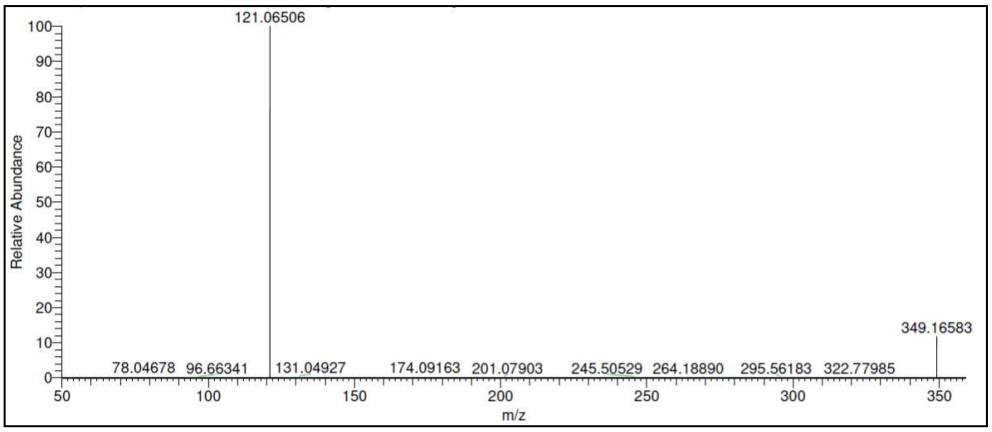

Figure S12 - HRMS spectrum of **3c**.

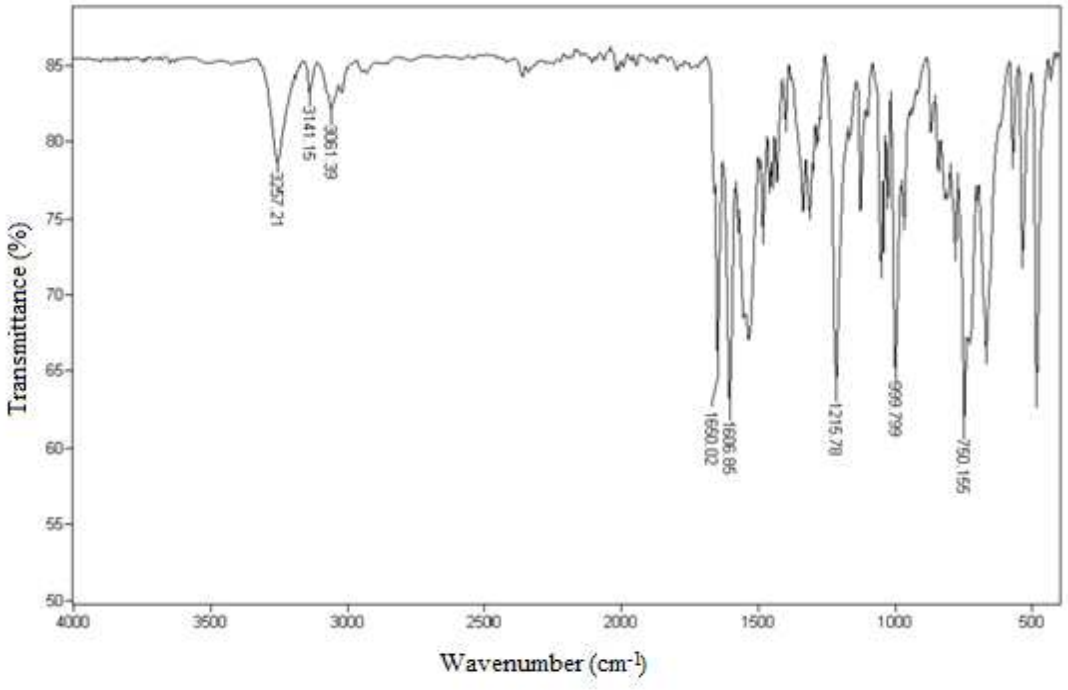

Figure S13 - IR spectrum (ATR) of **3d**.

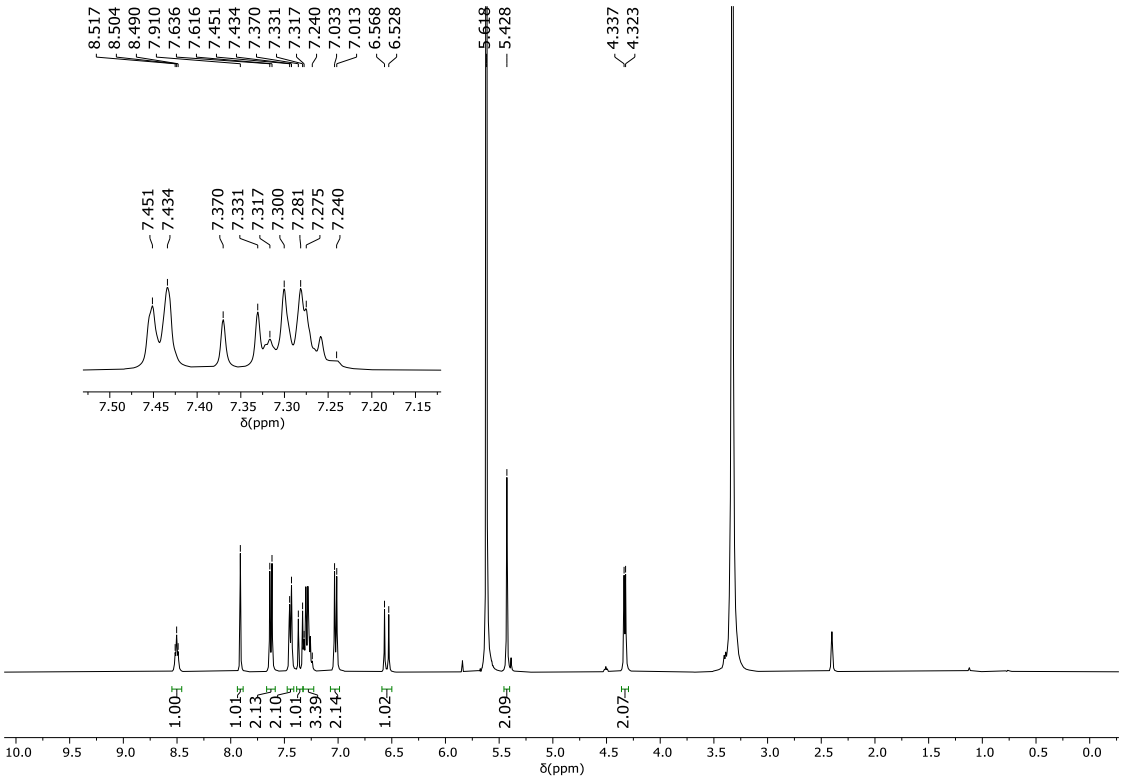

Figure S14 - ^{1}H NMR spectrum (400 MHz, DMSO-d_6) of **3d**.

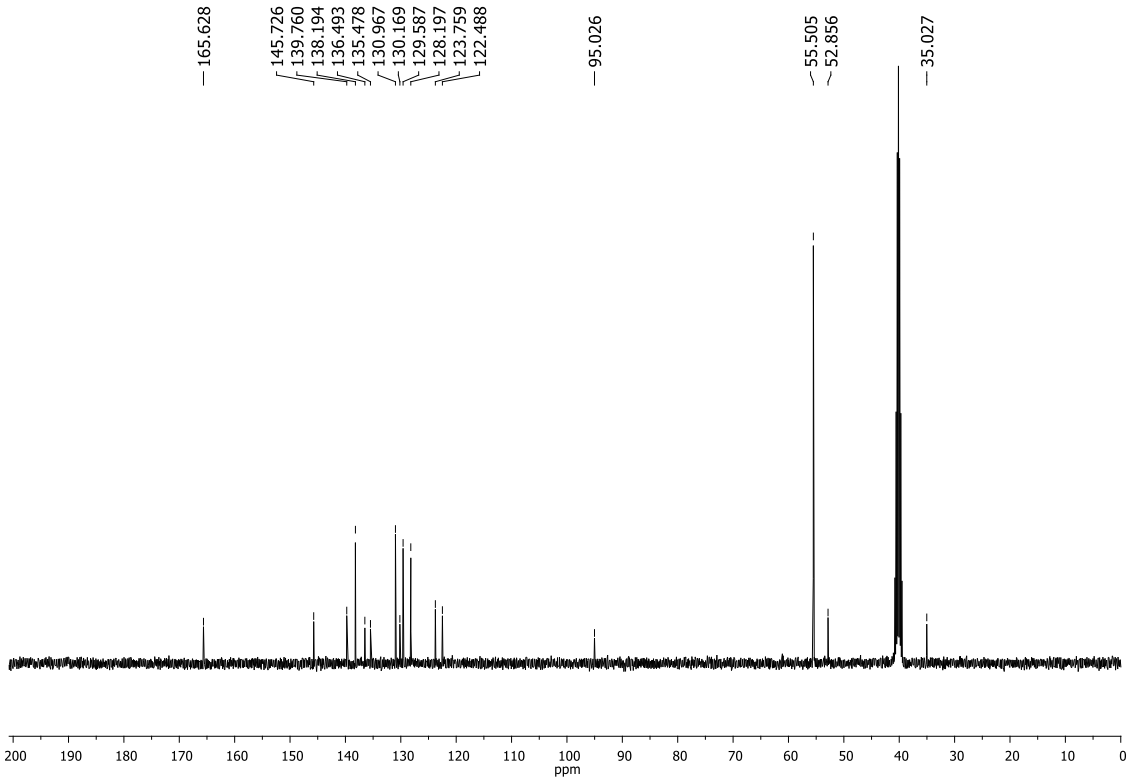

Figure S15 - ^{13}C NMR spectrum (100 MHz, DMSO-d_6) of **3d**.

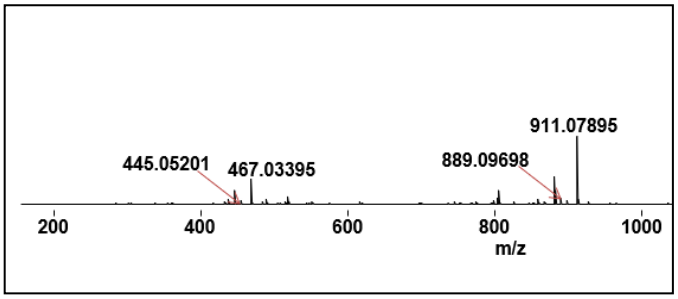

Figure S16 - HRMS spectrum of **3d**.

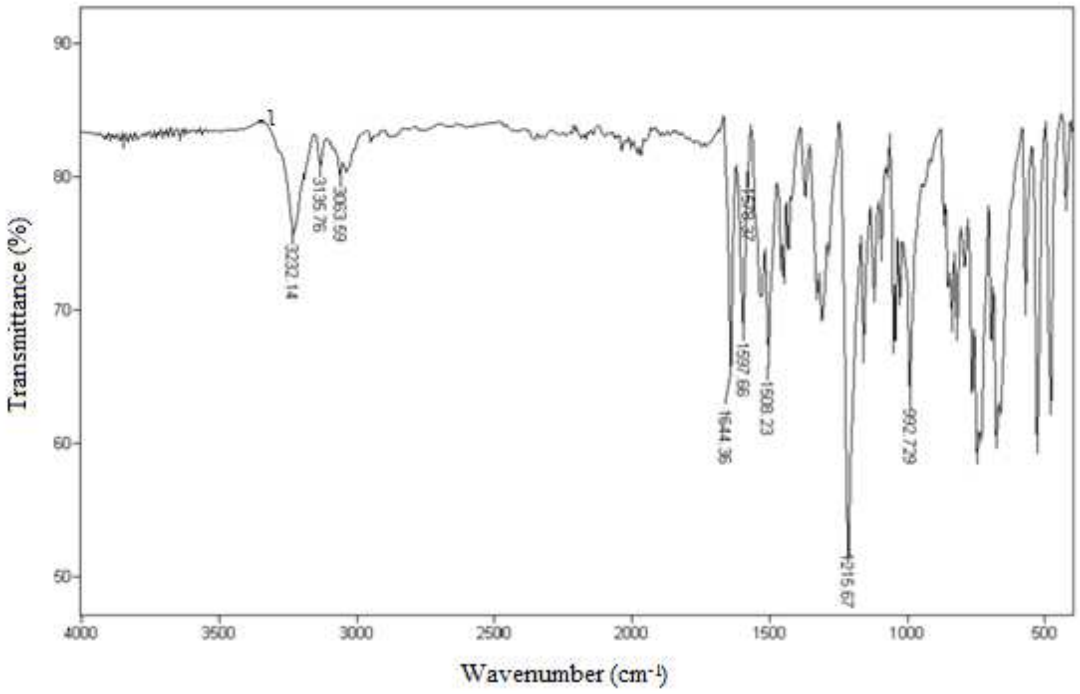

Figure S17 - IR spectrum (ATR) of **3e**.

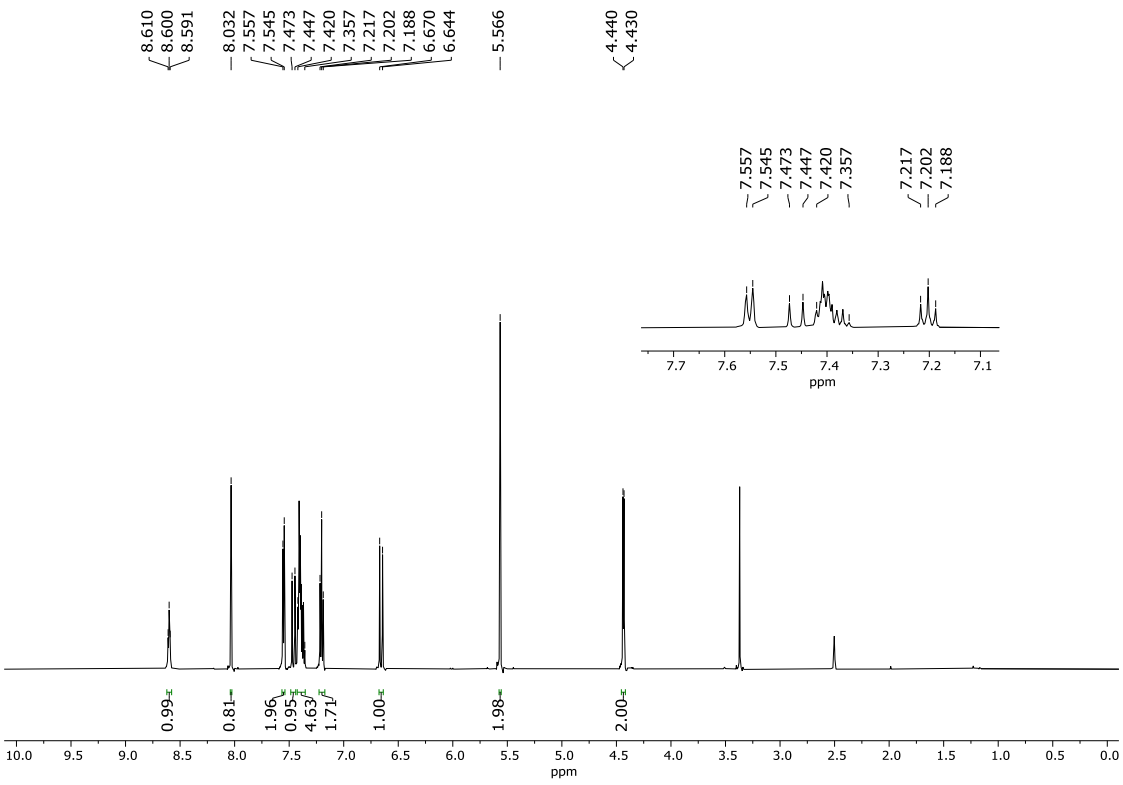

Figure S18 - ^{1}H NMR spectrum (600 MHz, DMSO-d_6) of **3e**.

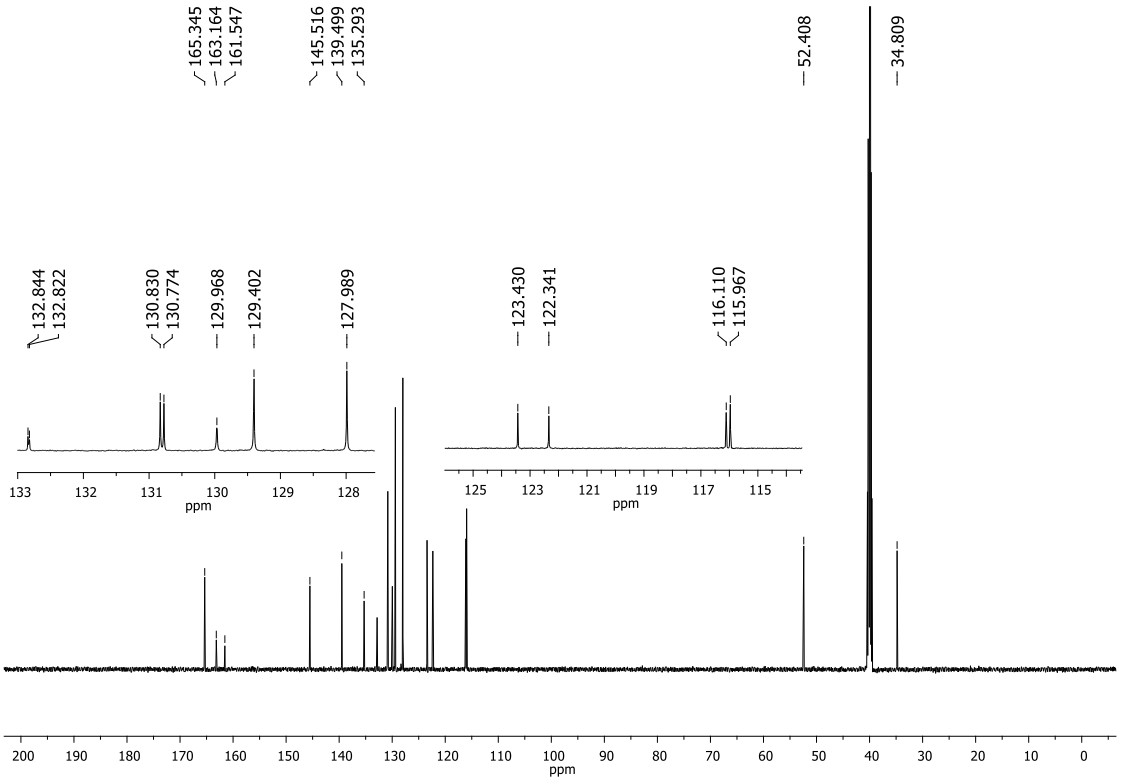

Figure S19 - ^{13}C NMR spectrum (150 MHz, DMSO-d_6) of **3e**.

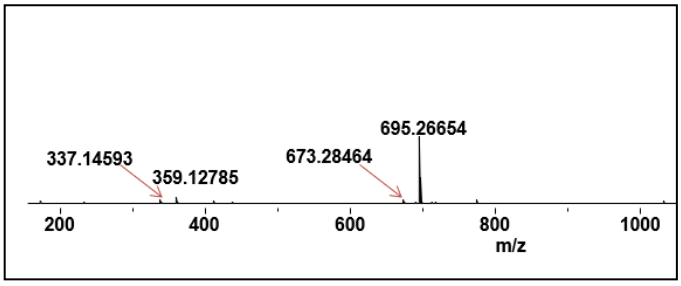

Figure S20 - HRMS spectrum of **3e**.

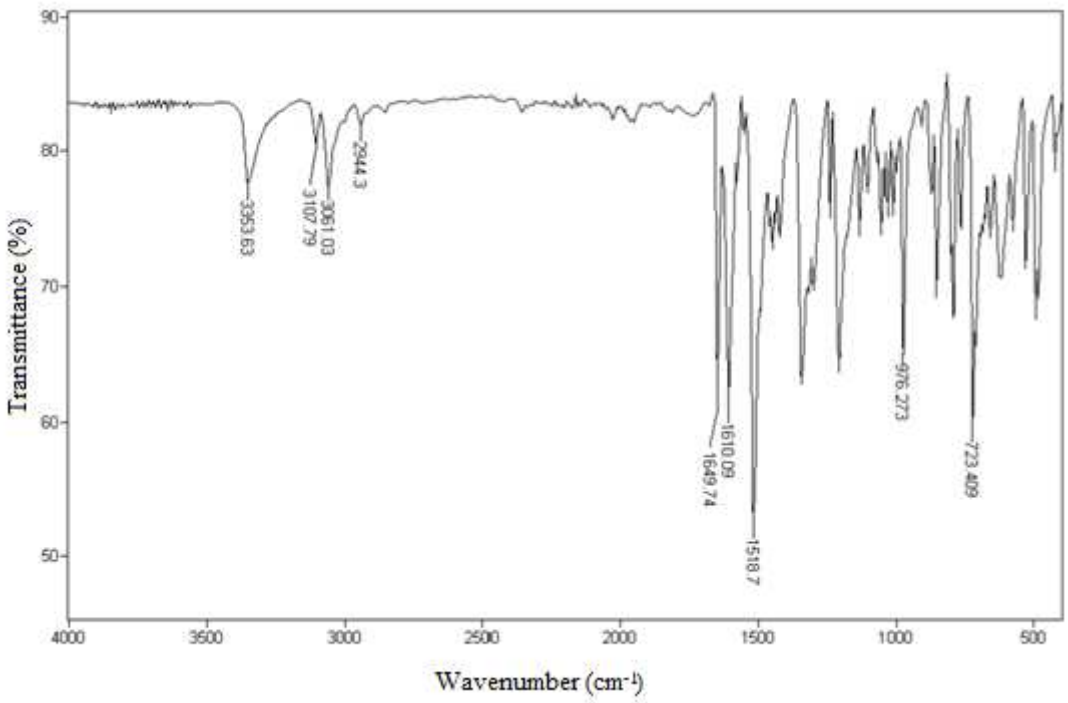

Figure S21 - IR spectrum (ATR) of **3f**.

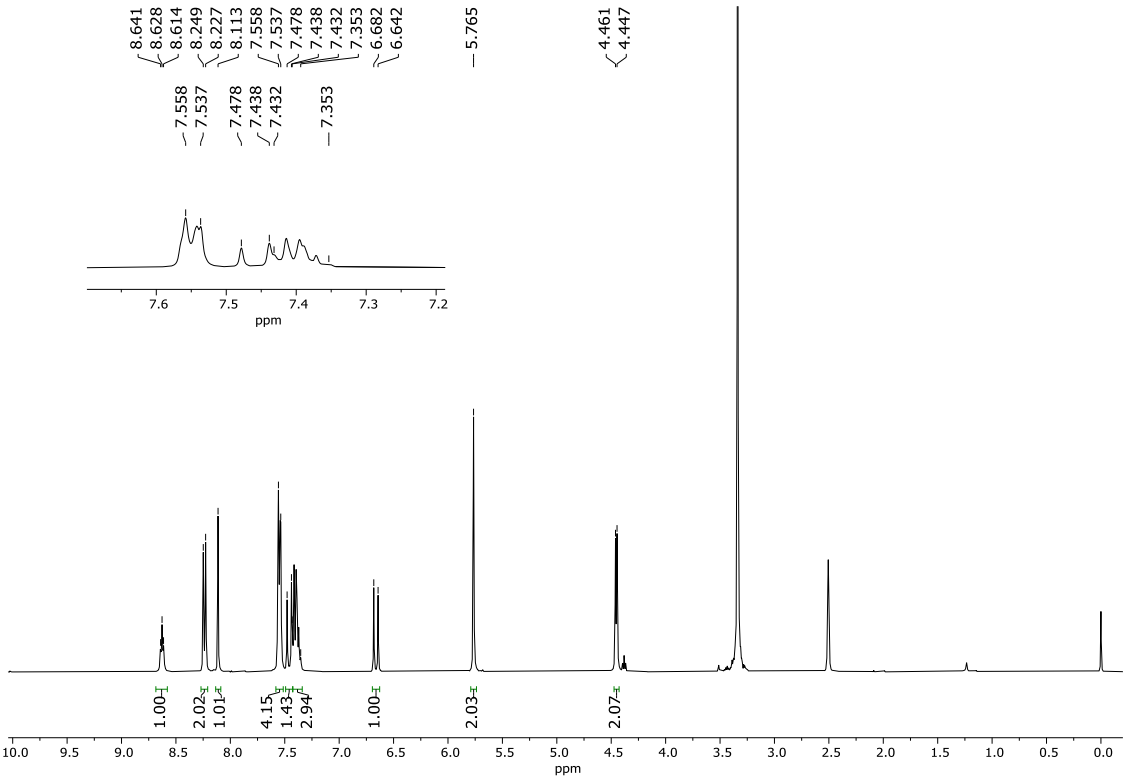

Figure S22 - ^{1}H NMR spectrum (400 MHz, DMSO-d_6) of **3f**.

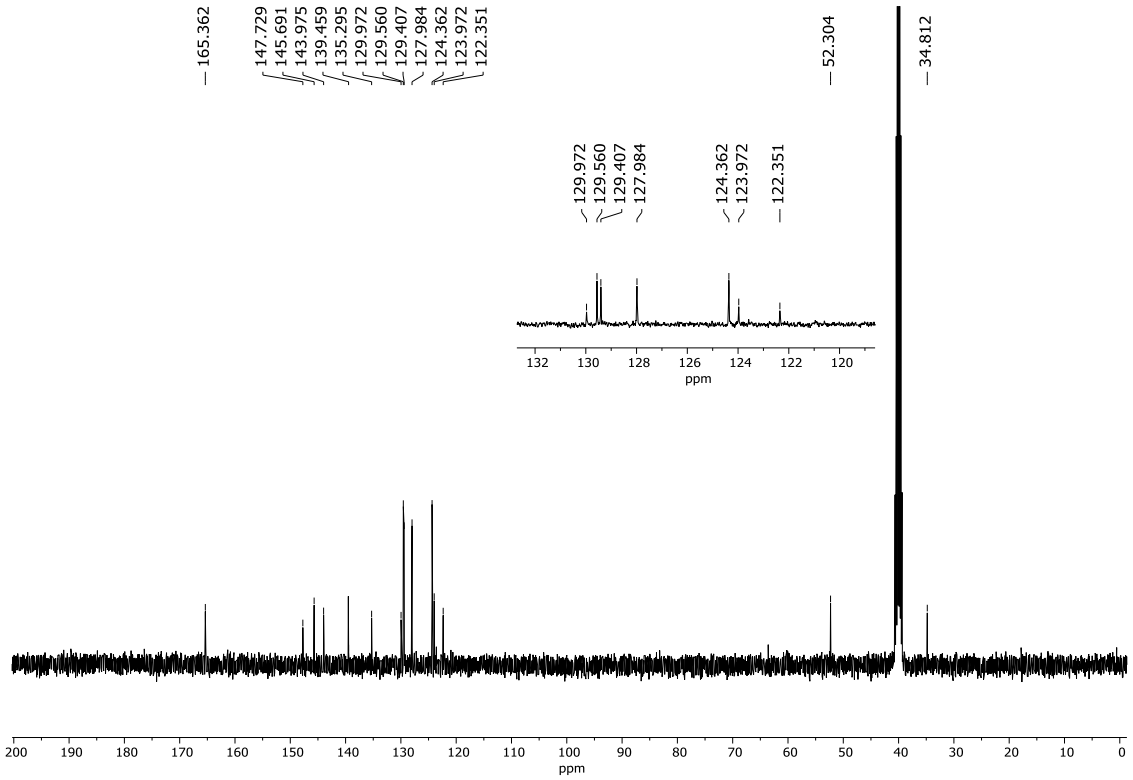

Figure S23 - ^{13}C NMR spectrum (100 MHz, DMSO-d_6) of **3f**.

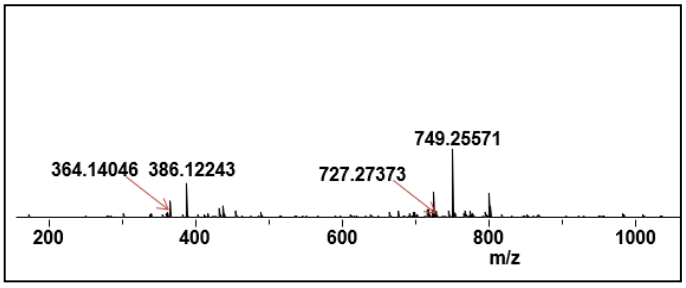

Figure S24 - HRMS spectrum of **3f**.

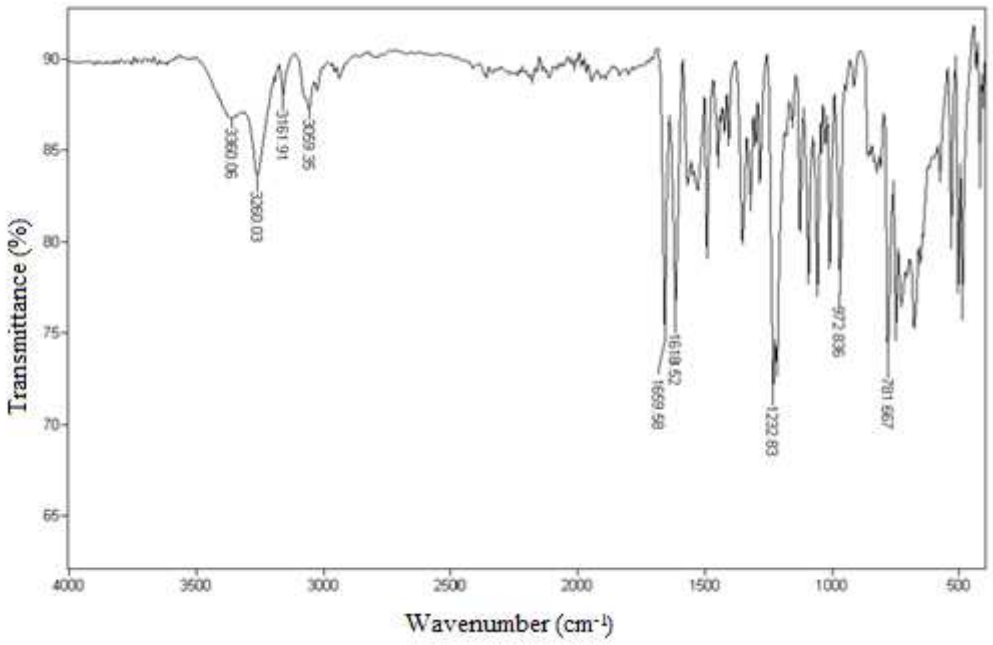

Figure S25 - IR spectrum (ATR) of **3g**.

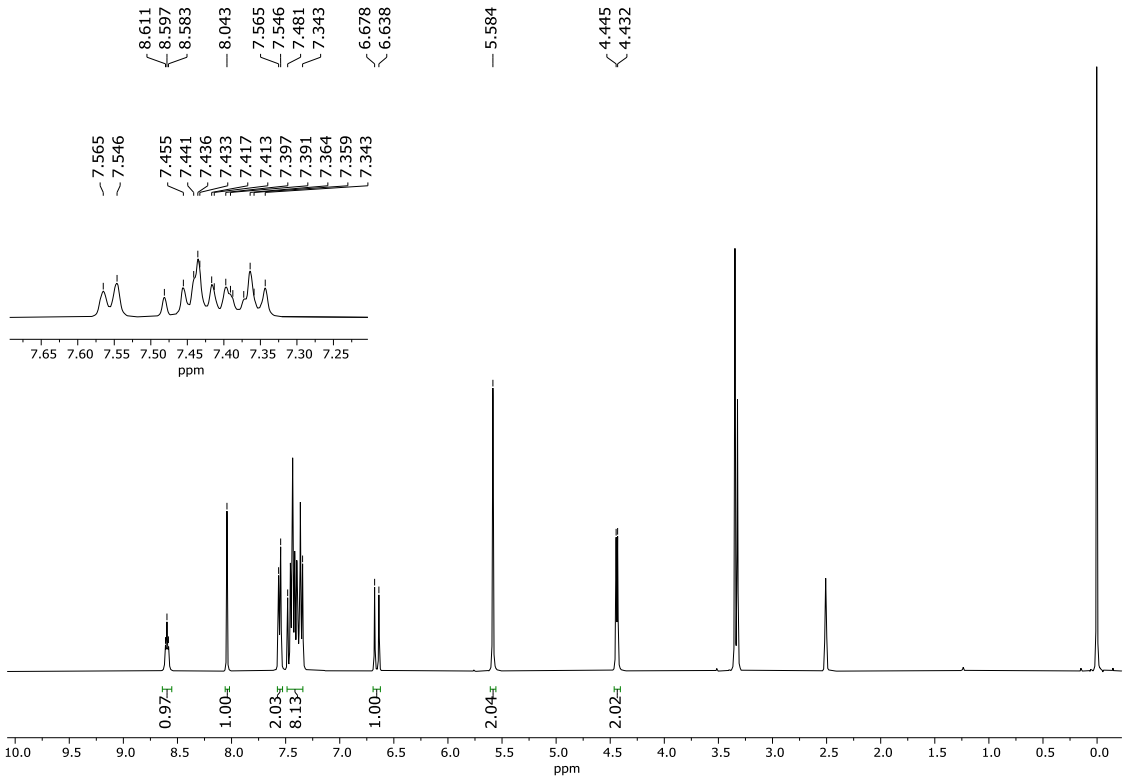

Figure S26 - ^{1}H NMR spectrum (400 MHz, DMSO-d_6) of **3g**.

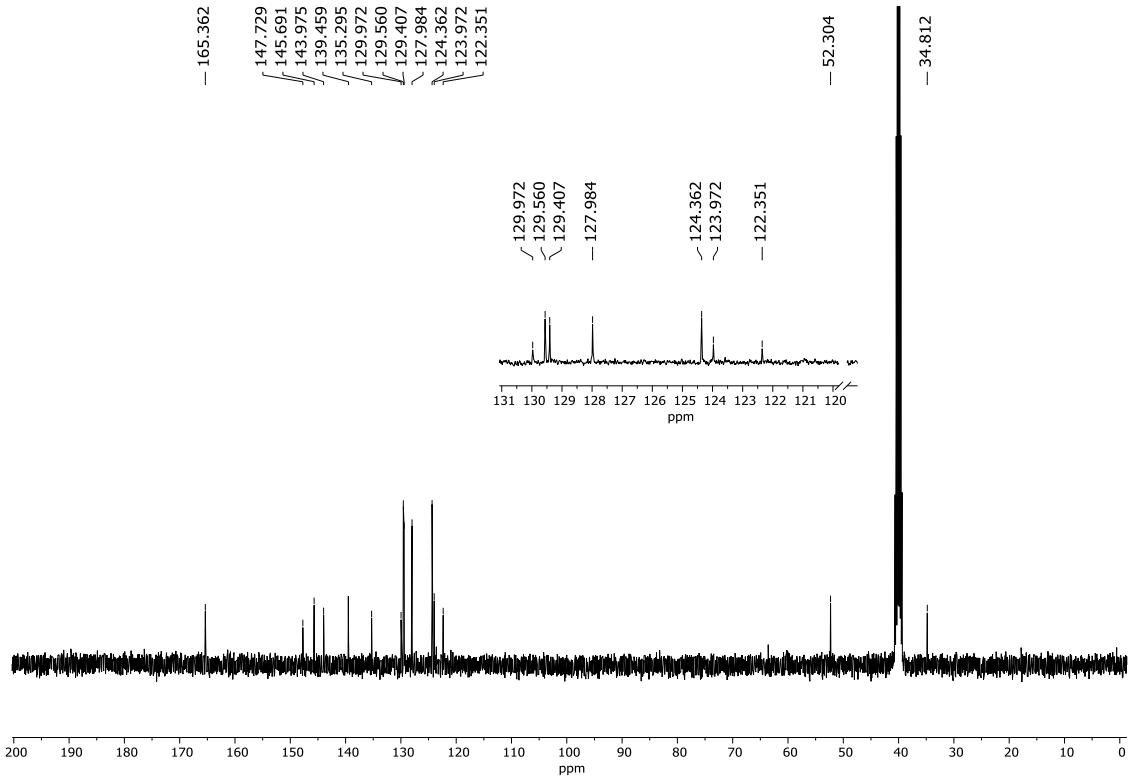

Figure S27 - ^{13}C NMR spectrum (100 MHz, DMSO-d_6) of **3g**.

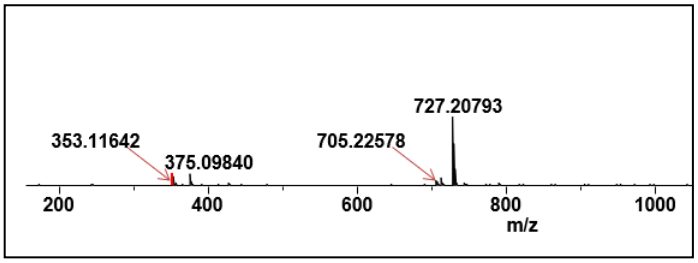

Figure S28 - HRMS spectrum of **3g**.

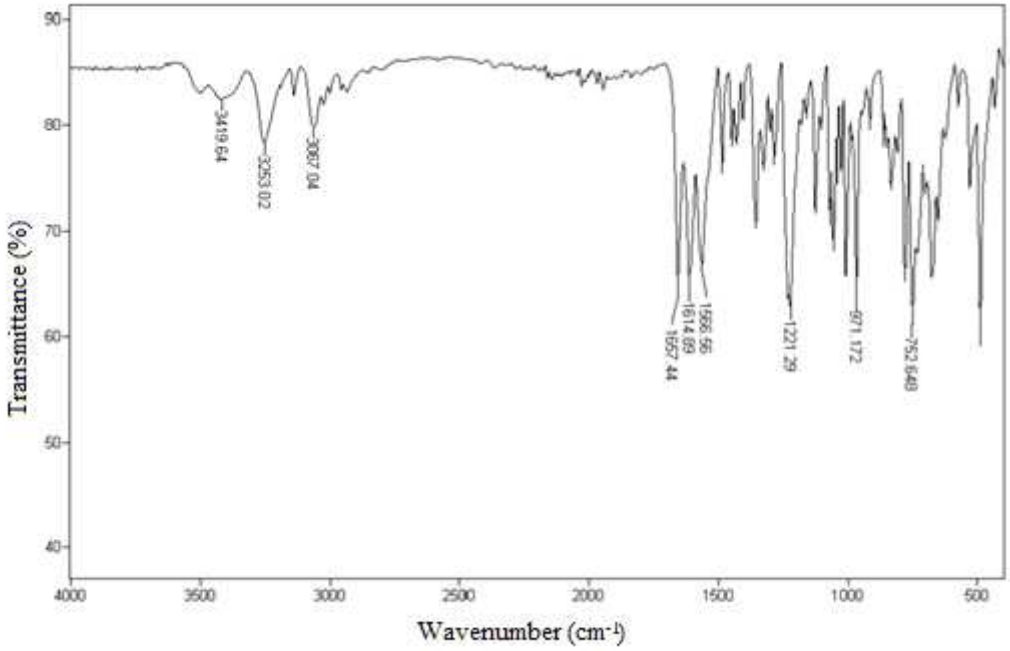

Figure S29 - IR spectrum (ATR) of **3h**.

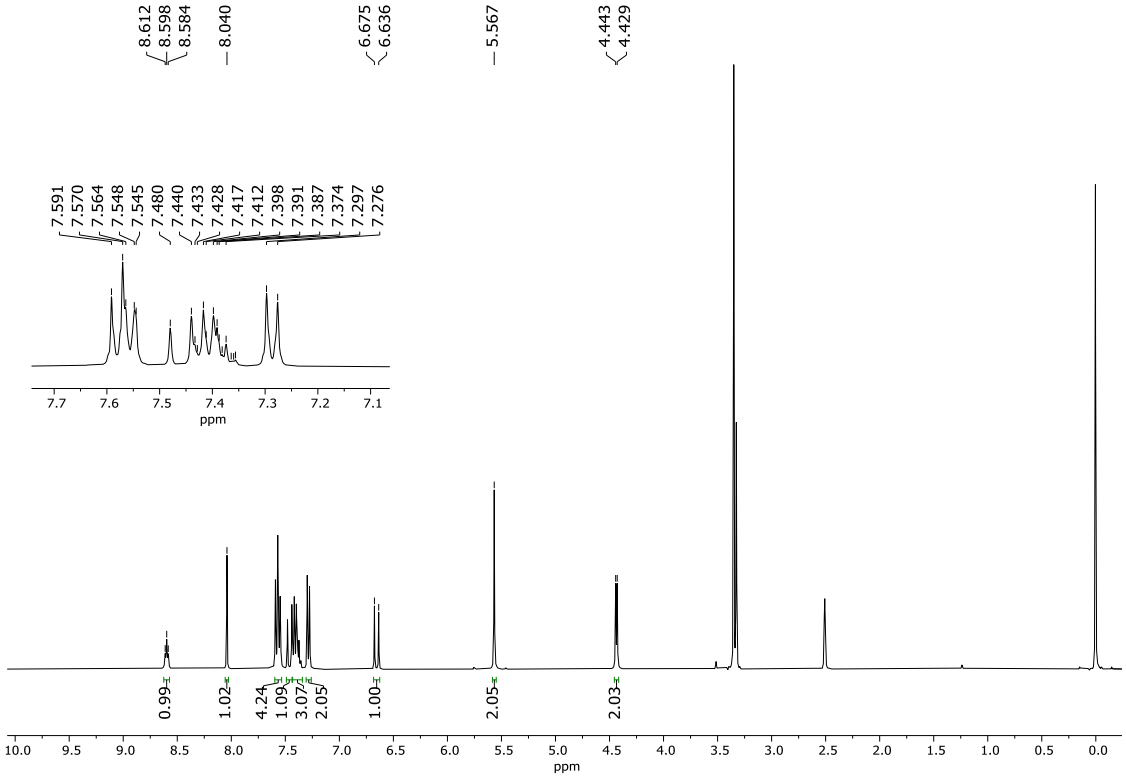

Figure S30 - ^{1}H NMR spectrum (400 MHz, DMSO-d_6) of **3h**.

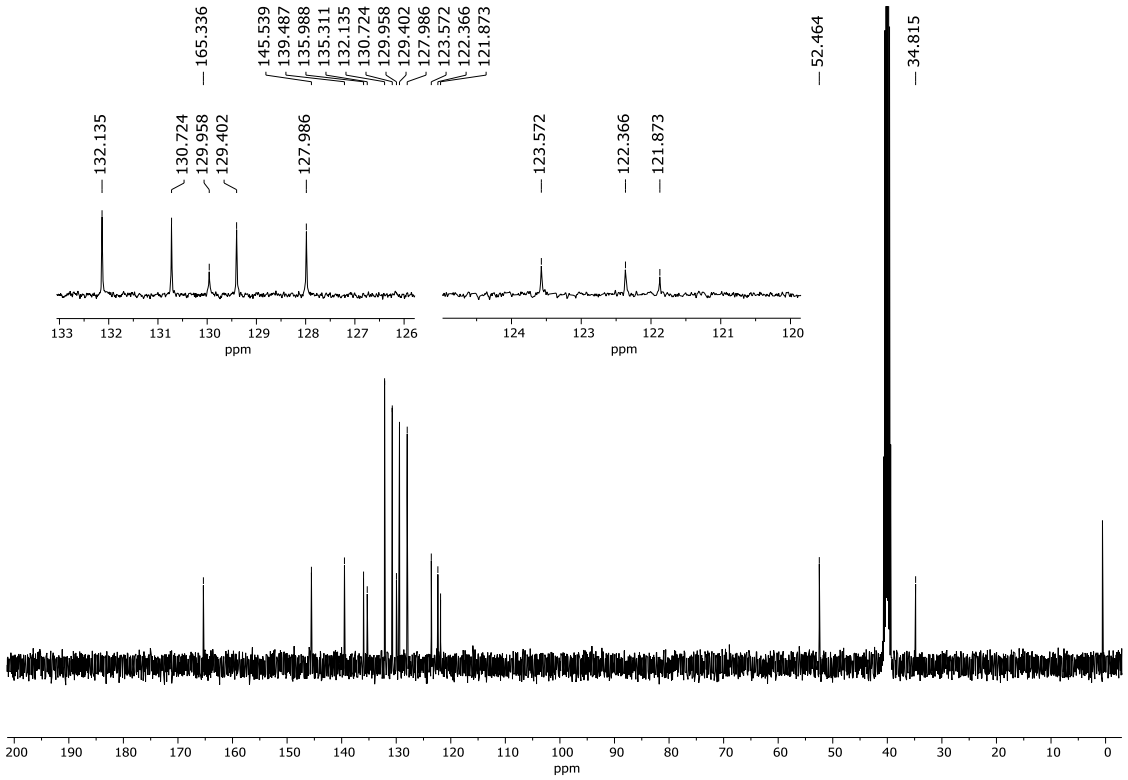

Figure S31 - ^{13}C NMR spectrum (100 MHz, DMSO-d_6) of **3h**.

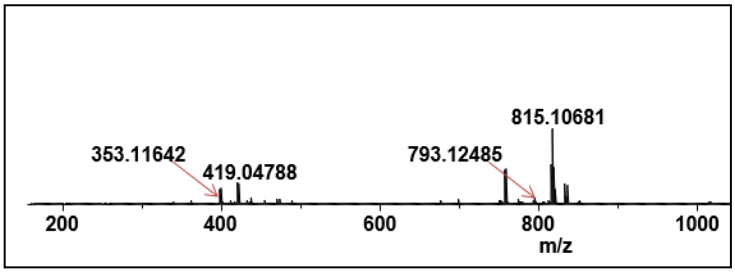

Figure S32 - HRMS spectrum of **3h**.

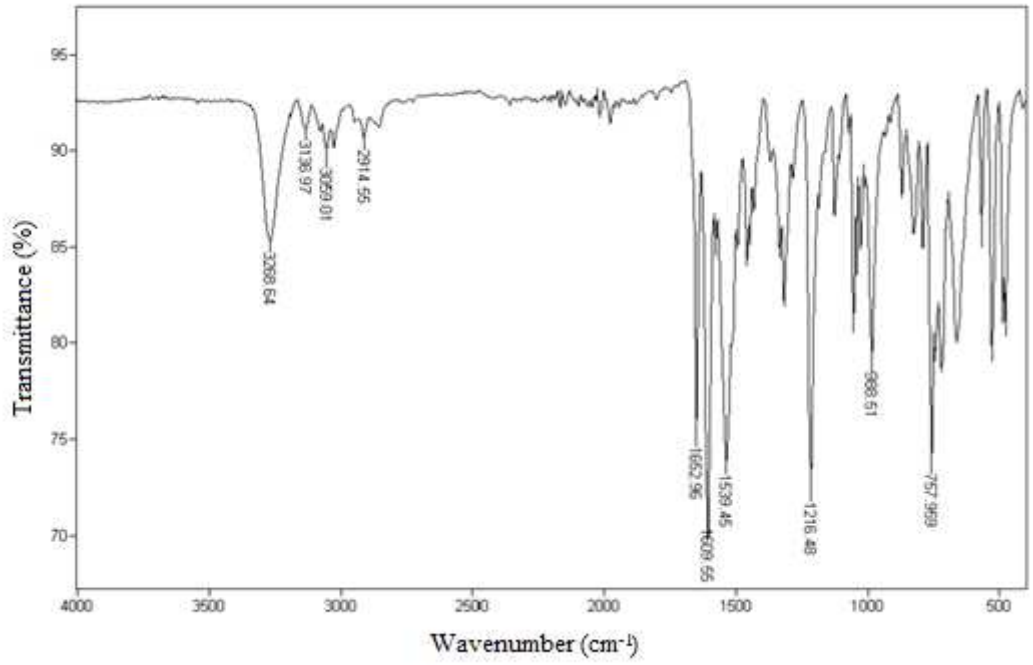

Figure S33 - IR spectrum (ATR) of **3i**.

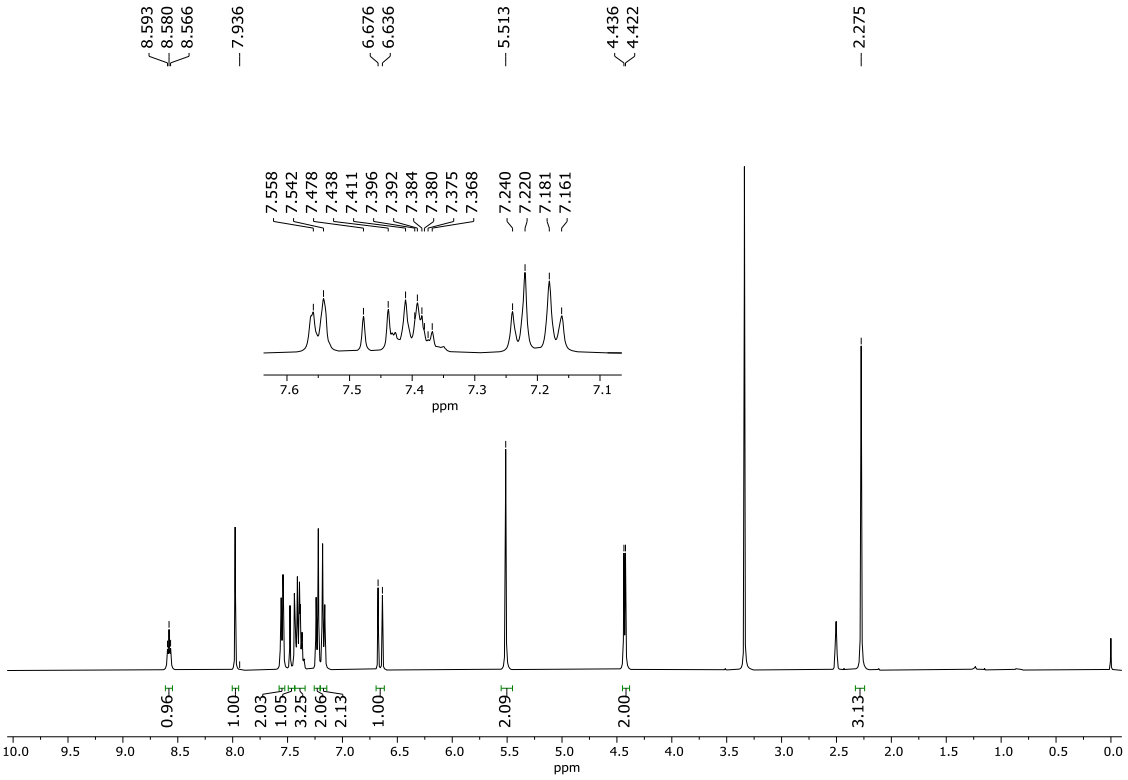

Figure S34 - ^{1}H NMR spectrum (400 MHz, DMSO-d_6) of **3i**.

.

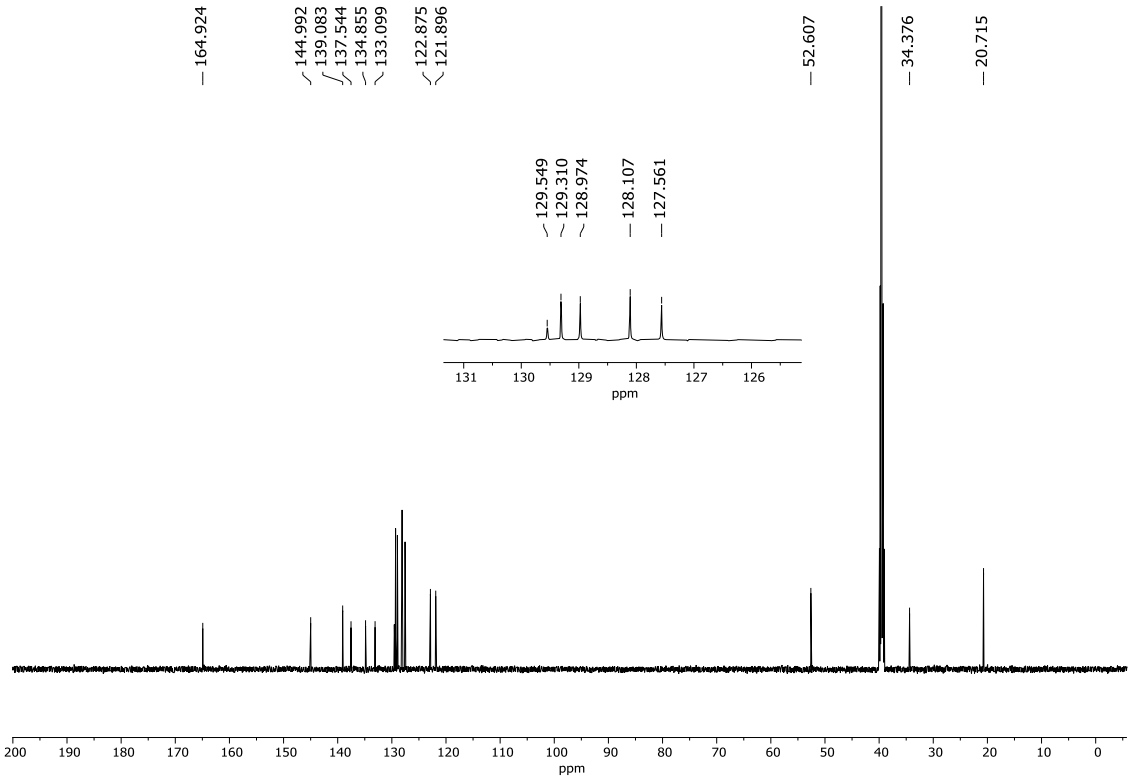

Figure S35 - ^{13}C NMR spectrum (100 MHz, DMSO-d_6) of **3i**.

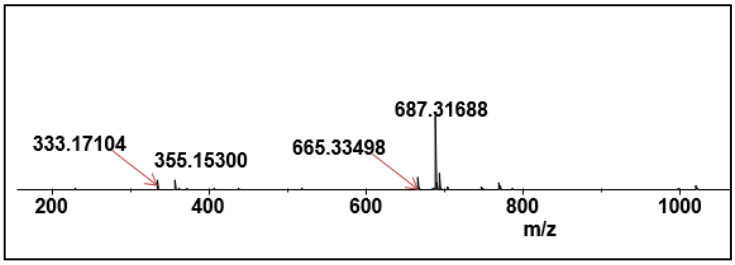

Figure S36 - HRMS spectrum of **3i**.

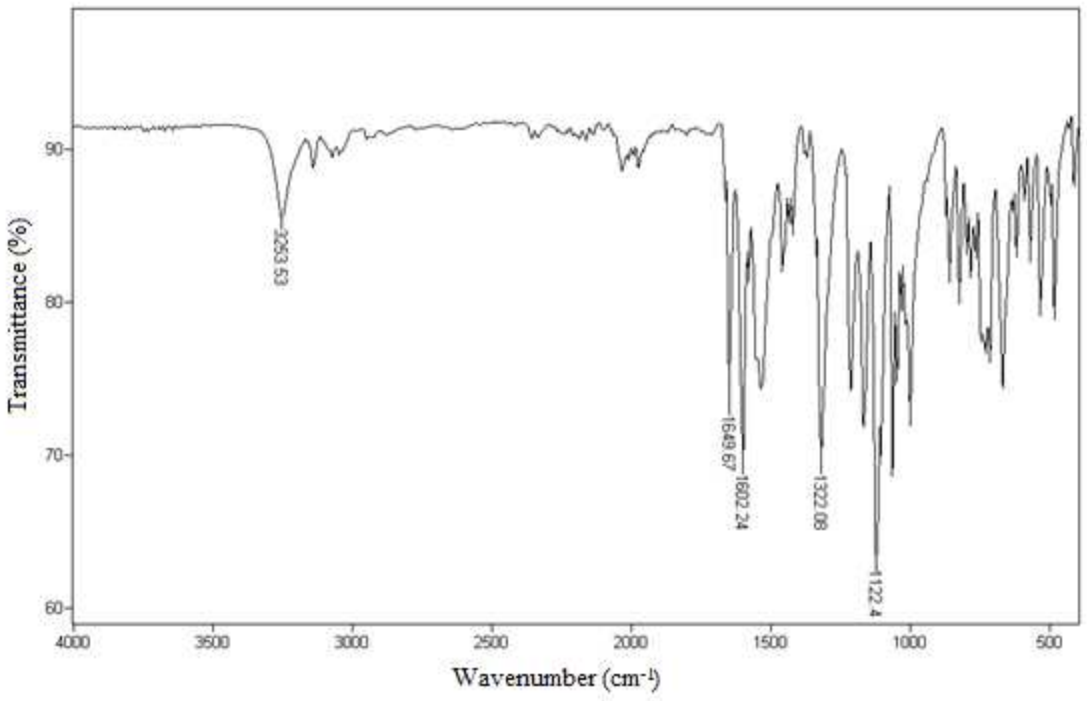

Figure S37 - IR spectrum (ATR) of **3j**.

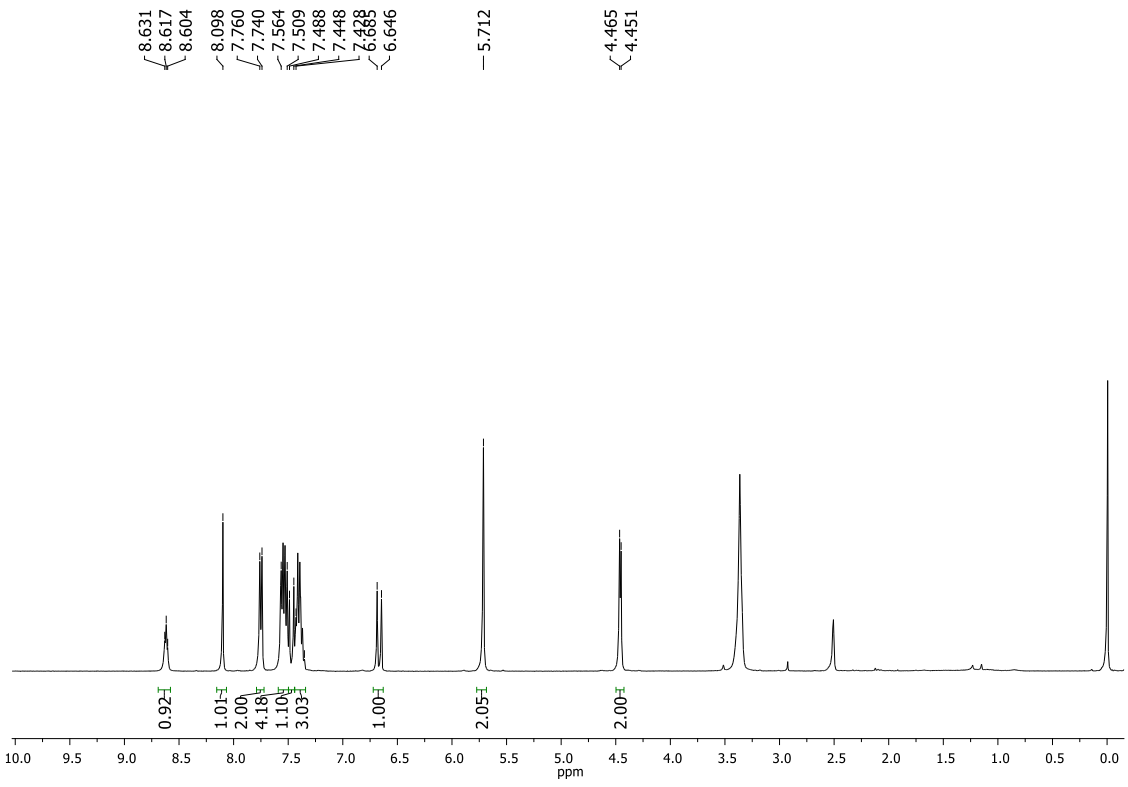

Figure S38 - ^{1}H NMR spectrum (400 MHz, DMSO-d_6) of **3j**.

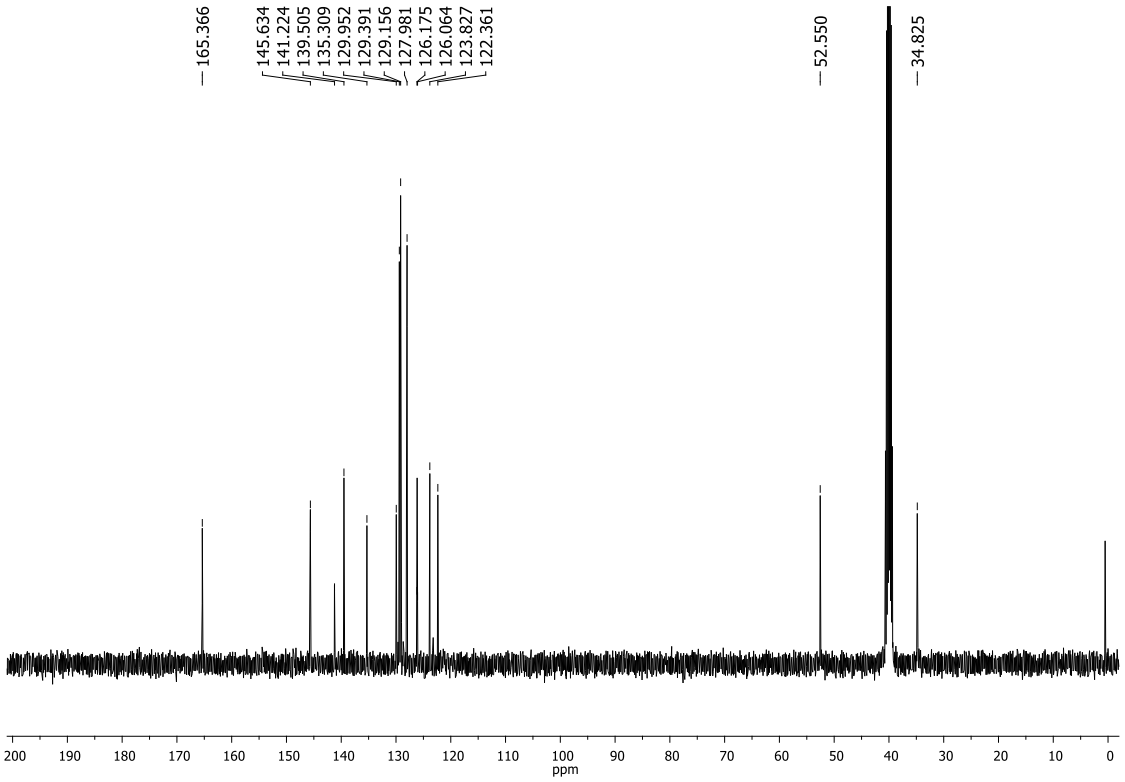

Figure S39 - ^{13}C NMR spectrum (100 MHz, DMSO-d_6) of **3j**.

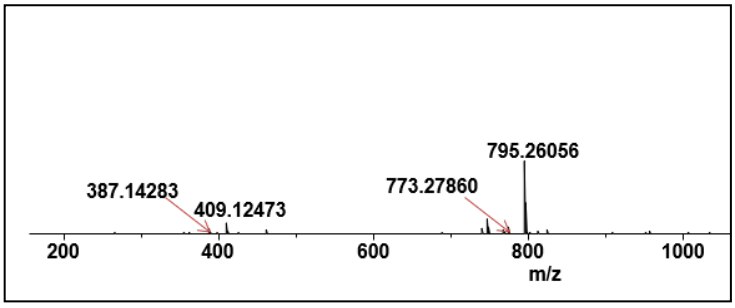

Figure S40 - HRMS spectrum of **3j**.

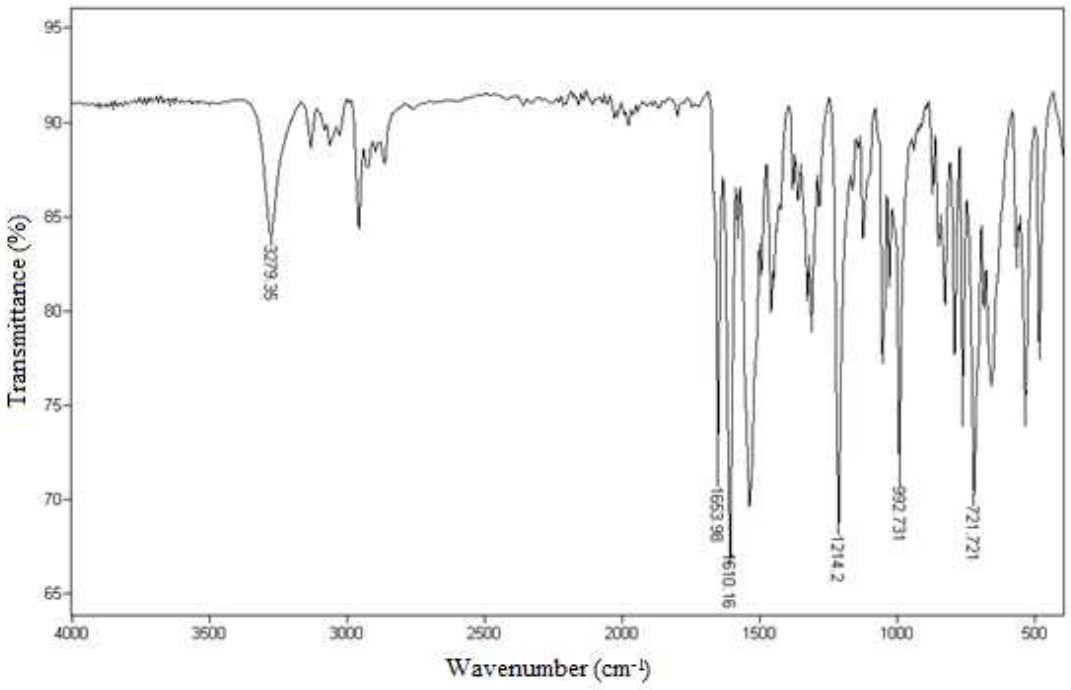

Figure S41 - IR spectrum (ATR) of **3k**.

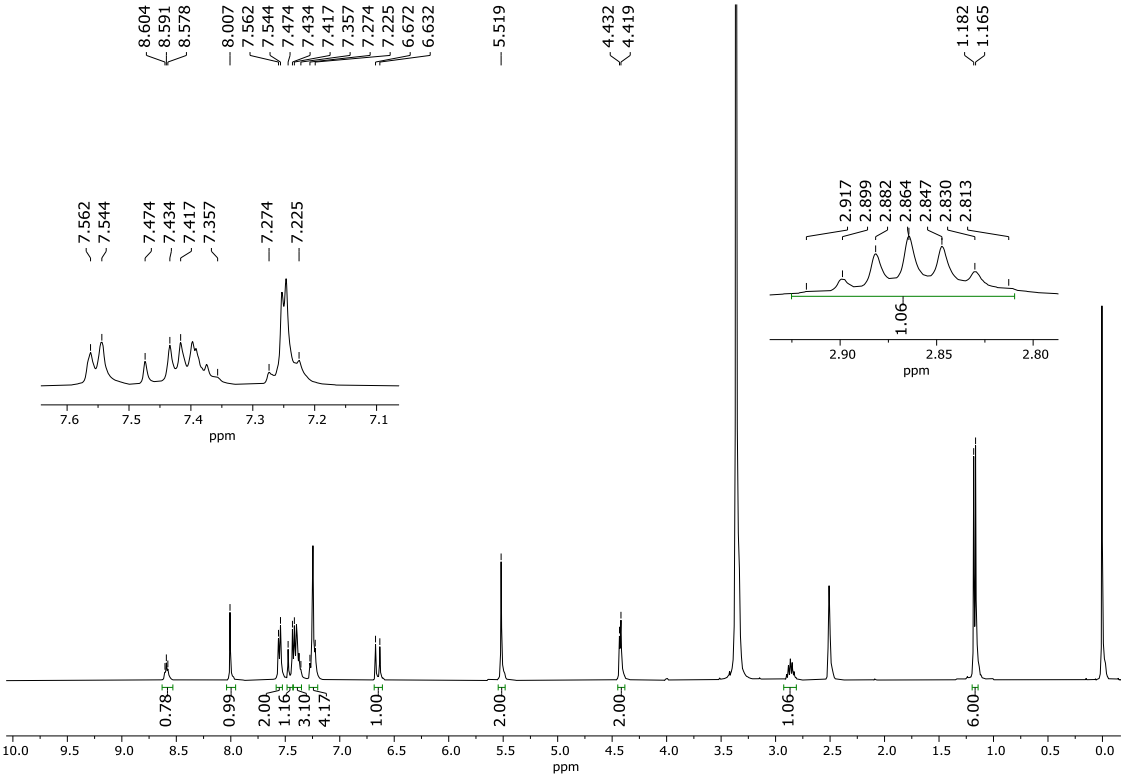

Figure S42 - ^{1}H NMR spectrum (400 MHz, DMSO-d_6) of **3k**.

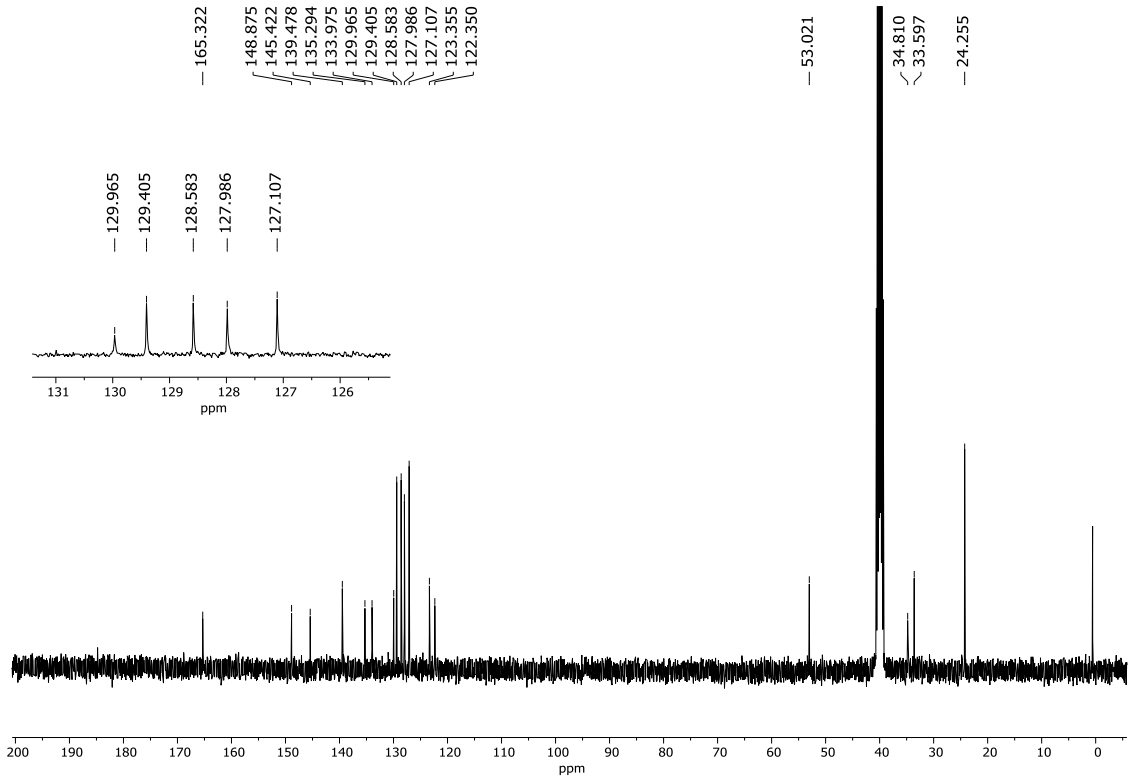

Figure S43 - ^{13}C NMR spectrum (100 MHz, DMSO-d_6) of **3k**.

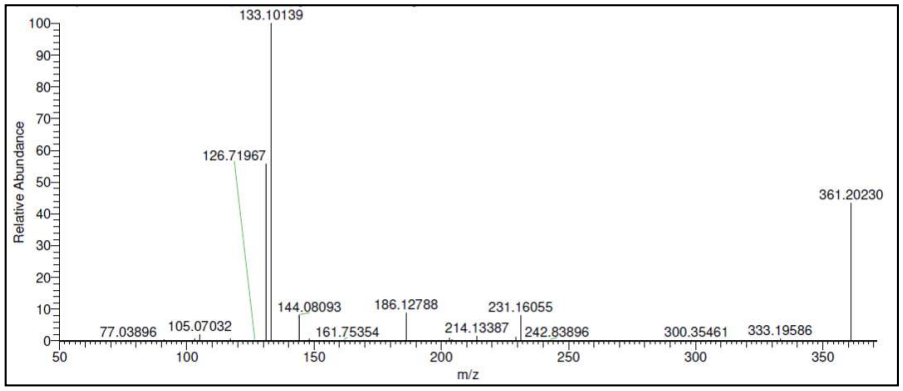

Figure S44 - HRMS spectrum of **3k**.

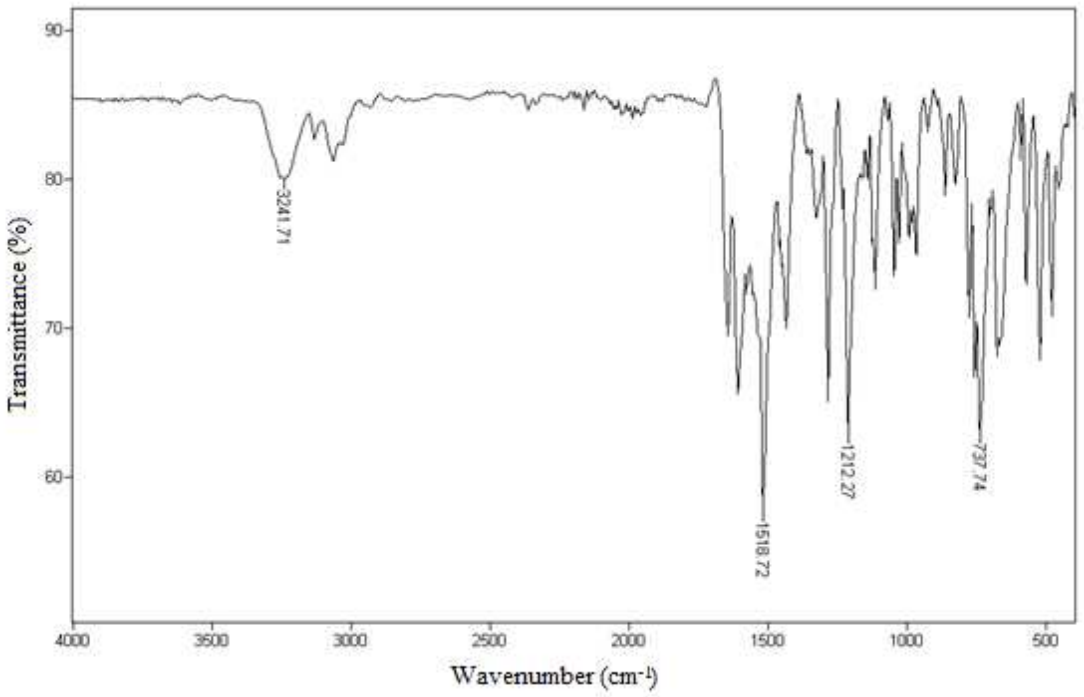

Figure S45 - IR spectrum (ATR) of **3l**.

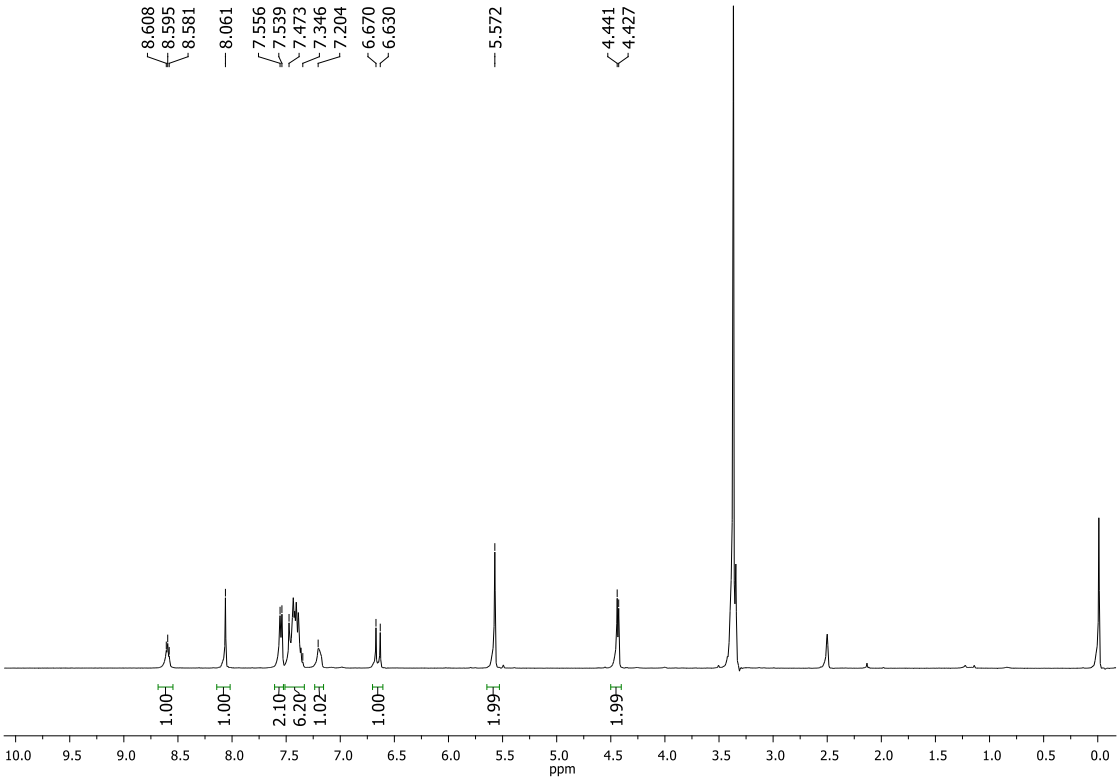

Figure S46 - ^{1}H NMR spectrum (400 MHz, DMSO-d_6) of **3l**.

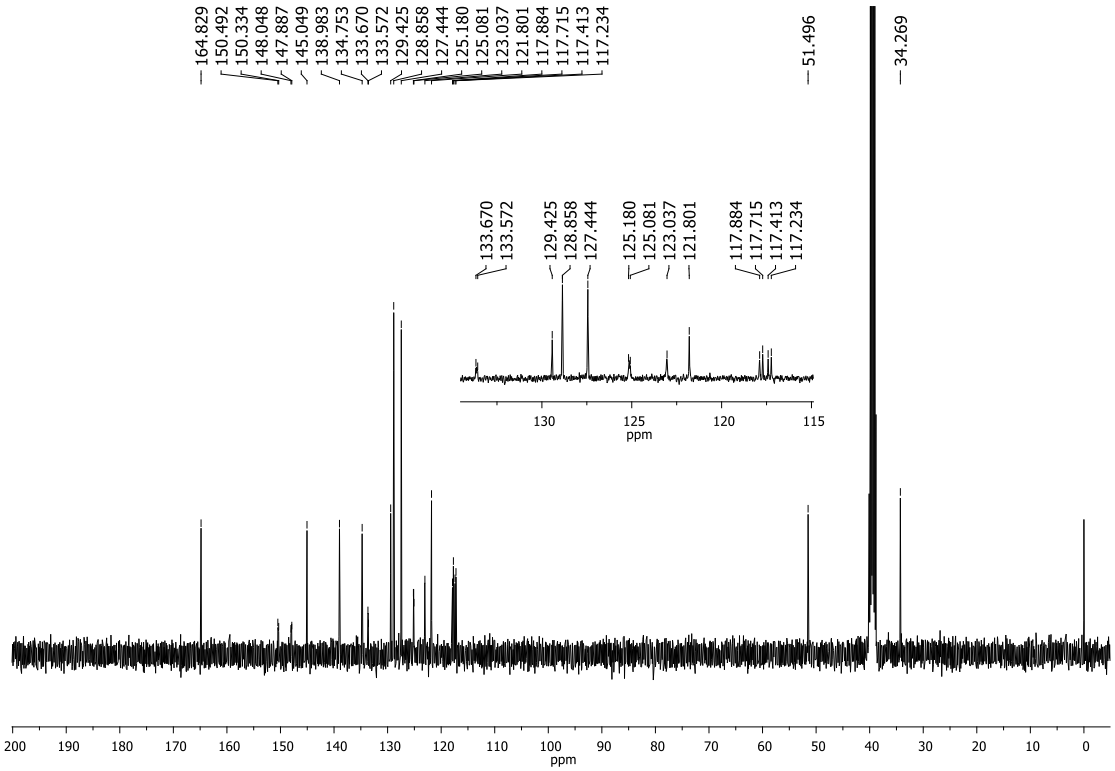

Figure S47 - ^{13}C NMR spectrum (100 MHz, DMSO-d_6) of **3l**.

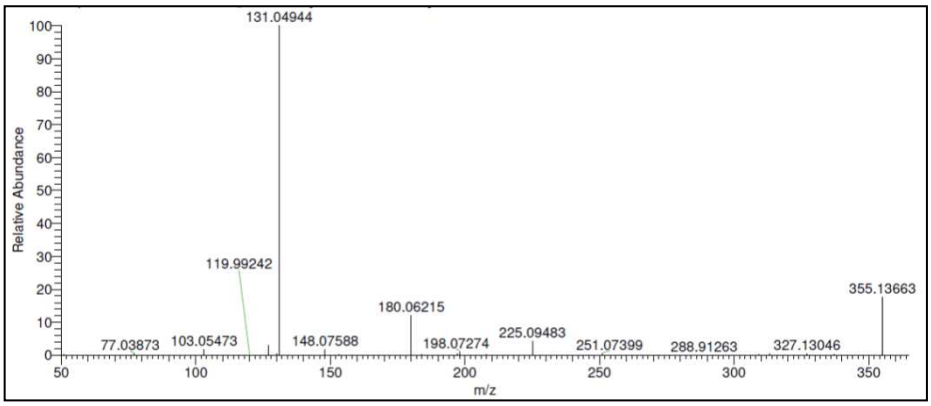

Figure S48 - HRMS spectrum of **3l**.

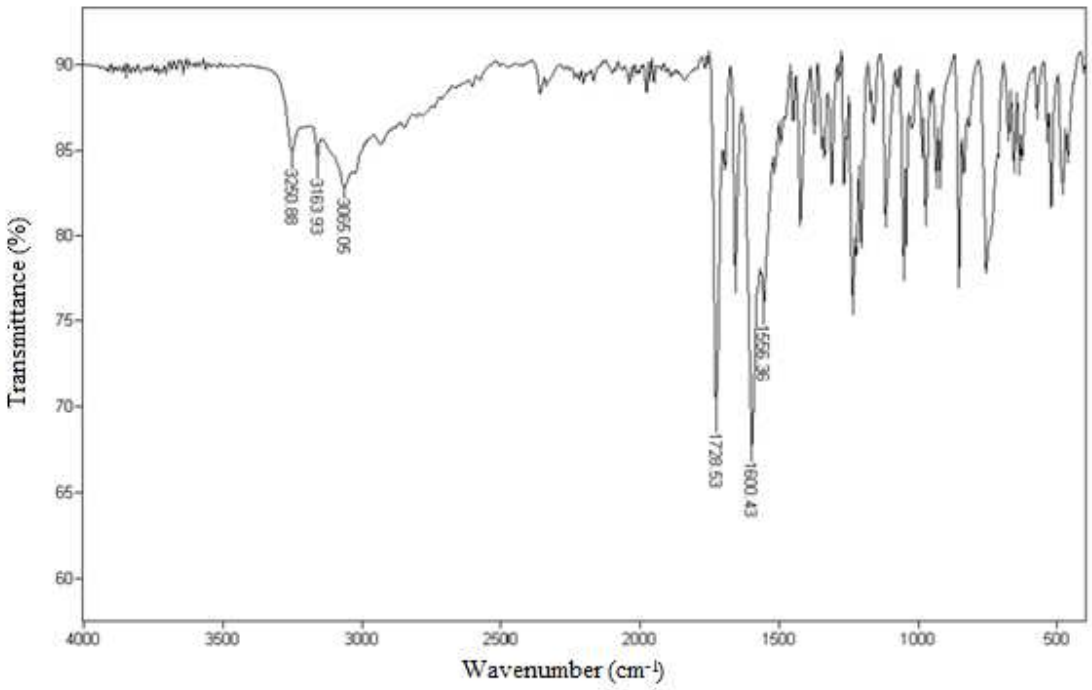

Figure S49 - IR spectrum (ATR) of **3m**.

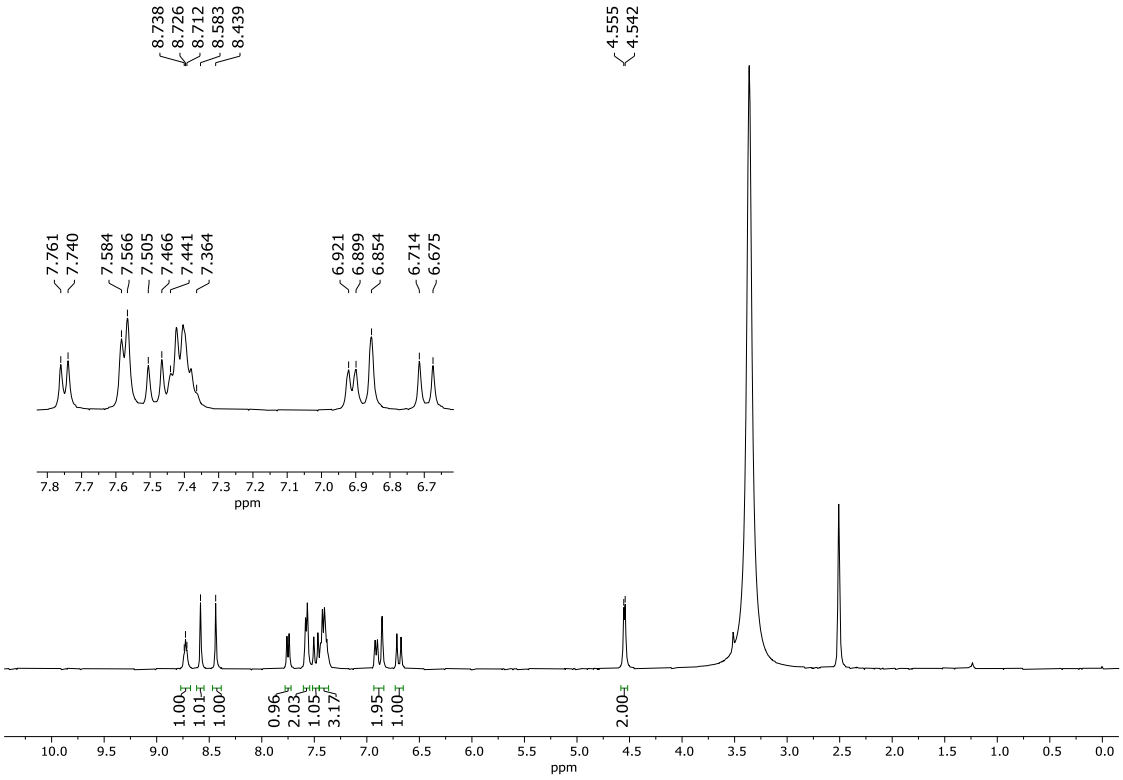

Figure S50 - ^{1}H NMR spectrum (400 MHz, DMSO-d_6) of **3m**.

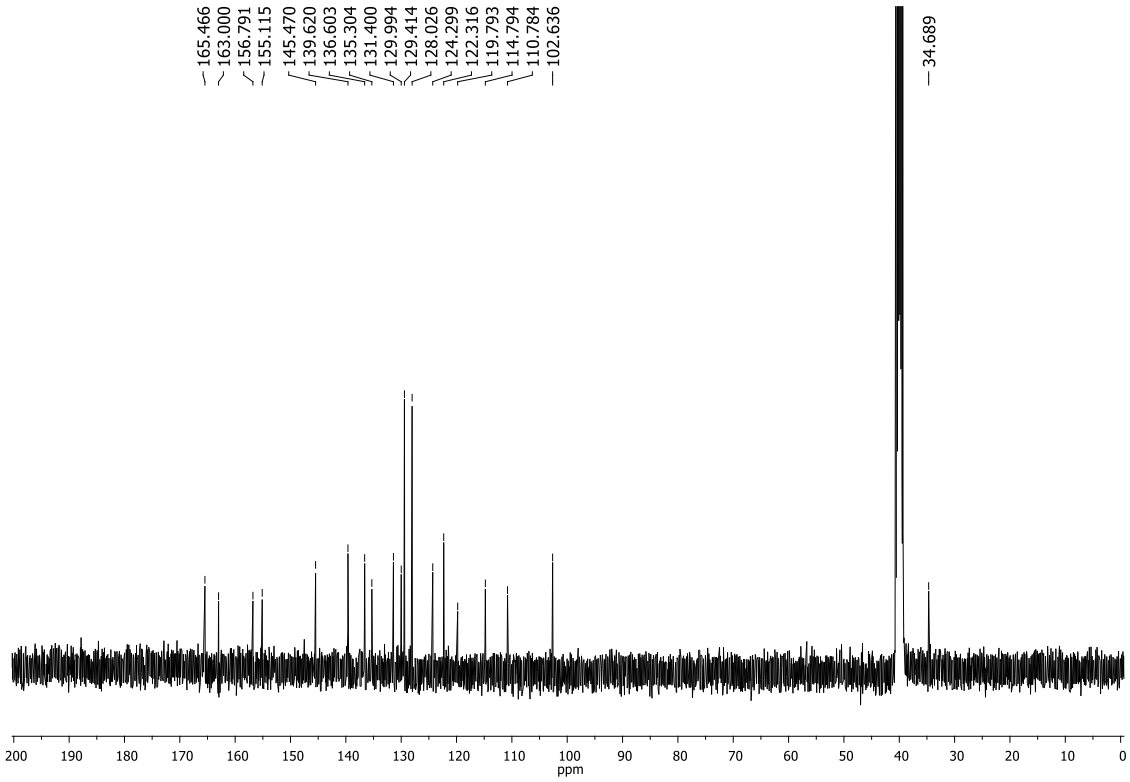

Figure S51 - ^{13}C NMR spectrum (100 MHz, DMSO-d_6) of **3m**.

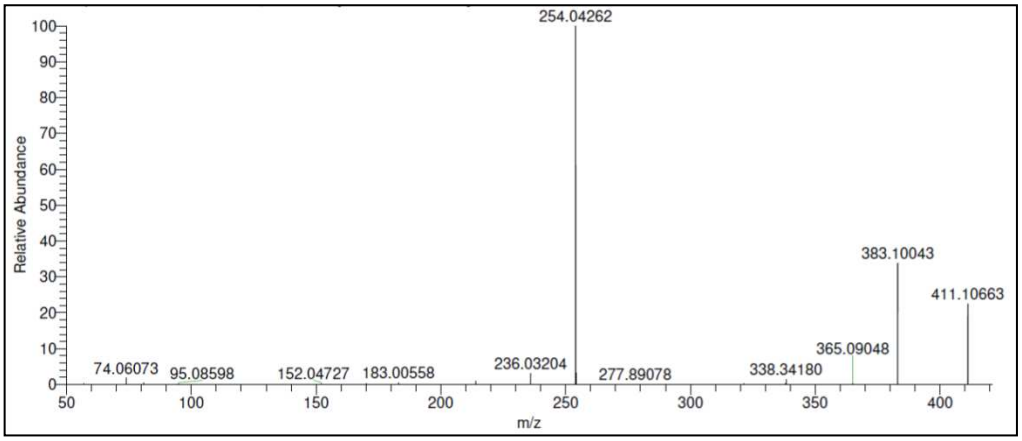

Figure S52 - HRMS spectrum of **3m**.

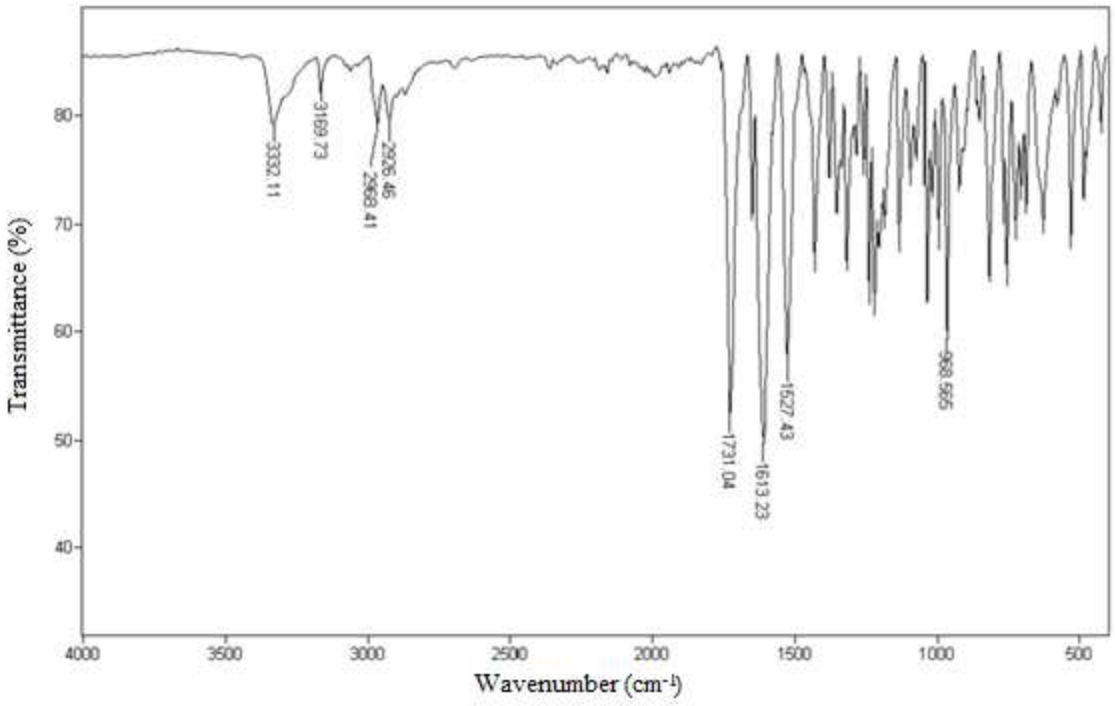

Figure S53 - IR spectrum (ATR) of **3n**.

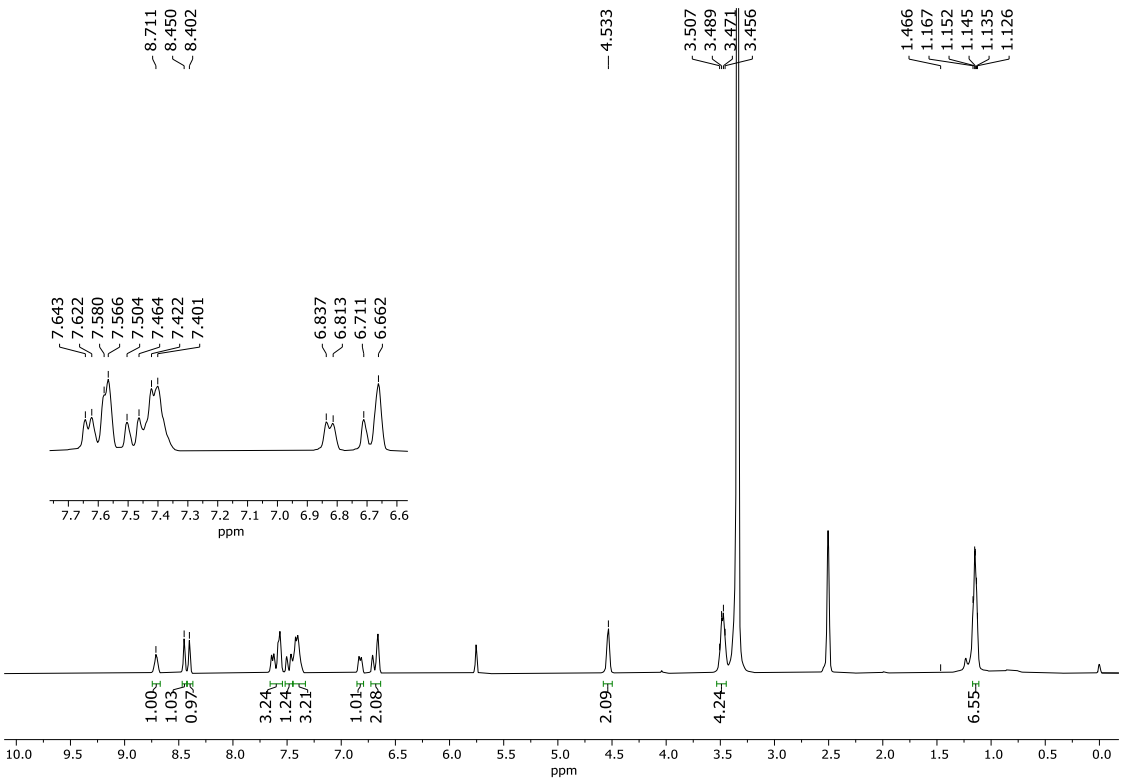

Figure S54 - ^{1}H NMR spectrum (400 MHz, DMSO-d_6) of **3n**.

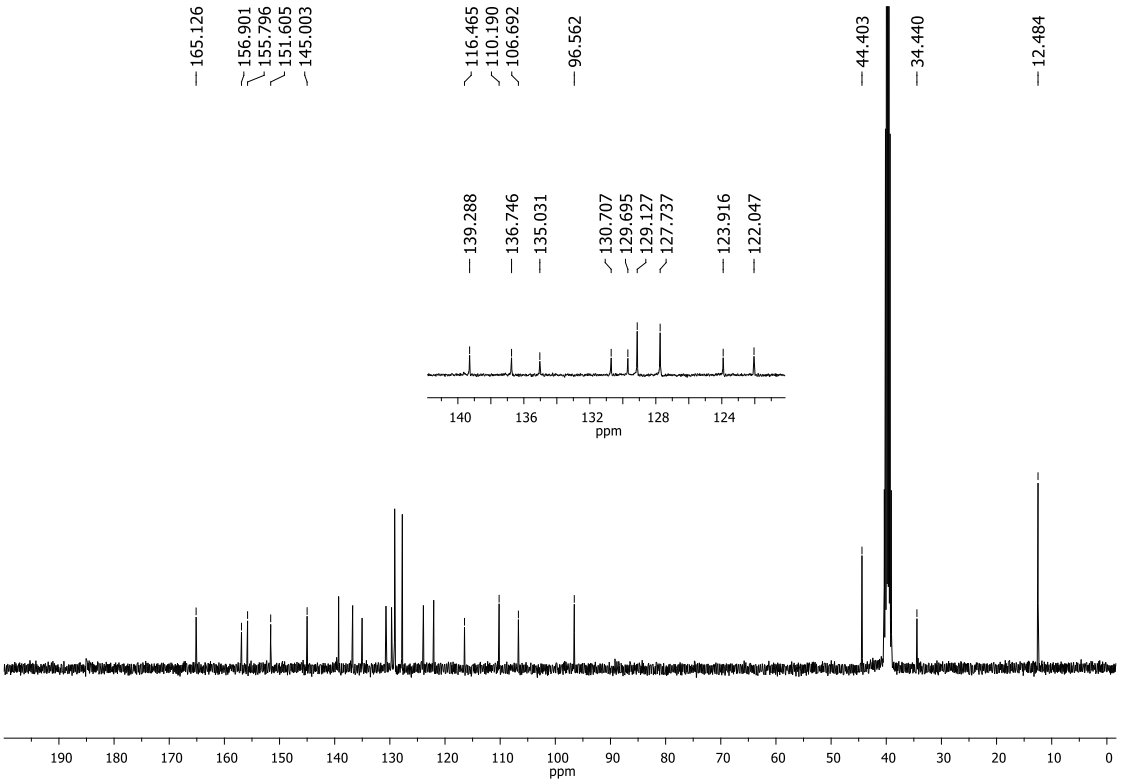

Figure S55 - ^{13}C NMR spectrum (100 MHz, DMSO-d_6) of **3n**.

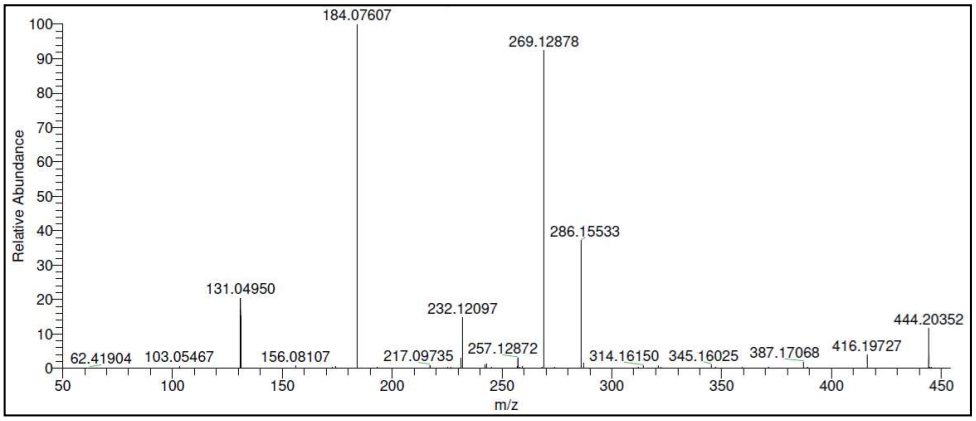

Figure S56 - HRMS spectrum of **3n**.

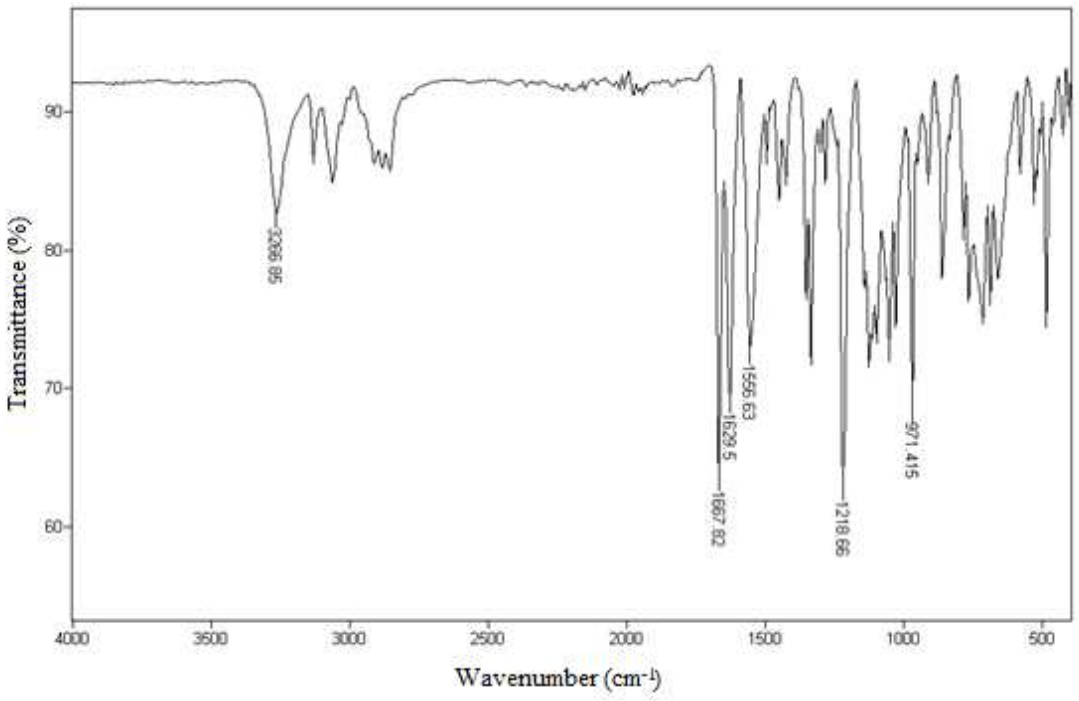

Figure S57 - IR spectrum (ATR) of **6a**.

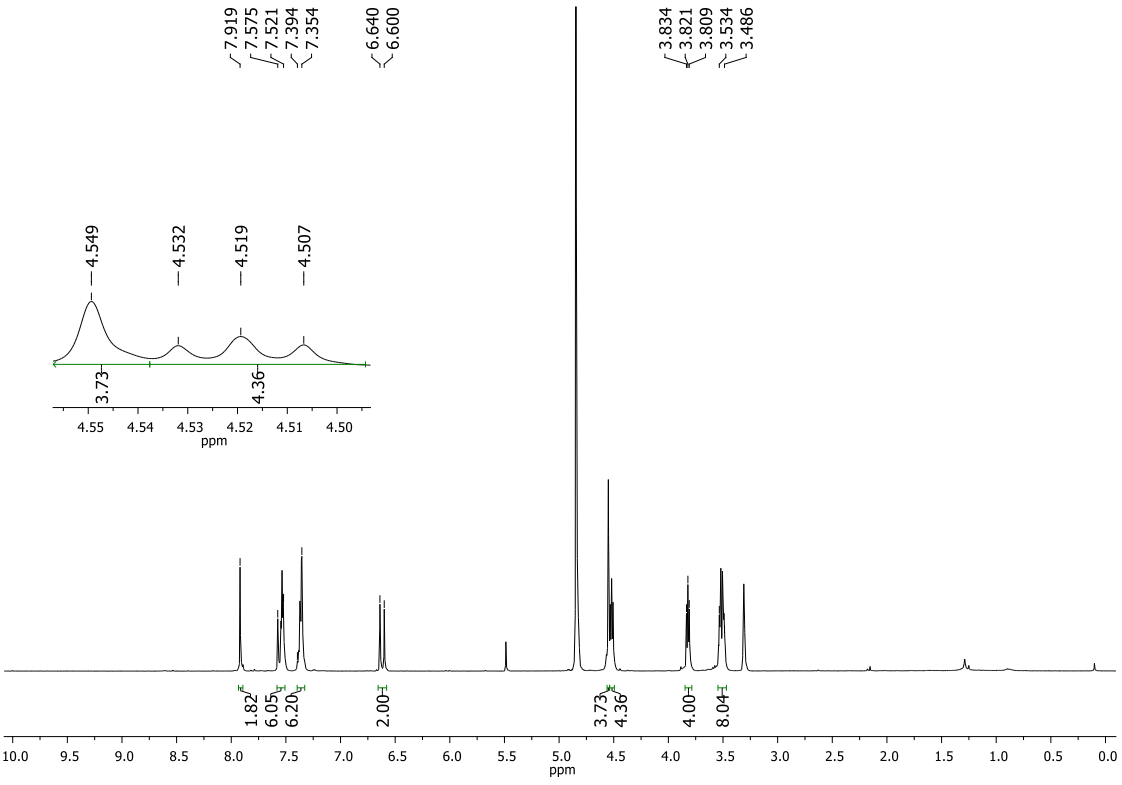

Figure S58 - ^{1}H NMR spectrum (400 MHz, CD_3OD) of **6a**.

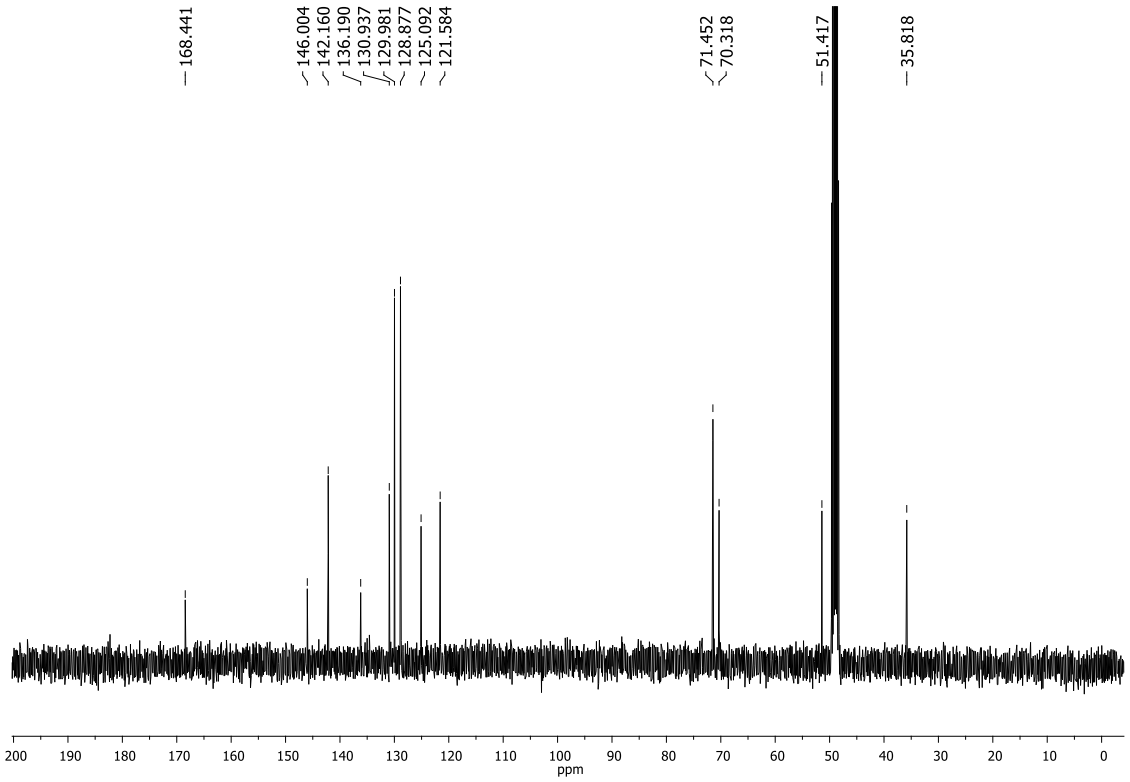

Figure S59 - ^{13}C NMR spectrum (100 MHz, CD_3OD) of **6a**.

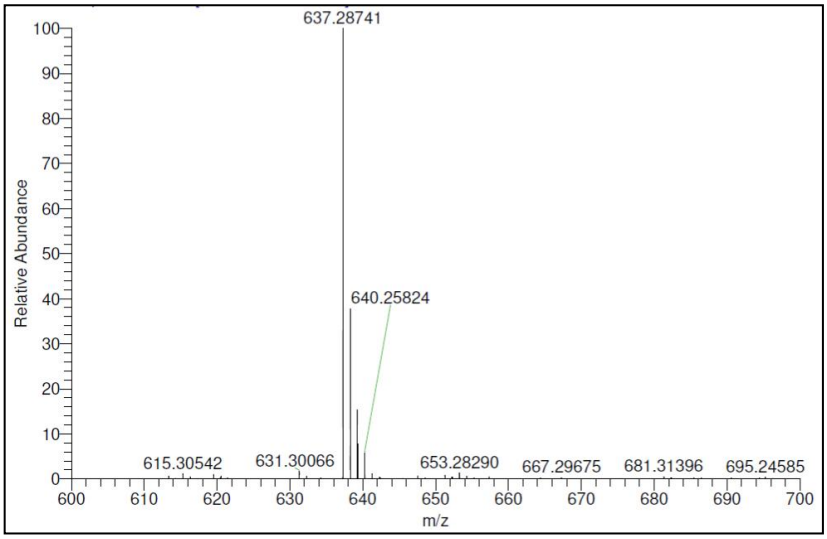

Figure S60 - HRMS spectrum of **6a**.

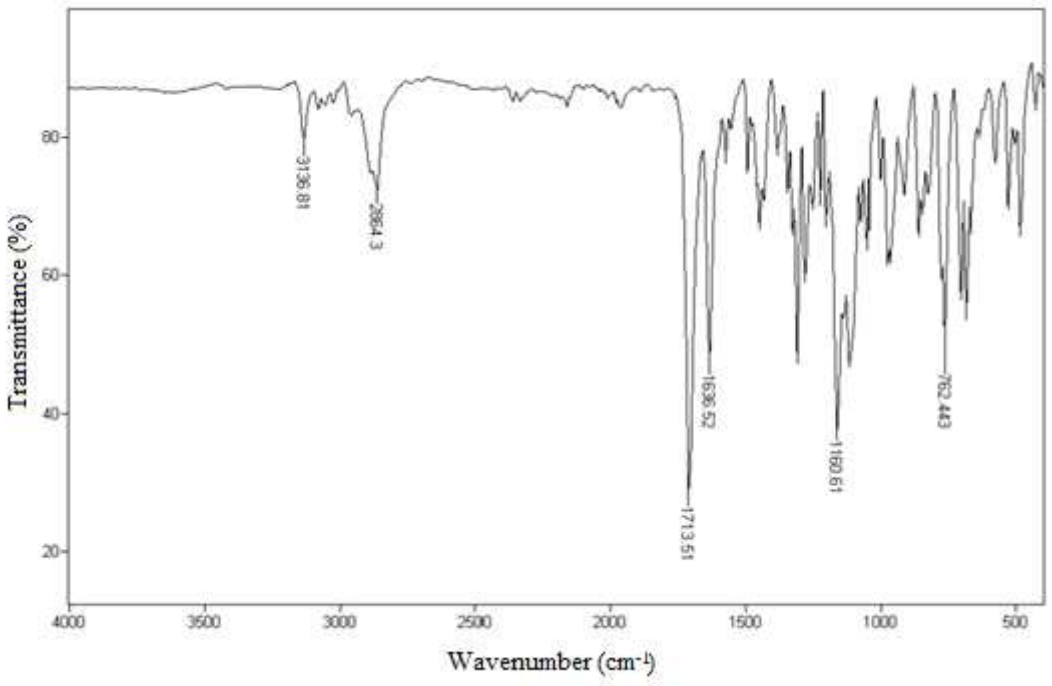

Figure S61 - IR spectrum (ATR) of **6b**.

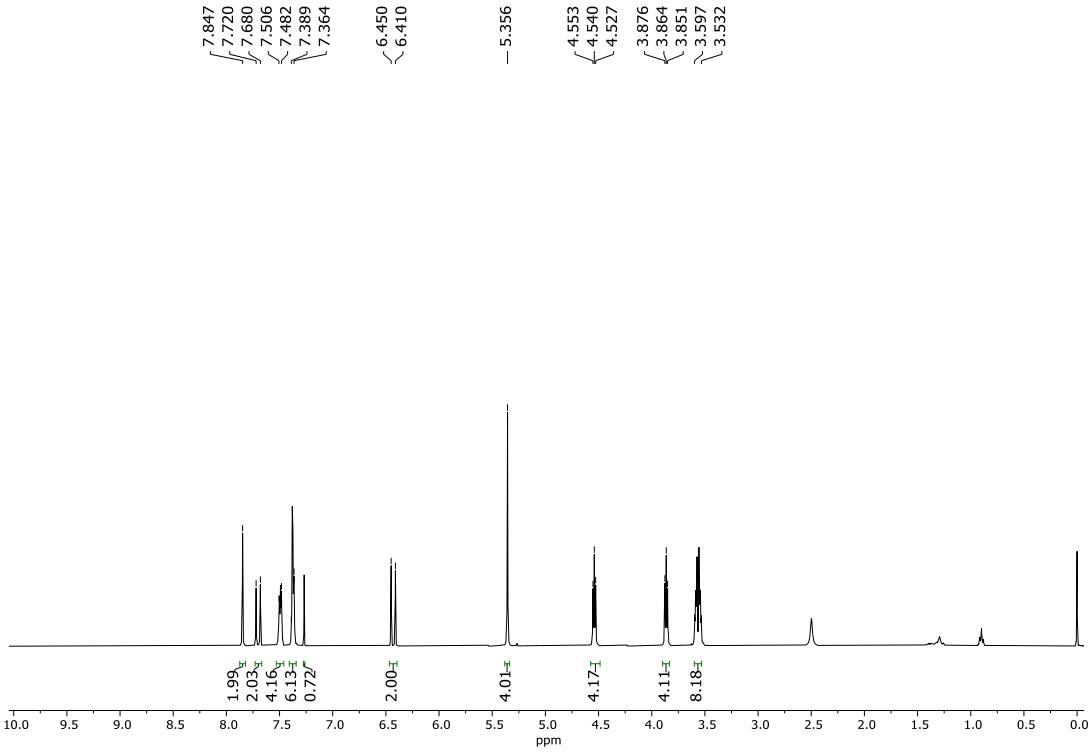

Figure S62 - ^{1}H NMR spectrum (400 MHz, $CDCl_3$) of **6b**.

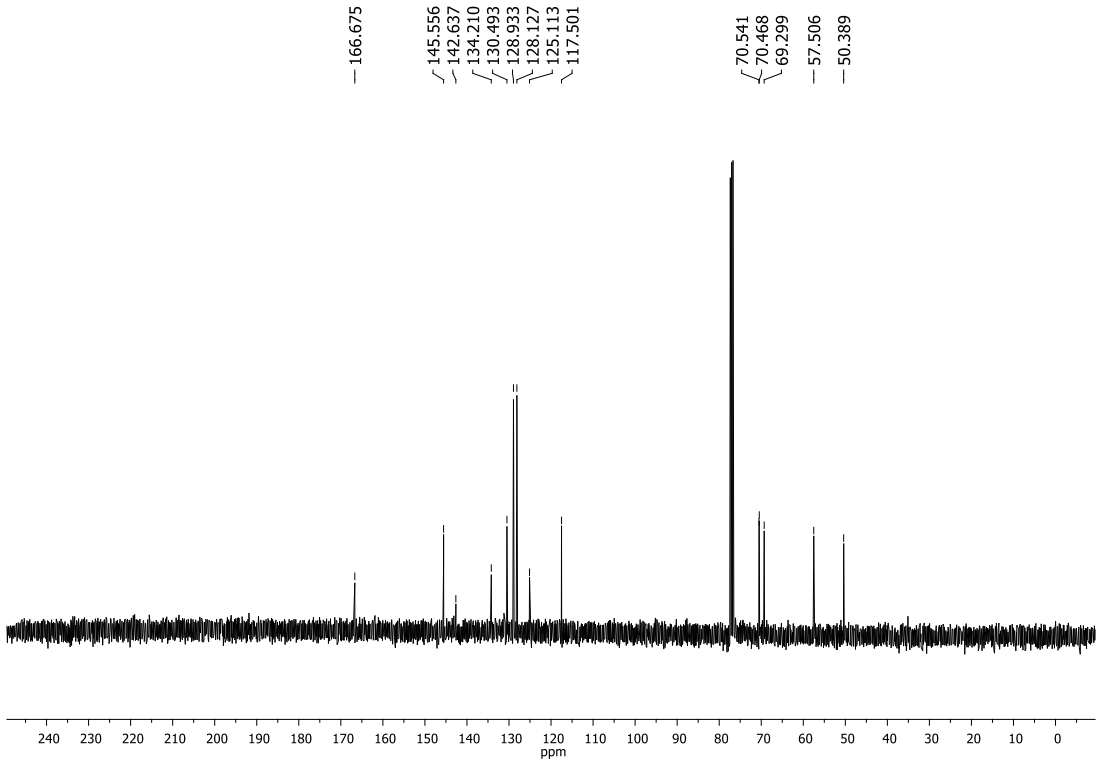

Figure S63 - ^{13}C NMR spectrum (100 MHz, $CDCl_3$) of **6b**.

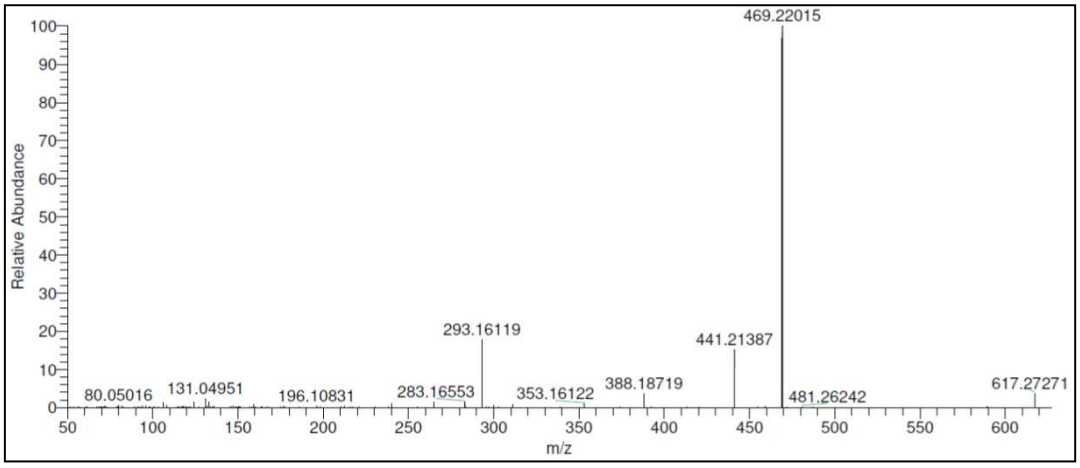

Figure S64 - HRMS spectrum of **6b**.

CAPÍTULO 4 – ARTIGO DE PESQUISA 2

Synthesis of cinnamic acid ester derivatives with antiproliferative and antimetastatic activities on murine melanoma cells

Juliana Alves do Vale[1]§, Michelle Peixoto Rodrigues[2]§, Ângela Maria Almeida Lima[2], Samira Soares Santiago[2], Graziela Domingues de Almeida Lima[1], Alisson Andrade Almeida[3], Leandro Licursi de Oliveira[1], Gustavo Costa Bressan[3**], Róbson Ricardo Teixeira[2**], Mariana Machado-Neves[1*]

[1]Department of General Biology, Federal University of Viçosa, Viçosa, Minas Gerais, Brazil
[2]Department of Chemistry, Federal University of Viçosa, Viçosa, Minas Gerais, Brazil
[3]Department of Biochemistry and Molecular Biology, Federal University of Viçosa, Viçosa, Minas Gerais, Brazil

§These authors contributed equally to this work

Publicado: Biomedicine & Pharmacotherapy, 148, 112689, 2022

ABSTRACT

Melanoma is the most aggressive skin cancer, and its incidence has continued to rise during the past decades. Conventional treatments present severe side effects in cancer patients, and melanoma can be refractory to commonly used anticancer drugs, which justify the efforts to find new potential anti-melanoma drugs. An alternative to promote the discovery of new pharmacological substances would be modifying chemical groups from a bioactive compound. Here we describe the synthesis of seventeen cinnamate derived from cinnamic acid and their bioactivity evaluation against melanoma cells. The compound phenyl 2,3-dibromo-3-phenylpropanoate (**3q**) was the most effective against murine B16-F10 cells, as observed in cytotoxicity and cell migration assays. Simultaneously, this compound showed low cytotoxic activity on non-tumor cells. At the highest concentration, the compound **3q** was able to trigger apoptosis, whereas, at lower concentrations, it affected the cell cycle and melanoma cell proliferation. Furthermore, cinnamate **3q** impaired cell invasion, adhesion, and colonization. In conclusion, these results highlight the antiproliferative and antimetastatic potential of cinnamic acid derivatives on melanoma.

Keywords: cinnamic acid; cinnamates; anticancer drug discovery; anti-melanoma; antitumoral activity; B16-F10 cell line.

1. INTRODUCTION

Melanoma is the most aggressive form of skin cancer, associated with high mortality rates [1-3]. The prognosis of this cancer may be favorable if detected early, being treated by surgical excision with adequate safety margins [4]. However, the prognosis is unfavorable in advanced stages, when the melanoma exhibits high metastatic ability and resistance to existing drugs [1,5]. At this stage, the treatment may involve classical chemotherapy, immune-, and targeted molecular therapies. Although these treatments have improved the clinical outcome of a significant proportion of patients, there are still either refractory cases or those exhibiting side effects [6-8]. For that reason, it is imperative to make progress in the research for novel chemical structures that can serve as leads for the development of new drugs against melanoma.

Nature is a source of compounds with relevant biological activities [9-12]. Among those substances, cinnamic acid, also called 3-phenyl-2-propenoic acid, consists of a naturally occurring aromatic carboxylic acid found in plant tissues, mainly cinnamon oils and coca leaves. This acid exhibits a substance with a scaffolded structure in *cis* and *trans* configurations, being the *trans* the most frequent configuration [13-15]. Studies have demonstrated distinct pharmacological effects to cinnamic acid and its derivatives with low toxicity to living organisms, including antimicrobial, antifungal, antioxidant, anti-inflammatory, leishmanicidal, and antitumoral activities [13,16-21].

In vitro antitumor and antimetastatic activities of cinnamic acid have been reported in several cancer cell lines, including melanoma [15,17,18], by preventing cell multiplication [22], inducing apoptosis in cells with irreversible DNA damage, promoting disruption of the cytoskeleton [18], and reducing the invasive capacity of cancer cells [15,23]. Notwithstanding, structural changes in the cinnamic acid molecule can generate derivatives more potent than the parent cinnamic acid [21,24,25]. For instance, cinnamic acid derivatives have shown antitumor activity on melanoma [25,26], hepatocellular carcinoma [27,28], colon cancer [27,29,30], breast cancer [27,29-31], nasopharyngeal carcinoma [32], and lung cancer [30,33,34]. Several mechanisms of action have been proposed for cinnamic acid derivatives, such as inhibition of histone deacetylases and metalloproteinases activity, which may cause cancer cell death and reduce cancer invasion, respectively [33,35]. Moreover, these

derivatives can play more than one role in antitumor activity, such as inhibition of cell proliferation, induction of apoptosis, and disruption of the stages of metastasis [25-27,30-32].

Therefore, this study aimed to synthesize compounds derived from cinnamic acid and perform a drug screening to detect the most active derivative compound against melanoma cells. To this end, we used the B16-F10 cell line due to its recognized aggressiveness, as well as *in vitro* assays to evaluate the effect of the selected compound on apoptotic, proliferative, and antimetastatic melanoma activities. Our results might indicate future directions to study the mechanism of action of these esters derived from cinnamic acid.

2. MATERIAL AND METHODS

2.1 Synthesis

2.1.1 Generalities

Solvents were purchased from F Maia (Charqueada, São Paulo, Brazil). Commercially available *N,N'*-dicyclohexylcarbodiimide (DCC), 4-*N,N'*-dimethylaminopyridine (DMAP), *trans*-cinnamic acid, benzyl alcohol, 4-nitrobenzyl alcohol, 4-bromobenzyl alcohol, 4-chlorobenzyl alcohol, 4-trifluoromethoxybenzyl alcohol, 4-trifluoromethylbenzyl alcohol, 4-methoxybenzyl alcohol, 4-methylbenzyl alcohol, 4-isopropylbenzyl alcohol, phenol, eugenol, perillyl alcohol, carvacrol, timol, and vanilin were purchased from Sigma Aldrich (St. Louis, MO, USA) and used without further purification. The preparation of the compound 6-hydroxyisobenzofuran-1(3*H*)-one (**2o**) (cf. Scheme 1) has been previously described [21]. The NMR spectra were recorded on a Varian Mercury 300 instrument (Varian, Palo Alto, CA, USA) at 300 MHz (^{1}H) and 75 MHz (^{13}C) or on a Brucker spectrometer (Bruker Billerica, Massachusetts) at 400 MHz (^{1}H) and 100 MHz (^{13}C). For the acquisition of the spectra, deuterated chloroform ($CDCl_3$) and methanol (CD_3OD) were used as solvents. The ^{1}H-NMR data are presented as follows: chemical shift (δ) in ppm, multiplicity, number of protons, *J* values in Hertz (Hz). Multiplicities are indicated by the following abbreviations: s (singlet), d (doublet), m (multiplet), sept (septet), brs (broad singlet), d (doublet), ddt_{ap} (apparent doublet of doublet of triplets). For fluorine-containing derivatives, the multiplicity (quartet, q) of some carbon signals is described along with *J* values in Hertz. IR spectra were obtained using Varian 660-IR equipped with GladiATR (Varian, Palo Alto, CA, USA) scanning from 4000 to 500 cm^{-1}. Melting points were determined using a MQAPF-302 melting point apparatus (Microquímica, Santa Catarina, Brazil) and are uncorrected. The progress of the reactions was

monitored by thin layer chromatography (TLC). Flash column chromatography was performed using silica gel (60–230 mesh).

*2.1.2 General procedure for the synthesis of cinnamates 3a-3p, exemplified by the synthesis of benzyl cinnamate (**3a**)*

Benzyl alcohol (0.297 g, 2.75 mmol) was added to a 50 mL round-bottom flask containing 25.0 mL of dichloromethane, 0.370 g (2.50 mmol) of *trans*-cinnamic acid, 0.567 g (2.75 mmol) of DCC, and 0.0301 g (0.250 mmol) of DMAP. After 40 min of stirring at room temperature, the reaction mixture was filtered, and the resulting solution was washed with 10% m/v citric acid solution (2 x 20.0 mL), distilled water (15.0 mL), and brine (30.0 mL). The resulting organic phase was reserved, and the aqueous layer was extracted with dichloromethane (3 x 20.0 mL). The organic extracts were combined, and the resulting organic phase was dried by Na_2SO_4, filtered, and concentrated under reduced pressure. The resulting material was purified by silica gel column chromatography eluted with hexane-ethyl acetate (4:1 v/v). The described procedure afforded compound **3a** in 63% yield (0.374 g, 1.57 mmol). White solid, m.p. 33.1─33.6 ^{o}C, TLC: R_f = 0.52 (hexane-ethyl acetate 4:1 v/v). IR (ATR) $\bar{\nu}_{max}$/cm^{-1}: 3084, 3032, 2968, 2897, 1703, 1634, 1574, 1494, 1371, 1312, 1152. ^{1}H NMR (300 MHz, $CDCl_3$) δ: 5.27 (s, 2H), 6.50 (d, 1H, J_{trans} = 16.2 Hz), 7.35─7.54 (m, 10H), 7.75 (d, 1H, J_{trans} = 16.2 Hz). ^{13}C NMR (75 MHz, $CDCl_3$) δ: 66.3, 117.9, 128.1, 128.23, 128.25, 128.6, 128.9, 130.3, 134.4, 136.1, 145.1, 166.7. The preparation of compounds **3b-3p** followed the procedure used for compound **3a** production. All the compounds were characterized by IR and NMR (^{1}H and ^{13}C). Spectroscopic data are available in the supplementary material (Figures S1-S51).

*2.1.3 Data for 4-chlorobenzyl cinnamate (**3b**)*

White solid, obtained in 59% yield, m.p. 61.5─62.1 oC, purified by silica gel column chromatography eluted with hexane-ethyl acetate (4:1 v/v), TLC: R_f = 0.53 (hexane-ethyl acetate 4:1 v/v). IR (ATR) $\bar{\nu}_{max}$/cm^{-1}: 3057, 2935, 2887, 2121, 1706, 1633, 1574, 1493, 1312, 1282, 1171, 1090. ^{1}H NMR (300 MHz, $CDCl_3$) δ: 5.22 (s, 2H), 6.48 (d, 1H, J_{trans} = 16.0 Hz), 7.35─7.39 (m, 6H), 7.51─7.53 (m, 2H), 7.73 (d, 1H, J_{trans} = 16.0 Hz). ^{13}C NMR (75 MHz, $CDCl_3$) δ: 65.5, 117.6, 128.1, 128.8, 128.9, 129.6, 130.4, 134.1, 134.3, 134.6, 145.4, 166.6.

*2.1.4 Data for 4-nitrobenzyl cinnamate (**3c**)*

White solid, obtained in 68% yield, m.p. 114.5─115.7 °C, purified by silica gel column chromatography eluted with hexane-ethyl acetate (4:1 v/v), TLC: R_f = 0.31 (hexane-ethyl acetate 4:1 v/v). IR (ATR) $\bar{\nu}_{max}$/cm^{-1}: 3111, 3066, 2964, 2846, 1706, 1630, 1513, 1446, 1374, 1342, 1205, 1153. ^{1}H NMR (300 MHz, $CDCl_3$) δ: 5.34 (s, 2H), 6.51 (d, 1H, J_{trans} = 15.9 Hz), 7.39─7.41 (m, 3H), 7.52─7.58 (m, 4H), 7.76 (d, 1H, J_{trans} = 15.9 Hz), 8.23 (d, 2H, J = 8.4 Hz). ^{13}C NMR (75 MHz, $CDCl_3$) δ: 64.7, 117.1, 123.8, 128.2, 128.3, 128.9, 130.6, 134.1, 143.4, 146.0, 147.7, 166.4.

*2.1.5 Data for 4-bromobenzyl cinnamate (**3d**)*

White solid, obtained in 56% yield, m.p. 77.3─77.8 °C, purified by silica gel column chromatography eluted with hexane-ethyl acetate (4:1 v/v), TLC: R_f = 0.46 (hexane-ethyl acetate 4:1 v/v). IR (ATR) $\bar{\nu}_{max}$/cm^{-1}: 3057, 2974, 2939, 2885, 2117, 1704, 1633, 1574, 1489, 1369, 1311, 1282, 1167, 1067. ^{1}H NMR (300 MHz, $CDCl_3$) δ: 5.20 (s, 2H), 6.48 (d, 1H, J_{trans} = 15.9 Hz), 7.29 (d, 2H, J = 8.4 Hz); 7.38─7.40 (m, 3H), 7.50─7.53 (m, 4H), 7.74 (d, 1H, J_{trans} = 15.9 Hz). ^{13}C NMR (75 MHz, $CDCl_3$) δ: 65.5, 117.6, 122.3, 128.1, 128.9, 129.9, 130.4, 131.7, 134.3, 135.1, 145.4, 166.6.

*2.1.6 Data for 4-(trifluoromethyl)benzyl cinnamate (**3e**)*

White solid, obtained in 61% yield, m.p. 47.4─47.8 °C, purified by silica gel column chromatography eluted with hexane-ethyl acetate (4:1 v/v), TLC: R_f = 0.43 (hexane-ethyl acetate 4:1 v/v). IR (ATR) $\bar{\nu}_{max}$/cm^{-1}: 3062, 3032, 2929, 2117, 1713, 1633, 1578, 1450, 1327, 1207, 1154, 1106, 1065. ^{1}H NMR (300 MHz, $CDCl_3$) δ: 5.31 (s, 2H), 6.51 (d, 1H, J_{trans} = 16.1 Hz), 7.39─7.41 (m, 3H), 7.52─7.54 (m, 4H), 7.65 (d, 2H, J = 8.1 Hz), 7.76 (d, 1H, J_{trans} = 16.1 Hz). ^{13}C NMR (75 MHz, $CDCl_3$) δ: 65.3, 117.4, 124.0 (q, $J_{C\text{-}F}$ = 270.4 Hz), 125.5 (q, $J_{C\text{-}F}$ = 3.8 Hz), 128.1, 128.9, 130.4 (q, $J_{C\text{-}F}$ = 32.3 Hz), 130.5, 134.2, 140.1, 145.7, 166.5.

*2.1.7 Data for 4-methoxybenzyl cinnamate (**3f**)*

White solid, obtained in 61% yield, m.p. 62.3─63.4 °C, purified by silica gel column chromatography eluted with hexane-ethyl acetate (4:1 v/v), TLC: R_f = 0.51 (hexane-ethyl acetate 4:1 v/v). IR (ATR) $\bar{\nu}_{max}$/cm^{-1}: 3047, 2995, 2931, 2833, 2117, 1892, 1700, 1641, 1574, 1513,

1452, 1369, 1306, 1247, 1167, 1033. ^{1}H NMR (300 MHz, $CDCl_3$) δ: 3.82 (s, 3H), 5.20 (s, 2H), 6.48 (d, 1H, J_{trans} = 15.9 Hz), 6.93 (d, 2H, J = 8.4 Hz), 7.36─7.52 (m, 7H), 7.73 (d, 1H, J_{trans} = 15.9 Hz). ^{13}C NMR (75 MHz, $CDCl_3$) δ: 55.3, 66.2, 114.0, 118.1, 128.1, 128.2, 128.9, 130.1, 130.3, 134.4, 145.0, 159.7, 166.8.

*2.1.8 Data for 4-(trifluoromethoxy)benzyl cinnamate (**3g**)*

White solid, obtained in 64% yield, m.p. 34.0─35.1 °C, purified by silica gel column chromatography eluted with hexane-ethyl acetate (4:1 v/v), TLC: R_f = 0.48 (hexane-ethyl acetate 4:1 v/v). IR (ATR) $\bar{\nu}_{max}$/cm^{-1}: 3066, 2964, 2931, 2121, 1969, 1708, 1634, 1506, 1451, 1370, 1309, 1262, 1143, 1011. ^{1}H NMR (300 MHz, $CDCl_3$) δ: 5.25 (s, 2H), 6.49 (d, 1H, J_{trans} = 15.9 Hz), 7.23 (d, 2H, J = 8.4 Hz), 7.38─7.40 (m, 3H), 7.45 (d, 2H, J = 8.4 Hz), 7.52─7.55 (m, 2H), 7.75 (d, 1H, J_{trans} = 15.9 Hz). ^{13}C NMR (75 MHz, $CDCl_3$) δ: 65.3, 117.6, 120.4 (q, $J_{C\text{-}F}$ = 255.7 Hz), 121.0, 128.1, 128.9, 129.7, 130.4, 134.2, 134.8, 145.5, 149.1, 166.6.

*2.1.9 Data for 4-methylbenzyl cinnamate (**3h**)*

White solid, obtained in 72% yield, m.p. 40.3─41.6 °C, purified by silica gel column chromatography eluted with hexane-ethyl acetate (4:1 v/v), TLC: R_f = 0.47 (hexane-ethyl acetate 4:1 v/v). IR (ATR) $\bar{\nu}_{max}$/cm^{-1}: 3049, 3022, 2920, 2856, 2121, 1702, 1638, 1570, 1446, 1373, 1308, 1282, 1173. ^{1}H NMR (300 MHz, $CDCl_3$) δ: 2.38 (s, 3H), 5.23 (s, 2H), 6.49 (d, 1H, J_{trans} =15.9 Hz), 7.21 (d, 2H, J = 7.8 Hz), 7.33 (d, 2H, J = 7.8 Hz), 7.38─7.40 (m, 3H), 7.51─7.54 (m, 2H), 7.74 (d, 1H, J_{trans} = 15.9 Hz). ^{13}C NMR (75 MHz, $CDCl_3$) δ: 21.2, 66.3, 118.0, 128.1, 128.4, 128.9, 129.3, 130.3, 133.1, 134.4, 138.1, 145.0. 166.8.

*2.1.10 Data for 4-isopropylbenzyl cinnamate (**3i**)*

White solid, obtained in 75% yield, m.p. 38.1─38.5 °C, purified by silica gel column chromatography eluted with hexane-ethyl acetate (4:1 v/v), TLC: R_f = 0.52 (hexane-ethyl acetate 4:1 v/v). IR (ATR) $\bar{\nu}_{max}$/cm^{-1}: 3053, 2958, 2926, 2858, 2121, 1708, 1636, 1510, 1453, 1382, 1311, 1202, 1159, 1057. ^{1}H NMR (300 MHz, $CDCl_3$) δ: 1.28 (d, 6H, J = 6.9 Hz), 2.94 (sept, 1H, J = 6.9 Hz); 5.25 (s, 2H), 6.51 (d, 1H, J_{trans} = 15.9 Hz), 7.27 (d, 2H, J = 6.9 Hz), 7.37─7.39 (m, 5H), 7.52─7.54 (m, 2H), 7.75 (d, 1H, J_{trans} = 15.9 Hz). ^{13}C NMR (75 MHz, $CDCl_3$) δ: 24.0, 33.9, 66.4, 118.0, 126.7, 128.1, 128.6, 128.9, 130.3, 133.4, 134.4, 145.1, 149.1, 166.9.

*2.1.11 Data for 5-isopropyl-2-methylphenyl cinnamate (**3j**)*

White solid, obtained in 45% yield, m.p. 62.8─64.3 °C, purified by silica gel column chromatography eluted with hexane-ethyl acetate (4:1 v/v), TLC: R_f = 0.58 (hexane-ethyl acetate 4:1 v/v). IR (ATR) $\bar{\nu}_{max}$/cm^{-1}: 3062, 3032, 2960, 2926, 2868, 2023, 1721, 1628, 1578, 1497, 1448, 1308, 1237, 1138. ^{1}H NMR (300 MHz, $CDCl_3$) δ: 1.28 (d, 6H, J = 6.9 Hz), 2.21 (s, 3H), 2.93 (sept, 1H, J = 6.9 Hz), 6.70 (d, 1H, J_{trans} = 16.1 Hz), 6.97 (s, 1H), 7.06 (d, 1H, J = 7.7 Hz), 7.20 (d, 1H, J = 7.7 Hz), 7.44 (brs, 3H), 7.61 (brs, 2H), 7.92 (d, 1H, J_{trans} = 16.1 Hz). ^{13}C NMR (75 MHz, $CDCl_3$) δ: 15.9, 24.0, 33.6, 117.2, 119.8, 124.2, 127.4, 128.3, 129.0, 130.7, 130.9, 134.2, 146.5, 148.1, 149.3, 165.2.

*2.1.12 Data for 2-isopropyl-5-methylphenyl cinnamate (**3k**)*

White solid, obtained in 53% yield, m.p. 65.4─66.5 °C, purified by silica gel column chromatography eluted with hexane-ethyl acetate (4:1 v/v), TLC: R_f = 0.55 (hexane-ethyl acetate 4:1 v/v). IR (ATR) $\bar{\nu}_{max}$/cm^{-1}: 3057, 3024, 2960, 2922, 2852, 2117, 1724, 1637, 1505, 1448, 1308, 1242, 1144, 1080. ^{1}H NMR (300 MHz, $CDCl_3$) δ: 1.24 (d, 6H, J = 6.9 Hz), 2.35 (s, 3H), 3.07 (sept, 1H, J = 6.9 Hz), 6.69 (d, 1H, J_{trans} = 15.9 Hz), 6.92 (s, 1H), 7.06 (d, 1H, J = 8.0 Hz), 7.24 (d, 1H, J = 8.0 Hz), 7.43─7.45 (m, 3H), 7.60─7.63 (m, 2H), 7.90 (d, 1H, J_{trans} = 15.9 Hz). ^{13}C NMR (75 MHz, $CDCl_3$) δ: 20.8, 23.1, 27.2, 117.3, 122.8, 126.5, 127.1, 128.3, 129.0, 130.6, 134.2, 136.6, 137.2, 146.4, 148.0, 165.6.

*2.1.13 Data for 4-formyl-2-methoxyphenyl cinnamate (**3l**)*

White solid, obtained in 84% yield, m.p. 91.5─92.6 °C, purified by silica gel column chromatography eluted with hexane-ethyl acetate-chloroform (3:1:3 v/v), TLC: R_f = 0.47 (hexane-ethyl acetate-chloroform 3:1:3 v/v). IR (ATR) $\bar{\nu}_{max}$/cm^{-1}: 3059, 3012, 2929, 2852, 2738, 2117, 1979, 1725, 1701, 1633, 1595, 1500, 1423, 1391, 1307, 1265, 1132, 1029. ^{1}H NMR (300 MHz, $CDCl_3$) δ: 3.91 (s, 3H), 6.67 (d, 1H, J_{trans} = 15.9 Hz), 7.31 (d, 1H, J = 7.8 Hz), 7.42─7.61 (m, 7H), 7.90 (d, 1H, J_{trans} = 15.9 Hz), 9.96 (s, 1H). ^{13}C NMR (75 MHz, $CDCl_3$) δ: 56.1, 110.8, 116.3, 123.5, 124.8, 128.4, 129.0, 130.9, 134.0, 135.2, 145.0, 147.4, 152.1, 164.3, 191.1.

*2.1.14 Data for 4-allyl-2-methoxyphenyl cinnamate (**3m**)*

White solid, obtained in 67% yield, m.p. 79.5─80.6 °C, purified by silica gel column chromatography eluted with hexane-ethyl acetate (2:1 v/v), TLC: R_f = 0.59 (hexane-ethyl acetate 2:1 v/v). IR (ATR) $\bar{\nu}_{max}$/cm^{-1}: 3059, 3003, 2935, 2843, 1731, 1636, 1602, 1507, 1462, 1449, 1305, 1264, 1122, 1031. ^{1}H NMR (400 MHz, $CDCl_3$) δ: 3.40 (d, 2H, J = 6.8 Hz), 3.82 (s, 3H), 5.09─5.15 (m, 2H); 5.98 (ddt_{ap}, 1H, J_1 = 16.8 Hz, J_2 = 10.2 Hz and J_3 = 6.6 Hz), 6.67 (d, 1H, J_{trans} = 16.0 Hz), 6.78-6.82 (m, 2H), 7.03 (d, 1H, J = 8.0 Hz), 7.40─7.59 (m, 5H), 7.87 (d, 1H, J_{trans} = 16.0 Hz). ^{13}C NMR (100 MHz, $CDCl_3$) δ: 40.2, 55.9, 112.8, 116.2, 117.1, 120.7, 122.7, 128.3, 129.0, 130.6, 134.3, 137.1, 138.0, 139.0, 146.5, 151.0, 165.2.

*2.1.15 Data for (S) -(4-(prop-1-en-2-yl) cyclohex-1-en-1-yl) methyl cinnamate (**3n**)*

Colorless oil, obtained in 65% yield, purified by silica gel column chromatography eluted with hexane-ethyl acetate (4:1 v/v), TLC: R_f = 0.59 (hexane-ethyl acetate 4:1 v/v). IR (ATR) $\bar{\nu}_{max}$/cm^{-1}: 3062, 2968, 2925, 2837, 2118, 1710, 1636, 1578, 1496, 1450, 1307, 1280, 1158. ^{1}H NMR (400 MHz, $CDCl_3$) δ: 1.85─2.21 (m, 7H), 4.61 (brs, 2H), 4.73─4.74 (m, 2H), 5.82 (s, 1H), 6.47 (d, 1H, J_{trans} = 16.0 Hz), 7.36─7.40 (m, 3H), 7.52─7.54 (m, 2H), 7.70 (d, 1H, J_{trans} = 16.0 Hz). ^{13}C NMR (100 MHz, $CDCl_3$) δ: 20.8, 26.5, 27.3, 30.5, 40.9, 68.5, 108.8, 118.1, 125.9, 128.1, 128.9, 130.3, 132.7, 134.4, 144.9, 149.6, 166.9.

*2.1.16 Data for 3-oxo-1,3-dihydroisobenzofuran-5-yl cinnamate (**3o**)*

White solid, obtained in 82% yield, m.p. 171.9─172.4 °C, purified by silica gel column chromatography eluted with hexane-ethyl acetate (3:1 v/v), TLC: R_f = 0.30 (hexane-ethyl acetate 3:1 v/v). IR (ATR) $\bar{\nu}_{max}$/cm^{-1}: 3074, 2928, 2852, 1755, 1725, 1633, 1577, 1481, 1451, 1158, 1138. ^{1}H NMR (300 MHz, $CDCl_3$) δ: 5.33 (s, 2H), 6.64 (d, 1H, J_{trans} = 16.0 Hz), 7.43─7.72 (m, 8H), 7.90 (d, 1H, J_{trans} = 16.0 Hz). ^{13}C NMR (75 MHz, $CDCl_3$) δ: 69.5, 116.3, 118.8, 123.1, 127.2, 128.2, 128.4, 129.0, 131.0, 133.8, 143.6, 147.6, 151.4, 165.0, 170.2.

*2.1.17 Data for phenyl cinnamate (**3p**)*

White solid, obtained in 82% yield, m.p. 73.9─75.3 °C, purified by silica gel column chromatography eluted with hexane-ethyl acetate (2:1 v/v), TLC: R_f = 0.56 (hexane-ethyl

acetate 2:1 v/v). IR (ATR) $\bar{\nu}_{max}$/cm^{-1}: 3058, 2932, 1727, 1637, 1588, 1484, 1449, 1204, 1145, 910. ^{1}H NMR (300 MHz, $CDCl_3$) δ: 6.73 (d, 2H, J_{trans} = 16.0 Hz), 7.68─7.14 (m, 10H), 7.87 (d, 2H, J_{trans} = 16.0 Hz). ^{13}C NMR (75 MHz, $CDCl_3$) δ: 116.8, 121.3, 125.4, 128.0, 128.6, 129.0, 134.1, 146.5, 150.9, 165.5.

*2.1.18 General procedure for the synthesis of phenyl 2,3-dibromophenylpropanoate (**3q**)*

Phenyl cinnamate (0.100 g, 0.445 mmol) was added to a 25 ml round-bottom flask containing 6.0 ml of CCl_4. To this reaction mixture, it was added, dropwise, a solution of bromine dissolved in CCl_4 until a reddish color remains. The reaction remained under magnetic stirring at 40 ºC for 8 hours. After this period, 15.0 mL of saturated sodium bicarbonate solution were added, and the aqueous phase was extracted with dichloromethane (3 x 20.0 mL). The organic extracts were combined, and the resulting organic phase was dried over anhydrous sodium sulfate, filtered, and concentrated under reduced pressure. The compound **3q** was not submitted to any subsequent purification method. The described procedure afforded compound **3q** in 86% yield (0.141 g, 0.367 mmol). White solid, m.p. 121.3─122.7 ^{o}C, TLC: R_f = 0.86 (hexane-ethyl acetate 2:1 v/v). IR (ATR) $\bar{\nu}_{max}$/cm^{-1}: 3010, 1764, 1626, 1576, 1494, 1265, 1196, 695, 602. ^{1}H NMR (300 MHz, $CDCl_3$/ CD_3OD) δ: 5.01 (d, 1H, J = 12.0 Hz), 5.41 (d, 1H, J = 12.0 Hz), 7.43─7.15 (m, 10 H). ^{13}C NMR (75 MHz, $CDCl_3$/ CD_3OD) δ: 46.7, 50.5, 120.9, 126.5, 128.0, 128.9, 129.4, 129.5, 137.2, 150.2, 166.4.

2.2 Cell culture, culture conditions, and compound dilution

Metastatic melanoma cells (B16-F10) were kindly provided by Dr. Mirian T. Paes Lopes (Department of Pharmacology, Universidade Federal de Minas Gerais, Belo Horizonte, Minas Gerais, Brazil). Embryonic fibroblasts cell line (NIH3T3) and African green monkey kidney cell line (Vero) were kindly provided by Dr. Juliana Lopes Rangel Fietto (Department of Biochemistry and Molecular Biology, Universidade Federal de Viçosa, Viçosa, Minas Gerais, Brazil). The cells were grown in RPMI-1640 medium (pH 7.2; Sigma Aldrich) at 37 °C under 5% CO_2 atmosphere, supplemented with 10% (v/v) of fetal bovine serum (FBS) (LGC Biotecnologia, Cutia, São Paulo, Brazil), 100 g/mL streptomycin, and 100 units/mL penicillin. The compounds, in turn, were diluted in DMSO, aliquoted, and stored at -20 ^{o}C to avoid freeze-thaw cycles.

2.3 Screening assays

Trans-cinnamic acid and the seventeen compounds were submitted to screening assays, such as cell viability and migration, to select the most active compound(s) that were used in subsequent assays. Cell viability was assessed using the MTT (3-(4,5 dimethylthiazol-2-yl)-2,5 diphenyltetrazolium bromide; Sigma Aldrich) metabolization. First, B16-F10 cells at 1.0 x 10^4 cells/well were seeded onto 96-well plates containing 100 μL complete RPMI-1640 medium and incubated for 24 h. Later, the cells were incubated with 100 μM *trans*-cinnamic acid and the compounds **3a**–**3q** (treatment groups). This concentration of 100 μM was chosen in the preliminary analysis of cytotoxic effect based on protocols that analyze IC_{50} in a range between 0 and 200 μM. Wells containing cells treated with 0.4% DMSO corresponded to the control culture. After 48 h incubation, MTT solution was added to each well at a final concentration of 5 mg/mL and incubated at 37 ^oC for 3 h. The MTT solution was then removed, and DMSO (100 μL/well) was added to solubilize the formazan. Absorbance was measured at 540 nm in a plate reader (Sinergy HT, Biotek, Winooski, Vermont, USA). Results were normalized considering the control culture. The half-maximal inhibitory concentration (IC_{50}) was obtained after treating B16-F10 cells with the cinnamic acid and the most active compound(s) at increasing concentrations (0–200 μM) as described by Siqueira et al. [36]. The active compounds detected by the B16-F10 cell viability assay were then incubated with Vero (8.0 x 10^4 cells/well) and NIH3T3 cells (1.0 x 10^4 cells/well) to evaluate their potential to reduce the viability of normal/nontumor cells. This incubation followed the same procedure described above.

The ability of *trans*-cinnamic acid and its derivatives compounds (**3a** – **3q**) to inhibit cell migration was analyzed using the wound-healing assay. Thus, B16-F10 cells were seeded onto a 24-well plate (1.0 x 10^5 cells/well) and allowed to reach full confluence after incubation overnight at 37 °C under 5% CO_2 atmosphere. Monolayers were then wounded using a sterile 200 μL pipette tip. Cells were washed twice with phosphate-buffered saline (PBS) to remove detached cells and treated with the compounds at 50 and 25 μM, which are submultiples values of 100 μM. The DMSO vehicle treatment (0.4% v/v) was used as a control. Photos of the wound were taken using an inverted microscope EVOS® (Life Technologies, Carlsbad, California, USA). Wound closure rates were then calculated quantitatively as the difference between wound width at 0 h and 24 h. Results were expressed as a percentage of cell migration.

2.4 Post-screening assays using the selected compound 3q

2.4.1 Apoptosis assays

The apoptotic activity of the compound **3q** was analyzed using acridine orange (AO) and ethidium bromide (EB), and annexin V/FITC staining. First, B16-F10 cells were plated in 24 wells (1.0 x 10^5 cells/well) and incubated for 24 h. The cells were then treated with 25, 50, and 100 μM of compound **3q** for 48 h, while DMSO (0.4% v/v) was used as vehicle control. The plate was centrifuged, and the supernatant removed. Each well was stained with 200 μL of a dye solution containing PBS with AO (50 μg/mL; Sigma Aldrich) and EB (50 μg/ mL; Sigma Aldrich) in a 1:1 ratio for 5 min. Later on, the cells were washed with PBS and centrifuged at 1,500 rpm several times. AO is a vital dye that stains viable and non-viable cells, whereas EB stains only non-viable cells. Viable cells present membrane integrity and show a green nucleus with a round intact structure. Non-viable cells, in turn, exhibit damaged membranes and either a dense orange or a red nucleus due to co-staining with EB. These results indicate apoptosis and necrosis, respectively [37]. Ultimately, ten microscopic images of different fields were evaluated under a fluorescence microscope EVOS® (Thermo Fisher Scientific, Waltham, Massachusetts, USA) at 200 x magnification, and the cells were classified into viable and non-viable cells (%).

Subsequently, apoptosis was evaluated by flow cytometry. B16-F10 cells were seeded on a 6-well plate at a density of 2.5 x 10^5 cells/well. The cells were treated with compound **3q** at 25, 50, and 100 μM for 48 h. DMSO (0.4% v/v) was used as a vehicle control. Later, these cells were labeled using Annexin V/FITC apoptosis detection kit (Merck, Kenilworth, Nova Jersey, USA), according to the manufacturer's protocol, and analyzed by flow cytometry (FACS Verse, BD Bioscience, Franklanes, New Jersey, USA). The results were expressed as percentage of cells in early events of apoptosis (annexin-V^+/PI^-), in late apoptosis (annexin-V^+/PI^+), and necrotic cells (annexin-V^-/PI^+).

2.4.2 Cell proliferation assays

Trypan blue exclusion assay, Ki-67 immunofluorescence, and cell cycle assay were performed to assess the capacity of B16-F10 cells to proliferate after treatment with compound **3q**. For this experiment and the subsequent experiments, concentrations below the IC_{50} of compound **3q** (60.28 μM) and submultiples values of 100 μM were chosen. Firstly, B16-F10 cells (2.5 x 10^4 cells/well) were seeded onto a microplate with a 24-well plate for 24

h. The compound **3q** was then diluted in RPMI-1640 medium and evaluated at 6.25, 12.5, 25, and 50 μM for 24 h and 48 h. The negative group received medium supplemented with DMSO (0.4% v/v). After the incubation period, cells were trypsinized, pelleted, and re-suspended in 300 μL of RPMI-1640 medium supplemented with FBS (10% v/v). The counting of non-living cells stained with trypan blue was carried out using a Neubauer chamber (Kasvi, Paraná, Brazil).

Moreover, Ki-67 immunofluorescence was assessed using B16-F10 cells (2.0 x 10^4 cells/well with a coverslip) treated with compound **3q** at 6.25, 12.5, 25, and 50 μM and DMSO (0.4% v/v; control) for 24 and 48 h. The samples were fixed with 4% paraformaldehyde for 20 min and washed with PBS. Then, they were permeabilized and blocked with 0.5% v/v Triton X-100/PBS and 3% m/v bovine serum albumin (BSA) for 60 min. The cells were washed with PBS three times and incubated with the primary antibody anti-Ki-67 (1:100, Abcam, #ab16667) for 60 min. After PBS washing, the cells were incubated with a secondary antibody anti-rabbit IgG Alexa Fluor 488 (1:100, ThermoFisher Scientific, #A11008) for 60 min. Slides were mounted using Prolong Diamond® with 4′,6-diamidino-2-phenylindole (DAPI, Thermo Fisher Scientific) used as a nuclear counterstain. The fluorescence was recorded using an inverted fluorescence microscope EVOS® (Life Technologies) with DAPI LED CUBE and GFP LED CUBE filters.

Finally, a cell cycle assay analyzed B16-F10 cells seeded on a 6-well plate (2.5 x 10^5 cells/well) and treated with compound **3q** at 12.5, 25, and 50 μM for 24 and 48 h. DMSO (0.4%v/v) was used as vehicle control. Then, the cells were fixed in 70% ethanol, washed in PBS, and incubated for 60 min in PBS containing propidium iodide (50 μg/mL, Sigma Aldrich) and RNase A (0.2 mg/mL, Invitrogen, Carlsbad, California). The samples were analyzed by flow cytometry (FACS Verse, BD Bioscience).

2.4.3 Cell invasion assay

The matrigel matrix (BD Biosciences) was diluted with serum-free RPMI-1640 culture medium at a 1:12 ratio. The upper chamber of the transwell (8.0 μm polycarbonate membrane, Corning, Corning, New York, USA) was coated with a 35 μL diluted matrigel matrix and incubated at 37 °C for 2 h for full condensation. Then, B16-F10 cells were re-suspended with a serum-free RPMI-1640, treated with **3q** at 6.25, 12.5, 25, and 50 μM, and inoculated into the upper chamber matrigel-precoated (5.0 x 10^4 cells; 100 μL/well). The DMSO-vehicle treatment (0.4% v/v) was used as a control. The well was filled with 650 μL of culture

medium containing 10% v/v FBS as a chemoattractant. After 24 h, filter inserts were removed from the wells. The cells on the upper surface of the filter were wiped with a cotton swab, while the chambers with the cells that invaded the lower surface were fixed in methanol for 30 min, washed, and stained with toluidine blue (1% v/v, Sigma) for 15 min. Images from ten fields were randomly chosen and captured using an inverted microscope (Leica Microsystems, Wetzlar, Germany). The cells were counted using the Image J software, and the results were expressed as a percentage of cell invasion.

2.4.4 Cell-matrix adhesion assay

B16-F10 cells were trypsinized and then treated with 6.25, 12.5, 25, and 50 μM of compound **3q** or the vehicle DMSO (0.4% v/v) for 30 min. Subsequently, the cells were plated in a 96-well plate (1.0 x 10^4 cell/well) precoated with 20 μg/mL fibronectin (BD Biosciences) and incubated for 4 h at 37 °C for adhesion. Later on, the cells were washed with PBS, and the adherent cells were analyzed by the MTT method. The absorbance was measured at 540 nm.

2.4.5 Colony formation assay

B16-F10 cells were seeded in 6-well plates in triplicate at the density of 1.0 x 10^3 cells/well. After 24 h, the cells were treated with the compound **3q** at 6.25, 12.5, 25, and 50 μM and DMSO (control) for 24 h. The complete medium was exchanged for complete medium with 2% FBS, and the cells were cultured for 7 days. The colonies formed were then fixed and stained with toluidine blue solution (1% v/v, Sigma Aldrich) and methanol (20% v/v). Colonies were counted using Image J software, and the results were expressed as a percentage of the untreated control cultures.

2.4.6 Actin cytoskeleton staining assay

B16-F10 cells at 2.0 x 10^4 cells/well were seeded on 24-well plates containing coverslips. After 24 h, the cells were treated with compound **3q** at 6.25, 12.5, 25, and 50 μM for 24 h. The cells treated with the vehicle DMSO (0.4% v/v) and RPMI-1640 medium were used as a control. Subsequently, the coverslips were fixed with 4% paraformaldehyde for 20 min, washed with PBS, and then permeabilized and blocked with 0.5% v/v Triton X-100/PBS and 2% m/v BSA for 60 min. The cells were washed with PBS three times. The cells were

then incubated with 1.4 μL of rhodamine phalloidin (6.6 μM; Thermo Fisher Scientific) diluted in 250 μL of PBS for 20 min. Then, the slides were mounted using DAPI (Thermo Fisher Scientific) as a nuclear counterstain. The fluorescence was recorded using an inverted fluorescence microscope EVOS® (Life Technologies) with DAPI LED CUBE and RFP LED CUBE filters.

2.5 Statistical analysis

The results were obtained from three independent experiments, each experiment with triplicate. They were submitted to one-way analysis of variance (ANOVA) followed by Dunnett's test, using the GraphPad Prism 6.0 statistical software (GraphPad Software Inc., San Diego, CA, USA). Results were shown as mean ± standard error of the mean (S.E.M.). Differences were considered significant when *p < 0.05, **p < 0.01, ***p < 0.001 and ****p < 0001.

3. RESULTS

3.1 Synthesis of cinnamates derived from cinnamic acid

The cinnamates **3a-3p** were prepared using the Steglich esterification [38] between the *trans*-cinnamic acid (**1**) and different hydroxylated compounds **2a-2p**, using DCC as coupling reagent. The cinnamic acid derivatives **3a-3p** were obtained in satisfactory yields (45%-84%) after purification by silica gel column chromatography (Scheme 1). DIC was used as a coupling reagent only in the synthesis of compound **3c**. The reaction with DCC, in this case, formed a mixture from which the purification of **3c** by silica gel column chromatography was not possible. Compound **3p** was chosen for the preparation of **3q** since *trans*-cinnamic acid and phenol were reagents available in higher quantities (compared to other hydroxylated reagents used in this investigation) for the preparation of **3q**. Purification procedures were not necessary and the compound **3q** was afforded in good yield (86%) (Scheme 2).

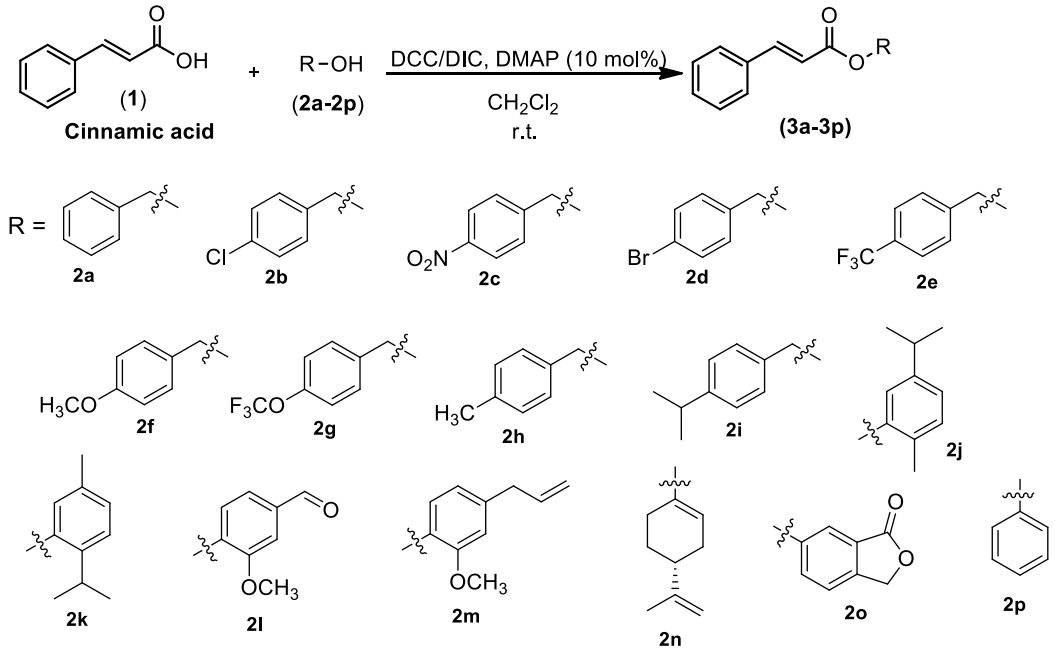

Scheme 1 - Synthesis of cinnamic acid derivatives **3a-3p**.

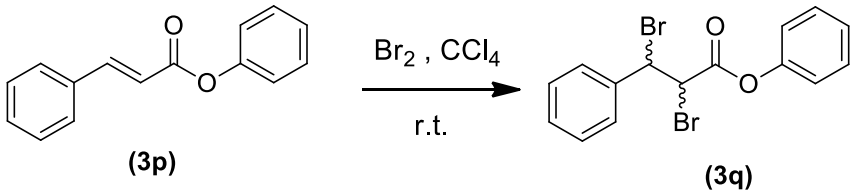

Scheme 2 - Synthesis of phenyl 2,3-dibromophenylpropanoate (**3q**).

3.2 Screening assays

The results from the cell viability assay showed that 100 μM of cinnamates **3l** and **3q** decreased the viability of B16-F10 cells compared to the DMSO-treated cells (Figure 1). The IC_{50} of these compounds were 193.9 μM and 60.28 μM, respectively (Figure S52), whereas cinnamic acid presented IC_{50} > 200 μM. Additionally, we evaluated the effect of these two compounds (**3l** and **3q**) on Vero and NIH3T3 cells. The compound **3l** significantly reduced the viability of these two non-tumorigenic cell lines and B16-F10 melanoma cells (Figure 2A). Conversely, the compound **3q** exhibited no effect on the viability of Vero and NIH3T3 cells in contrast to B16-F10 cells (Figure 2B). With regards to wound-healing assay, we observed that the compounds **3l**, **3p**, and **3q,** at the concentration of 50 μM**,** were capable of inhibiting cell migration when compared to DMSO control (Figure 3A). At 25 μM, in turn, only the compound **3q** significantly suppressed B16-F10 cell migration (Figure 3B and C). Based on the results from screening assays, the compound **3q** was selected to be tested by the post-screening assays.

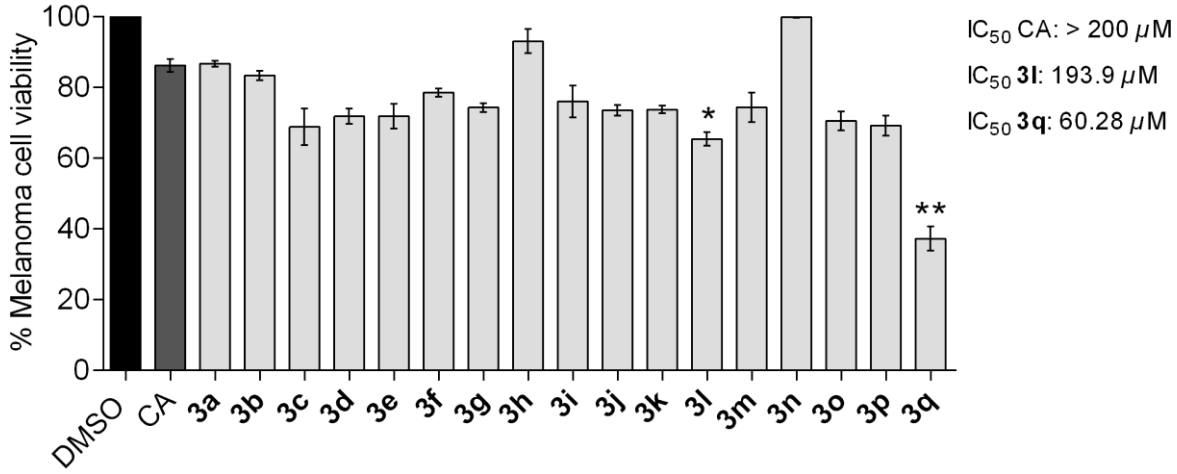

Figure 1 - Effect of seventeen compounds on cell viability of melanoma cells. B16-F10 metastatic melanoma was treated with 100 μM of each compound for 48 h. Each bar shows the percentage of survival of melanoma cells determined by MTT assay. *Trans*-cinnamic acid (CA) and the compounds that showed statistical difference in relation to the control were selected for IC_{50} evaluation. Mean ± S.E.M. *$p < 0.05$, **$p < 0.01$ versus control by one-way ANOVA and Dunnett's post-hoc test.

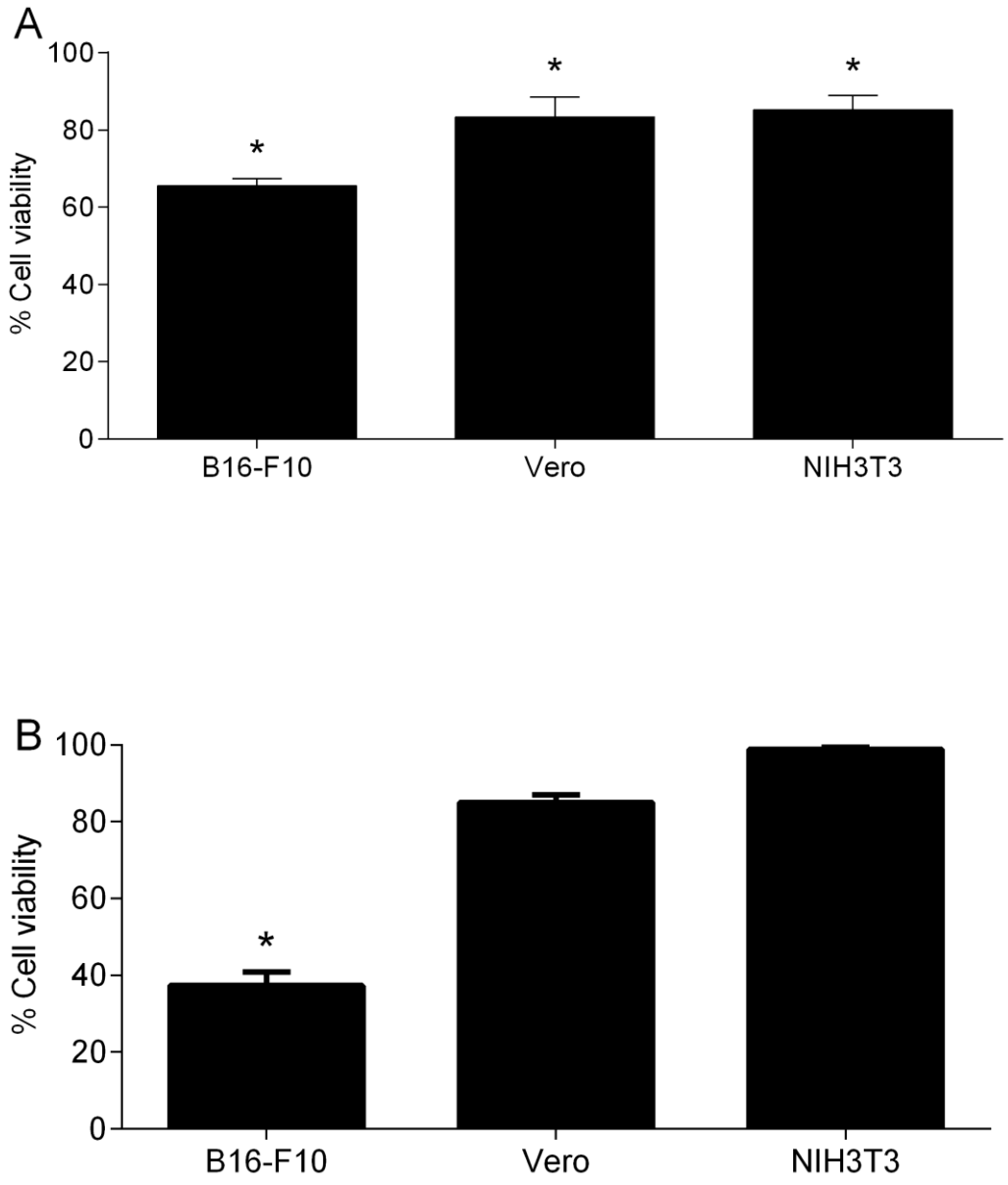

Figure 2 - Effect of the most active compounds on cell viability of non-tumorigenic cells in comparison with B16-F10. Vero (African green monkey kidney epithelial cells) and NIH3T3 (Embryonic fibroblasts cells) were treated with 100 μM of the compounds **3l** (A) and **3q** (B) for 48 h. Each bar shows the mean of percentage of survival of B16-F10, Vero, and NIH3T3 cells determined by MTT assay. Data were normalized based on DMSO control. Mean ± S.E.M. *$p < 0.05$ versus control by one-way ANOVA and Dunnett's post-hoc test.

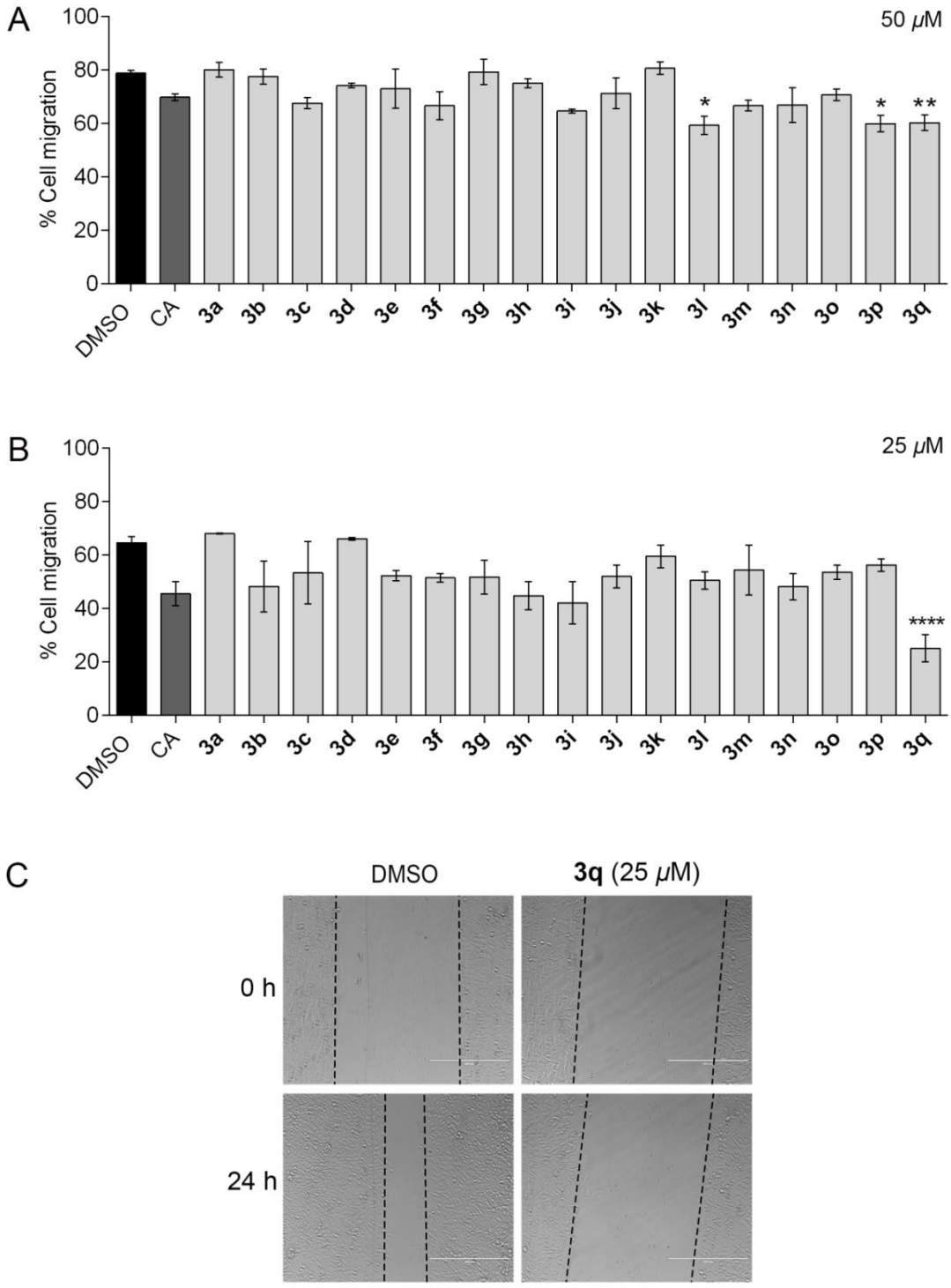

Figure 3 - Effect of cinnamic acid derivatives on wound healing of B16-F10 melanoma cells *in vitro*. (A) B16-F10 metastatic melanoma was wounded with a pipette tip and then treated with 50 μM of *trans*-cinnamic acid (CA) and each synthesized compound for 24 h. (B) Melanoma cells were wounded with a pipette tip and then treated with 25 μM of CA and each synthesized compound for 24 h. (C) Representative images of the wound were taken at 0 h and 24 h after treatment with 25 μM of compound **3q**; scale bars: 400 μM. Mean ± S.E.M. *p < 0.05, **p < 0.01 and ****p<0.0001 versus control by one-way ANOVA and Dunnett's post-hoc test.

Based on these results, the subsequent *in vitro* assays were performed to evaluate the apoptotic, antiproliferative, and antimetastatic activity of the selected compound **3q** on B16-F10 metastatic lineage. These tests were conducted using concentrations ≤ 50 μM, which are lower than the IC_{50} of this compound (60.28 μM). Concentrations > 50 μM induce cell death in B16-F10, which is not desirable once it is important to maintain the cell viability during the experiments.

3.3 Post-screening assays

*3.3.1 Apoptotic effect of compound **3q** on melanoma cells*

Double staining with AO and EB showed that B16-F10 cells treated with 100 μM compound **3q** for 48 h decreased the percentage of viable cells and increased the percentage of non-viable cells compared to the control ($p < 0.0001$; Figures 4A and B). This compound did not cause cell death at concentrations of 25 and 50 μM ($p > 0.05$; Figures 4A and B). Annexin V/PI staining assay, in turn, indicated that compound **3q** at 100 μM significantly increased annexin-V positive cells after 48 h incubation compared to control ($p < 0.0001$; Figures 4C and D). At this concentration, the percentage of cells in early events of apoptosis reached 15.3% (Figures 4D, left), while the values increased ten times approximately in late apoptosis (Figure 4D, right). Importantly, necrotic cells were little observed in this assay (Figures 4A and B).

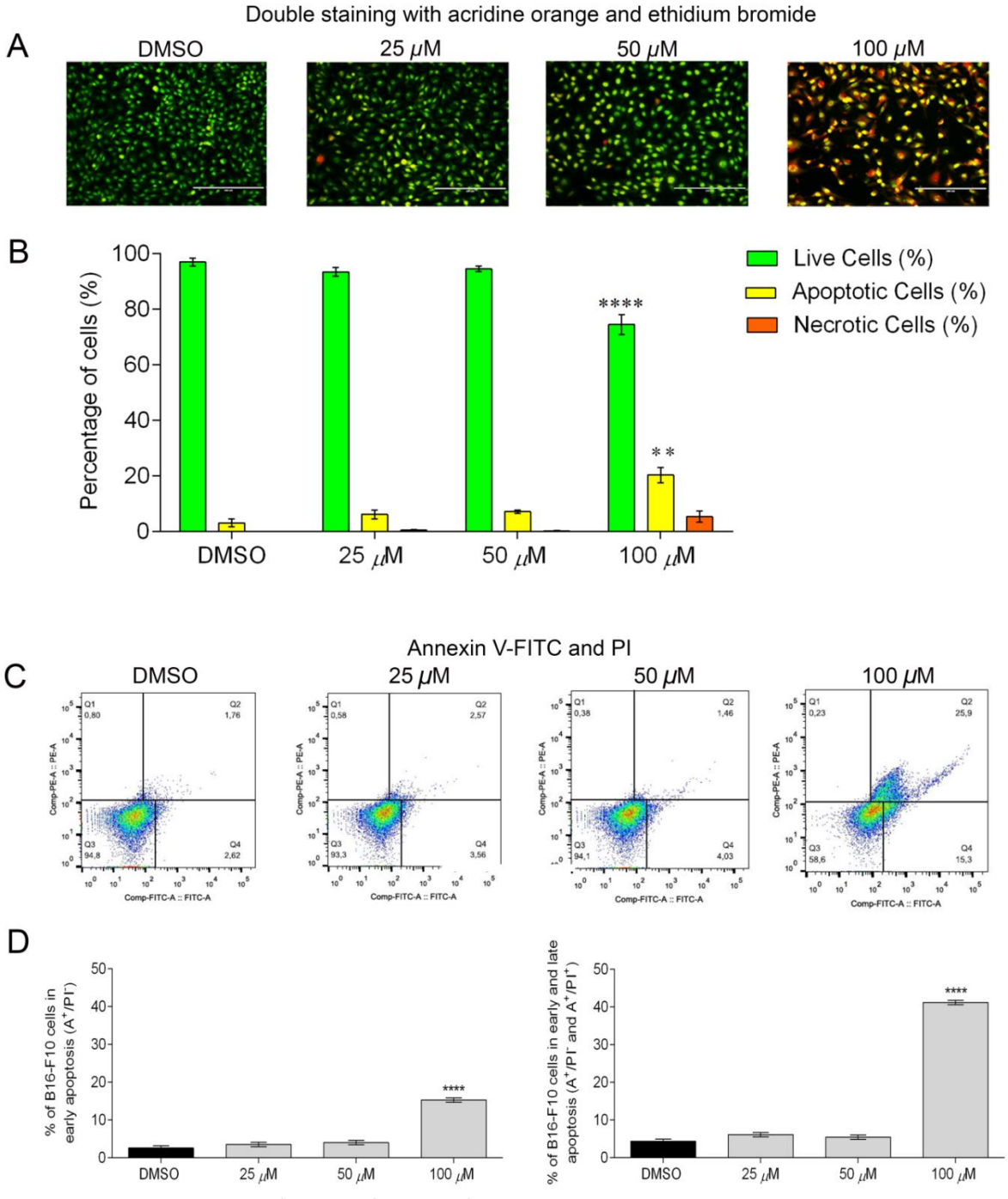

Figure 4 - Effect of compound **3q** on melanoma cell death. (A) Photomicrography showing the living cells and cells in either apoptosis or necrosis stained with acridine orange and ethidium bromide after 48 h incubation with 25, 50, and 100 μM of compound **3q**. Scale bars: 200 μM. (B) Percentage of live cells, apoptotic cells, and necrotic cells. (C) B16-F10 cells treated with 25, 50, and 100 μM of **3q** compound for 48 h, and labeled using annexin-V/FITC and PI kit. (D) The graphs show percentage of apoptotic cells (annexin-V positive cells). The percentage of cells in early apoptosis is represented on the left side and the percentage of cells in early and late apoptosis is on the right side. Mean ± S.E.M. **p < 0.01 and ****p<0.0001 versus control by One-way ANOVA and Dunnett's post-hoc test.

*3.3.2 Antiproliferative effect of compound **3q** on melanoma cells*

Trypan blue method revealed that compound **3q** reduced B16-F10 cell proliferation at all concentrations tested after 24 h of treatment, whereas this compound, after 48 h incubation, reduced this process only at 25 and 50 μM (Figure 5A). Similarly, Ki-67 immunolabeling (Figure 5B) showed a low number of Ki67-positive B16-F10 cells after 24 h incubation with compound **3q** at 6.25, 12.5, 25, and 50 μM. After 48 h, in turn, the compound reduced the proliferative activity of B16-F10 at the concentrations of 25 and 50 μM (Figure S53).

Once the compound **3q** impaired the proliferative activity of B16-F10, we evaluated the effect of this compound on its cell cycle. In this assay, we observed that compound **3q** at 50 μM increased the duration of the G2/M phase compared to the control group, followed by 25 μM after 24 h treatment (Figure 5C, left). After 48 h, in turn, this cell cycle phase was increased by the compound **3q** at the concentration of 12.5 μM (Figure 5C, right). Moreover, we observed a reduction in the proportion of cells exhibiting S phase after 24 h treatment with compound **3q** at 50 μM (Figure 5C, left), and after 48 h treatment with this compound at the three concentrations tested (Figure 5C, right). These alterations significantly reduced the proportion of cells in G0/G1 phase only after 24 h treatment with compound **3q** at 25 μM (Figure 5C, left).

*3.3.3 Antimetastatic effect of compound **3q** on melanoma cells*

We evaluated the effect of compound **3q** on the invasion and adhesion of metastatic B16-F10 cells. Cell invasion decreased after 24 h of treatment with compound **3q** at 6.25 (22.1%), 12.5 (41.9%), 25 (58%), and 50 μM (71.4%) compared to DMSO-treated cells (Figures 6A and B). Likewise, cell adhesion was significantly decreased at 12.5 (18.2%), 25 (22.6%), and 50 μM (37.5%) (Figure 6C). Moreover, the compound **3q** altered the colony formation assay by reducing the number of colonies when incubated in concentrations of 6.25 (9.7%), 12.5 (39.8%), 25 (89.6%), and 50 μM (96.5%) compared to the control (Figure 6D).

Regarding actin cytoskeleton staining assay, B16-F10 cells from the control group were highly labeled by rhodamine phalloidin, exhibiting a spindle shape and microfilaments forming parallel fibers (Figure 6E). Cells incubated with the compound **3q** at 50 μM for 24 h, in turn, showed a rounded morphology and low labeling, indicating a reduction of polymerized actin. In addition, we detected a relevant decrease in the microfilament density

within the peripheral cytoplasm and an accumulation of fragmented F-actin close to the nucleus in B16-F10 cells treated with compound **3q** at 50 μM.

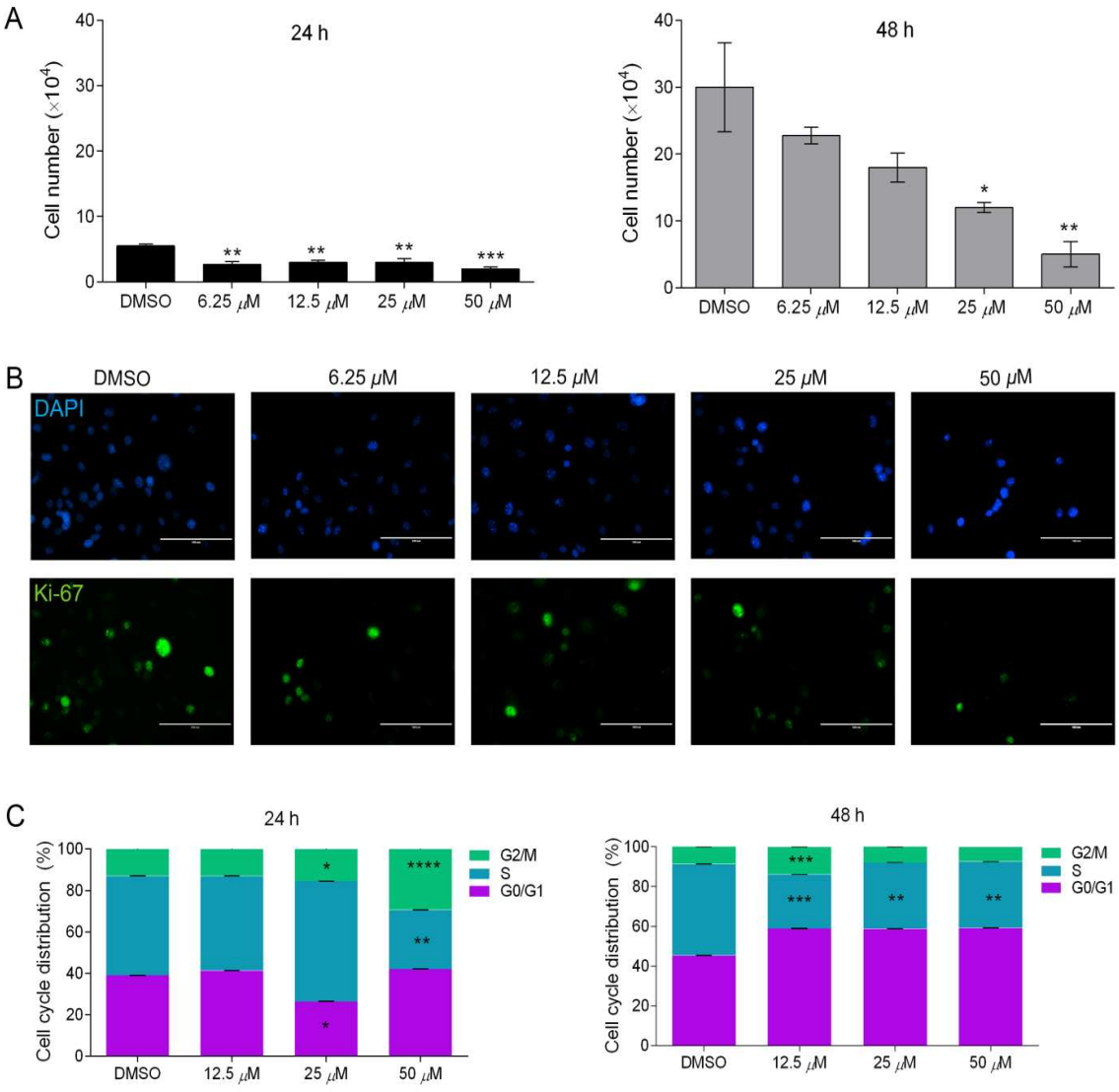

Figure 5 - Effect of compound **3q** on melanoma cell proliferation and cell cycle progression. B16-F10 cells were treated with 6.25, 12.5, 25, and 50 μM of compound **3q**. Cells treated with DMSO 0.4% v/v were used as a control. (A) Cell growth was determined with trypan blue exclusion at 24 and 48 h after incubation. (B) Representative photomicrography of Ki-67 (green) and DAPI (blue) immunolabeling after 24 h of treatment. Scale bars: 100 μM. (C) Cell cycle was evaluated using propidium iodide (PI) fluorochrome and flow cytometry analysis after 24 h and 48 h incubation. Mean ± S.E.M. *p < 0.05, **p < 0.01, ***p < 0.001 and ****p < 0.0001 versus control by One-way ANOVA and Dunnett's post-hoc test.

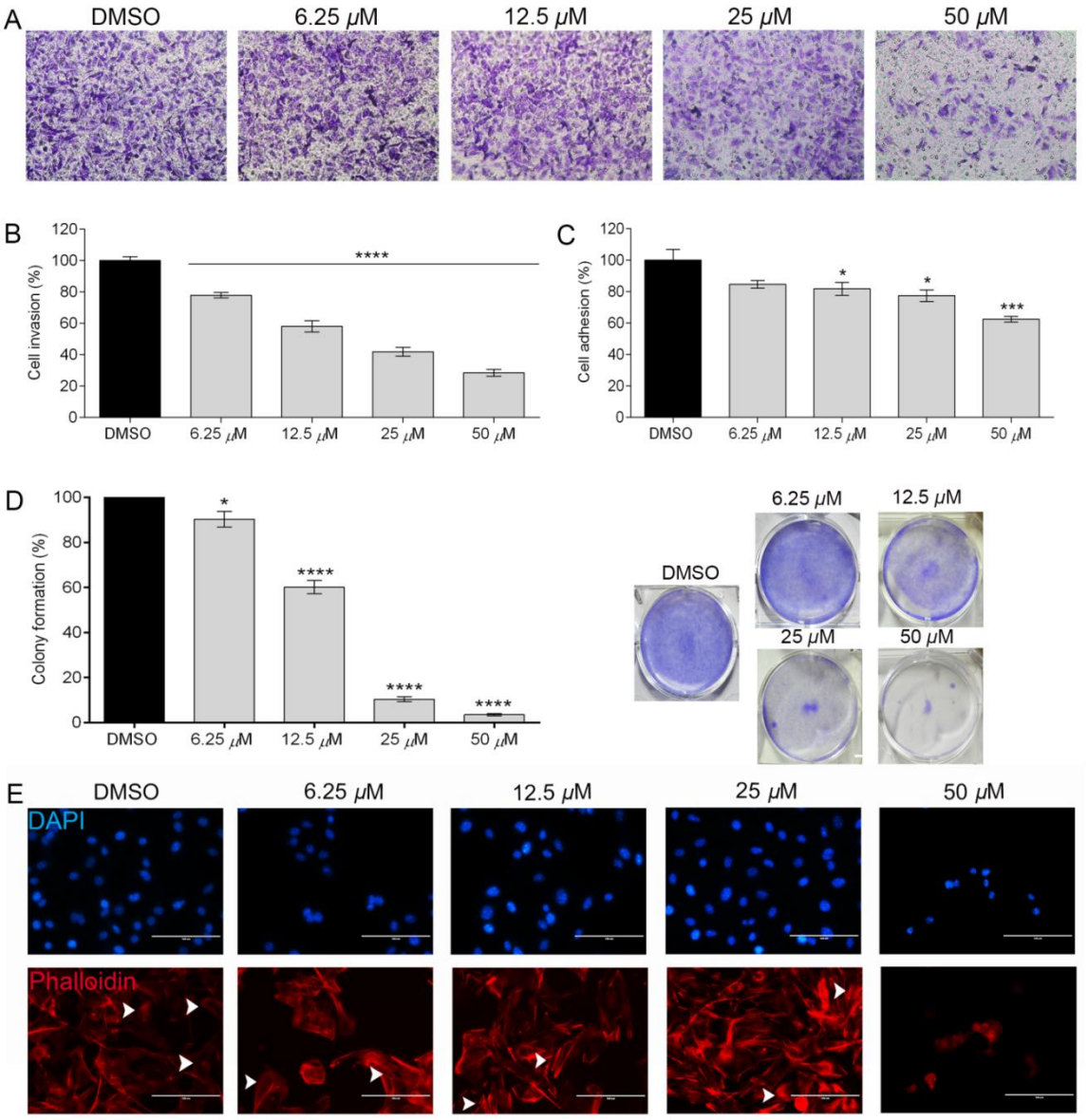

Figure 6 - Effects of compound **3q** on metastatic behavior of B16-F10 cells. (A) Photomicrography represents the cells invasion through matrigel-coated transwell. (B) The bar graph represents the percentage of invasive cell that were treated with 6.25, 12.5, 25, and 50 μM of compound **3q** for 24 h. (C) The bar graph represents the percentage of adhered cell that were treated with 6.25, 12.5, 25, and 50 μM of compound **3q** for 4 h. (D) The bar graph represents the percentage of colony formation after 7 days of assay and the photomicrography represents the formation of B16-F10 colonies after treatment with 6.25, 12.5, 25 and 50 μM of compound **3q**. (E) Photomicrography of Rhodamine Phalloidin staining (red) and DAPI (blue) preparations, evidencing stress fibers (white arrows). The cells were treated for 24 h with increasing concentrations of compound **3q**. Mean ± S.E.M. *$p < 0.05$, ***$p < 0.001$ and ****$p < 0.0001$ versus control by One-way ANOVA and Dunnett's post-hoc test. Scale bars: 100 μM.

4. DISCUSSION

This study aimed to identify the most active compound among seventeen synthesized from *trans*-cinnamic acid, based on its biological activity against melanoma cells. These substances were yielded and submitted to *in vitro* screening assays in which only the compound **3q** was eligible. This selective step is crucial during the early stages of the drug-discovery process, providing pharmacological and toxicological data for understanding drug candidate performance [39]. Moreover, through *in vitro* assays, it is possible to optimize the drug screening and reduce the number of laboratory animals in *in vivo* studies following the 3R's principles [8,40,41]. Compound **3q** was chosen due to its ability to reduce the viability and migration of B16-F10 melanoma cells. This finding is relevant considering the aggressive behavior of B16-F10 cells. B16-F10 cell line is a recognized model for human melanoma and has attractive characteristics for studies focused on antimetastatic agents, such as high metastatic capacity and dose-dependent resistance to chemotherapeutic drugs [1,3,6-8,11,25,42-46]. Moreover, compound **3q** presented low IC_{50} on melanoma cells in comparison to *trans*-cinnamic acid, confirming its ability to inhibit cell viability. Overall, low IC_{50} is associated with a drug with a high inhibitory effect [47]. Meanwhile, compound **3q** did not impair the viability of non-tumorigenic cells (Vero and NIH3T3 cells), demonstrating its selectivity to act on tumor cells only. This behavior is desirable for selecting drug candidates against cancer because they must be safe for illness treatment [48,49].

Herein, *trans*-cinnamic acid showed a non-significant cytotoxic effect on B16-F10 cells, different from previous studies [15,18]. Methodological parameters regarding melanoma cell lineages, IC_{50} value, and cinnamic acid concentration differed between studies. Niero and Machado-Santelli [18], for example, used a human melanoma cell line (HT-144) and a human melanocyte cell line derived from blue nevus (NGM) in their experiments. Liu et al. [15] evaluated the cytotoxic effect of cinnamic acid against the human cell lines MEL 1011, A375, and SKMEL 28. It is known that molecular characteristics of the cell lines, such as genomic and transcriptional profiles, can influence the resistance and susceptibility of cells to an anticancer drug, altering the experimental planning and result interpretation [8,50,51]. Moreover, cinnamic acid was tested here at micromolar concentrations, while other studies [15,18] tested this compound at millimolar concentrations. This difference influences the IC_{50} value that, in turn, defines the concentrations of cinnamic acid to be applied in *in vitro* cell migration, invasion, adhesion, colony formation, proliferation, and cell cycle assays.

The derivative compound **3q** markedly inhibited the migration, invasion, adhesion,

and colonization of B16-F10 melanoma cells. Cell migration, for instance, is a physiological event involved in many biological processes, such as embryo development, tissue formation, immune defense, and cancer metastasis [52]. The ability of tumor cells to migrate within the body comprises one stage of a series of progressive events that characterize the metastatic process, which includes cell detachment, adhesion, colonization, and surveillance [53-55]. Altogether, these steps contribute to the aggressiveness of metastasis with consequent high mortality rates [1,3,8,51]. It is worth mentioning that the inhibition of these events by the compound **3q** did not result from its cytotoxic effect. Otherwise, we used this compound at concentrations lower than its IC_{50} in the *in vitro* assays to maintain the viability of B16-F10 cells and permit their treatment with it for exposure periods between 24 and 48 h. Accordingly, we could verify how the compound **3q** exerted effects on these cells [11,37].

In light of the foregoing, one possible explanation for the antimetastatic activity of compound **3q** was its effect on the actin cytoskeleton. Results from rhodamine phalloidin immunostaining revealed an alteration in the actin arrangement in B16-F10 cells when exposed to compound **3q**, probably by reducing its polymerization. Indeed, actin microfilaments are indispensable for cell locomotion [56]. Studies have reported that cell migration and invasion can be altered by remodeling the actin cytoskeleton [57,58]. Niero and Machado-Santelli [18] observed interference of cinnamic acid on cytoskeleton dynamics by labeling actin with phalloidin. Thus, we may suggest that compound **3q** played a role in actin disarrangement leading to reduced cell migration, invasion, adhesion, and colonization.

Our results showed that compound **3q** triggered apoptosis on B16-F10 melanoma cells at concentrations higher than IC_{50} value, while lower concentrations affected the cell cycle, reducing cell proliferation and metastatic capacity. These data may open novel directions to understand the potential antitumor effect of novel cinnamic acid derivatives and their role in cancer. Natural and synthetic products can affect cancer cell behavior, leading to cell death, inhibition of tumor cell proliferation, and metastasis [59]. Acridine orange and annexin V/PI staining assays were performed to evaluate whether the reduction in cell viability of B16-F10 caused by compound **3q** occurred by apoptosis. These analyses showed low melanoma cell viability via inducing cell death by apoptosis. Importantly, necrotic cells, which is considered a toxic and degradative process of cell death [60], were little noticed in this assay. Once tumor cells typically resist apoptosis-programmed cell death processes [61], apoptosis inducers have been prominent in the discovery of anticancer drugs [62]. Studies have already reported that cinnamic acid and its derivatives can induce the death of tumor cells by apoptosis

[18,32,30,63,64]. Cytoskeletal damage is a characteristic of pre-apoptotic, and here we saw that compound **3q** interfered with cytoskeletal dynamics [18]. Therefore, we may suggest that the alterations caused in the cytoskeleton reflect characteristics of apoptotic processes.

Finally, compound **3q** interfered with B16-F10 cell proliferation. Previous studies showed that compounds derived from cinnamic acid are known to impair melanoma cell proliferation [18,25] and other cell lines, such as leukemia and breast cell lines [30,22,65]. Herein, we observed a reduction in the Ki67-positive cells after exposure to compound **3q** for 24 and 48 h, confirming the results obtained by the trypan blue assay. The cell proliferation marker Ki-67, a nuclear protein, is widely used in cancer diagnosis because its expression is dependent on the phases of the cell cycle [66]. Additionally, we decided to analyze the cell cycle once several cell cycle regulators have emerged as potential therapeutic drugs for cancer treatment [67]. Our results showed that compound **3q** delayed the cell cycle after 24 and 48 h of treatment, causing a decrease in cells in the S phase and, consequently, a reduction in Ki-67 marking. Studies reported that Ki- 67 tends to accumulate in the S phase [68,69]. Sun and Kaufman [70] and Sun et al. [71] found that depletion of Ki-67 retard the entry of the cells in the S phase of the cell cycle. Sova et al. [22] showed that cinnamic acid can interfere with the cell cycle of carcinoma cell lines, indicating that novel cinnamic acid derivatives inhibit cell growth by induction of cell death. Collectively, these findings indicated that compound **3q** impacts the cell cycle of melanoma cell lines and, consequently, cell proliferation. One possible mechanism of compound **3q** may be related to the p53 function. This transcription factor is associated with many stress signals, such as DNA damage and oncogene activation, inducing cell cycle arrest and apoptosis, inhibiting cell proliferation, and causing cell death [72]. Loss or gain of p53 function can directly alter cell migration, promote cancer cell invasion, and regulate integrin expression and activation, interfering in the cell adhesion [73,74]. Moreover, compound **3q** may interfere with the remodeling of the actin cytoskeleton and, consequently, cause changes in cell migration and invasion [57,58]. Therefore, we suggest that our next step should be to study the role of compound **3q** in the expression of transcription factor p53. The success of compound **3q** on the screening assays may be related to the addition of bromine atoms to the double bond of cinnamic acid structure since cinnamic acid is a natural substance with a scaffolded structure [13,14]. The halogens play a role in drug discovery and the design of ligand inhibitors. This fact is because halogen bonds can be introduced into organic compounds to improve their ligand affinities without disrupting other structural interactions [75,76]. Moreover, halogens have been frequently found in the structures of anticancer agents, even for melanoma [77]. Within this context,

compound **3p** was converted into **3q**. The dibrominated compound **3q** showed the lowest IC_{50}. Thus, as the addition of bromine atoms in the double acyclic bond resulted in a significant reduction in cell viability, we may suggest that the presence of the bromine group in novel compounds may be associated with their superior activity [78]. Xu et al. [79] developed a detailed database survey and quantum chemistry calculation concerning halogen bonds (C-X, X = F, Cl, Br, I). This investigation showed that the ratio of heavy organohalogens (Cl, Br, I) to organofluorine increased during drug discovery and development. This fact revealed that more fluorinated leads and candidates are eliminated than other organohalogens, whereas drug discovery and development move on. The halogen bond plays a positive role in tuning ADMET property. Besides, the authors found that 16.6% of halogen bonds are formed between heavy organohalogens and water molecules, apart from 82.4% of halogen bonds formed between heavy organohalogens and biopolymer, such as proteins. Considering that most biopolymers reside in an aqueous environment and a drug may interact with many kinds of biopolymers to exert their therapeutic effects, these 16.6% halogen bonds would play relevant physiological roles. Therefore, it is plausible that the presence of the bromine atoms in the structure of compound **3q** resulted in beneficial effects concerning ADMET properties of compound **3q** and its interactions in an aqueous medium with biological targets.

Considering compounds **3a-3i** with benzylic groups, the modification of introducing only the benzyl group ($C_6H_5CH_2$-) into the cinnamic acid skeleton did not alter the percentage of metabolic active B16-F10 cells (approximately 86% for CA e **3a**). While the percentage of cell viability inhibition for the chlorinated compound **3b** was nearly 17%, this activity corresponded to approximately 30% for the brominated counterpart compound **3d**. In terms of compounds **3c**, **3e**, **3f**, and **3g**, which possess polar groups, the cell viability did not change considerably among them. Comparing the cinnamates **3h** and **3i**, which have aliphatic groups, the presence of the bulkier isopropyl group in the structure was more effective (~ 24%) than the methyl group (~ 7%) in inhibiting cell viability. The compounds **3a** (with a benzyl group) and **3p** (with a phenyl group) differ from each other by one methylene group. Although small, this structural difference between the compounds impacted the percentage of viable cells (~ 13% for the former and ~ 31% for the latter). While compounds **3j** and **3k** differ in terms of the position of the isopropyl and methyl groups, they presented identical effects on B16-F10 cells. Regarding derivatives **3l** and **3m**, which are quite similar in terms of their structures, compound **3l** with the polar group aldehyde was more effective in inhibiting cell viability. The derivatives **3o** and **3p** had similar effects (~ 30% of cell viability inhibition) on B16-F10

cells. Thus, the introduction of an isobenzofuranone functionality was not beneficial regarding the biological response. Finally, the introduction of an alicyclic portion (compound **3m**) into the cinnamic acid skeleton did not interfere with cell viability.

5. CONCLUSIONS

In this study, we evaluated seventeen esters derived from *trans*-cinnamic acid. From these compounds, one presented superior cytotoxicity against the B16-F10 cell line and reduced cell migration, being the derivative compound **3q** the most active. This compound has two bromine atoms attached to the acyclic portion, suggesting that the presence of the bromine atoms may be associated with their superior activity. It is plausible that the presence of the bromine atoms in the structure of compound **3q** resulted in beneficial effects regarding its ADMET properties and its interactions in an aqueous medium with biological targets. At 100 μM concentration, the compound **3q** may trigger apoptosis in melanoma cells. Moreover, low concentrations of this compound affected the cell cycle of the B16-F10 cell line, reducing cell proliferation and its ability to metastasize by migration, invasion, adhesion, and colonization activities. Therefore, this compound may be a candidate for the development of novel antiproliferative and antimetastatic drugs based on cinnamic acid derivatives.

Declaration of Competing Interest

The authors declare that they have no competing interests.

Acknowledgements

This work was supported by the Coordenação de Aperfeiçoamento de Pessoal de Nível Superior (CAPES) [doctor fellowship to JAV], Conselho Nacional de Desenvolvimento Científico e Tecnológico (CNPq; Grant number 485011/2012-3 and 420648/2016-0 to G.C.B., 431330/2018-2 to G.D.A.L., and 420077/2018-9 to M.M.-N.), and Fundação de Amparo à Pesquisa do Estado de Minas Gerais (FAPEMIG; Grant number APQ-01637-13, APQ-02556-15, and RED-00140-16 to G.C.B., and PPM-0621-18 to MMN). The funders were not involved in the study design, collection, analysis or interpretation of data, writing of the report, or in the decision to submit the article for publication.

Supplementary material

Appendix A. Supporting information Supplementary data associated with this article can be found in the online version at doi:10.1016/j.biopha.2022.112689.

6. REFERENCES

[1] Mattia, G., Puglisi, R., Ascione, B., Malorni, W., Carè, A., Matarrese, P., 2018. Cell death-based treatments of melanoma: Conventional treatments and new therapeutic strategies. Cell Death Dis. 9:112, 1-14. https://doi.org/10.1038/s41419-017-0059-7.

[2]American Cancer Society, 2021. Cancer Facts & Figures 2021. https://www.cancer.org/research/cancer-facts-statistics/all-cancer-facts-figures/cancer-facts-figures-2021.html (accessed 26 November 2021).

[3] Atkins, M.B., Curiel-Lewandrowski, C., Fisher, D.E., Swetter, S.M., Tsao, H., Aguirre-Ghiso, J.A., Soengas, M.S., Weeraratna, A.T., Flaherty, K.T., Herlyn, M., Sosman, J.A., Tawbi, H.A., Pavlick, A.C., Cassidy, P.B., Chandra, S., Chapman, P.B., Daud, A., Eroglu, Z., Ferris, L.K., Fox, B.A., Gershenwald, J.E., Gibney, G.T., Grossman, D., Hanks, B.A., Hanniford, D., Hernando, E., Jeter, J.M., Johnson, D.B., Khleif, S.N., Kirkwood, J.M., Sancy, A., 2021. The State of Melanoma: Emergent Challenges and Opportunities. Clin Cancer Res. 27(10), 2678–2697. https://doi.org/doi:10.1158/1078-0432.CCR-20-4092.

[4] Maverakis, E., Cornelius, L.A., Bowen, G.M., Phan, T., Patel, F.B., Fitzmaurice, S., He, Y., Burrall, B., Duong, C., Kloxin, A.M., Sultani, H., Wilken, R., Martinez, S.R., Patel, F., 2015. Metastatic melanoma – A review of current and future treatment. Options Acta Derm. Venereol. 95, 516–524. https://doi.org/10.2340/00015555-2035.

[5] Kumar, S., Weaver, V.M., 2009. Mechanics, malignancy, and metastasis: The force journey of a tumor cell. Cancer Metastasis Rev. 28, 113–127. https://doi.org/10.1007/s10555-008-9173-4.

[6] Bhatia, S., Tykodi, S.S., Thompson, J.A., 2009. Treatment of metastatic melanoma: An overview. Oncology 23, 488–496. PMID: 19544689, PMCID: PMC2737459.

[7] Shaffer, S.M., Dunagin, M.C., Torborg, S.R., Torre, E.A., Emert, B., Krepler, C., Beqiri, M., Sproesser, K., Brafford, P.A., Xiao, M., Eggan, E., Anastopoulos, I.N., Vargas-Garcia, C.A., Singh, A., Nathanson, K.L., Herlyn, M., Raj, A., 2017. Rare cell variability and drug-induced reprogramming as a mode of cancer drug resistance. Nature 546, 431-435. https://doi.org/10.1038/nature22794.

[8] Vale, J.A., Lima, G.D.A., Almeida, A.A., Teixeira, R.R., Neves, M.M., 2020. Melanoma cell lines as a model for high-throughput drug screening, in: Watanabe, H.S. (Ed.), Horizons in cancer research. Nova Science Publishers, Nova York, pp. 85-145.

[9] Chinembiri, T.N., Plessis, L.H., Gerber, M., Hamman, J.H., Plessis, J., 2014. Review of natural compounds for potential skin cancer treatment. Molecules 19, 11679-11721. https://doi.org/10.3390/molecules190811679.

[10] Albuquerque, K.R.S., Pacheco, N.M., Casao, T.R.L., Melo, F.C.S.A., Novaes, R.D., Gonçalves, R.V., 2018. Applicability of plant extracts in preclinical studies of melanoma: A systematic review. Mediators of Inflamm. ID 6797924. https://doi.org/10.1155/2018/6797924.

[11] Almeida, A.A., Lima, G.D.A., Simão, M.V.R.C., Moreira, G.A., Siqueira, R.P., Zanatta, A.C., Vilegas, W., Machado-Neves, M., Bressan, G.C., Leite, J.P.V., 2020. Screening of plants from the Brazilian Atlantic Forest let to identification of Athenaea velutina (Solanacea) as a novel source of antimetastatic agents. Int. J. Exp. Path. 101, 106–121. https://doi.org/10.1111/iep.12351.

[12] Agarwal, G., Carcache, P.J.B., Addo, E.M., Kinghorn, A.D., 2019. Current status and contemporary approaches to the discovery of antitumor agents from higher plants. Biotechnol. Adv. 38, 1–27. https://doi.org/10.1016/j.biotechadv.2019.01.004.

[13] Chavarria, D., Silva, T., Martins, D., Bravo, J., Summavielle, T., Garrido, J., Borges, F., 2015. Exploring cinnamic acid scaffold: Development of promising neuroprotective lipophilic antioxidants. Med. Chem. Comm. 6, 1043-1053. https://doi.org/10.1039/c5md00018a.

[14] Ullah, S., Parka, Y., Ikram, M., Lee, S., Park, C., Kang, D., Yang, J., Akter, J., Yoon, S., Chun, P., Moon, H.R., 2018. Design, synthesis and anti-melanogenic effect of cinnamamide derivatives. Bioorg. Med. Chem. 26(21), 5672-5681. https://doi.org/10.1016/j.bmc.2018.10.014.

[15] Liu, L., Hudgins, W.R., Shack, S., Yin, M.Q., Samid, D., 1995. Cinnamic acid: A natural product with potential use in cancer intervention. Int. J. Cancer. 62, 345-350. https://doi.org/10.1002/ijc.2910620319.

[16] Tawata, S., Taira, S., Kobamoto, N., Zhu, J., Ishihara, M., Toyama, S., 1996. Synthesis and antifungal activity of cinnamic acid esters. Biosci. Biotech. Biochem. 60, 909-910. https://doi.org/10.1271/bbb.60.909.

[17] Ekmekcioglu, C., Feyertag, J., Marktl, W., 1998. Cinnamic acid inhibits proliferation and modulates brush border membrane enzyme activities in Caco-2 cells. Cancer Lett. 128, 137-144. https://doi.org/10.1016/S0304-3835(98)00073-1.

[18] Niero, E.L., Machado-Santelli, G.M., 2013. Cinnamic acid induces apoptotic cell death and cytoskeleton disruption in human melanoma cells. J. Exp. Clin. Cancer Res. 32. https://doi.org/10.1186/1756-9966-32-31.

[19] Orlikova, B., Legrand, N., Panning, J., Dicato, M., Diederich, M., 2014. Anti-inflammatory and anticancer drugs from nature, in: Zappia, V., Panico, S., Russo, G.L., Budillon, A., Della Ragione, F. (Eds.), Adv. Nutr. Cancer. Springer Berlin Heidelberg, Berlin, Heidelberg, pp. 123-143. https://doi.org/10.1007/978-3-642-38007-5_8.

[20] Laverty, G., McCloskey, A.P., Gorman, S.P., Gilmore, B.F., 2015. Anti-biofilm activity of ultrashort cinnamic acid peptide derivatives against medical device-related pathogens. J. Pept. Sci. 21, 770-778. https://doi.org/10.1002/psc.2805.

[21] Rodrigues, M.P., Tomaz, D.C., de Souza, L.A., Onofre, T.S., de Menezes, W.A., Almeida-Silva, J., Suarez-Fontes, A.M., de Almeida, M.R., da Silva, A.M., Bressan, G.C., Vannier-Santos, M.A., Fietto, J.L.R., Teixeira, R.R., 2019. Synthesis of cinnamic acid derivatives and leishmanicidal activity against *Leishmania braziliensis*. Eur. J. Med. Chem. 183, 111688. https://doi.org/10.1016/j.ejmech.2019.111688.

[22] Sova, M., Zizac, Z., Stankovic, J.A.A., Prijatelj, M., Turk, S., Jurani, Z.D., Mlinari -Rascan, I., Gobec, S., 2013. Cinnamic acid derivatives induce cell cycle arrest in carcinoma cell lines. J. Med. Chem. 9, 633-641. https://doi.org/10.2174/1573406411309050002.

[23] Yen, G-C., Chen, Y-L., Sun, F-M., Chiang, Y-L., Lu, S-H., Wenga, C-J., 2011. A comparative study on the effectiveness of *cis*- and *trans*-form of cinnamic acid treatments for inhibiting invasive activity of human lung adenocarcinoma cells. Eur. J. Pharm. Sci. 44, 281–287. https://doi.org/10.1016/j.ejps.2011.08.006.

[24] De, P., Baltas, M., Bedos-Belval, F., 2011. Cinnamic acid derivatives as anticancer agents - A review. Curr Med Chem. 18, 1672-1703. https://doi.org/10.2174/092986711795471347.

[25] Lima, G.D.A., Rodrigues, M.P., Mendes, T.A.O., Moreira, G.A., Siqueira, R.P., da Silva, A.M., Vaz, B.G., Fietto, J.L.R., Bressan, G.C., Machado-Neves, M., Teixeira, R.R., 2018. Synthesis and antimetastatic activity evaluation of cinnamic acid derivatives containing 1,2,3-triazolic portions. Toxicol. *In Vitro*. 53, 1-9. https://doi.org/10.1016/j.tiv.2018.07.015.

[26] Peng, X., Wang, Z., Liu, Y., Peng, X., Liu, Y., Zhu, S., Zhang, Z., Qiu, Y., Jin, M., Wang, R., Zhang, Q., Kong, D., 2017. Oxyfadichalcone C inhibits melanoma A375 cell proliferation and metastasis via suppressing PI3K/Akt and MAPK/ERK pathways. Life Sci. 206, 35-44. https://doi.org/10.1016/j.lfs.2018.05.032.

[27] Ling, Y., Guo, J., Yang, Q., Zhu, P., Miao, J., Gao, W., Peng, Y., Yang, J., Xu, K., Xiong, B., Liu, G., Tao, J., Luo, L., Zhu, Q., Zhang, Y., 2018. Development of novel β-carboline-based hydroxamate derivatives as HDAC inhibitors with antiproliferative and antimetastatic activities in human cancer cells. Eur. J. Med. Chem. 144, 398-409. https://doi.org/10.1016/j.ejmech.2017.12.061.

[28] Ruwizhi, N., Aderibigbe, B.A., 2020. Cinnamic acid derivatives and their biological efficacy. Int. J. Mol. Sci. 21, 5712. https://doi.org/10.3390/ijms21165712.

[29] Pontiki, E., Hadjipavlou-Litina, D., Litinas, K., Geromichalos, G., 2014. Novel cinnamic acid derivatives as antioxidant and anticancer agents: Design, synthesis and modeling studies. Molecules 19, 9655-9674. https://doi.org/10.3390/molecules19079655.

[30] Reddy, N.D., Shoja, M.H., Biswas, S., Nayak, P.G., Kumar, N., Rao, C.M., 2016. An appraisal of cinnamyl sulfonamide hydroxamate derivatives (HDAC inhibitors) for anti-cancer, anti-angiogenic and anti-metastatic activities in human cancer cells. Chemo-Bio Interact. 253,112-124. https://doi.org/10.1016/j.cbi.2016.05.008.

[31] Sinka, I., Kiss, A., Mernyák, E., Wölfling, J., Schneider, G., Ocsovszki, I., Kuo, C.Y., Wang, H., Zupkó, I., 2018. Antiproliferative and antimetastatic properties of 3-benzyloxy-16-hydroxymethylene-estradiol analogs against breast cancer cell lines. Eur. J. Pharm. Sci. 123, 362–370. https://doi.org/10.1016/j.ejps.2018.07.029.

[32] Qi, G., Chen, J., Shi, C., Wang, Y., Mi, S., Shao, W., Yu, X., Ma, Y., Ling, J., Huang, J., 2016. Cinnamic acid (CINN) induces apoptosis and proliferation in human nasopharyngeal carcinoma cells. Cell. Physiol. Biochem. 40, 589-596. https://doi.org/10.1159/000452572.

[33] Tsai, C.M., Yen, G.C., Sun, F.M., Yang, S.F., Weng, C.J., 2013. Assessment of the anti-invasion potential and mechanism of select cinnamic acid derivatives on human lung adenocarcinoma cells. Mol. Pharm.10, 1890-1900. https://dx.doi.org/10.1021/mp3006648.

[34] Rathee, D., Lather, V., Grewal, A.S., Dureja, H., 2018. Targeting matrix metalloproteinases with novel diazepine substituted cinnamic acid derivatives: Design, synthesis, *in vitro* and *in silico* studies. Chem. Cent. J. 12. https://doi.org/10.1186/s13065-018-0411-8.

[35] Anantharaju, P.G., Reddy, D.B., Padukudru, M.A., Chitturi, CH.M.K., Vimalambike, M.G., Madhunapantula, S.V., 2017. Induction of colon and cervical cancer cell death by cinnamic acid derivatives is mediated through the inhibition of Histone Deacetylases (HDAC). PLoS ONE 12, e0186208. https://doi.org/10.1371/journal.pone.0186208.

[36] Siqueira, R.P., Barbosa, E.A.A., Polêto, M.D., Righetto, G.L., Seraphim, T.V., Salgado, R.L., Ferreira, J.G., Barros, M.V.A., de Oliveira, L.L., Laranjeira, A.B.A., Almeida, M.R., Júnior, A.S., Fietto, J.L.R., Kobarg, J., de Oliveira, E.B., Teixeira, R.R., Borges, J.C., Yunes, J.A., Bressan, G.C., 2015. Potential antileukemia effect and structural analyses of SRPK inhibition by N-(2-(Piperidin-1-yl)-5-(Trifluoromethyl)Phenyl) Isonicotinamide (SRPIN340). PLoS ONE 10, e0134882. https://doi.org/10.1371/journal.pone.0134882.

[37] Marvibaigi, M., Amini, N., Supriyanto, E., Majid, F.A.A., Jaganathan, S.K., Jamil, S., Almaki, J.H., Nasiri, R., 2016. Antioxidant activity and ROS-dependent apoptotic effect of *Scurrula ferruginea* (Jack) danser methanol extract in human breast cancer cell MDA-MB-231. PLoS ONE 11, e0158942. https://doi.org/10.1371/journal.pone.0158942.

[38] Sova, M., Perdih, A., Kotnik, M., Kristan, K., Rižner, T.L., Solmajer, T., Gobec, S., 2006. Flavonoids and cinnamic acid esters as inhibitors of fungal 17β-hydroxysteroid dehydrogenase: A synthesis QSAR and modelling study. Bioorganic Med. Chem. 14, 7404–7418. https://doi.org/10.1016/j.bmc.2006.07.027.

[39] Dorato, M.A., Buckley, L.A., 2007. Toxicology testing in drug Discovery and development. Current protocols in toxicology, John Wiley & Sons, Inc. https://doi.org/10.1002/0471141755.tx1901s31.

[40] Michelini, E., Cevenini, L., Mezzanotte, L., Coppa, A., Roda, A., 2010. Cell-based assays; fuelling drug discovery. Anal. Bioanal. Chem. 398, 227-238. https://doi.org/10.1007/s00216-010-3933-z.

[41] Tannenbaum, J., Bennett, B., 2015. Russel and Burch's 3Rs then and now: the need for clarity in definition and purpose. J. Am. Assoc. Lab. Animal Sci. 54, 120-132.

[42] Cillo, C., Dick, J.E., Ling, V., Hill, R.P., 1987. Gnereation of drug-resistant variants in metastatic B16 mouse melanoma cell lines. Cancer Res. 47, 2604-2608.

[43] Overwijk, W.W., Restifo, N.P., 2001. B16 as a mouse model for human melanoma. Curr. Protoc. Immunol. Chapter 20:Unit 20.1. https://doi.org/10.1002/0471142735.im2001s39.

[44] Moreira, G.A., Lima, G.D.A., Siqueira, R.P., Barros, M.V.A., Adjanohoun, A.L.M., Santos, V.C., Barbosa, E.A.A., Loterio, R.K., Paiva, J.C., Gonçalves, V.H.S., Viol, L.C.S., Silva, E.A.M., Júnior, A.S., Almeida, M.R., Fietto, J.L.R., Machado-Neves, M., Ferreira, R.S., Teixeira, R.R., Bressan, G.C., 2018. Antimetastatic effect of the pharmacological inhibition of serine/arginine-rich protein kinases (SRPK) in murine melanoma. Toxicol. Appl. Pharmacol. 356, 214-223. https://doi.org/10.1016/j.taap.2018.08.012.

[45] Almeida, A.A., Lima, G.D.A., Eiterer, M., Rodrigues, L.A., Vale, J.A., Zanatta, A.C., Bressan, G.C., Oliveira, L.L., Leite, J.P.V., 2021. A Withanolide-rich fraction of Athenaea velutina induces apoptosis and cell cycle arrest in melanoma B16F10 cells. Plant Med. 1-12. https://doi.org/10.1055/a-1395-9046.

[46] Santos, F.S., Vale, J.A., Santos, L.S., Gontijo, T.B., Lima, G.D.A., Oliveira, L.L., Machado-Neves, M., Teixeira, R.R., Freitas, R.P., 2021. J. Braz. Chem. Soc. 32(12), 2174-2185. https://dx.doi.org/10.21577/0103-5053.20210109.

[47] Berrouet, C., Dorilas, N., Rejniak, K.A., Tuncer, N., 2020. Comparison of drug inhibitory effects (IC_{50}) in monolayer and spheroid cultures. Bull. Math. Biol. 82, 68. https://doi.org/10.1007/s11538-020-00746-7.

[48] Sheng, L., Yang, Y., Zhang, Y., Li, N., 2019. Chemical constituents of *Patrinia heterophylla* Bunge and selective cytotoxicity against six human tumor cells. J. Ethnopharmacol. 236, 129–135. https://doi.org/10.1016/j.jep.2019.03.005.

[49] Tosun, F., Beutler, J.A., Ransom, T.T., Miski, M., 2019. Anatolicin, a highly potent and selective cytotoxic sesquiterpene coumarin from the root extract of *Heptaptera anatolica*. Molecules 24, 1153. https://doi.org/10.3390/molecules24061153.

[50] Vicent, K.M., Postovit, L-M., 2017. Investigating the utility of human melanoma cell lines as tumour models. Oncotarget 8, 10498-10509. https://doi.org/10.18632/oncotarget.14443.

[51] Couto, G.K., Segatto, N.V., Oliveira, T.L., Seixas, F.K., Schachtschneider, K.M., Collares, T., 2019. The Melding of Drug Screening Platforms for Melanoma. Front. Oncol. 9, 512. https://doi.org/10.3389/fonc.2019.00512.

[52] Pijuan, J., Barceló, C., Moreno, D.F., Maiques, O., Sisó, P., Marti, R.M., Macià, A., Panosa, A., 2019. *In vitro* cell migration, invasion, and adhesion assays: from cell imaging to data analysis. Front. Cell. Dev. Biol., 7, 1-16. https://doi.org/10.3389/fcell.2019.00107.

[53] Gray-Schopfer, V., Wellbrock, C., Marais, R., 2007. Melanoma biology and new targeted therapy. Nature 445, 851-857. https://doi.org/10.1038/nature05661.

[54] Schroeder, A., Heller, D.A., Winslow, M.M., Dahlman, J.E., Pratt, G.W., Langer, R., Jacks, T., Anderson, D.G., 2012. Treating metastatic cancer with nanotechnology. Nat. Rev. Cancer. 12, 39-50. https://doi.org/10.1038/nrc3180.

[55] Anderson, R.L., Balasas, T., Callaghan, J., Coombes, R.C., Evans, J., Hall, J.A., Kinrade, S., Jones, D., Jones, P.S., Jones, R., Marshall, J.F., Panico, M.B., Shaw, J.A., Steeg, P.S., Sullivan, M., Tong, W., Westwell, A.D., Ritchie, J.W.A., 2019. A framework for the development of effective anti-metastatic agentes. Nat. Rev. 16, 185-204. https://doi.org/10.1038/s41571-018-0134-8.

[56] Yamazaki, D., Kurisu, S., Takenawa, T., 2005. Regulation of cancer cell motility through actin reorganization. Cancer Sci. 96, 379–386. https://doi.org/10.1111/j.1349-7006.2005.00062.x.

[57] Yamaguchi, H., Condeelis, J., 2007. Regulation of the actin cytoskeleton in cancer cell migration and invasion. Biochim. et Biophys. Acta. 1773, 642–652. https://doi.org/10.1016/j.bbamcr.2006.07.001.

[58] Nersesian, S., Williams, R., Newsted, D., Shah, K., Young, S., Evans, P.A., Allingham, J.S., Craig, A.W., 2018. Effects of modulating actin dynamics on HER2 cancer cell motility and metastasis. Sci. Rep. 8, 17243. https://doi.org/10.1038/s41598-018-35284-9.

[59] Chen, H., Liu, R.H., 2018. Potential mechanisms of action of dietary phytochemicals for cancer prevention by targeting cellular signaling transduction pathways. J Agric Food Chem. 66(13), 3260-3276. https://doi.org/10.1021/acs.jafc.7b04975.

[60] Elmore, S., 2007. Apoptosis: A review of programmed cell death. Toxicol. Pathol. 35, 495-516. https://doi.org/10.1080/01926230701320337.

[61] Hanahan, D., Weinberg, R.A., 2011. Hallmarks of cancer: the next generation. Cell 144, 646-674. https://doi.org/10.1016/j.cell.2011.02.013.

[62] Llanos, G.G., Araujo, L.M., Jiménez, I.A., Moujir, L.M., Rodríguez, J., Jiménez, C., Bazzocchi, I.L., 2017. Structure-based design, synthesis, and biological evaluation of withaferin A-analogues as potent apoptotic inducers. Eur. J. Med. Chem. 140, 52-64. http://dx.doi.org/10.1016/j.ejmech.2017.09.004.

[63] Sadeghi, S., Davoodvandi, A., Pourhanifeh, M.H., Sharifi, N., ArefNezhad, R., Sahebnasagh, R., Moghadam, S.A., Sahebkar, A., Mirzaei, H., 2019. Anti-cancer effects of cinnamon: Insights into its apoptosis effects. Eur. J. Med. Chem. 178, 131-140. https://doi.org/10.1016/j.ejmech.2019.05.067.

[64] Ruwizhi, N., Aderibigbe, B.A., 2020. Cinnamic acid derivatives and their biological efficacy. Int. J. Mol. Sci. 21, 5712. https://doi.org/10.3390/ijms21165712.

[65] Hunke, M., Martinez, W., Kashyap, A., Bokoskie, T., Pattabiraman, M., Chandra, S., 2018. Antineoplastic actions of cinnamic acids and their dimers in breast cancer cells: A comparative study. Anticancer Res. 8, 4469-4474. https://doi.org/10.21873/anticanres.12749.

[66] Chierico, L., Rizzello, L., Guan, L., Joseph, A.S., Lewis, A., Battaglia, G., 2017. The role of the two splice variants and extranuclear pathway on Ki-67 regulation in non-cancer and cancer cells. PloS ONE 12, e0171815. https://doi.org/10.1371/journal.pone.0171815.

[67] Bai, J., Li, Y., Zhang, G., 2017. Cell cycle regulation and anticancer drug discovery. Cancer Biol. Med. 14, 348-362. https://doi.org/10.20892/j.issn.2095-3941.2017.0033.

[68] Miller, I., Min, M., Yang, C., Tian, C., Gookin, S., Carter, D., Spence, S.L., 2018. Ki67 is a graded rather than a binary marker of proliferation versus quiescence. Cell Rep. 24, 1105–1112. https://doi.org/10.1016/j.celrep.2018.06.110.

[69] Sobecki, M., Mrouj, K., Colinge, J., Gerbe, F., Jay, P., Krasinska, L., Dulic, V., Fisher, D., 2017. Cell-cycle regulation accounts for variability in Ki-67 expression levels. Cancer Res. 77, 2722-2734. https://doi.org/10.1158/0008-5472.CAN-16-0707.

[70] Sun, X., Kaufman, P.D., 2018. Ki-67: more than a proliferation marker. Chromosoma 127, 175–186. https://doi.org/10.1007/s00412-018-0659-8.

[71] Sun, X., Bizhanova, A., Matheson, T.D., Yu, J., Zhu, L.J., Kaufman, P.D., 2017. Ki-67 contributes to normal cell cycle progression and inactive X heterochromatin in p21 checkpoint-proficient human cells. Mol. Cell. Biol. 37, e00569-16. https://doi.org/10.1128/MCB.00569-16.

[72] Chen, J., 2016. The cell-cycle arrest and apoptotic functions of p53 in tumor initiation and progression. Cold Spring Harb. Perspect. Med. 6, a026104. https://doi.org/10.1101/cshperspect.a026104.

[73] Araki, K., Ebata, T., Guo, A.K., Tobiume, K., Wolf, S.J., Kawauchi, K., 2015. p53 regulates cytoskeleton remodeling to suppress tumor progression. Cell. Mol. Life Sci. 72, 4077–4094. https://doi.org/10.1007/s00018-015-1989-9.

[74] Ebata, T., Hirata, H., Kawauchi, K., 2016. Functions of the tumor suppressors p53 and Rb in actin cytoskeleton remodeling. BioMed Res. Int. 9231057. http://dx.doi.org/10.1155/2016/9231057.

[75] Voth, A.R., Khuu, P., Oishi, K., Ho, P.S., 2009. Halogen bonds as orthogonal molecular interactions to hydrogen bonds. Nat. Chem. 1, 74–79. https://doi.org/10.1038/nchem.112.

[76] Wilcken, R., Zimmermann, M.O., Lange, A., Joerger, A.C., Boeckler, F.M., 2013. Principles and applications of halogen bonding in medicinal chemistry and chemical biology. J Med Chem. 56(4), 1363-88. https://doi.org/10.1021/jm3012068.

[77] Valko-Rokytovska, M., Bruchata, K., Simkova, J., Milkovicova, M., Kostecka, Z., 2016. Current trends in the treatment of malignant melanoma. Neoplasma 63, 333-341. https://doi.org/10.4149/301_151015N533.

[78] Chung, P.Y., Lam, P.L., Zhou, Y., Gasparello, J., Finotti, A., Chilin, A., Marzaro, G., Gambari, R., Bian, Z., Kwok, W.M., Wong, W.Y., Wang, X., Lam, A.K-Y., Chan, A.S-C., Ma, J.Y.W., Chui, C.H., Lam, K.H., Tang, J.C.O., 2018. Targeting DNA binding for NF-

κB as an anticancer approach in hepatocellular carcinoma. Cells 7, 177. https://doi.org/10.3390/cells7100177.

[79] Xu, Z., Yang, Z., Liu, Y., Lu, Y., Chen, K., Zhu, W., 2014. Halogen bond: its role beyond drug-target binding affinity for drug discovery and development. J Chem Inf Model. 54(1), 69-78. https://doi.org/10.1021/ci400539q.

SUPPLEMENTARY MATERIAL

SPECTROSCOPIC DATA

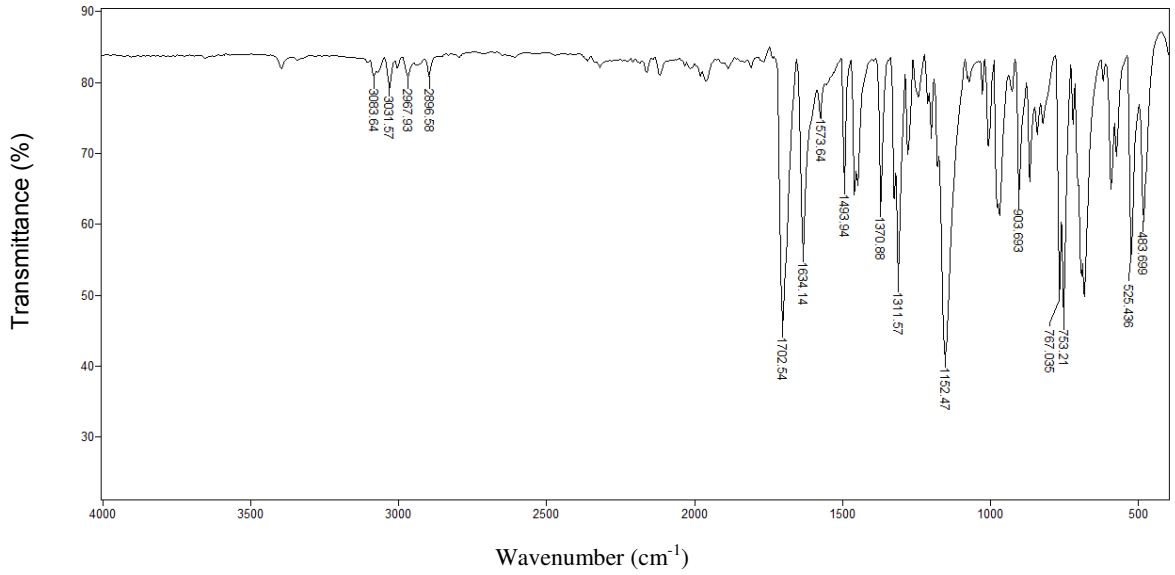

Figure S1 - IR spectrum (ATR) of benzyl cinnamate (**3a**).

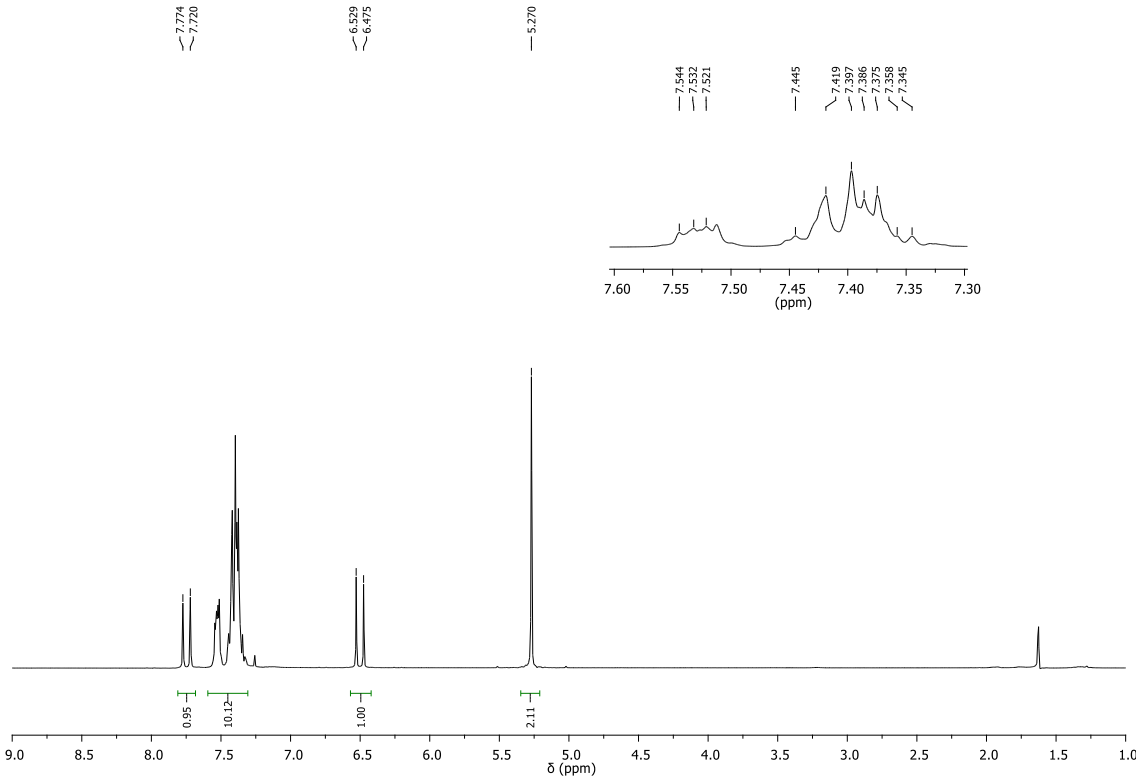

Figure S2 - ^{1}H NMR spectrum (300 MHz, $CDCl_3$) of benzyl cinnamate (**3a**).

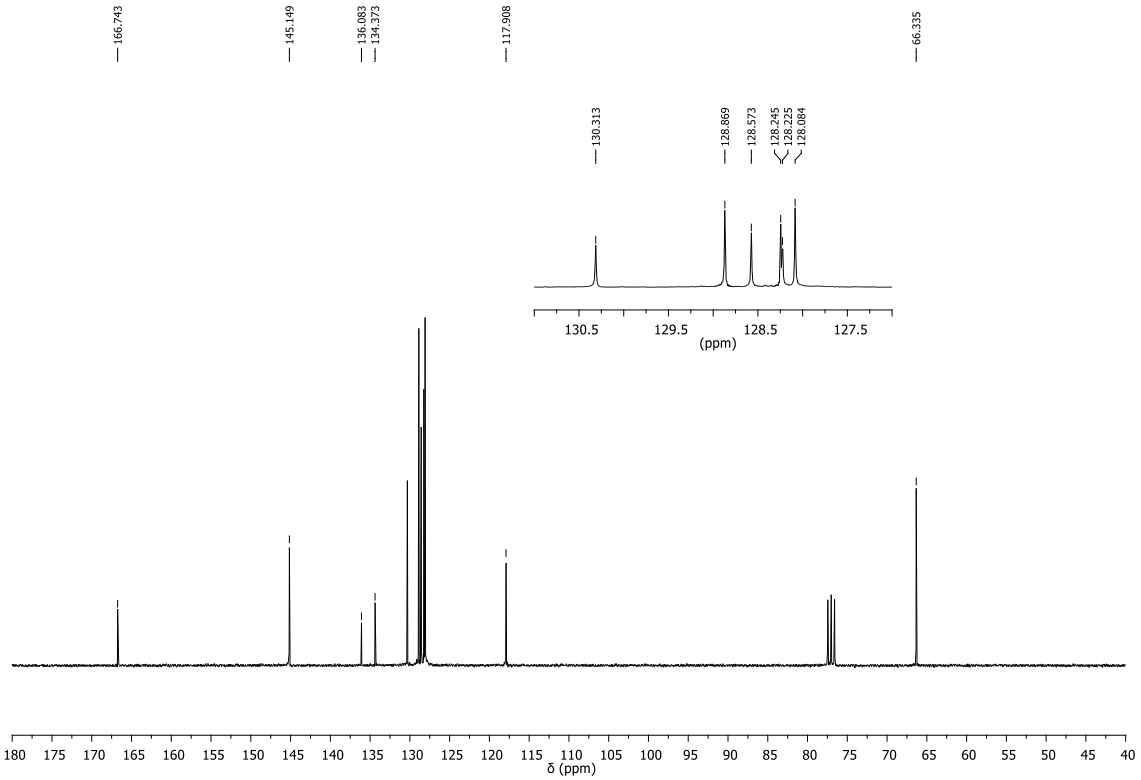

Figure S3 - ^{13}C NMR spectrum (75 MHz, $CDCl_3$) of benzyl cinnamate (**3a**).

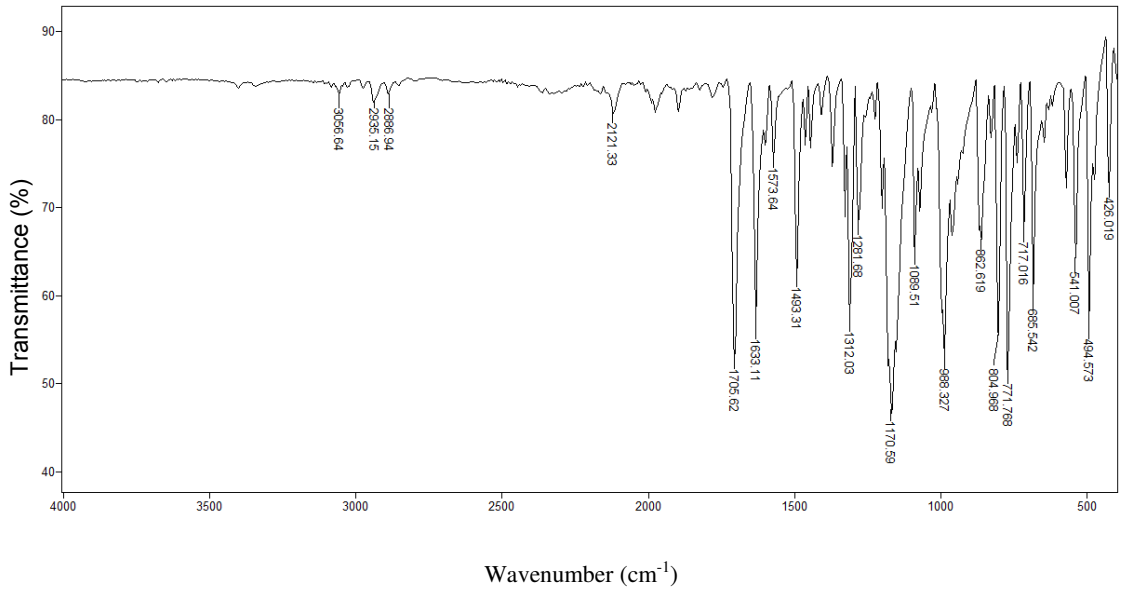

Figure S4 - IR spectrum (ATR) of 4-chlorobenzyl cinnamate (**3b**).

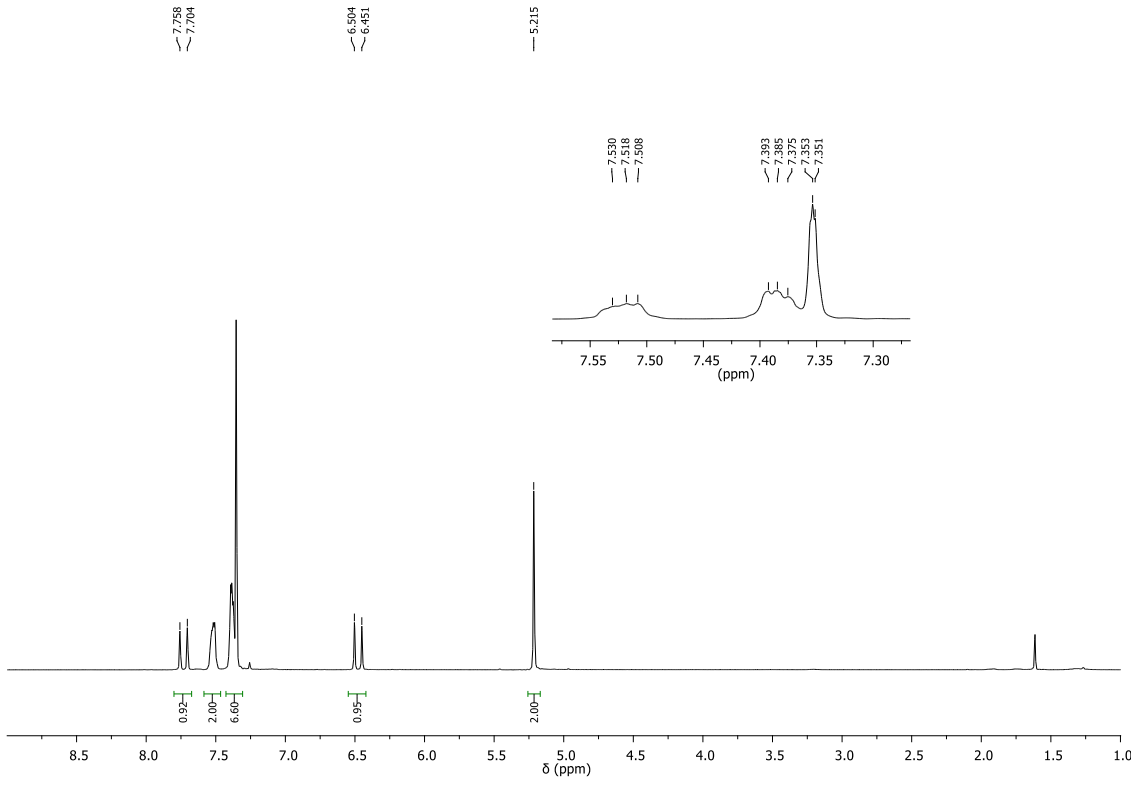

Figure S5 - ^{1}H NMR spectrum (300 MHz, $CDCl_3$) of 4-chlorobenzyl cinnamate (**3b**).

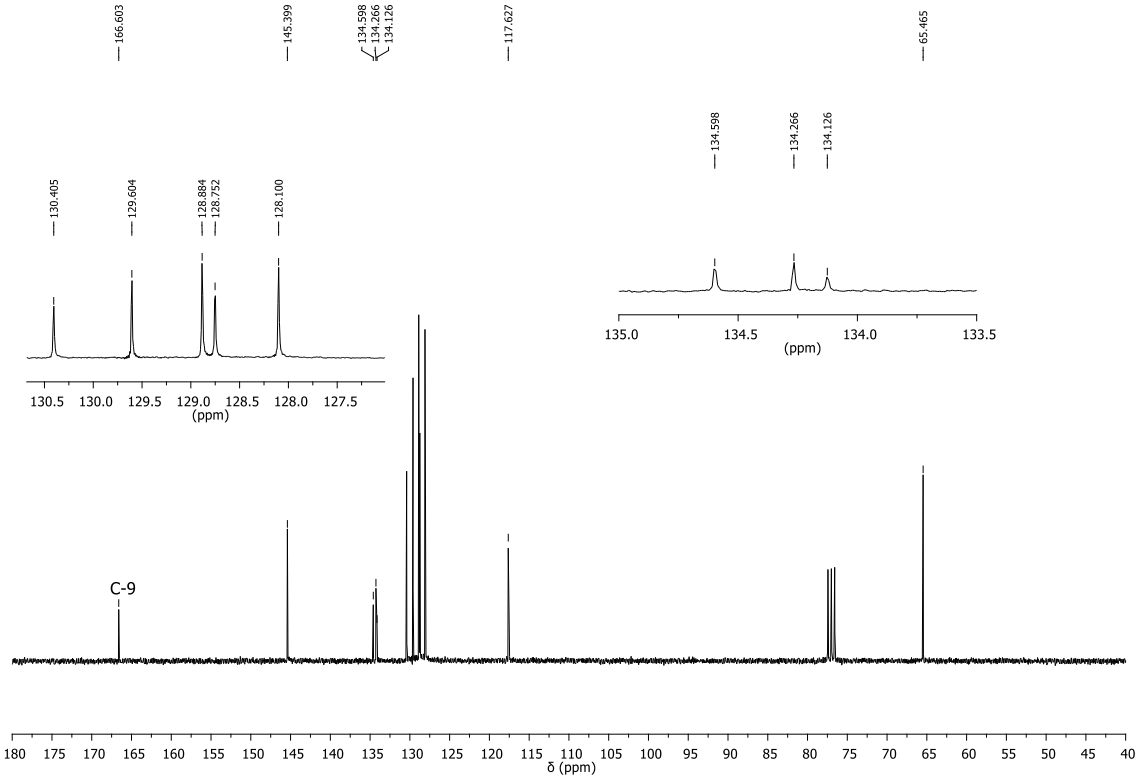

Figure S6 - ^{13}C NMR spectrum (75 MHz, $CDCl_3$) of 4-chlorobenzyl cinnamate (**3b**).

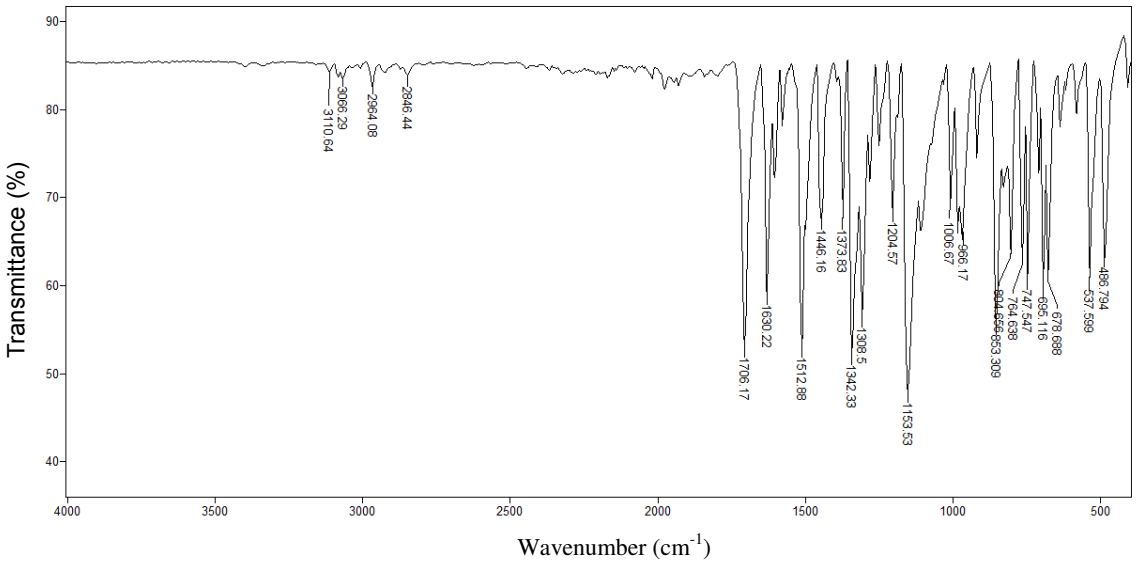

Figure S7 - IR spectrum (ATR) of 4-nitrobenzyl cinnamate (**3c**).

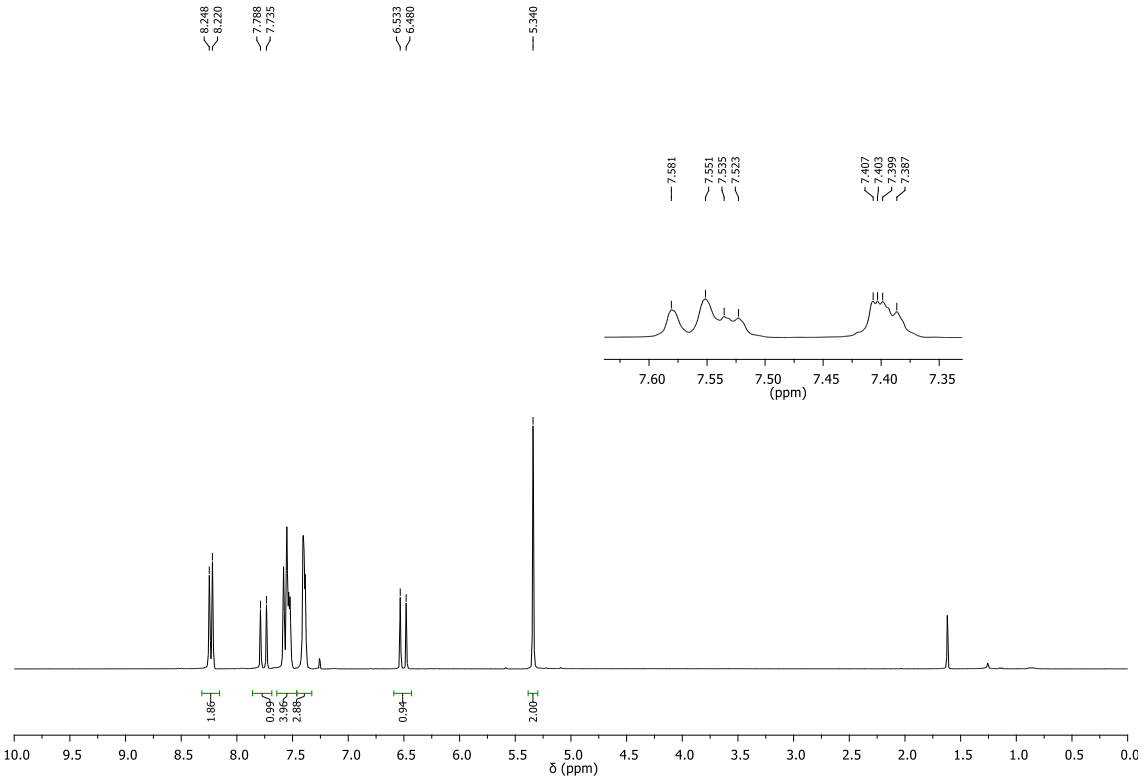

Figure S8 - ^{1}H NMR spectrum (300 MHz, $CDCl_3$) of 4-nitrobenzyl cinnamate (**3c**).

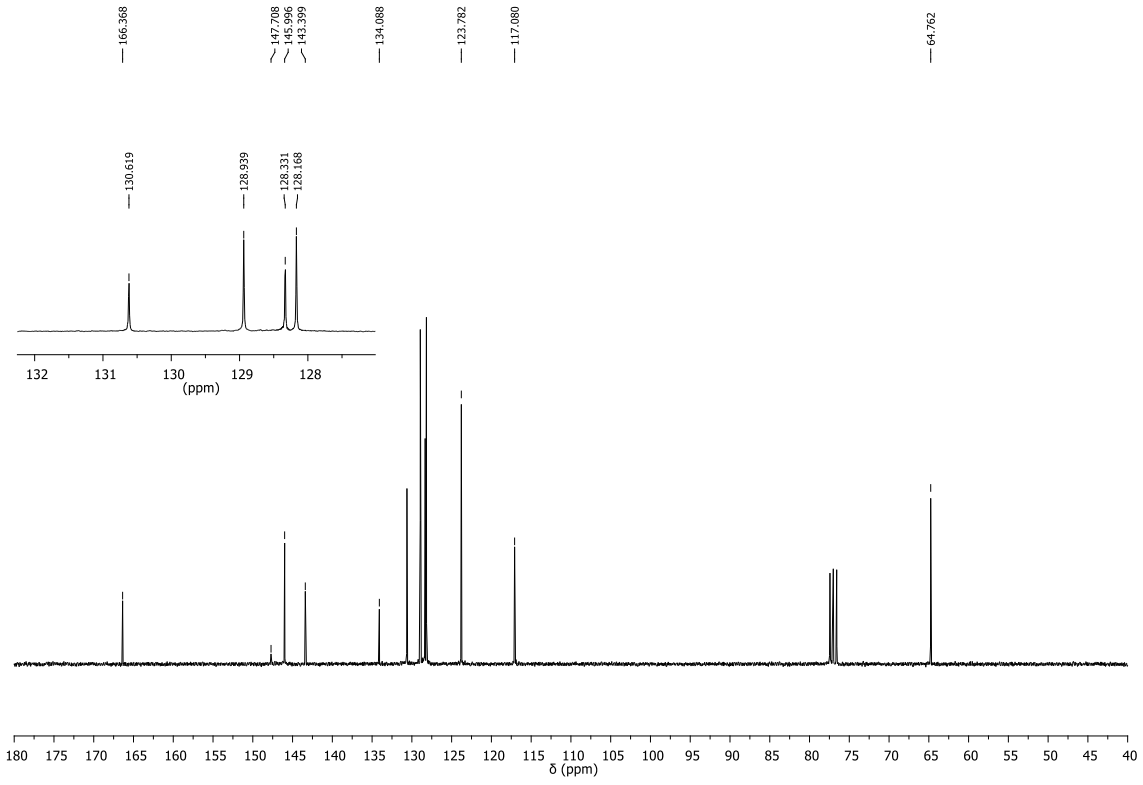

Figure S9 - ^{13}C NMR spectrum (75 MHz, $CDCl_3$) of 4-nitrobenzyl cinnamate (**3c**).

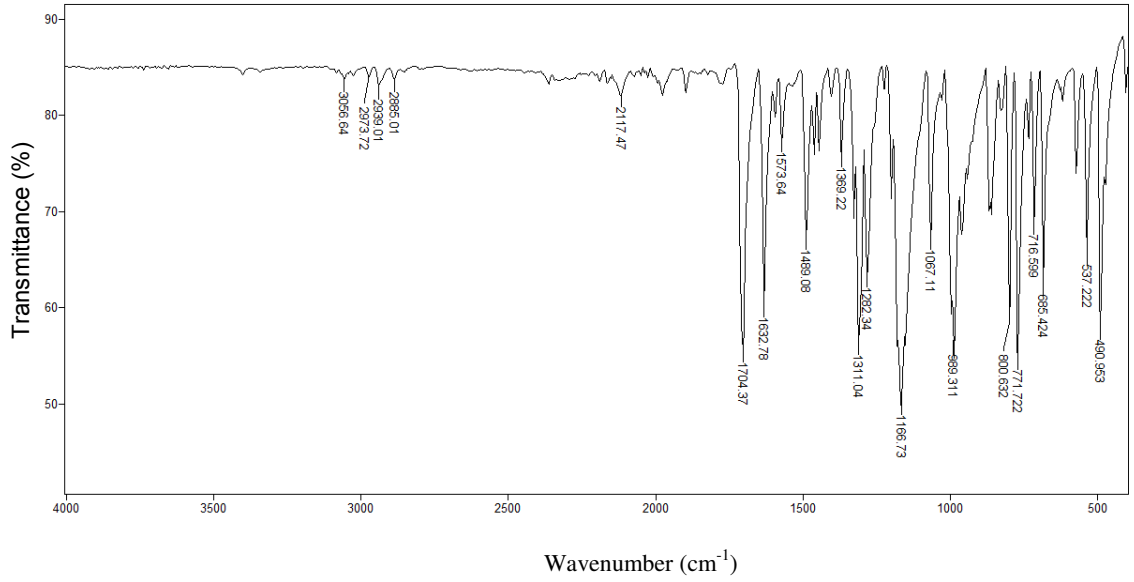

Figure S10 - IR spectrum (ATR) of 4-bromobenzyl cinnamate (**3d**).

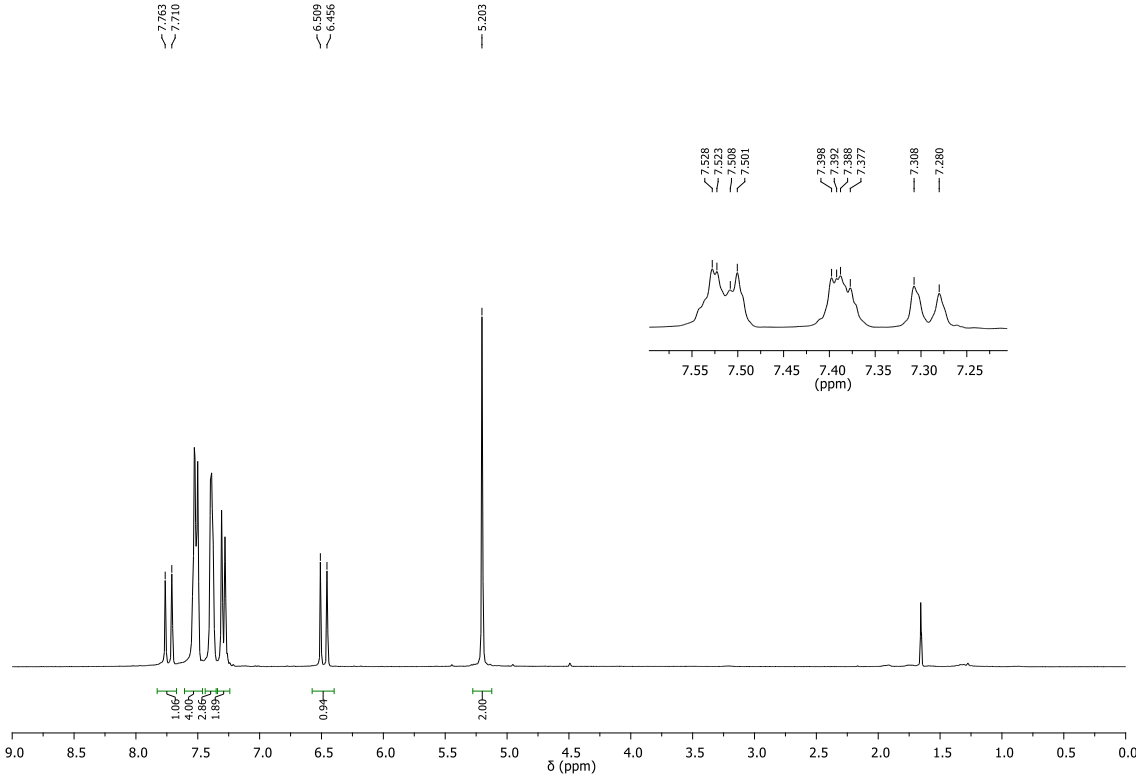

Figure S11 - ^{1}H NMR spectrum (300 MHz, $CDCl_3$) of 4-bromobenzyl cinnamate (**3d**).

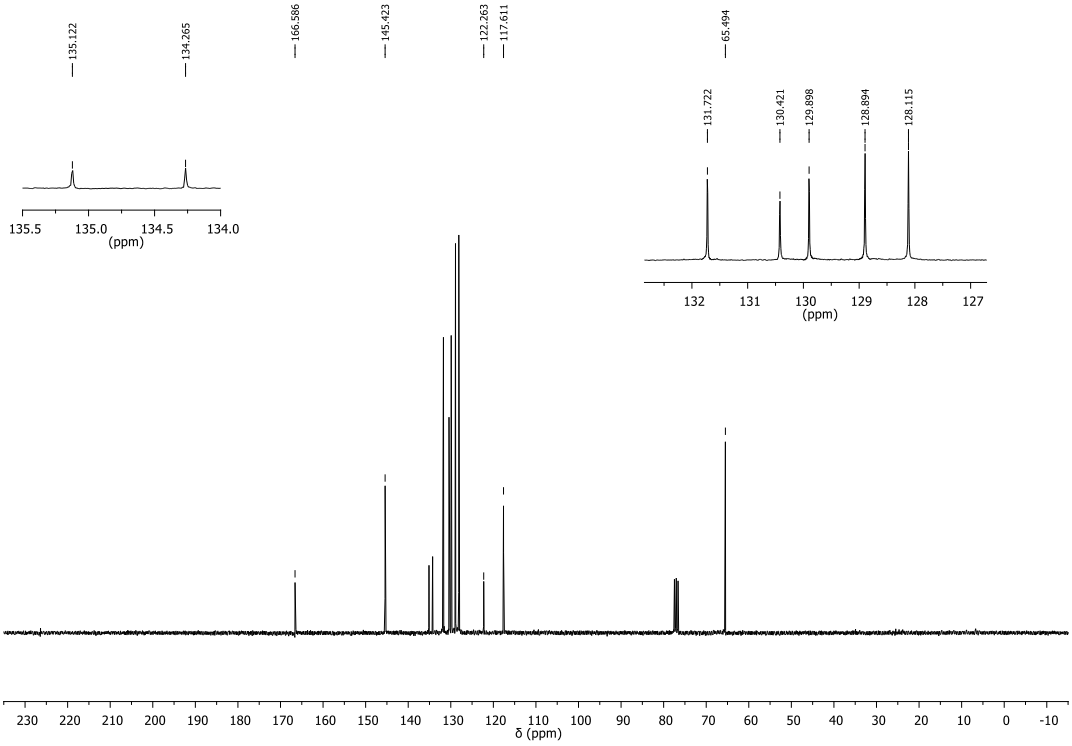

Figure S12 - ^{13}C NMR spectrum (75 MHz, $CDCl_3$) of 4-bromobenzyl cinnamate (**3d**).

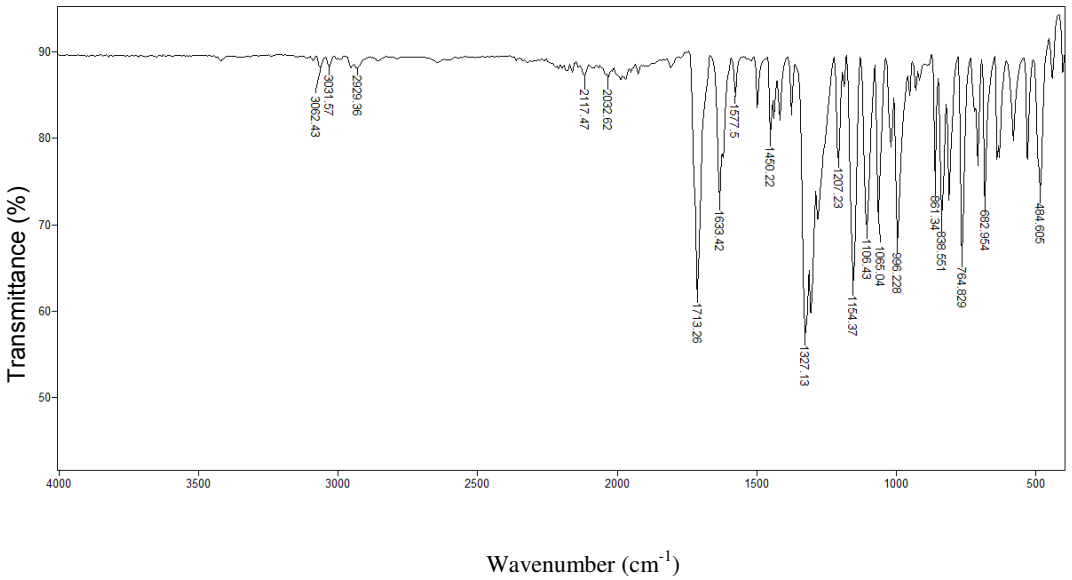

Figure S13 - IR spectrum (ATR) of 4-(trifluoromethyl)benzyl cinnamate (**3e**).

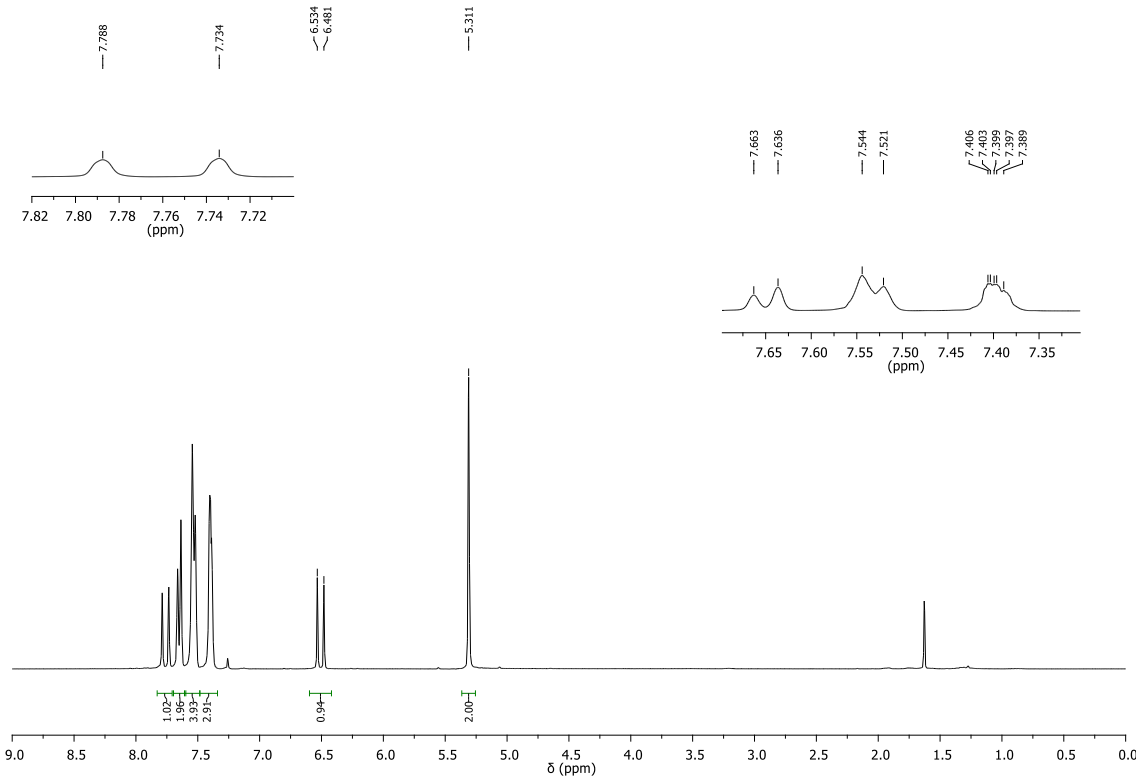

Figure S14 - ^{1}H NMR spectrum (300 MHz, $CDCl_3$) of 4-(trifluoromethyl)benzyl cinnamate (**3e**).

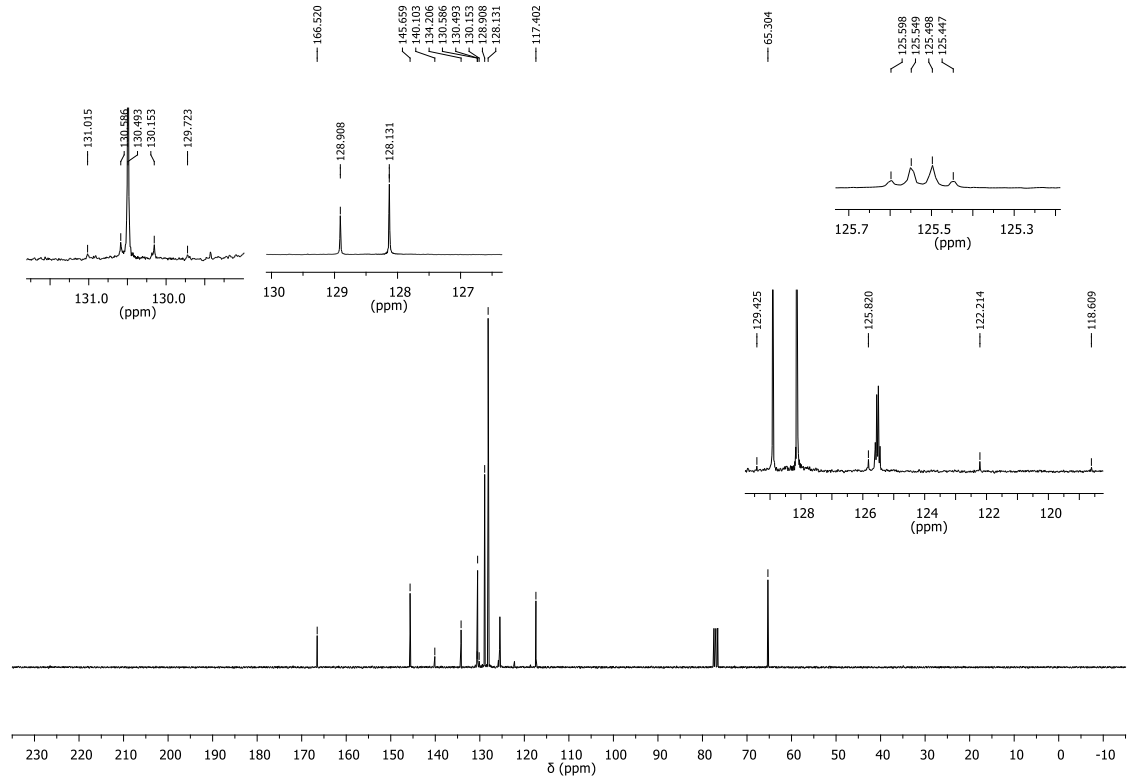

Figure S15 - ^{13}C NMR spectrum (75 MHz, $CDCl_3$) of 4-(trifluoromethyl)benzyl cinnamate (**3e**).

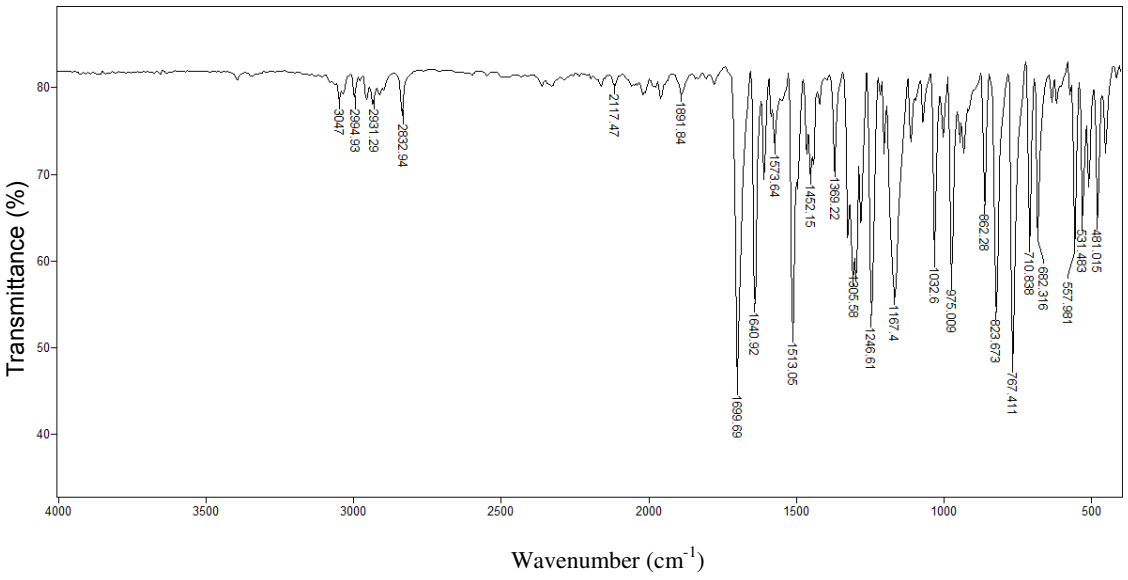

Figure S16 - IR spectrum (ATR) of 4-methoxybenzyl cinnamate (**3f**).

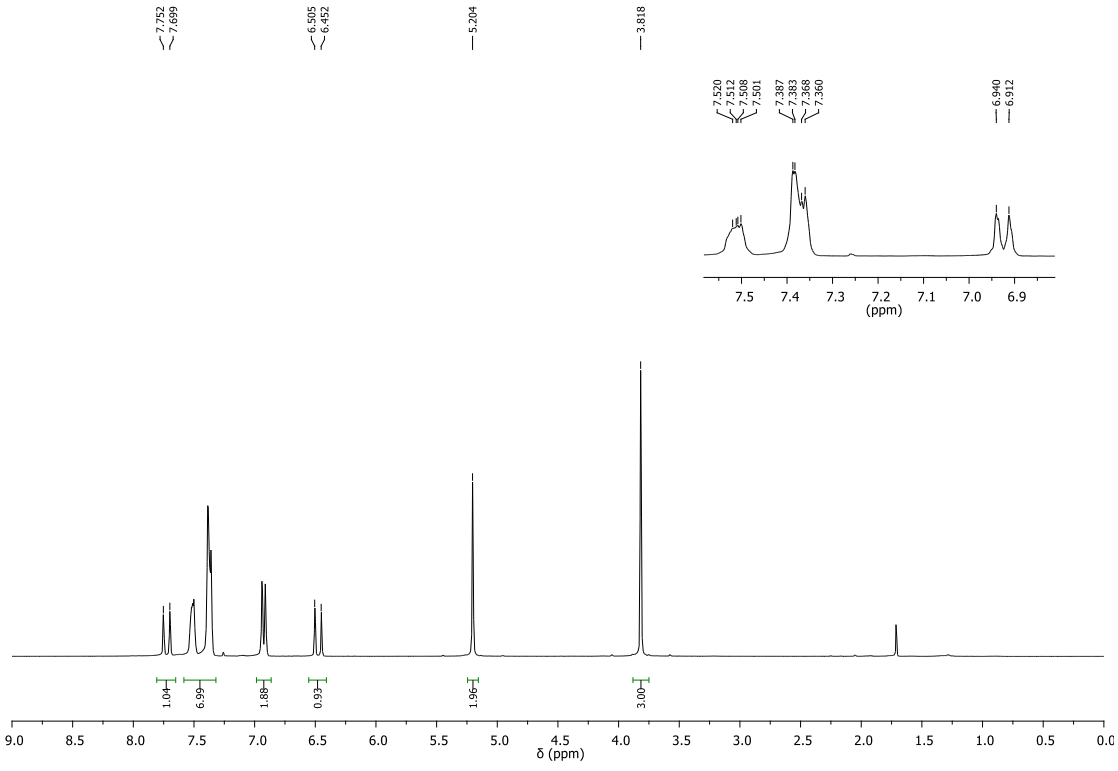

Figure S17 - ^{1}H NMR spectrum (300 MHz, $CDCl_3$) of 4-methoxybenzyl cinnamate (**3f**).

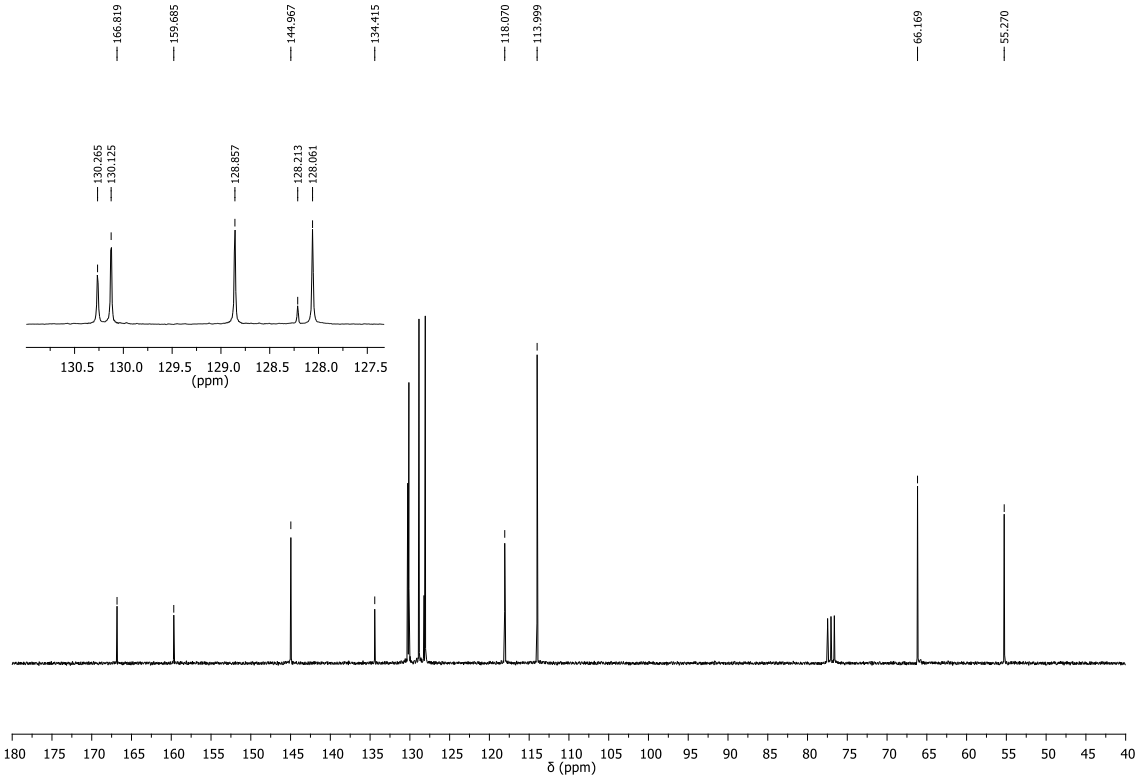

Figure S18 - ^{13}C NMR spectrum (75 MHz, $CDCl_3$) of 4-methoxybenzyl cinnamate (**3f**).

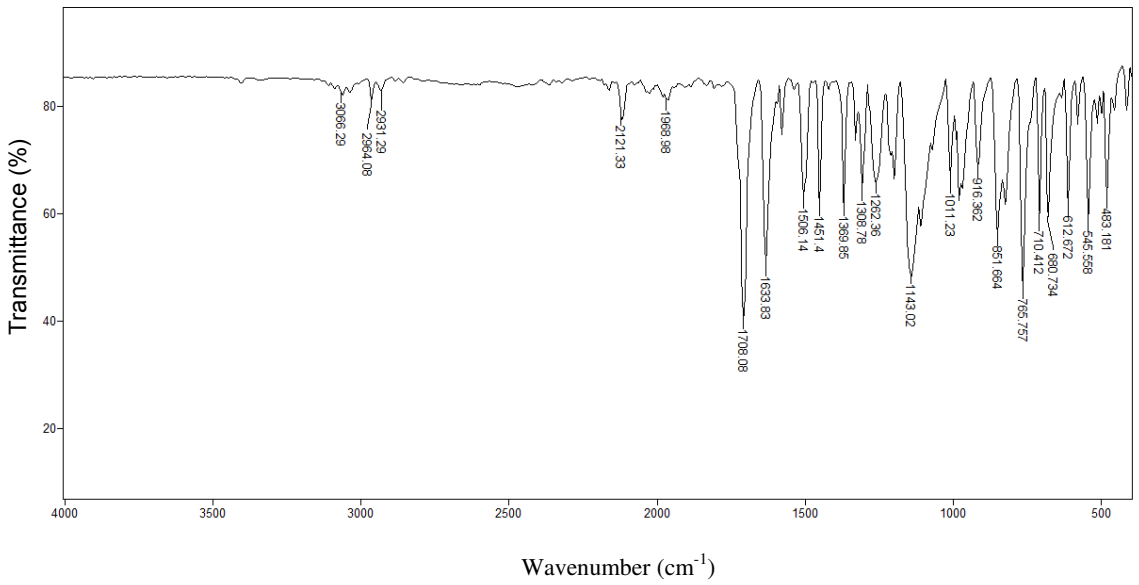

Figure S19 - IR spectrum (ATR) of 4-(trifluoromethoxy)benzyl cinnamate (**3g**).

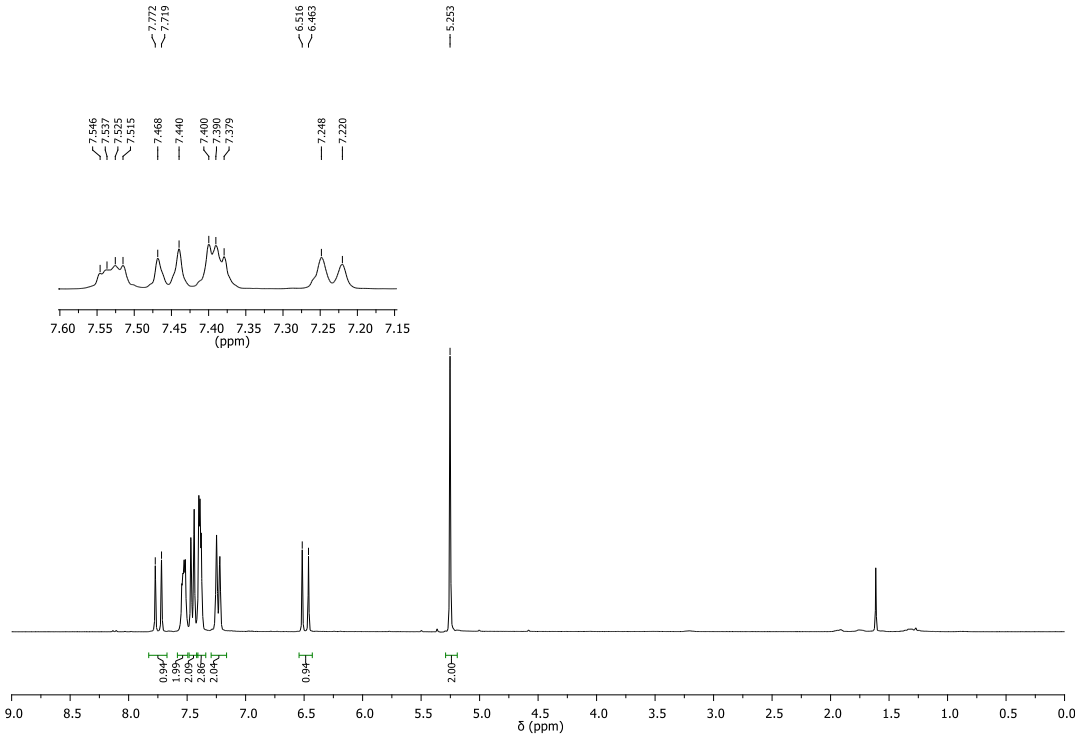

Figure S20 - ^{1}H NMR spectrum (300 MHz, $CDCl_3$) of 4-(trifluoromethoxy)benzyl cinnamate (**3g**).

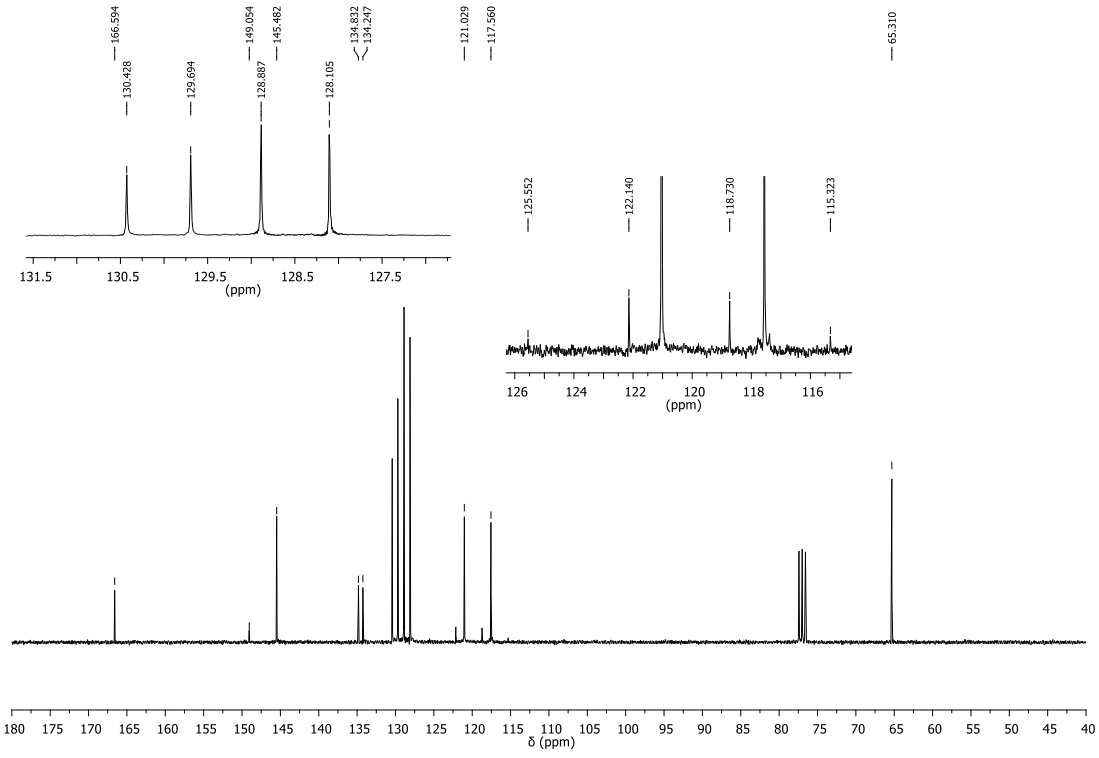

Figure S21 - ^{13}C NMR spectrum (75 MHz, $CDCl_3$) of 4-(trifluoromethoxy)benzyl cinnamate (**3g**).

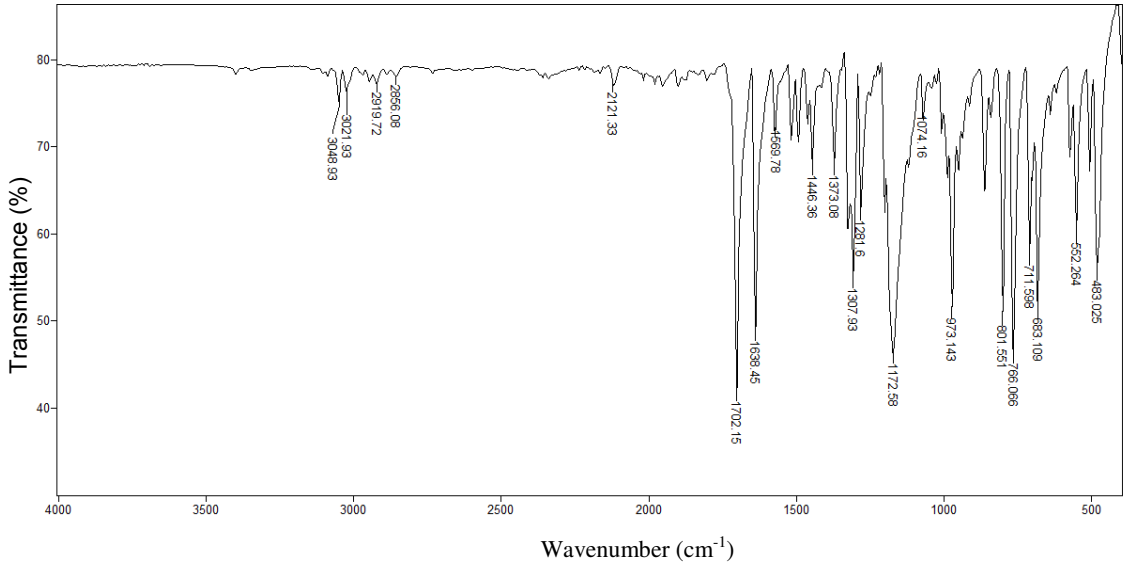

Figure S22 - IR spectrum (ATR) of 4-methylbenzyl cinnamate (**3h**).

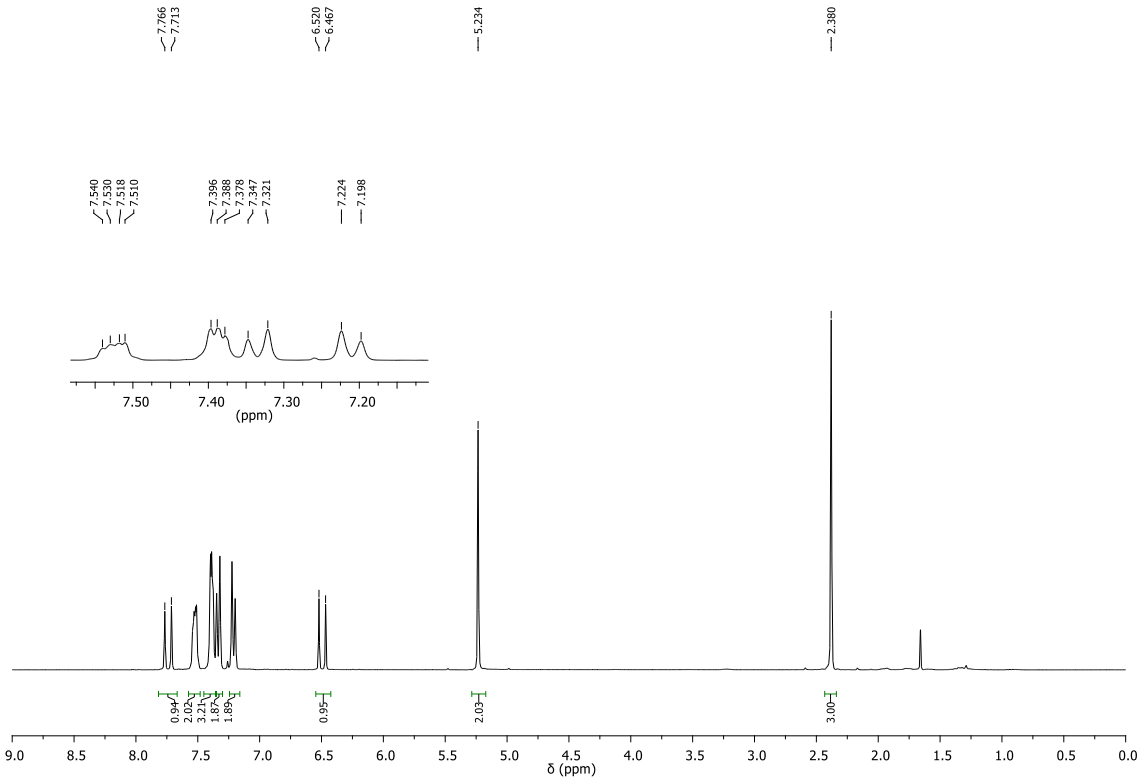

Figure S23 - ^{1}H NMR spectrum (300 MHz, $CDCl_3$) of 4-methylbenzyl cinnamate (**3h**).

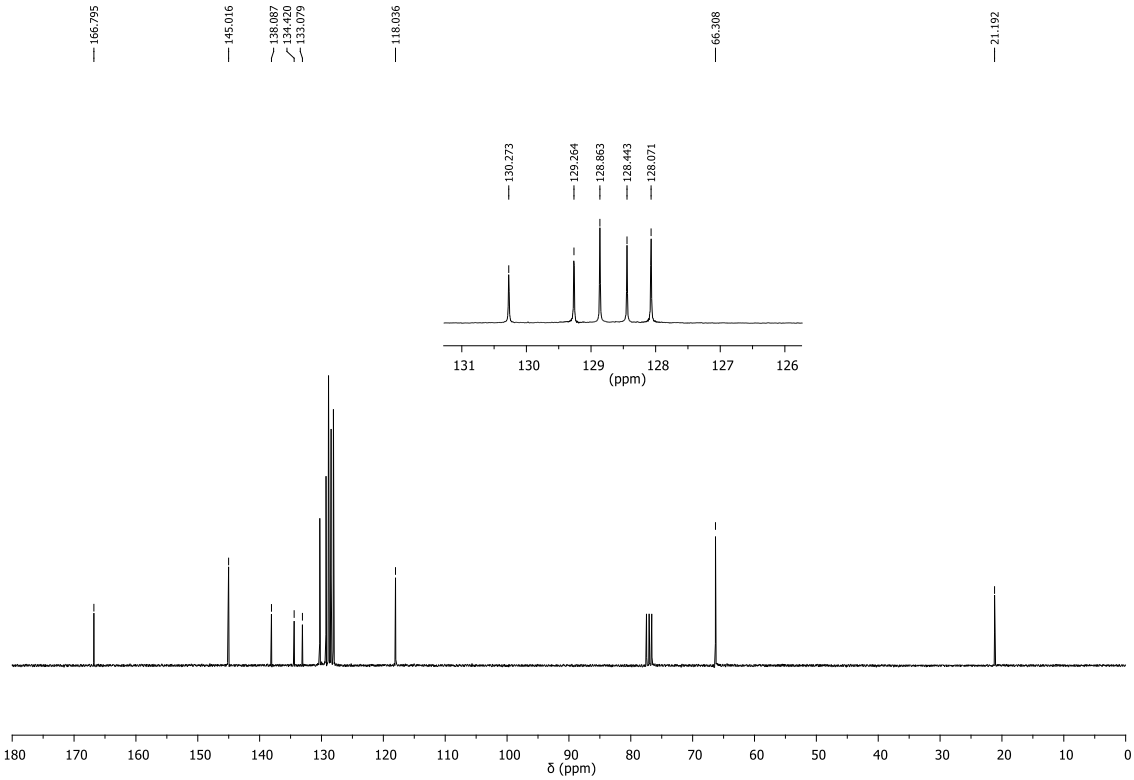

Figure S24 - ^{13}C NMR spectrum (75 MHz, $CDCl_3$) of 4-methylbenzyl cinnamate (**3h**).

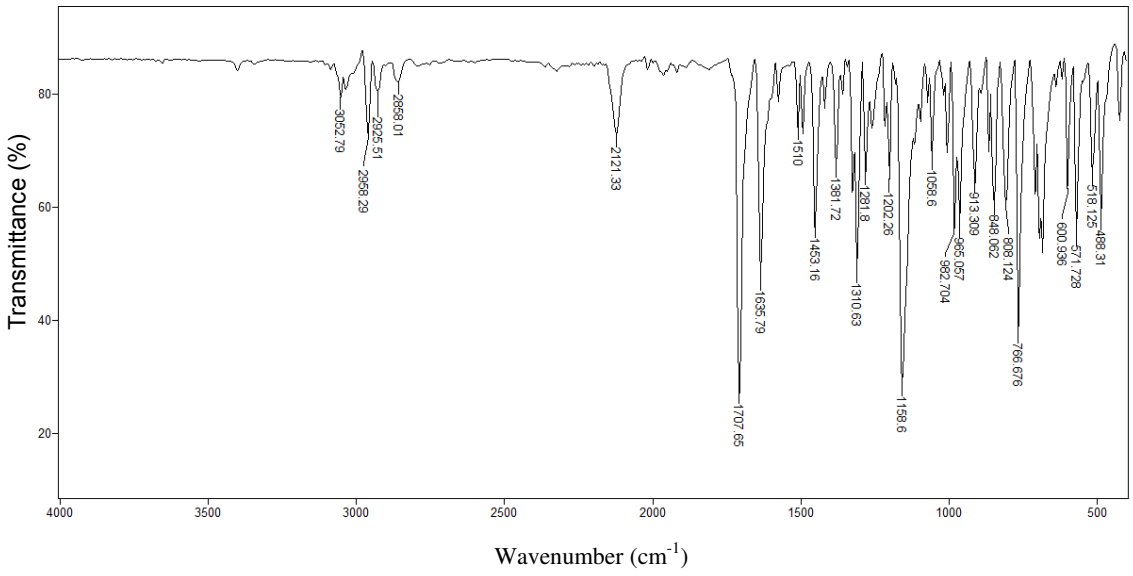

Figure S25 - IR spectrum (ATR) of 4-isopropylbenzyl cinnamate (**3i**).

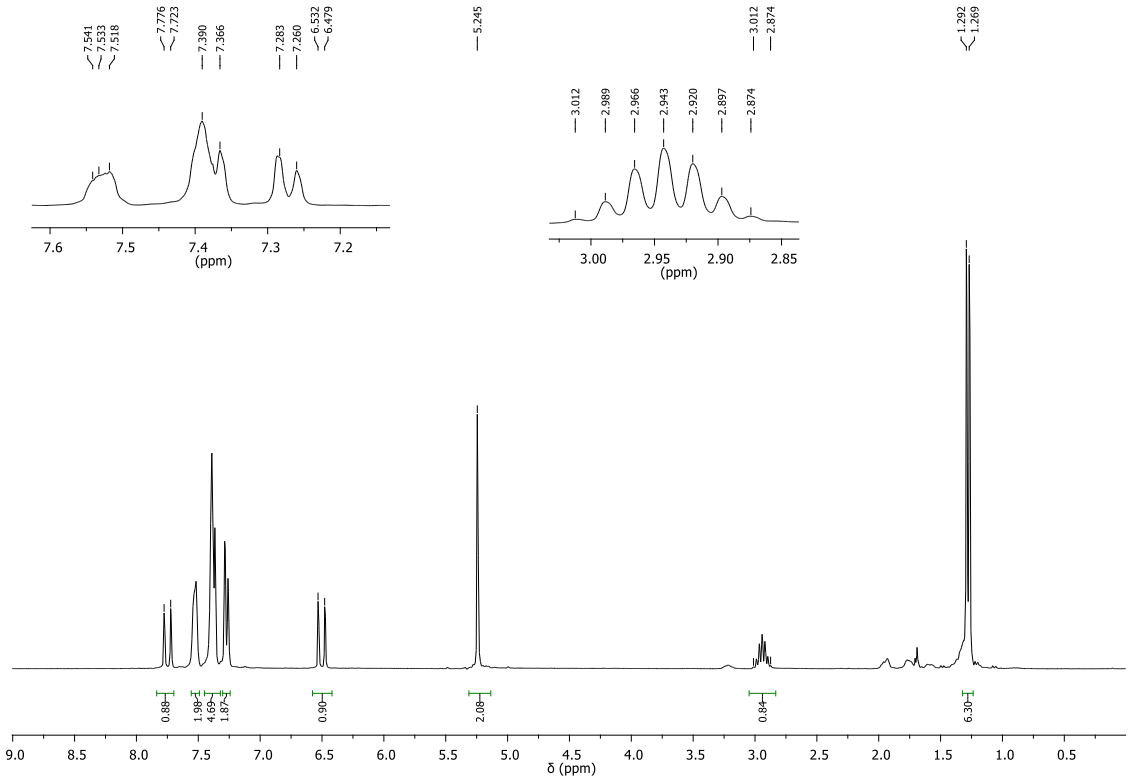

Figure S26 - ^{1}H NMR spectrum (300 MHz, $CDCl_3$) of 4-isopropylbenzyl cinnamate (**3i**).

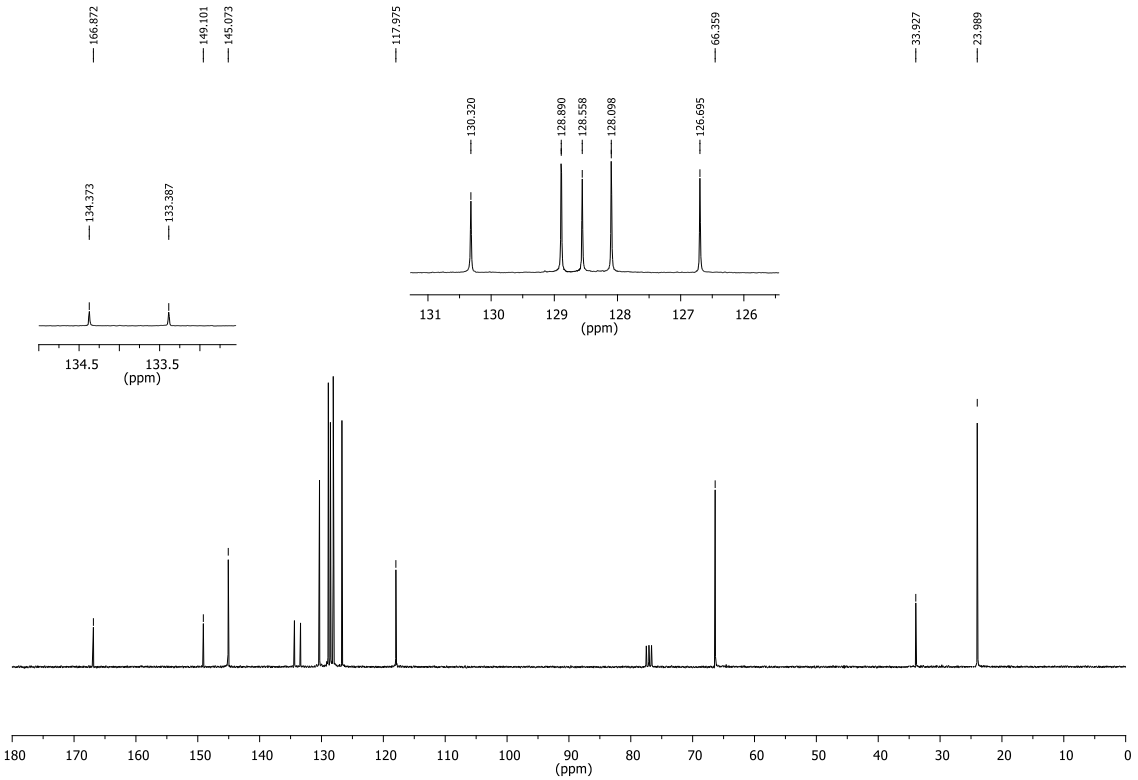

Figure S27 - ^{13}C NMR spectrum (75 MHz, $CDCl_3$) of 4-isopropylbenzyl cinnamate (**3i**).

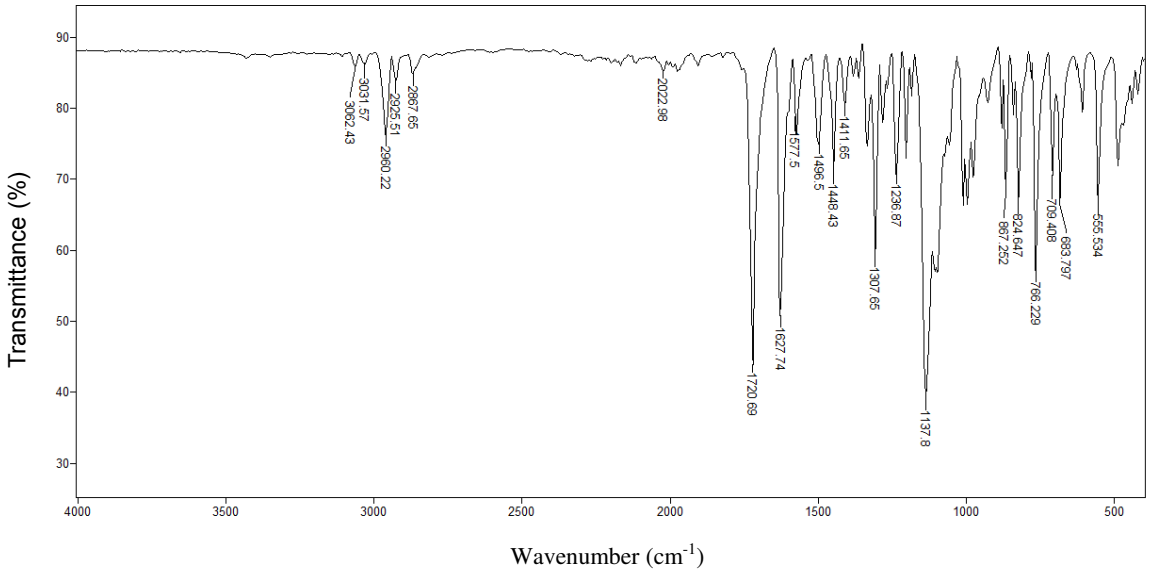

Figure S28 - IR spectrum (ATR) of 5-isopropyl-2-methylphenyl cinnamate (**3j**).

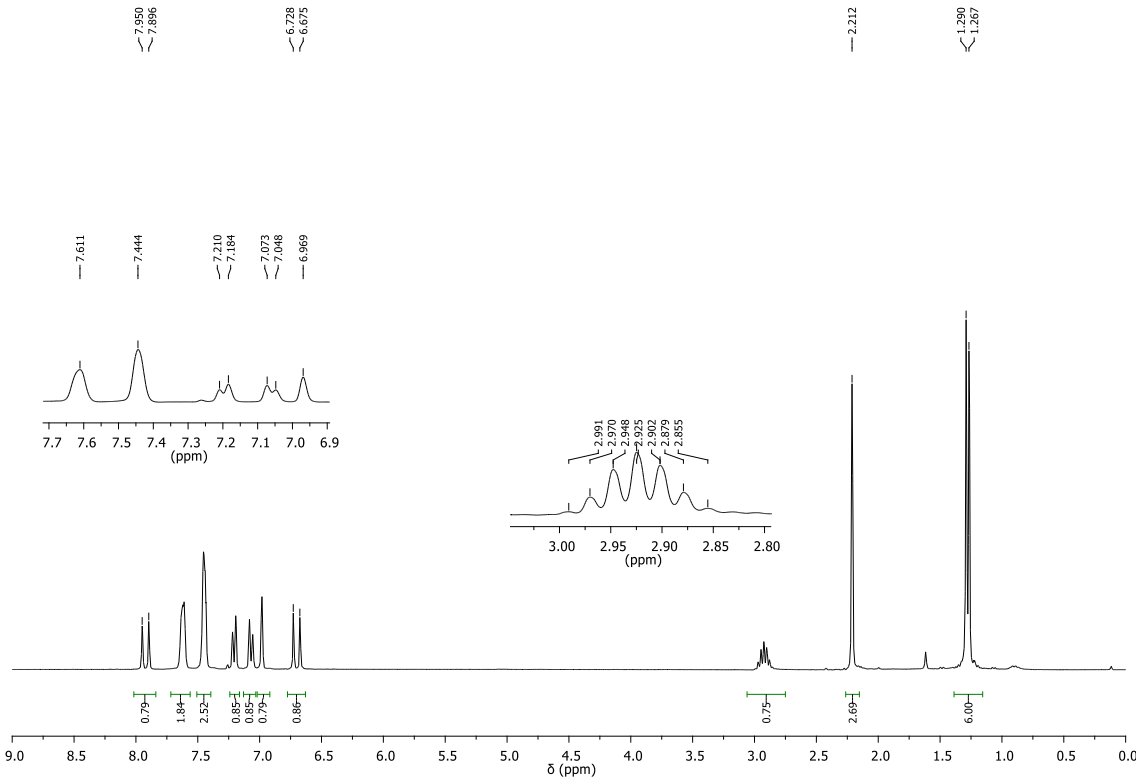

Figure S29 - ^{1}H NMR spectrum (300 MHz, $CDCl_3$) of 5-isopropyl-2-methylphenyl cinnamate (**3j**).

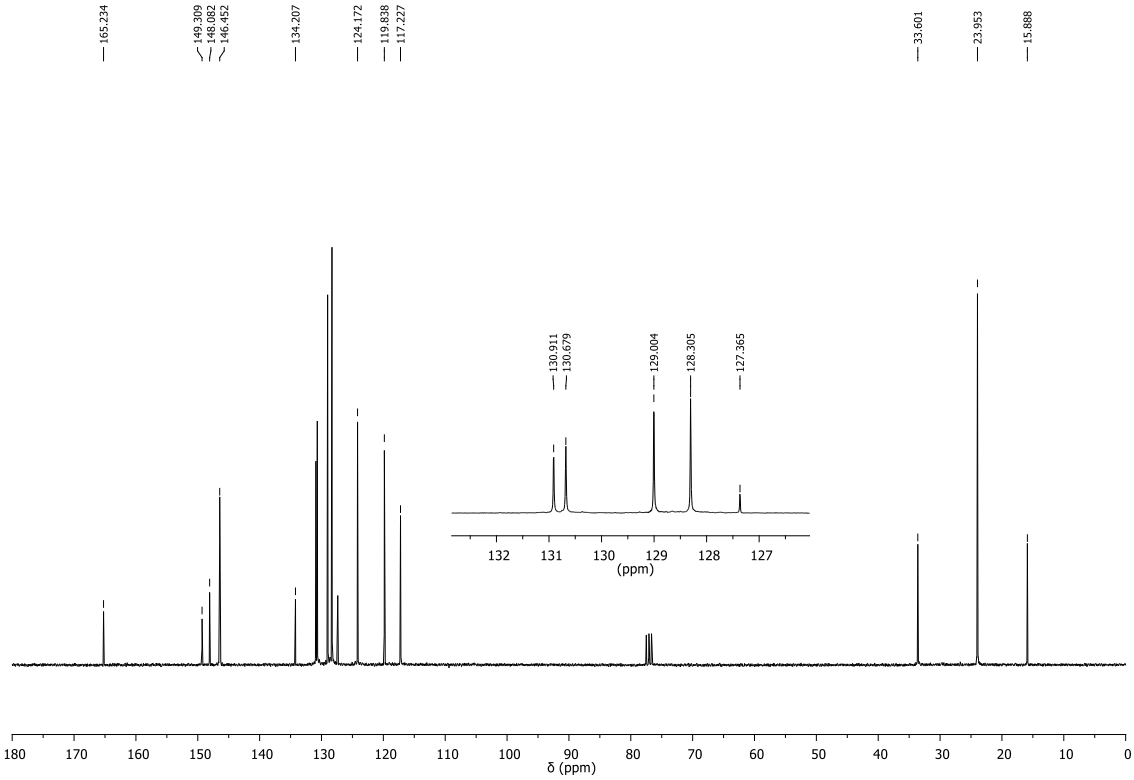

Figure S30 - ^{13}C NMR spectrum (75 MHz, $CDCl_3$) of 5-isopropyl-2-methylphenyl cinnamate (**3j**).

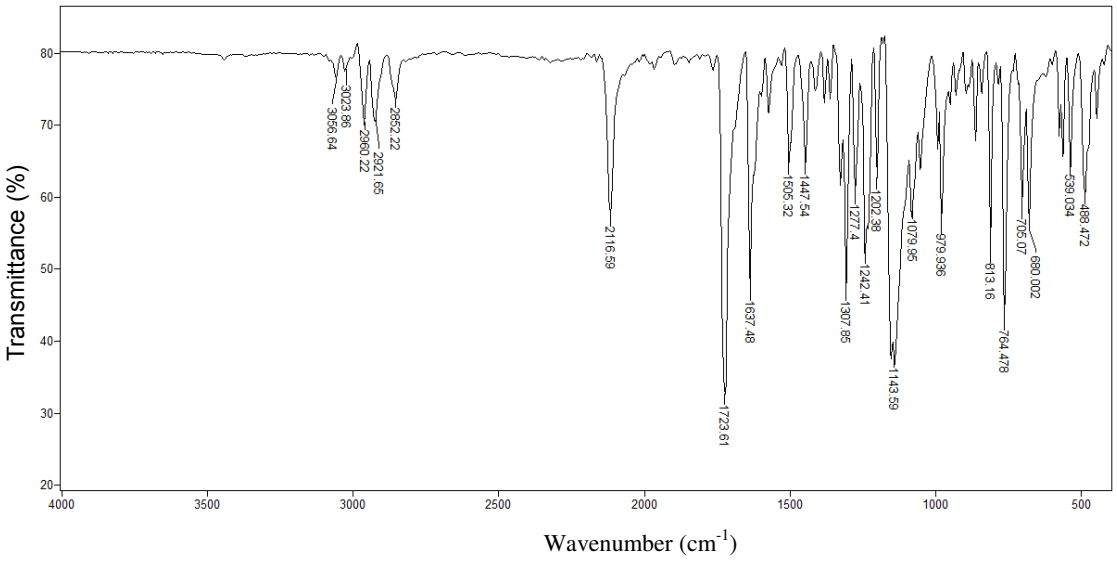

Figure S31 - IR spectrum (ATR) of 2-isopropyl-5-methylphenyl cinnamate (**3k**).

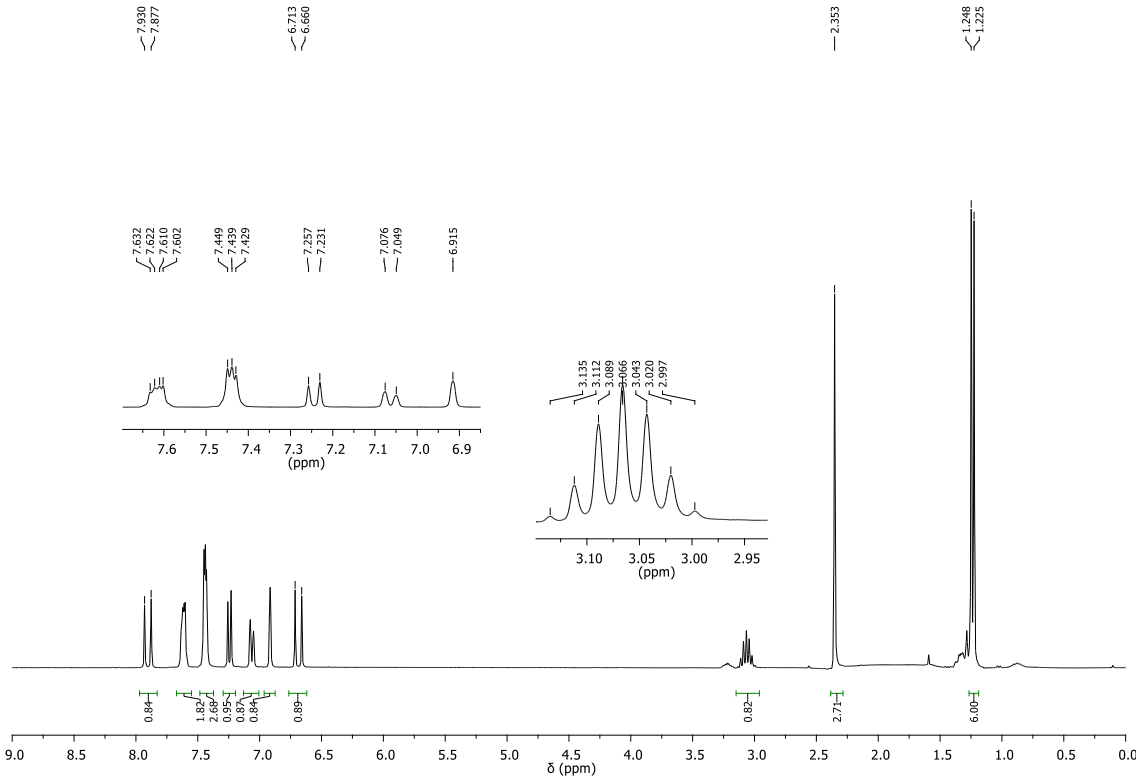

Figure S32 - ^{1}H NMR spectrum (300 MHz, $CDCl_3$) of 2-isopropyl-5-methylphenyl cinnamate (**3k**).

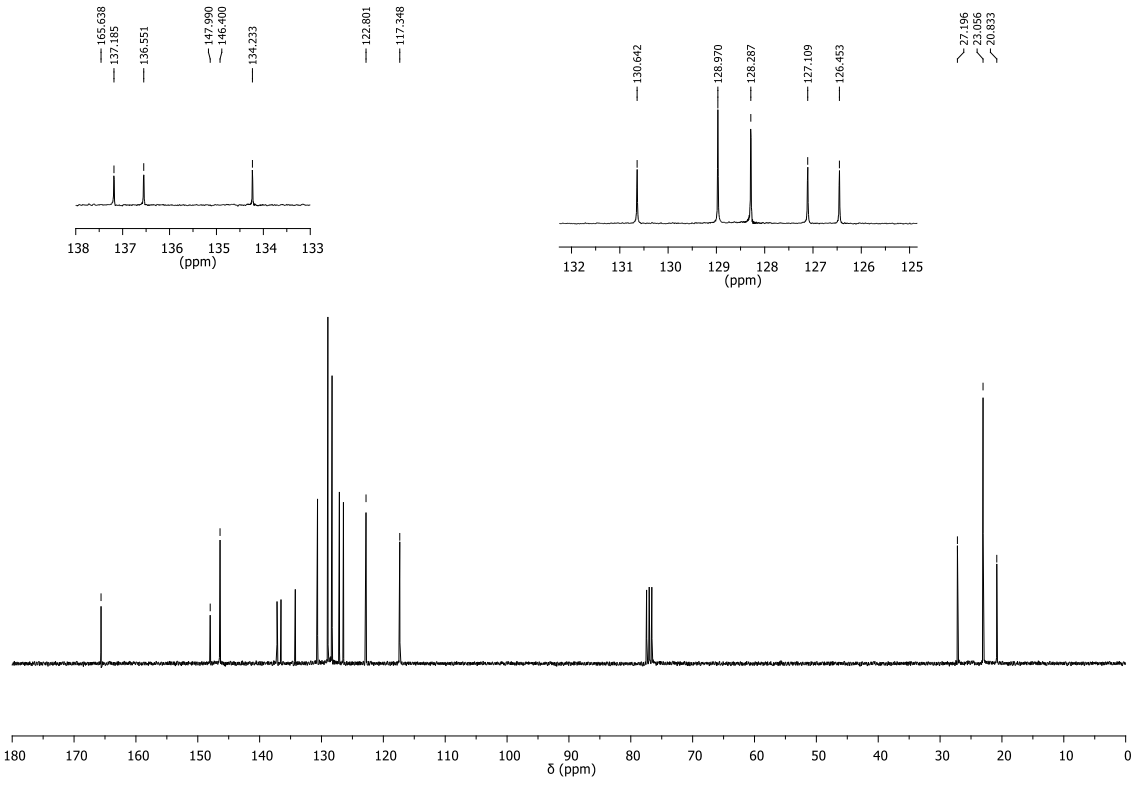

Figure S33 - ^{13}C NMR spectrum (75 MHz, $CDCl_3$) of 2-isopropyl-5-methylphenyl cinnamate (**3k**).

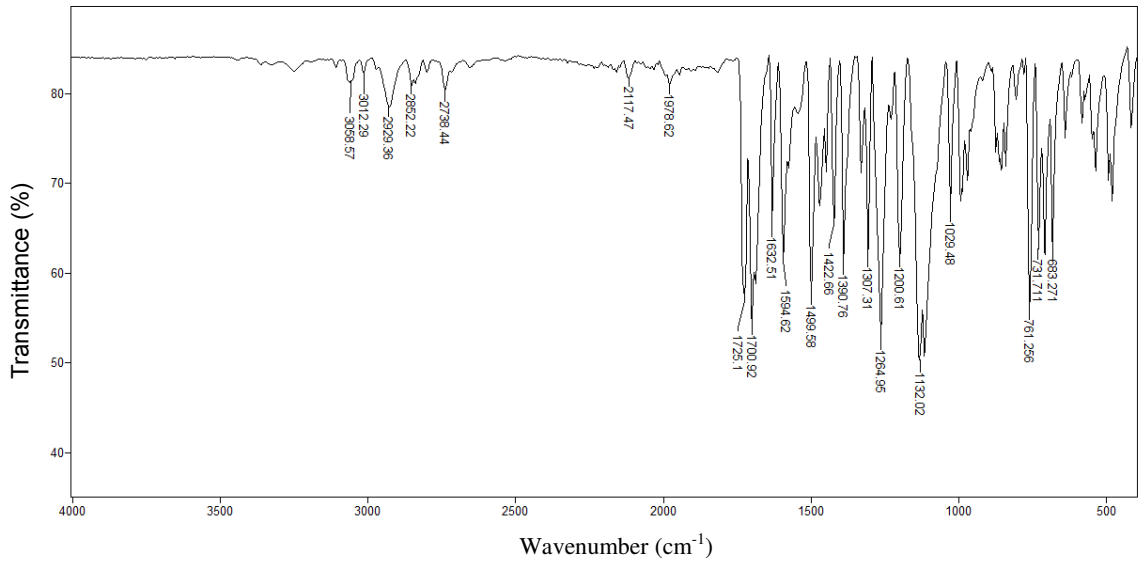

Figure S34 - IR spectrum (ATR) of 4-formyl-2-methoxyphenyl cinnamate (**3l**).

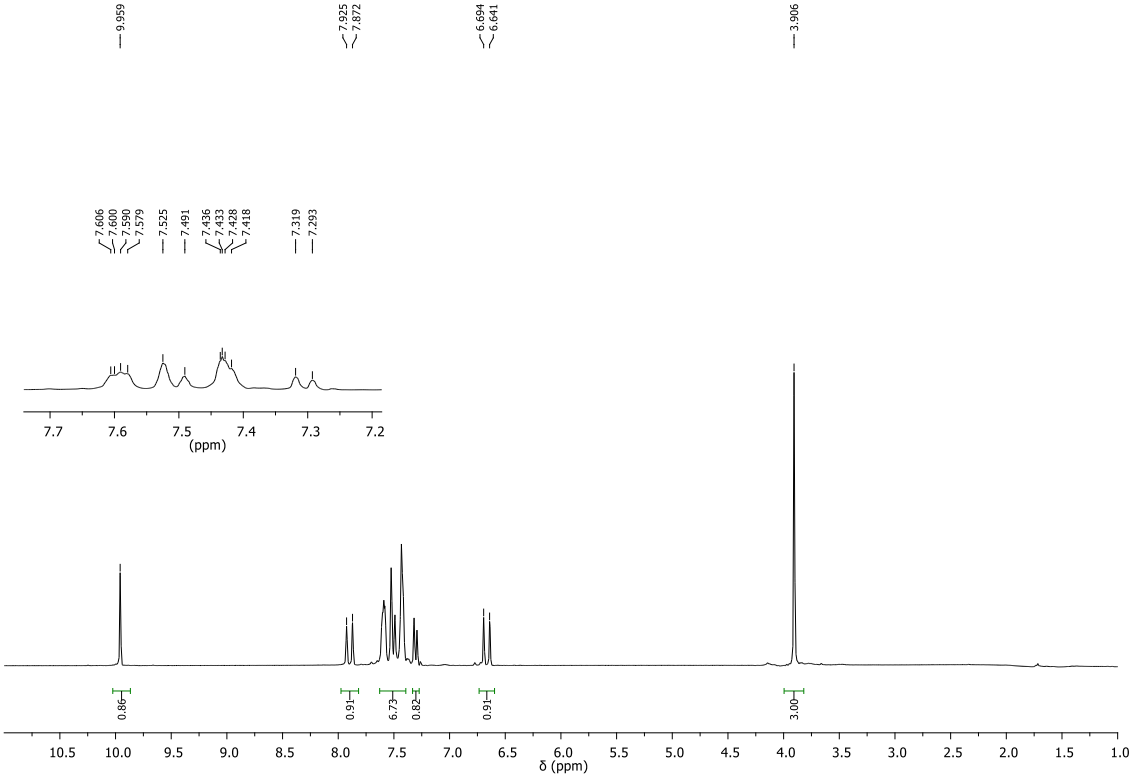

Figure S35 - ^{1}H NMR spectrum (300 MHz, $CDCl_3$) of 4-formyl-2-methoxyphenyl cinnamate (**3l**).

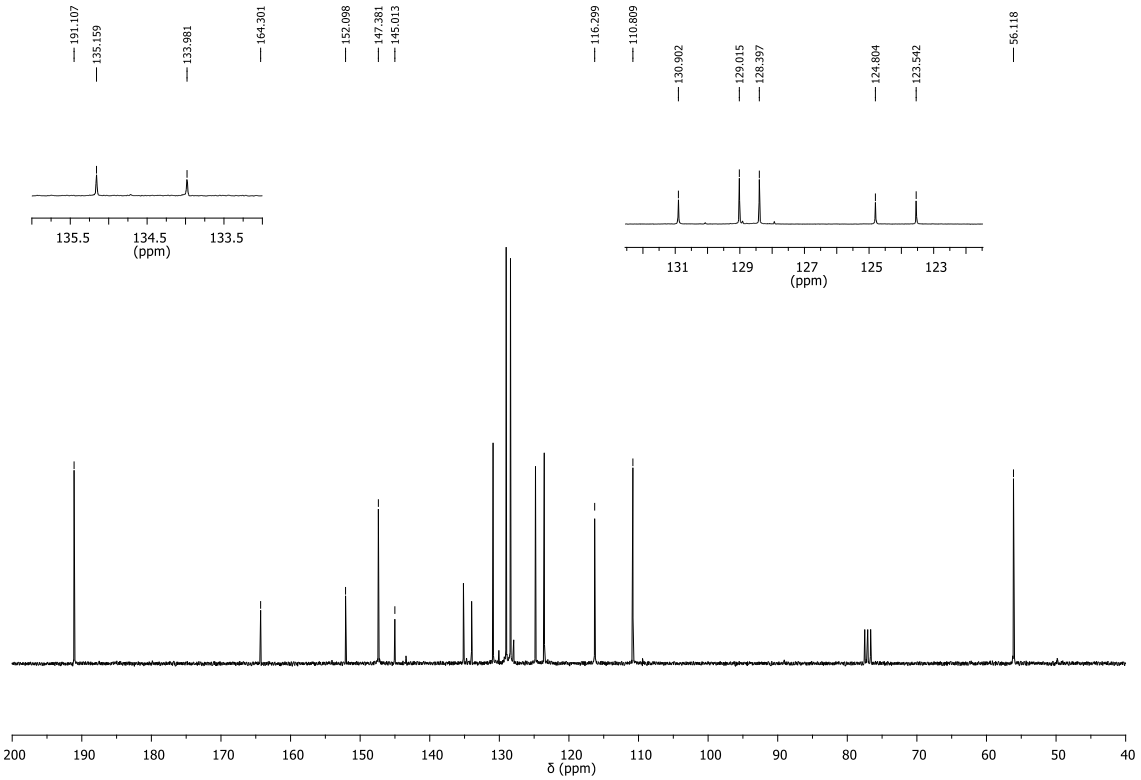

Figure S36 - ^{13}C NMR spectrum (75 MHz, $CDCl_3$) of 4-formyl-2-methoxyphenyl cinnamate (**3l**).

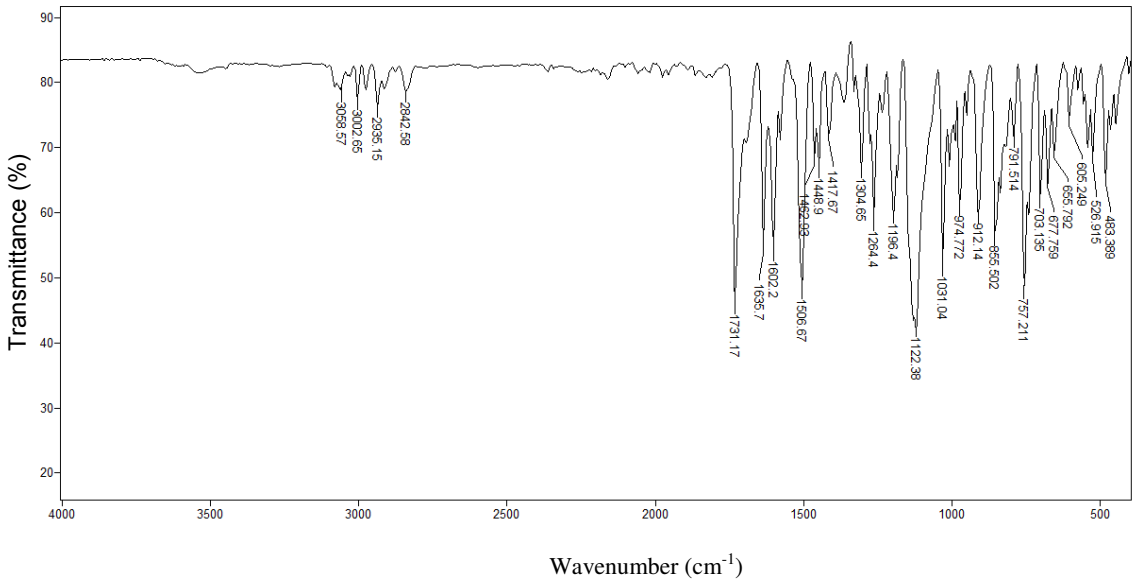

Figure S37 - IR spectrum (ATR) of 4-allyl-2-methoxyphenyl cinnamate (**3m**).

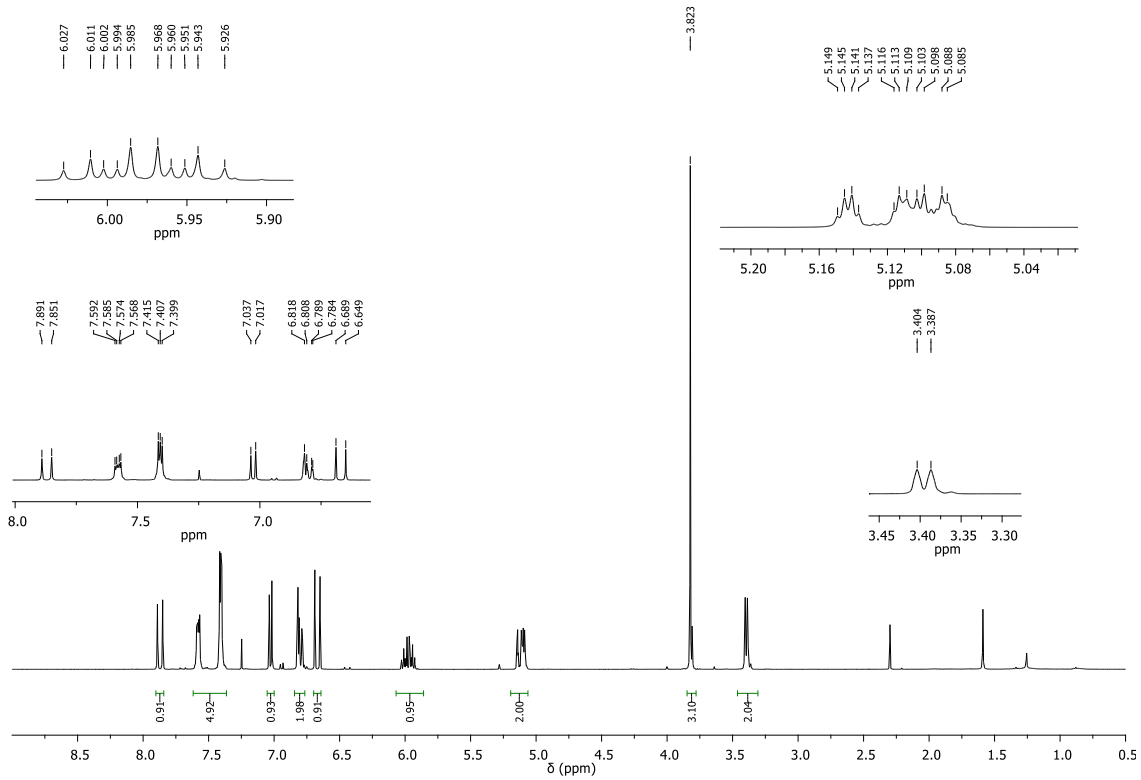

Figure S38 - ^{1}H NMR spectrum (400 MHz, $CDCl_3$) of 4-allyl-2-methoxyphenyl cinnamate (**3m**).

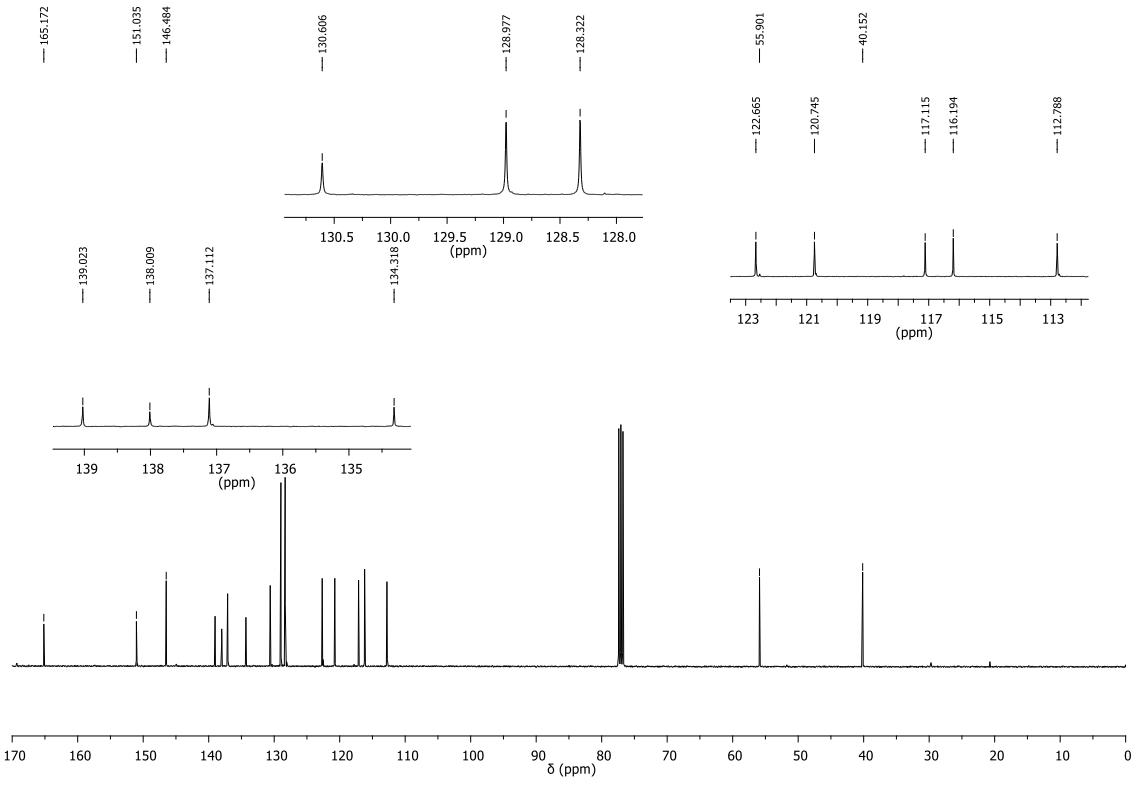

Figure S39 - ^{13}C NMR spectrum (100 MHz, $CDCl_3$) of 4-allyl-2-methoxyphenyl cinnamate (**3m**).

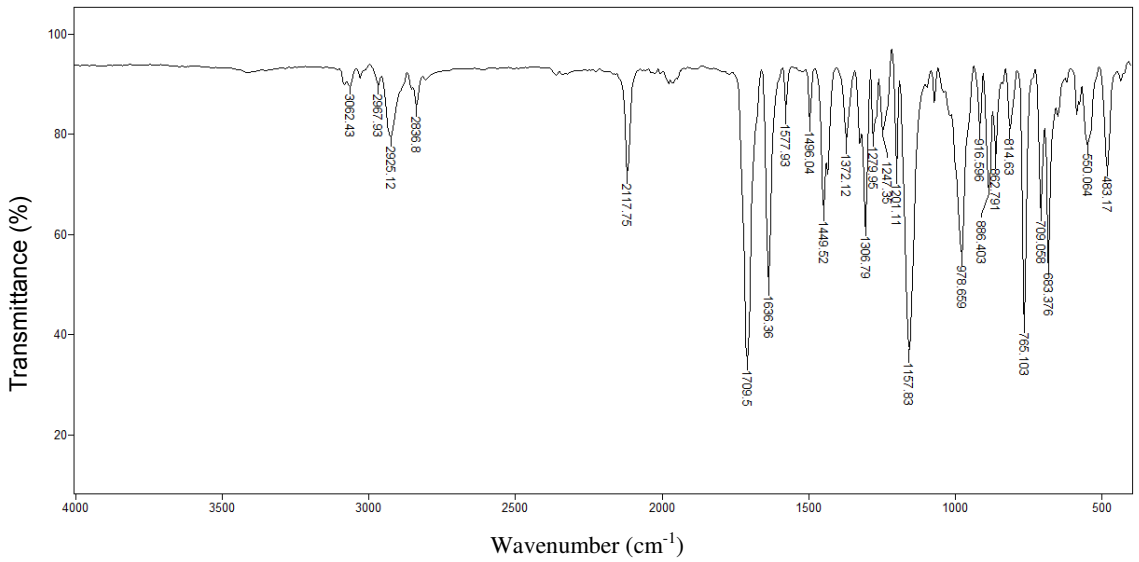

Figure S40 - IR spectrum (ATR) of (*S*)-(4-(prop-1-en-2-yl) cyclohex-1-en-1-yl)methyl cinnamate (**3n**).

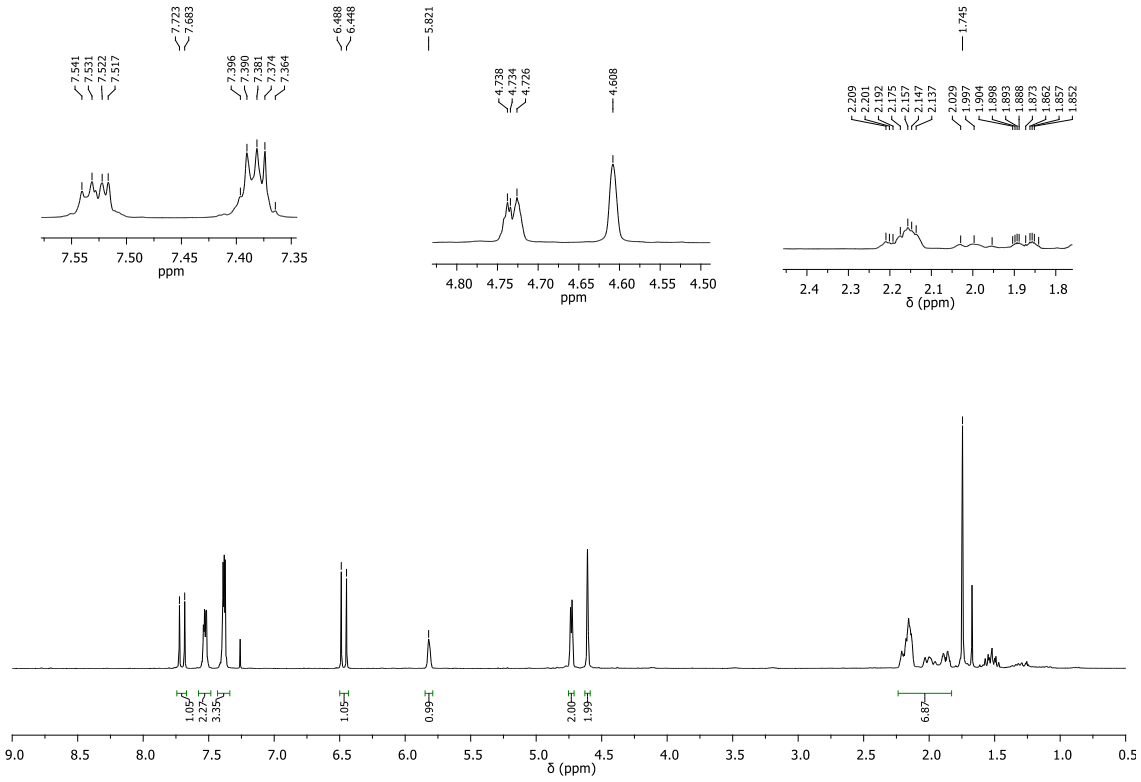

Figure S41 - ^{1}H NMR spectrum (400 MHz, $CDCl_3$) of (*S*)-(4-(prop-1-en-2-yl) cyclohex-1-en-1-yl)methyl cinnamate (**3n**).

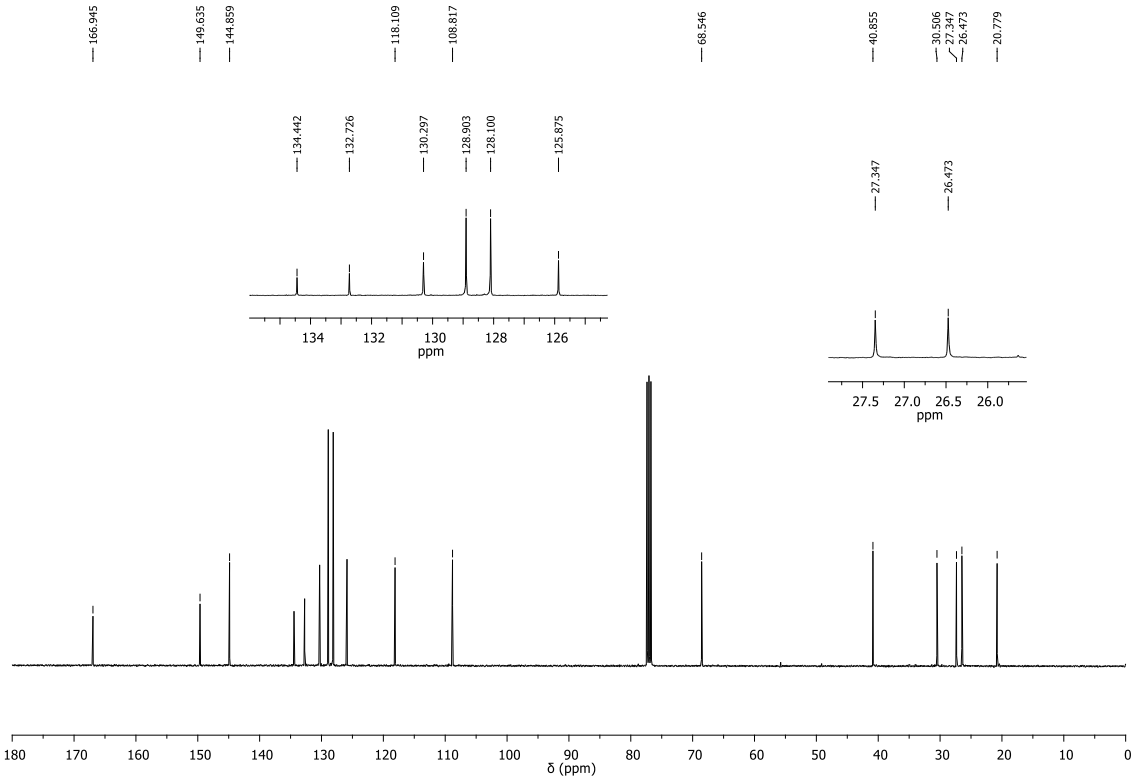

Figure S42 - ^{13}C NMR spectrum (100 MHz, $CDCl_3$) of (*S*)-(4-(prop-1-en-2-yl) cyclohex-1-en-1-yl)methyl cinnamate (**3n**).

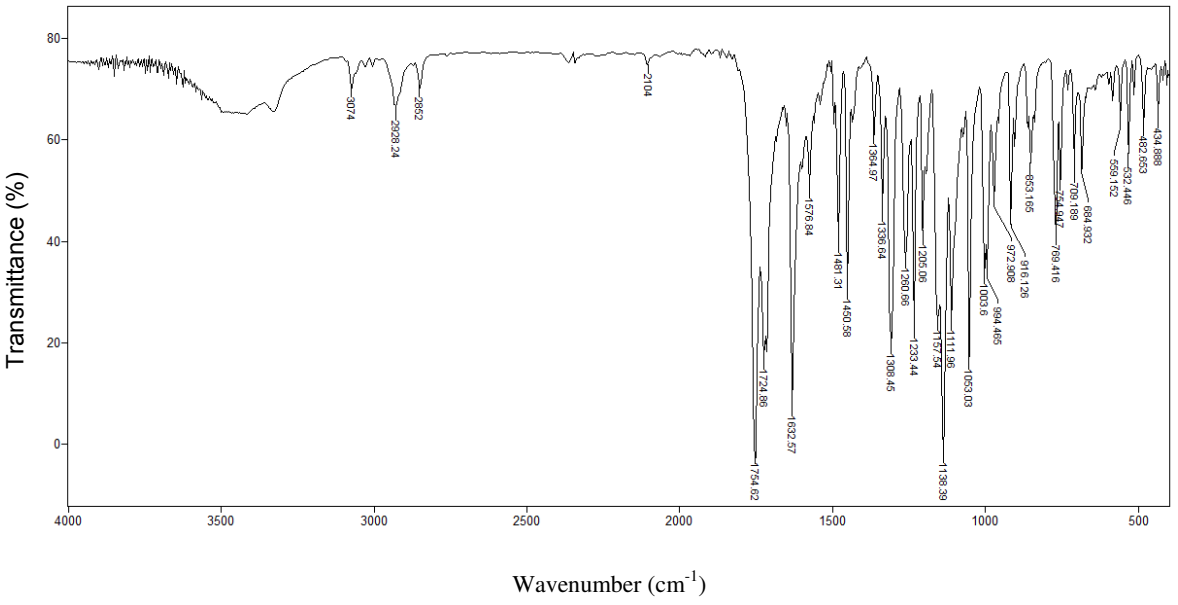

Figure S43 - IR spectrum (KBr) of 3-oxo-1,3-dihydroisobenzofuran-5-yl cinnamate (**3o**).

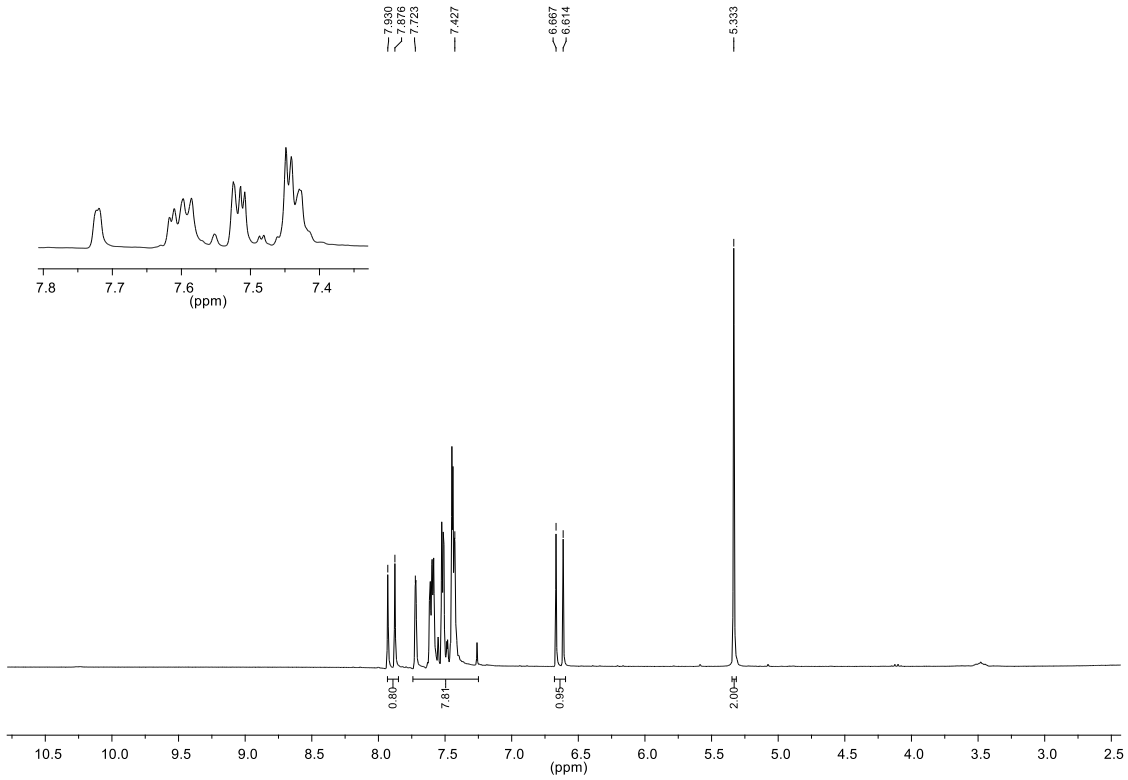

Figure S44 - ^{1}H NMR spectrum (300 MHz, $CDCl_3$) of 3-oxo-1,3-dihydroisobenzofuran-5-yl cinnamate (**3o**).

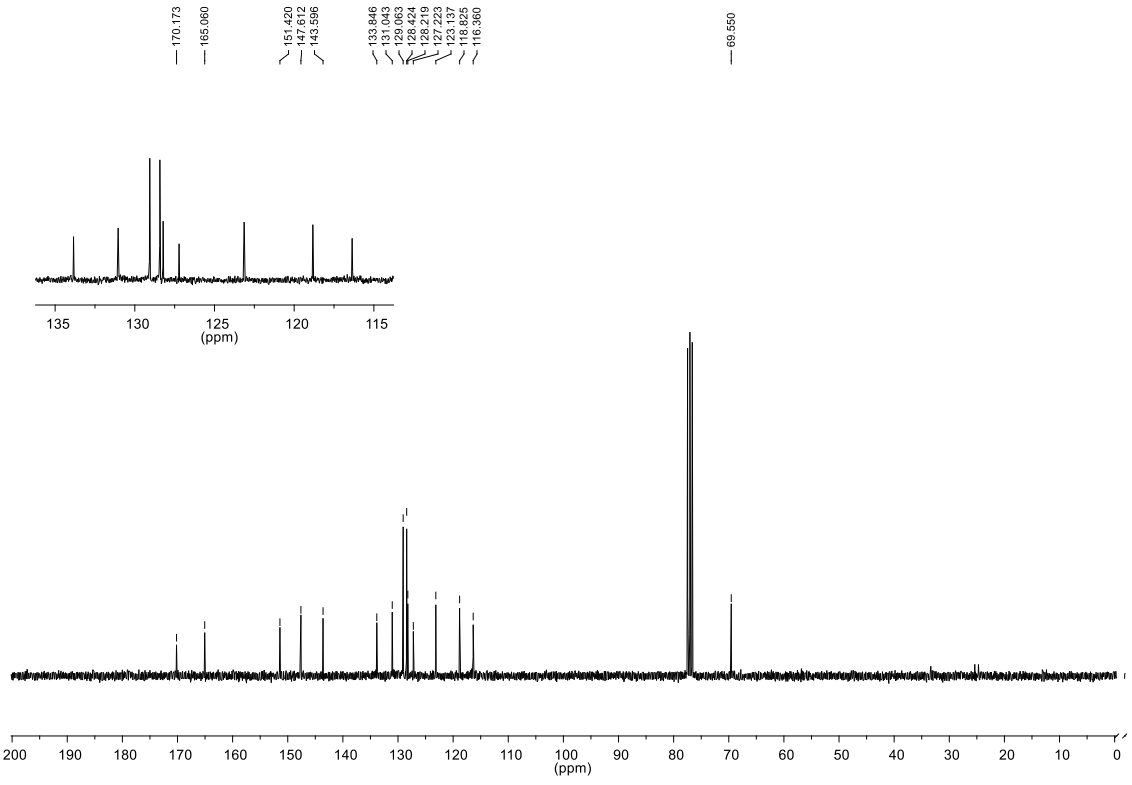

Figure S45 - ^{13}C NMR spectrum (75 MHz, $CDCl_3$) of 3-oxo-1,3-dihydroisobenzofuran-5-yl cinnamate (**3o**).

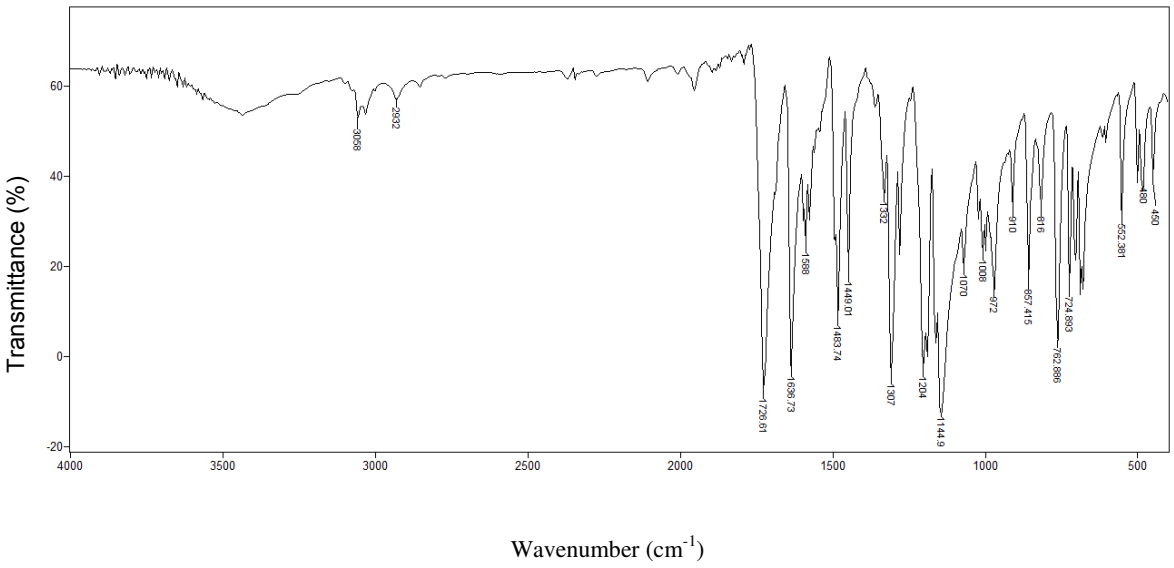

Figure S46 - IR spectrum (KBr) of phenyl cinnamate (**3p**).

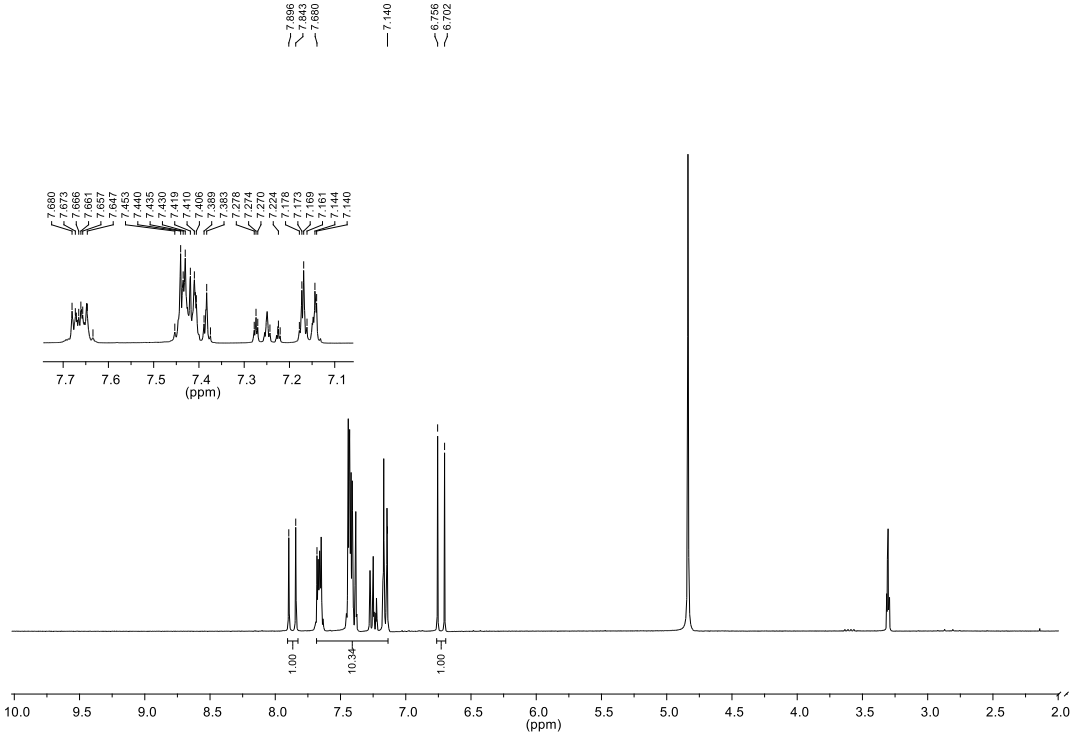

Figure S47 - ^{1}H NMR spectrum (300 MHz, CD_3OD) of phenyl cinnamate (**3p**).

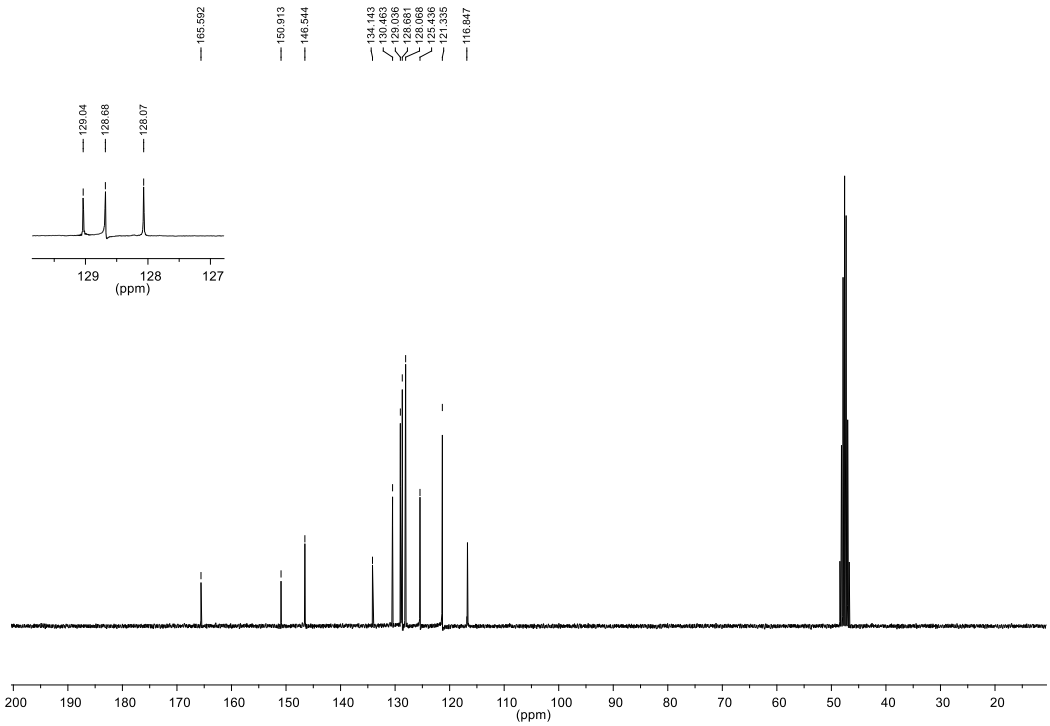

Figure S48 - ^{13}C NMR spectrum (75 MHz, CD_3OD) of phenyl cinnamate (**3p**).

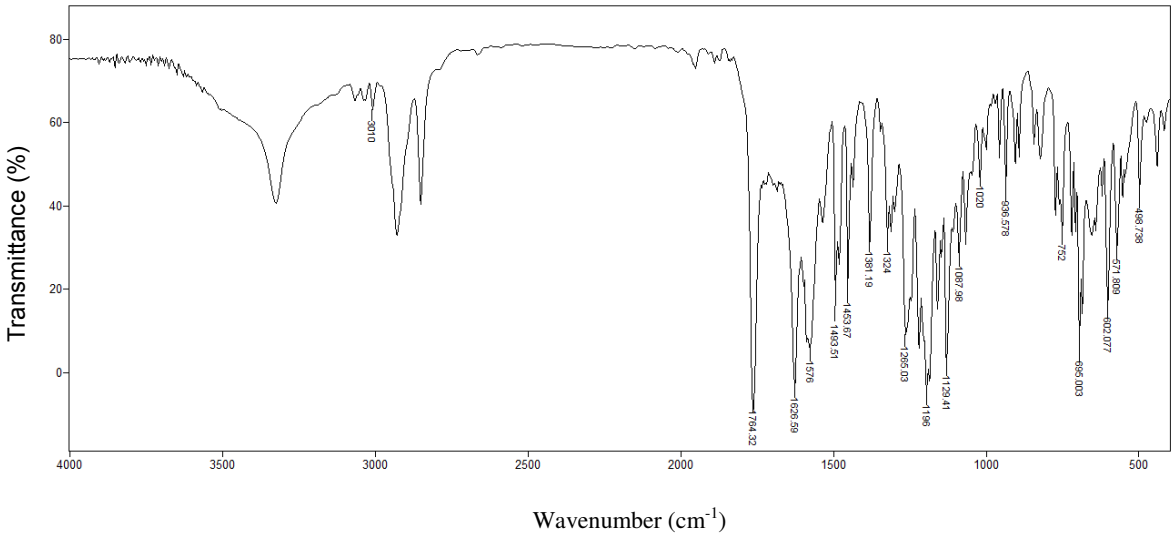

Figure S49 - IR spectrum (KBr) of phenyl 2,3-dibromophenylpropanoate (**3q**).

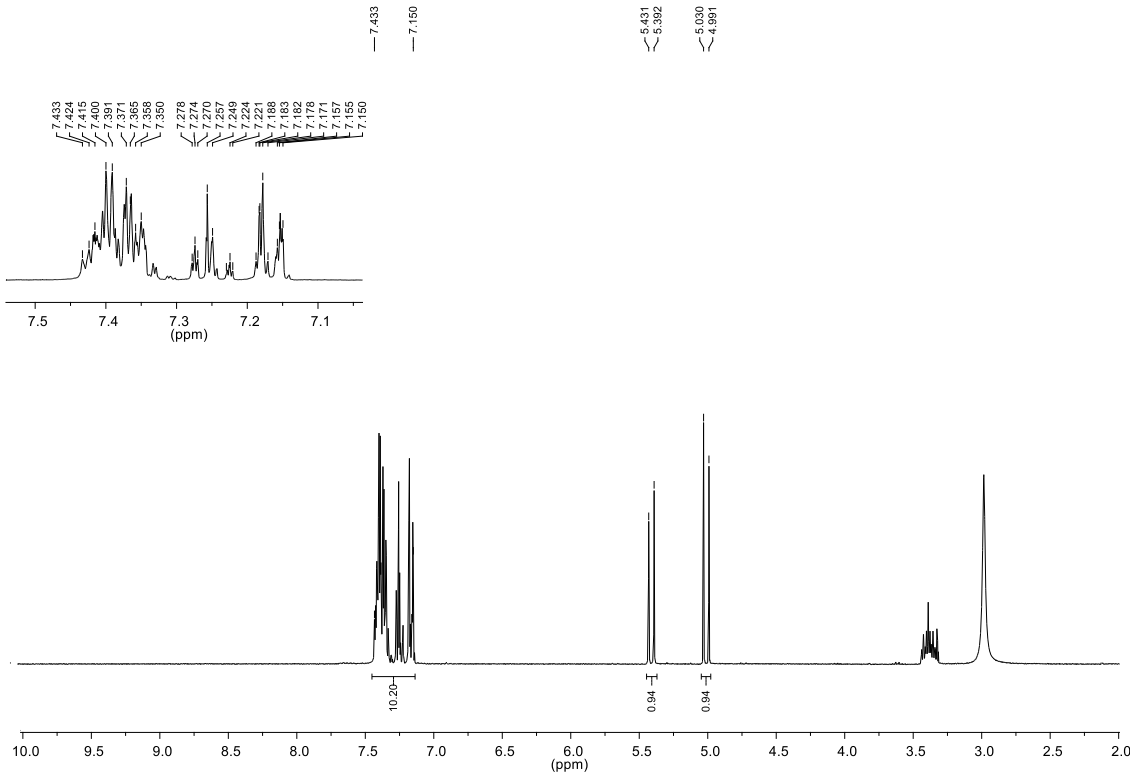

Figure S50 - ^{1}H NMR spectrum (300 MHz, $CDCl_3/CD_3OD$) of phenyl 2,3-dibromophenylpropanoate (**3q**).

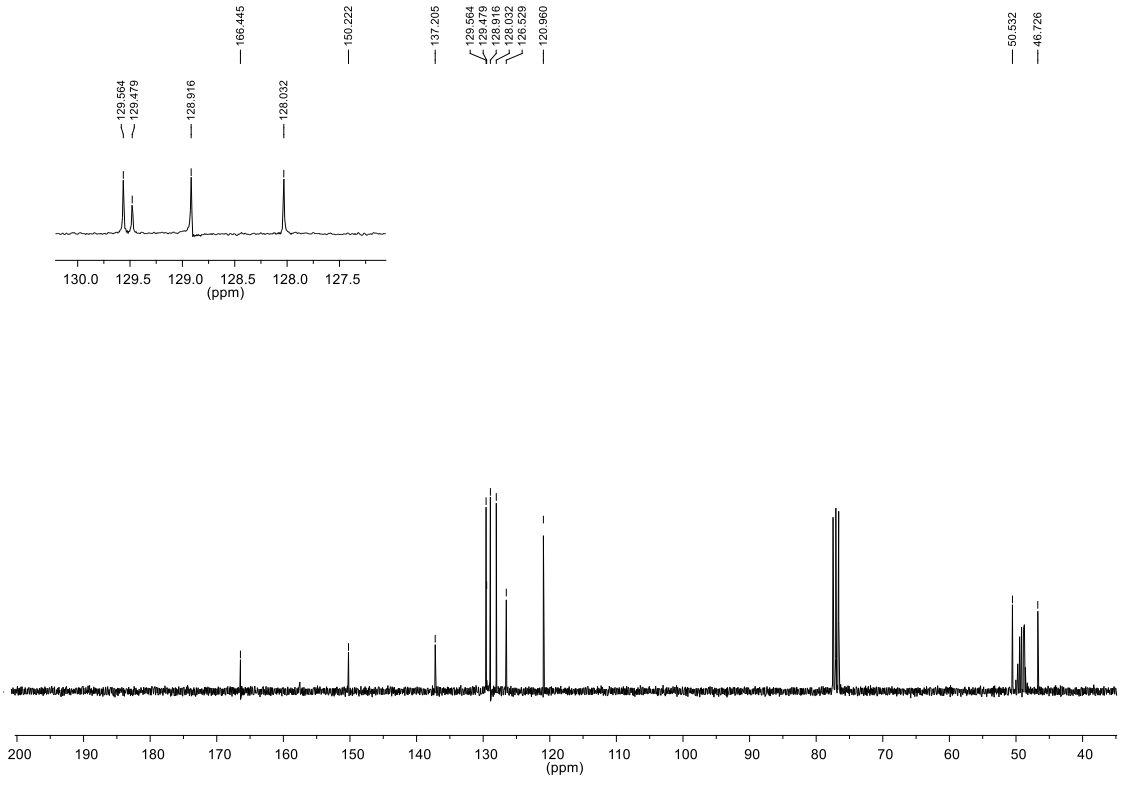

Figure S51 - ^{13}C NMR spectrum (75 MHz, $CDCl_3/CD_3OD$) of phenyl 2,3-dibromophenylpropanoate (**3q**).

BIOLOGICAL DATA

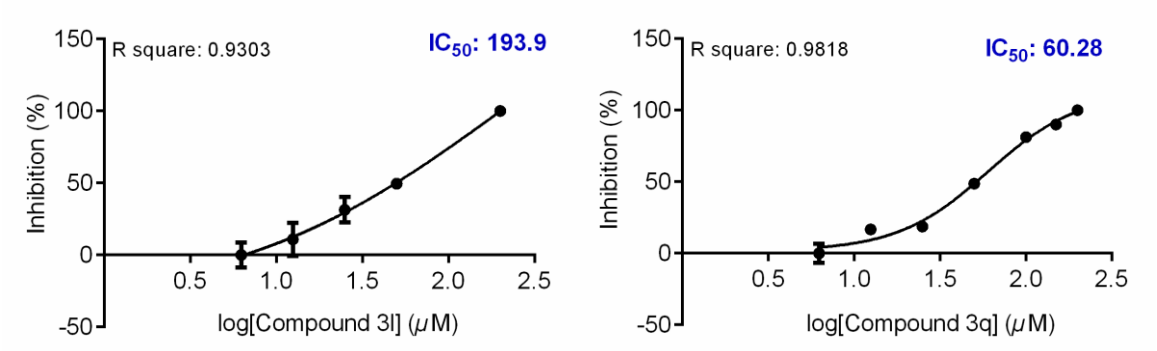

Figure S52 - Half-maximal inhibitory concentration (IC_{50}) and coefficient of determination (R2) values for cinnamic acid derivatives. B16-F10 metastatic melanoma were treated with increasing concentrations (0 – 200 μM) of the compounds **3l** or **3q** for 48 h.

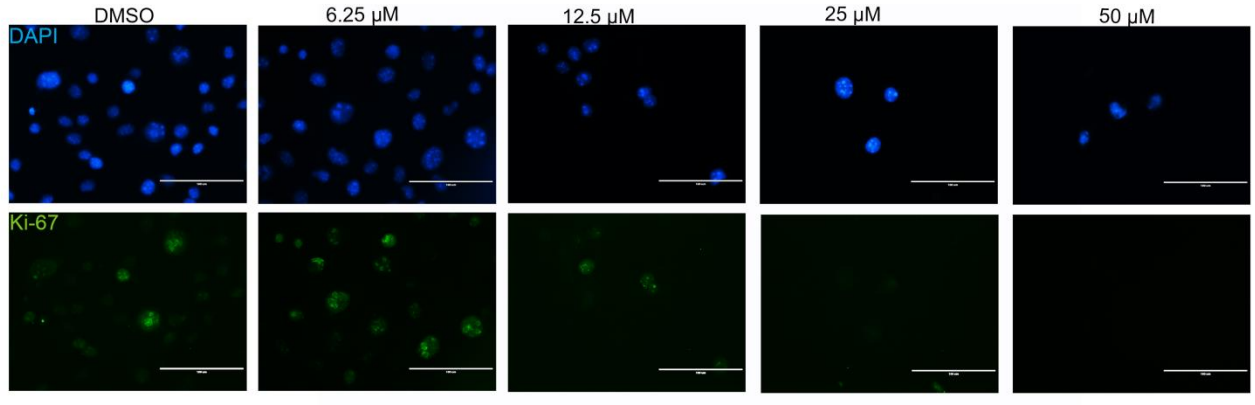

Figure S53 - Effect of **3q** compound on proliferation of B16-F10 melanoma cells. B16-F10 cells were treated with 6.25, 12.5, 25 and 50 μM of compound. DMSO 0.4% was used by control. Representative photomicrography of Ki-67 (green) and DAPI (blue) immunofluorescence after 48 h of treatment; scale bars: 100 μM.

1. CONSIDERAÇÕES FINAIS

O melanoma é um câncer altamente agressivo, metastático e, portanto, letal. Os atuais tratamentos terapêuticos causam inúmeros efeitos colaterais nos pacientes e o melanoma é normalmente refratário à maioria deles. Portanto, dada à gravidade da doença e a dificuldade de tratamentos que extirpem o tumor e melhorem a qualidade de vida dos pacientes, faz-se necessária a prospecção de compostos com potencial atividade antimelanoma. Nesse contexto, o ácido cinâmico é um composto que possibilita a síntese de novos compostos derivados, os quais podem ser ainda mais potentes que o original. Portanto, a presente tese teve por objetivo avaliar a atividade de derivados do ácido cinâmico com potencial antimelanoma.

O capítulo um apresentou uma introdução geral do assunto, enquanto o capítulo dois descreveu sobre o uso das células de melanoma no *screening* de compostos. Já os capítulos três e quatro expuseram resultados significativos sobre compostos derivados do ácido cinâmico com potencial antimelanoma. Os compostos selecionados foram o **3q** e o **6b**, ambos são ésteres derivados do ácido cinâmico, chamados de cinamatos. Tais compostos impactaram a atividade celular de melanoma B16-F10, ao alterar a viabilidade e a proliferação celular, gerar morte celular e interferir no comportamente metastático dessas células. Tomados em conjunto, esses dados mostraram o potencial dos derivados do ácido cinâmico para o desenvolvimento de novos compostos para o tratamento do melanoma metastático. Como perspectiva, pretende-se realizar trabalhos futuros para acessar os mecanismos de ação dos compostos selecionados por meio de ensaios moleculares, além de ensaios *in vivo*, a fim de complementar e acrescer os resultados encontrados.

2. LISTA DE PUBLICAÇÕES, COAUTORES E OUTROS TRABALHOS RELEVANTES

Nesta Tese:

- **Vale, J.A.**; Lima, G.D.A.; Almeida, A.A.; Teixeira, R.R.; Neves, M.M. 2020. Melanoma cell lines as a model for high-throughput drug screening, in: Watanabe, H.S. (Ed.), Horizons in cancer research. Nova Science Publishers, Nova York, 85-145.

- Santos, F.S.; **Do Vale, J.A.**; Santos, L.S.; Gontijo, T.B.; Lima, G.D.A.; Oliveira, L.L.; Neves, M.M.; Teixeira, R.R.; Freitas, R.P. Synthesis of Novel Cinnamides and a Bis Cinnamate Bearing 1,2,3-Triazole Functionalities with Antiproliferative and Antimetastatic Activities on Melanoma Cells. Journal of the Brazilian Chemical Society (Online), 32, 2174-2185, 2021.

- **Vale, J.A.**; Rodrigues, M. P.; Lima, A.M.A.; Santiago, S.S.; Lima, G.D.A.; Almeida, A.A.; Oliveira, L.L.; Bressan, G.C.; Teixeira, R.R.; Machado-Neves, M. Synthesis of Cinnamic Acid Ester Derivatives with Antiproliferative and Antimetastatic Activities on Murine Melanoma Cells. Biomedicine & Pharmacotherapy, 148, 112689, 2022.

Outras publicações:

- **Vale, J.A.**; Souza, A.P.M.; Lima, G.D.A.; Gonçalves, V.H.S; Moreira, G.A.; Barros, M.V.A.; Pereira, W.L.; Lazaroni e Merchid, N.C.; Fietto, J.L.R.; Bressan, G.C.; Teixeira, R.R.; Neves, M. M. Effect of the topical administration of N-(2-(4- bromophenylamino)-5-(trifluoromethyl)phenyl)nicotinamide compound in a murine subcutaneous melanoma model. Anti-Cancer Drugs, 31(7), 718-727, 2020.

- Almeida, A.A.; Lima, G.D.A.; Eiterer, M.; Rodrigues, L.A.; **Vale, J.A.**; Zanatta, A.C.; Bressan, G.C.; Oliveira, L.L.; Leite, J.P.V. A withanolide-rich fraction of Athenaea velutina induces apoptosis and cell cycle arrest in melanoma B16F10 cells. Planta Medica (Internet), 1-12, 2021.

Patentes dos artigos: Submetidas.